Exploiting the Bioenergetics of Disease-Causing Lymphocytes for Selective Immunomodulation.

by

Daniel R. Wahl

A dissertation submitted in partial fulfillment
of the requirements for the degree of
Doctor of Philosophy
(Chemical Biology)
in The University of Michigan
2010

Doctoral Committee:

Professor Gary D. Glick, Co-Chair
Professor James L. M. Ferrara, Co-Chair
Professor Carol A. Fierke
Associate Professor Kristina I. Hakansson
Associate Professor Philip D. King
Associate Professor Pavan R. Reddy

For my loving wife, Suzanne

ACKNOWLEDGEMENTS

This dissertation could not have been completed without the support and guidance of my friends, family and colleagues. I must first thank my advisors, Gary Glick and Jamie Ferrara. Gary has always been willing to take time to help me refine my ideas and force me to think critically about this project. In doing so, Gary has helped me change from someone who simply enjoys science into an actual scientist. I am deeply grateful to Jamie for welcoming me into his world-class laboratory mid-Ph.D. to further my studies. Jamie has spent endless hours critically discussing this project with me and has made every resource available to test our ideas. Gary and Jamie have helped me to an intellectual place that I could not have reached on my own, sometimes despite my fierce resistance. Most importantly, their high standards have taught me to demand excellence of myself and my work. I am truly thankful to both of you.

I would also like to thank the members of my dissertation committee: Carol Fierke, Kristina Hakansson, Phil King, and Pavan Reddy. Thank you for taking time out of your schedules to serve on my committee and ensure my progress through graduate school. Your thoughtful suggestions and insight into this research have helped bring it to its current state.

I am also grateful to the current and former members of the Glick and Ferrara laboratories: Craig Byersdorfer, Joanne Cleary, Shawn Clouthier, Tasha Francis, Rich Frazee, Erin Gatza, Chris Grondin, Magic Jang, Kathi Lowler, Gina Ney, Evelyn Nieves, Sophie Paczesny, Isao Tawara, Tom Sundberg, Lara Swenson, and Li Wang. Your humor, intellect and enthusiasm have made the lab a pleasant place to spend my days. I am especially grateful to Erin Gatza for her development of this project and for all the time she spent teaching me once I joined the Ferrara laboratory. I would also like to specially thank Tony Opipari for his enthusiasm regarding cellular metabolism and Tom Sundberg for his peer mentorship early in my graduate career. In addition, I thank Gary, Jamie, Craig and Erin for taking time to help edit and critique this dissertation.

I would also like to thank the other laboratories that helped to make this work possible. In particular, Faith Strickland, Sushmay Yarlagadda and Brian Petersen in Bruce Richardson's laboratory provided the T cell samples used in Chapter 2. Additionally, James Bain, Olga Ilkayev and Chris Newgard at Duke University provided the acyl-carnitine analysis discussed in Chapter 3.

Finally, I must thank my family. My parents, Rich and Sandy, and my siblings, Matt, Pete and Katie, have always believed in me and encouraged me to pursue my dreams. Most importantly, I would like to thank my wife, Suzanne. Your unconditional love and support (and editing prowess) has made this thesis possible.

Table of Contents

LIST OF FIGURES

Figure

LIST OF TABLES

Table

LIST OF ABBREVIATIONS

$\Delta\psi_m$	Mitochondrial membrane potential
γc	Common gamma chain
α-KG	α-ketoglutarate
α-KGDH	α-ketoglutarate dehydrogenase
1,3-BPG	1,3-bisphosphoglycerate
2DG	2-deoxyglucose
2PG	2-phosphoglycerate
3PG	3-phosphoglycerate
4-HPR	N-(4-hydroxyphenyl) retinamide
ACC	Acetyl coA carboxylase
ACL	ATP-citrate lyase
ACTH	Adrenocorticotropic hormone
AICD	Activation induced cell death
ALL	Acute lymphoblastic leukemia
AML	Acute myelogenous leukemia
AMPK	AMP-activated protein kinase
AP-1	Activator protein 1
APC	Antigen presenting cell

APL	Acute promyelocytic leukemia
ASK	Apoptosis signal-regulated kinase
ATG	Anti-thymocyte globulin
ATO	Arsenic trioxide
B6	C57BL/6
BCR	B cell receptor
BMT	Bone marrow transplant
BrdU	5-bromo-2-deoxyuridine
BSA	Bovine serum albumin
BSO	Buthionine sulfoxide
CBR	Central benzodiazepine receptor
CD	Cluster of differentiation
CDK	Cyclin-dependent kinases
CFSE	Carboxyfluorescein diacetate succinimidyl ester
CMV	Cytomegalovirus
CoA	Coenzyme A
ConA	Concanavalin A
COX	Cyclooxygenase
CPT	Carnitine palmitoyltransferase
CRAC	Ca^{2+} release-activated Ca^{2+}
CTL	Cytotoxic T lymphocyte
Cu,Zn-SOD	Copper, Zinc superoxide dismutase
cyt C	Cytochrome C

DAG	Diacylglyceride
DC	Dendritic cell
DCF	Dichlorofluorescein
DHAP	Dihydroxyacetone phosphate
DHE	Dihydroethidium
DHEA	Dehydroepiandrosterone
dsDNA	Double-stranded DNA
DTH	Delayed-type hypersensitivity
EAE	Experimental autoimmune encephalitis
EC_{50}	Effective concentration that produces a response in 50% of cells
ECP	Extracorporeal photopheresis
ERK	Extracellular signal-regulated kinase
ETC	Electron transport chain
F1	B6D2F1
F6P	Fructose-6-phosphate
FAD	Flavin adenine dinucleotide
FAO	Fatty acid oxidation
FASL	FAS ligand
FATP	Fatty acid transport proteins
FBP	Fructose-1,6-bisphosphate
FBS	Fetal bovine serum
FCCP	Carbonylcyanide-p-trifluoromethoxyphenylhydrazone

FDG	2-[^{18}F]-Fluoro-2-deoxy-D-glucose
FMN	Flavin mononucleotide
FSC	Forward light scatter
G6P	Glucose-6-phosphate
G6PDH	Glucose-6-phosphate dehydrogenase
GABA	γ-aminobutyric acid
GAP	Glyceraldehydes-3-phosphate
GAPDH	GAP dehydrogenase
GC	Glucocorticoid
G-CSF	Granulocyte-colony stimulating factor
GLUT	Glucose transporter
GSH	Glutathione (reduced)
GSSG	Glutathione (oxidized)
GVHD	Graft-versus-host disease
H_2O_2	Hydrogen peroxide
HIF	Hypoxia-inducible factor
HK	Hexokinase
HSC	Hematopoietic stem cell
HSCT	Hematopoietic stem cell transplant
HSV	Herpes simplex virus
IDH	Isocitrate dehydrogenase
IFN	Interferon
IL	Interleukin

IP_3	Inositol-1,4,5-triphosphate
KLH	Keyhole limpet hemocyanin
LAT	Linker-of-activated T cells
LCMV	Lymphocytic choriomeningitis virus
LDH	Lactate dehydrogenase
LPS	Lipopolysaccharide
LSK^+	Lin^- c-Kit^+ Sca-1^+
Ly5.2	B6-Ly5.2
MAPK	Mitogen-activated protein kinase
MCT	Monocarboxylate transporter
MCT	Monocarboxylate transporter
MDA	Malondialdehyde
MDH	Malate dehydrogenase
MDRP	Multidrug resistance protein
MEF	Mouse embryonic fibroblast
MHC	Major histocompatability complex
MHV	Mouse γ-herpes virus
miHA	Minor histocompatibility antigen
MMF	Mycophenolate mofetil
MnSOD	Manganese superoxide dismutase
MnTBAP	Manganese(III)*meso*-tetrakis(4-benzoic acid) porphyrin
NAC	N-acetyl cysteine

NF-κB	Nuclear factor kappa-light-chain-enhancer of activated B cells
NFAT	Nuclear factor of activated T cells
NZB/W	F1 offspring of NZB and NZW mice
O_2^-	Superoxide anion
O_2	Oxygen
$OH^\bullet$	Hydroxyl radical
OSCP	Oligomycin sensitivity-conferring protein
OXPHOS	Oxidative phosphorylation
PBMCs	Peripheral blood mononuclear cells
PBR	Peripheral benzodiazepine receptor
PC	Pyruvate carboxylase
PDH	Pyruvate dehydrogenase
PE	Phycoerythrin
PEP	Phosphoenolpyruvate
PET	Positron emission tomography
PFK	Phosphofructokinase
PGI	Phosphoglucose isomerase
PGK	Phosphoglycerate kinase
PGM	phosphoglycerate mutase
PH	Pleckstrin homology
PHA	Phytohemagglutinin
PHA	Phytohemagglutinin

PI3-K	Phosphatidylinositol-3-kinase
PK	Pyruvate kinase
PKCθ	Protein kinase C-θ
PLCγ1	Phospholipase-C-γ 1
PMA	Phorbyl 12-myristate 13-acetate
PPC	pentose phosphate cycle
PTEN	Phosphatase and tensin homolog deleted on chromosome ten
PWM	Pokeweek mitogen
Q	Ubiquinone
$QH^{\cdot}$	Ubisemiquinone
QH_2	Ubiquinol
R5P	Ribose-5-phosphate
RA	Rheumatoid arthritis
RBC	Red blood cell
ROS	Reactive oxygen species
SCID	Severe-combined-immunodeficient
SDH	Succinate dehydrogenase
SLE	Systemic lupus erythematosus
SLP-76	SH2 domain containing leukocyte protein of 76kDa
SMP	Submitochondrial particle
SOD	Superoxide dismutase
STAT	Signal transducer and activator of transcription

TAC	Total antioxidant capacity
TBI	Total body irradiation
TCA	Tricarboxylic acid
TCR	T cell receptor
Th	T helper
Th_1	T helper type 1
Th_{17}	T helper type 17
Th_2	T helper type 2
Thy1.1	B6-Thy1.1
TIM	Triose phosphate isomerase
TLR	Toll-like receptor
TMRM	Tetramethyrhodamine
TNF	Tumor necrosis factor
Treg	Regulatory T cell
TSC	Tuberous sclerosis complex
TUNEL	Terminal deoxynucleotidyl transferase nick end labeling
U-^{13}C-Glucose	Uniformly labeled ^{13}C-glucose
WT	Wild type
X5P	Xylulose-5-phosphate
ZAP-70	ζ-chain-associated protein of 70 kDA

ABSTRACT

In diseases such as lupus or graft-versus-host disease (GVHD), lymphocytes react against self- or allo-antigen and mediate tissue damage. Current treatments for such diseases rely on non-specific immunosuppression and lead to opportunistic infections. Disease-causing lymphocytes perform numerous energetically demanding processes including proliferation and cytokine synthesis. While activated lymphocytes primarily utilize glycolysis *in vitro*, little is known regarding the bioenergetics of disease-causing lymphocytes *in vivo*. Understanding the metabolic pathways used by disease-causing lymphocytes could provide novel therapeutic targets that allow for selective immunomodulation. As such, the goal of this research is to characterize the pathways of cellular metabolism used by pathogenic lymphocytes and to exploit these pathways to treat disease.

Splenocytes from NZB/W mice with lupus up-regulate the oxidation of glucose rather than its conversion to lactate. This oxidative phenotype is distinct from acutely-activated T cells, which produce lactate at high rates. However, chronically-stimulated T cells have low rates of lactate production, suggesting that a reliance on oxidative metabolism could be a consequence of chronic stimulation.

In the setting of unirradiated GVHD, alloreactive donor T cells up-regulate OXPHOS but have low rates of glycolysis. This bioenergetic phenotype contrasts with control-stimulated T cells and proliferating bone marrow cells, which primarily up-regulate glycolysis. The oxidative phenotype of alloreactive donor T cells is associated with an increased mitochondrial membrane potential ($\Delta\psi_m$), increased levels of superoxide (O_2^-) and depleted antioxidants. These bioenergetic abnormalities suggest that GVHD-causing T cells could be sensitive to therapeutic agents that modulate the OXPHOS pathway or induce ROS-dependent apoptosis.

Bz-423 is a novel therapeutic that modulates the mitochondrial F_1F_o-ATPase, hyperpolarizes $\Delta\psi_m$, and induces O_2^--dependent apoptosis. We show that Bz-423 induces $\Delta\psi_m$ hyperpolarization, O_2^- production and apoptosis in alloreactive donor T cells *in vivo*. However, Bz-423 does not affect unstimulated T cells or proliferating cells in the bone marrow, which have low rates of OXPHOS and intact antioxidants. Bz-423 treatment reduces tissue damage and mortality in a model of nonirradiated GVHD, but does not inhibit immune reconstitution in fully irradiated syngeneic transplants. Hence, differences in cellular bioenergetics allow Bz-423 to selectively kill GVHD-causing lymphocytes without inducing non-specific immunosuppression.

CHAPTER 1

INTRODUCTION

Overview of the immune system. The immune system is a collection of specialized cells and molecules that protects an organism from foreign pathogens. In jawed vertebrates, the immune system has two components, termed the adaptive and innate immune systems (1, 2).

The adaptive immune system involves the recognition of specific molecules, which are known as antigens (1). In the context of an infection, antigens are often pathogen-derived peptides or polysaccharides. Specialized white blood cells, called B and T lymphocytes, recognize antigens using antigen receptors called the B cell receptor (BCR) and T cell receptor (TCR) (1). Each lymphocyte expresses an antigen receptor specific for a single antigen. When a lymphocyte encounters its cognate antigen, it becomes activated, meaning that it divides and differentiates into numerous progeny called clones, all of which recognize the same antigen and, if it is foreign, can aid in its clearance (Figure 1.1) (3). Differentiated lymphocytes that have acquired functions to aid in the immune response are termed effector cells.

In order for the adaptive immune response to be effective, the repertoire of lymphocyte antigen receptors must be sufficiently large so as to recognize the wide variety of pathogen-associated antigens. Indeed, on the order of 10^{15}

different T cell receptors can be theoretically generated (4, 5), while approximately 2 x 10^6 and 2.5 x 10^7 distinct T cell clones are estimated to exist in mice and humans, respectively (5-7). Following the expansion of lymphocyte clones and elimination of antigen, the immune response ceases and most effector cells die (8-12). However, some antigen-specific lymphocytes persist as memory cells, which can quickly mount an immune response upon reintroduction of antigen (13).

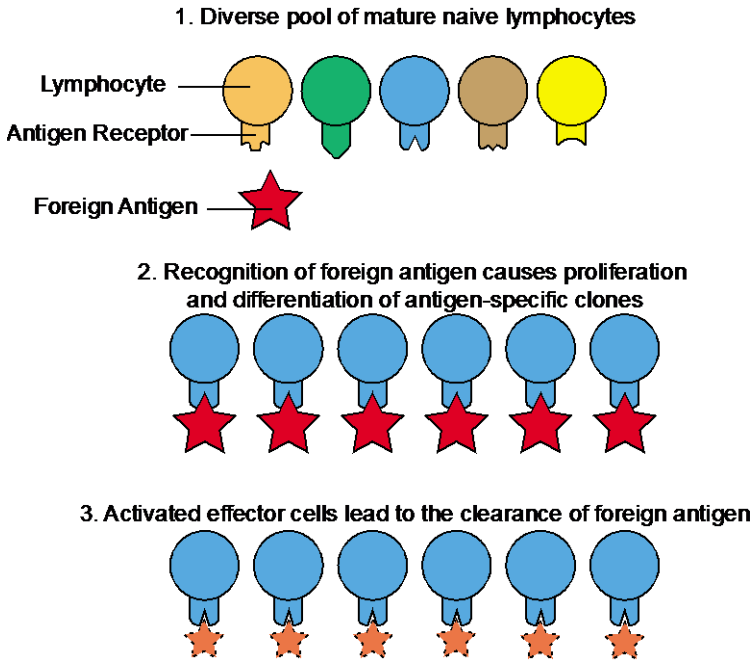

Figure 1.1. Antigen recognition and the adaptive immune response. (1) Mice and humans are populated by a diverse array of naïve lymphocytes that have not been stimulated by antigen. (2) Naïve lymphocytes that recognize foreign antigen begin to divide and give rise to a clonal population effector lymphocytes, all of which recognize the same antigen. (3) Effector lymphocytes eliminate the foreign antigen, and the immune response ceases. However, some effector lymphocytes differentiate into long-lived memory cells, which can respond quickly upon reintroduction of specific antigen. Adapted from (1).

Effector B cells are called plasma cells, and their primary function is antibody production (Figure 1.2) (14). Antibodies are a secreted form of the B cell receptor, which can bind to antigen (1). The binding of an antibody to antigen can have several consequences, depending on the nature of the antigen. Antibodies can neutralize soluble toxins and can coat the cell surface of bacteria that express antigen (1). This coating process is termed opsinization, and it can induce phagocytic cells to engulf bacteria or the complement system to lyse bacteria (1). Phagocytosis and the complement system are discussed further under innate immunity.

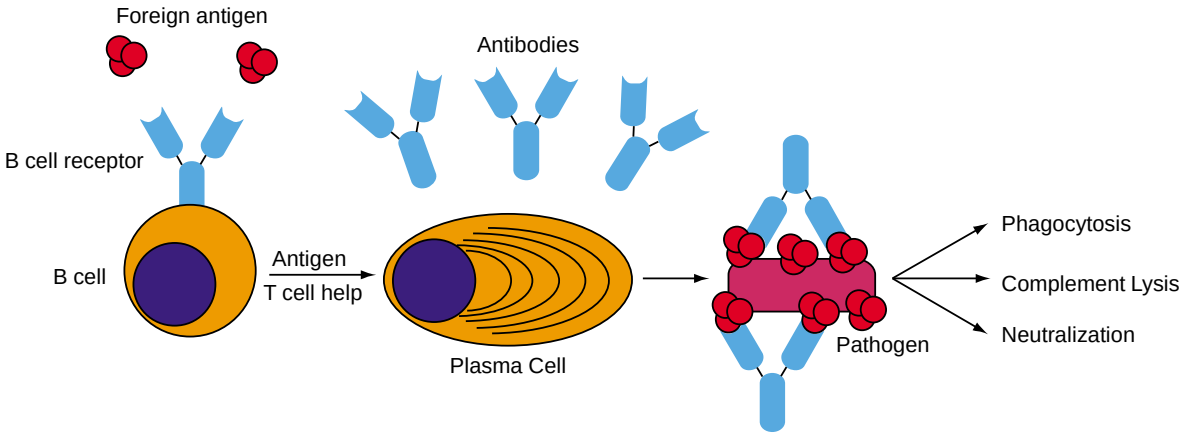

Figure 1.2. The production of antibodies by B cells. B cells recognize foreign antigen through their B cell receptors. Antigen-stimulation through the BCR, coupled with help from T cells causes B cells to differentiate into plasma cells, which produce large amount of secreted antibodies that recognize the stimulatory antigen. Antibodies coat the infectious pathogens leading to their clearance by phagocytosis or complement-mediated lysis. Alternatively, antibodies can bind to and neutralize foreign toxins. From (1).

The stimulation of T cells requires that antigen be bound to an accessory cell, termed an antigen presenting cell (APC, discussed below). There are two major classes of T cells, termed $CD4^+$ and $CD8^+$ based on the cell surface expression of the CD4 and CD8 glycoproteins (1). Effector $CD8^+$ cells express cytotoxic molecules that can kill infected target cells (Figure 1.3) (15). These cytotoxic molecules include FASL, which binds to cellular death receptors and induce apoptosis in target cells (15). $CD8^+$ T cells can also express perforin, which creates pores in target cells, and granzyme B, which passes through those pores and kills target cells by cleaving intracellular proteins and inducing apoptosis (16).

The effector functions of $CD4^+$ T cells primarily involve the synthesis of pro-inflammatory signaling molecules, termed cytokines (Figure 1.3) (17). Effector $CD4^+$ cells are termed helper T (Th) cells, because they help augment the activity of other immune cells. $CD4^+$ T cells can differentiate into several different types of helper T cells, each of which synthesizes different cytokines. Th type 1 (Th_1) $CD4^+$ T cells produce the cytokine IFN-γ, which promotes the killing of infected cells by phagocytes and $CD8^+$ T cells (18). The production of IL-4 by Th_2 $CD4^+$ T cells promotes antibody production by B cells (17). Activated $CD4^+$ T cells also express the cell surface protein CD40L, which stimulates B cell antibody production by signaling through CD40 on the B cell surface (19). Several other types of effector $CD4^+$ cells exist. Regulatory T cells (Tregs) dampen immune responses and are characterized by the expression of the transcription factor FoxP3. Finally, Th_{17} cells produce the cytokine IL-17 and

have recently been implicated in the clearance of pathogens such as tuberculosis (20), as well as the development of autoimmune diseases such as rheumatoid arthritis (21) and multiple sclerosis (22).

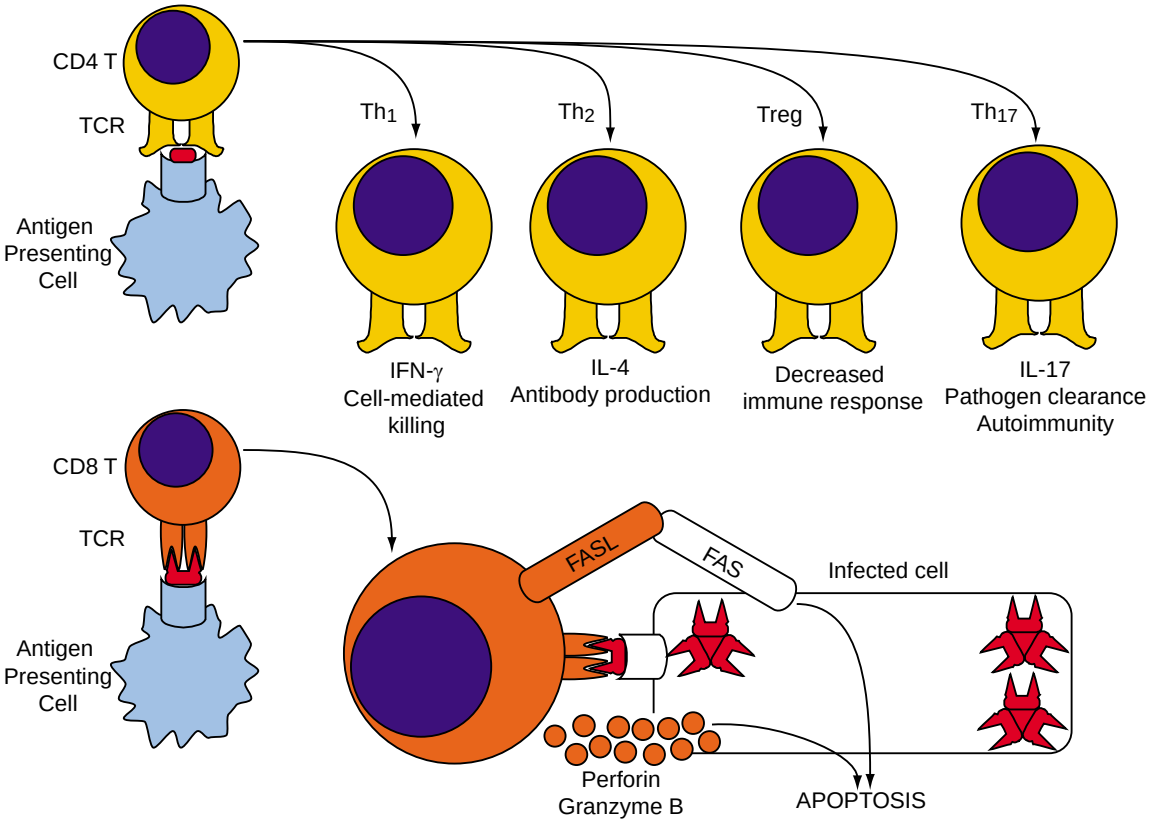

Figure 1.3. Effector functions of T cells. $CD4^+$ T cells (yellow) are stimulated by antigen (red) in the context of antigen presenting cells (blue). Depending on the environment at the time of stimulation, $CD4^+$ T cells can develop into Th_1, Th_2, Treg, or T_h 17 cells, which aid in various types of immune responses. $CD8^+$ T cells (orange) are stimulated by antigen (red) in the context of antigen presenting cells (blue). $CD8^+$ T cells differentiate into cytotoxic T cells, which express FASL, perforin and granzyme B. They can migrate to infected tissues and kill infected cells. Adapted from (1).

T cells can only recognize antigen when it is presented by cell surface proteins called the major histocompatability complex (MHC) (1). There are two classes of MHC, termed class I and class II (Figure 1.4). Class II MHC molecules are primarily expressed by professional APCs (dendritic cells, macrophages and B cells), which sample the extracellular environment and present these peptides to $CD4^+$ T cells (23). Class I MHC molecules are expressed on all nucleated cells and present intracellular antigen to $CD8^+$ T cells, although extracellular antigen can also be presented by class I MHC molecules in a process termed cross presentation (24). The expression of class I MHC on all nucleated cells allows cytotoxic $CD8^+$ T cells to recognize and kill infected cells, even if those cells are not professional APCs (1).

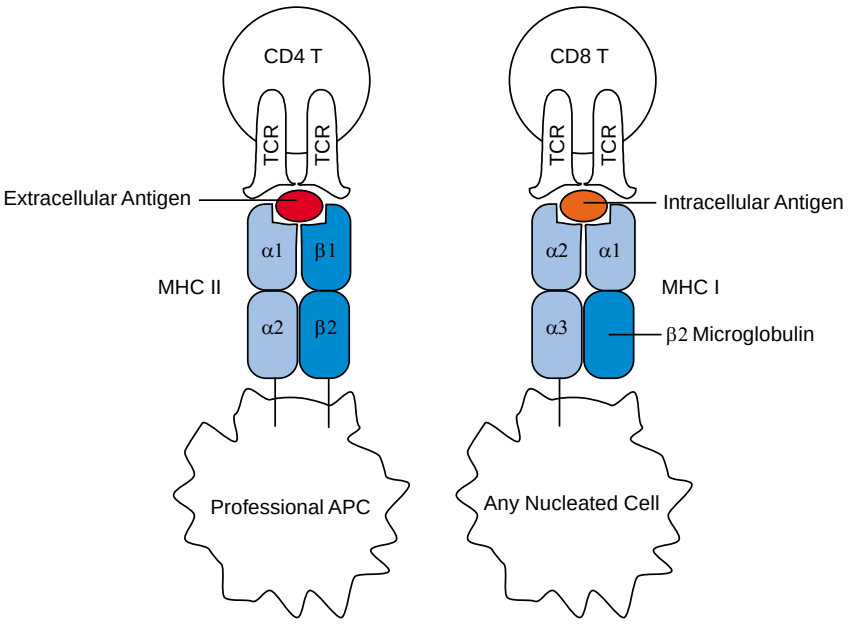

Figure 1.4. Antigen presentation to CD4 and CD8 T cells. CD4 T cells recognize antigen in the context of class II MHC expressed on professional APCs. CD8 T cells recognize antigen in the context class I MHC, which is expressed by all nucleated cells. (23, 24)

In contrast to the adaptive immune system, the innate immune system broadly protects against pathogens in an antigen-independent fashion (25). The first line of innate defense against pathogens is the epithelium of the skin, gut and lung, which serves as a physical barrier between the host and the outside environment (1). Once a pathogen enters a tissue, several cell types cooperate to aid in its removal. For example, macrophages are phagocytic cells that reside in connective tissues, the lung, the liver and the spleen (26). Macrophages express receptors that recognize molecular patterns on the surface of pathogens, which allows them to preferentially engulf pathogens rather than bystander self-tissue (27). For example, the polysaccharides frequently present in bacterial capsules are recognized by the mannose receptor on macrophages (28). Neutrophils are another type of phagocytic cell that quickly migrate from the blood to sites of infection and engulf pathogens (29, 30).

The innate immune system also contains several non-cellular components, including the complement system (31). The complement system is a set of soluble plasma proteins that can coat pathogens, leading to their direct lysis and the recruitment of phagocytes (1). The binding of the complement system to pathogens is stimulated either by the presence of specific molecular patterns on the pathogen surface, or the opsinization of the pathogen with antibodies (31).

Dendritic cells (DCs) function to link the innate and adaptive immune responses (Figure 1.5) (1). Immature DCs constantly phagocytose material at peripheral tissues such as the skin and the gut, and, after internally processing

this material, present it on their cell surface (1). Because of this activity, DCs are termed professional APCs. Macrophages and B cells can also function as professional APCs (1). Thus, the encounter of DC and pathogen leads to the presentation of pathogen-derived antigen on the surface of DCs (32). DCs also express molecules called Toll-like receptors (TLRs), which bind to common pathogen-derived molecules, such as bacterial lipopolysaccharide (LPS) and viral DNA (27). Signaling through TLRs causes DCs to undergo several changes known as “maturation” (1). These changes include the migration of DCs from peripheral tissue to lymphoid organs like the lymph nodes (LNs) or spleen (33). The DC maturation process also involves the up-regulation of important cell-surface stimulatory molecules such as CD80 and CD86 (27).

Once in the lymph node, DCs interact with T cells (1). If the TCR of a T cell recognizes the antigen presented by the DC, a signal passes through the TCR to stimulate the T cell (1). However, this signal by itself is insufficient to fully activate T cells (34). Mature DCs provide a second signal to T cells by binding CD80 or CD86 to the CD28 receptor on T cells (27). This second signal is termed costimulation. After receiving these two signals, activated T cells, divide, differentiate and can migrate to the site of infection. Because the expression of CD80 and CD86 is dependent on the exposure of DCs to pathogen-associated molecules, the second signal only comes from DCs bearing pathogen-related antigens (32). Thus, DCs bearing antigens derived from self-tissue (self-

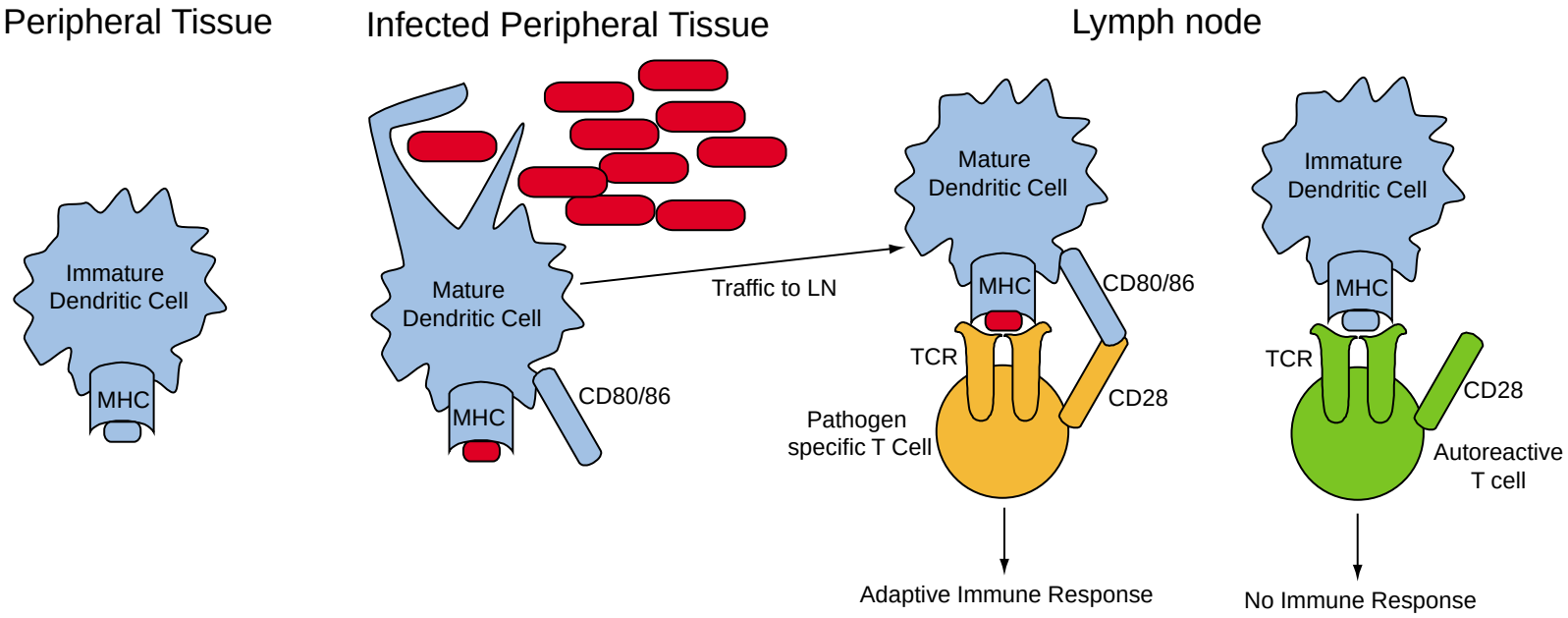

Figure 1.5. Dendritic cells bridge the innate and adaptive immune responses and limit autoreactivity. In the periphery, dendritic cells nonspecifically phagocytose and present processed antigens. In the absence of pathogens, these antigens are primarily from self-tissues (blue). When a tissue is infected, DCs phagocytose the pathogen and present its antigens on their cell surface (red). Pathogen-associated molecules activate the DC, causing it to migrate to the lymph node and increase the expression of costimulatory molecules such as CD80 and CD86. At the LN, DCs activate pathogen-specific lymphocytes by signaling through both the antigen receptor and through costimulatory interactions. DCs presenting self-antigen can also be found at LNs. However, these DCs have low levels of costimulatory molecules, which prevents the activation of potentially autoreactive lymphocytes. From (1)

antigens) have low expression of CD80 and CD86, which prevents potentially autoreactive T cells from inappropriately mediating immune responses (35, 36).

The cells of the immune system develop in the bone marrow from pluripotent hematopoietic stem cells (HSCs) (37). While B cells and the cells of innate immune system fully mature in the bone marrow, this is not the case for T cells (38). Following their formation in the bone marrow, T cell precursors migrate to the thymus, where they complete their development (39). The maturation of T cells in the thymus involves two steps that select for mature T cells capable of recognizing foreign antigens on APCs, but unlikely to recognize self antigens. The first selection process is termed positive selection, and it ensures that mature T cells contain a TCR that can bind to MHC molecules (40). If developing T cells are unable to interact with MHC molecules expressed on thymic epithelial cells, they die by neglect (41).

While the T cells that survive positive selection can recognize self-MHC molecules, many of these cells can also recognize self-antigen (40, 42). If these cells escaped the thymus, they would be predisposed to mount immune responses against self-tissue and might cause autoimmune diseases. The second selection, termed negative selection, kills many of these autoreactive T cells (42). Because the antigens found in the thymus are nearly all self-derived, T cells that *strongly* recognize antigen-MHC undergo apoptosis (42). Together, positive and negative selection function to minimize the number of non-reactive or autoreactive T cells present in the periphery.

Although positive and negative selection function to limit the number of autoreactive T cells in the periphery, these mechanisms are not perfect. In many diseases, such as rheumatoid arthritis, multiple sclerosis and systemic lupus erythematosus (SLE), B and T cells inappropriately respond to self-antigen, proliferate, differentiate into effector cells and cause tissue damage (43-45). The pathogenesis of SLE is covered in greater detail in Chapter 2.

Another type of lymphocyte-mediated disease occurs in the setting of transplantation. When foreign tissue is transplanted into a recipient, the recipient immune system mounts a response to it, as if it were a foreign pathogen (46). This response is called graft rejection. In the setting of a bone marrow transplant, it is the immune system, rather than peripheral tissue that is transplanted. In this setting, the transplanted immune system can recognize the host as “foreign” and mount an immune response, called graft-versus-host disease (GVHD) (47, 48). GVHD is covered in greater detail in Chapter 3.

Overview of lymphocyte glucose metabolism. Cells use glucose as a fuel source for a variety of purposes. The breakdown of glucose can provide ATP through both O_2-consuming and O_2-independent processes (49). For example, the conversion of glucose to pyruvate generates two molecules of ATP in an O_2-independent fashion (49). Pyruvate can either be secreted from cells as lactate, or enter the TCA cycle to generate ATP in an O_2-dependent fashion (49). Additionally, the metabolism of glucose by the pentose phosphate cycle (PPC), provides ribose molecules for nucleic acid synthesis and NADPH, which is an electron donor used for biomolecule synthesis and glutathione regeneration (50,

51). Finally, the breakdown of glucose can provide a carbon source for the synthesis of cellular fatty acids (52, 53). The principal enzymes involved in glucose metabolism are discussed below, with a particular emphasis placed on their expression and regulation in activated T cells and peripheral blood mononuclear cells (PBMCs) (Figure 1.6).

Cells import glucose according to its concentration gradient using facilitative glucose transporters (54). There are 14 different glucose transporters currently identified (GLUT1-14), each of which contains 12 transmembrane α-helical regions that form a central channel through which glucose passes (54-57). The best characterized glucose transporters are GLUT1-GLUT4, which are collectively termed class I glucose transporters. These glucose transporters vary based on their tissue distribution and their affinity for glucose (Table 1.1).

Table 1.1 Selected glucose transporters, their tissue distribution and K_m. From (54, 57).

	Primary Tissue	**K_m**
GLUT1	Ubiquitous	5 mM
GLUT2	Intestine, kidney, liver, pancreatic β cells	11 mM
GLUT3	Neurons	1 mM
GLUT4	Muscle and apidopse (insulin sensitive)	5 mM

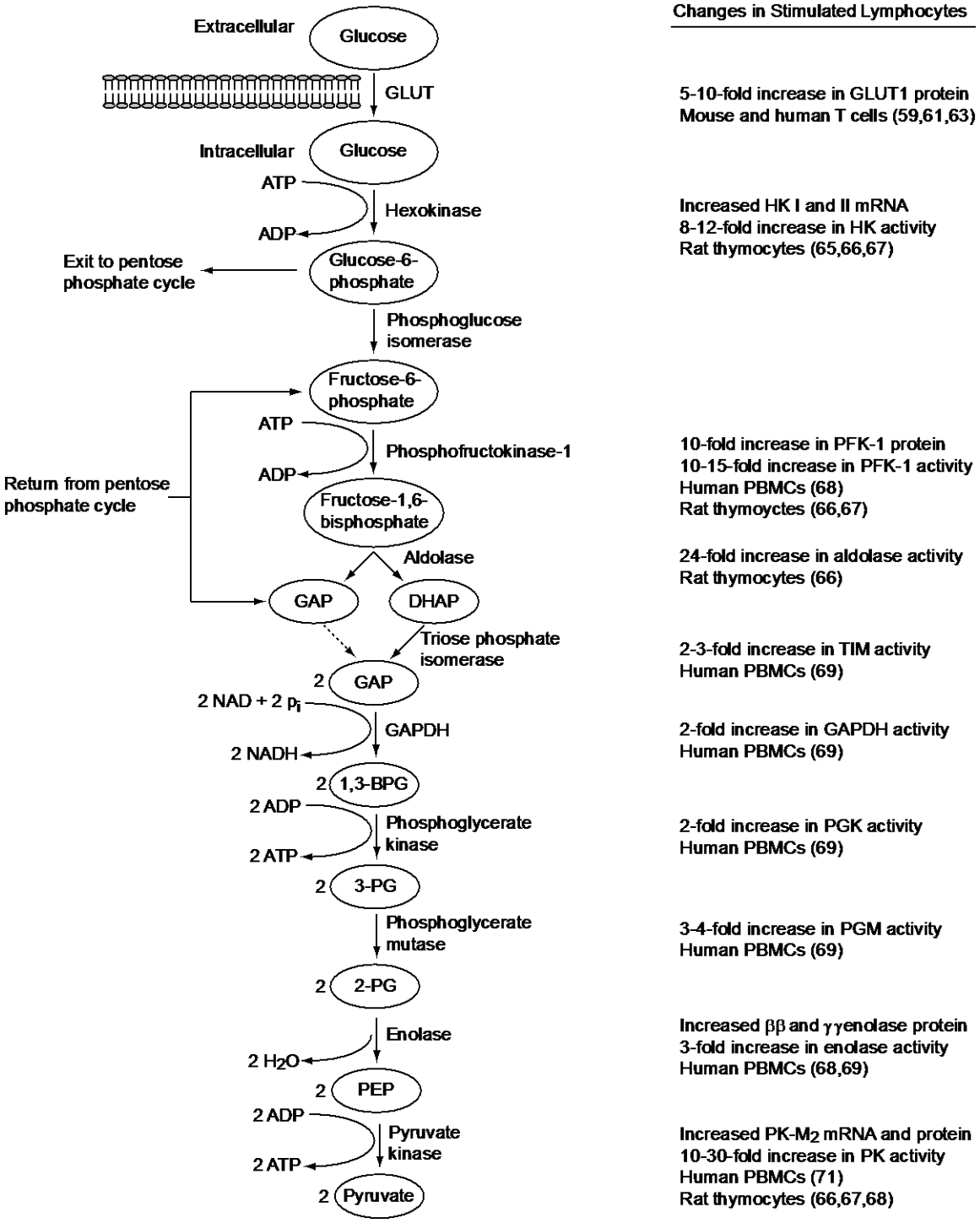

Figure 1.6. Reaction of glycolysis and their regulation in stimulated lymphocytes. Glycolysis proceeds along the pathway at left (49). Indicated lymphocyte populations were stimulated with agonistic antibodies or mitogens (58-67). Further details are provided in the text.

The major glucose transporter for lymphocytes is GLUT1 (58, 59, 68, 69), however GLUT3 expression has also been documented in human lymphocytes (60, 70). There is conflicting data regarding the expression of GLUT2 and the insulin-regulated GLUT4 in lymphocytes (60, 70, 71). For example, a microarray analysis detected GLUT4 transcripts in both human $CD4^+$ and $CD8^+$ T cells (71). However, RT-PCR analysis of human lymphocytes (70) and western blot analysis of human T cells (60) failed to detect evidence of GLUT4.

The expression of GLUT1 is an important regulator of cellular glucose metabolism in lymphocytes. Indeed, resting T cells that overexpress GLUT1 take up 5-fold more glucose than WT T cells (58). Several studies have addressed the effects of T cell stimulation on glucose transporter expression. Stimulation with anti-CD3 and anti-CD28 antibodies increases GLUT1 levels by 5-10-fold in both mouse and human $CD4^+$ T cells (58, 59). Similar results were observed when human T cells were stimulated with the mitogen phytohemagglutinin (PHA) (60). While PHA stimulation does not affect GLUT2 levels in lymphocytes (60), there is disagreement regarding the effects of stimulation on GLUT3. One study suggested that PHA stimulation of human lymphocytes increased GLUT3 levels 3-4-fold (70), while another suggested that PHA stimulation *decreased* GLUT3 expression (60). While the PHA concentrations used in these studies were similar (5-10 μg/ml), this discrepancy could be due to the different detection antibodies used (60, 70)

Once glucose is inside cells, hexokinase (HK) catalyzes the ATP-dependent phosphorylation of glucose to glucose-6-phosphate (G6P) (49).

Conversion to G6P traps glucose-derived carbons inside the cell and decreases intracellular [glucose], thereby maintaining the concentration gradient that drives glucose uptake (72). There are four different isozymes of HK (HK I-IV), each encoded by a separate gene (72). HK I and II are ubiquitously expressed in mammals, while HK III is expressed primarily in the liver and kidney (73). HK IV is expressed in hepatocytes and pancreatic β cells (72, 73). There are several modes by which HK activity is regulated. HK I-III, but not HK IV, are inhibited by their product G6P (72, 73). Additionally, insulin stimulates HK II activity in muscle and adipose (72, 73). On a transcriptional level, HK I and II mRNA are induced during hypoxia by the transcription factor hypoxia-inducible factor-1α (HIF-1α) (74).

T cells express HK I and II, and T cell stimulation increases HK activity. Indeed, expression of constitutively active AKT increases HK activity by 50% in non transformed lymphoid FL5.12 cells (75). Additionally, stimulation with the cytokine IL-7 increases HK II mRNA 2-3-fold in primary mouse T cells (76). HK activity also increases following T cell stimulation through the TCR. Both HK I and HK II mRNA increase 24-48 h after the stimulation of rat thymocytes with concanavalin A (conA) (61). Consistent with these results, two separate studies have shown that thymocyte HK activity increases 8-12-fold following conA stimulation (62, 63).

G6P can either enter the PPD (Figure 1.7) or continue along glycolysis. The entry of G6P into the PPC is catalyzed by glucose-6-phosphate dehydrogenase (G6PDH) (77). G6PDH and the subsequent PPC enzyme 6-

phosphogluconate dehydrogenase (6PGDH) convert G6P into ribulose-5-phosphate, thereby generating 1 molecule of CO_2 and 2 molecules of NADPH (49). Production of NAPDH through the PPC is required for generation of reduced glutathione and the synthesis of fatty acids (50, 51, 78). Ribulose-5-phosphate is then converted into xylulose-5-phosphate (X5P) or ribose-5-phosphate (R5P), which can exit the PPC and be used for nucleotide synthesis. Alternatively, two molecules of X5P and a single R5P can undergo reactions with transketolase and transaldolase, which generates 2 molecules of fructose-6-phosphate (F6P) and a single molecule of glyceraldehydes-3-phosphate (GAP) (49). Because both F6P and GAP are intermediates in the glycolytic pathway, these molecules can exit the PPC and reenter glycolysis (Figure 1.7) (49).

The activity of the PPC is regulated by G6P entry at G6PHD (77). G6PDH is encoded by a single gene and is subject to both transcriptional and post-translational regulation (77). Indeed, insulin signaling can increase G6PDH gene expression in a phosphatidylinositol-3-kinase (PI3-K) dependent fashion in rat hepatocytes (79). Stimulation of rat thymocytes with conA increases PPC activity 3-fold, however this study did not specifically measure the expression or activity of G6PDH (63).

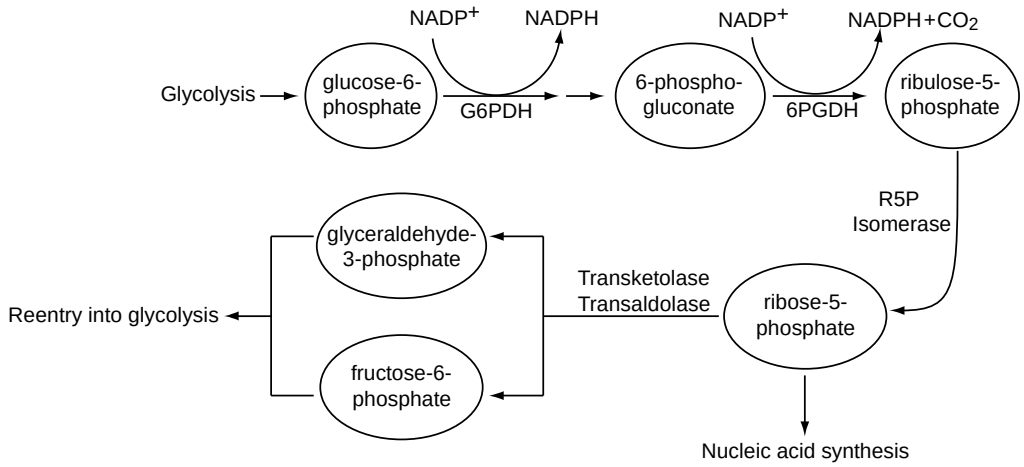

Figure 1.7. Pentose phosphate cycle. Glucose-6-phosphate enters the pentose phosphate cycle and is converted to ribulose-5-phosphate by glucose-6-phosphate dehydrogenase (GAPDH) and 6-phosphogluconate dehydrogenase (6PGDH), which generates 2 NADPH molecules and 1 CO_2. Ribulose-5-phosphate is converted to ribose-5-phosphate by ribulose-5-phosphate isomerase (R5P isomerase). Ribose-5-phosphate can be used for nucleic acid synthesis, or three ribose-5-phosphates can rearrange through the reactions of transketolase and transaldolase to form two fructose-6-phosphate molecules and one glyceraldehydes-3-phosphate, which can reenter glycolysis. From (49).

If G6P does not enter the PPC, it next reacts with phosphoglucose isomerase (PGI), which converts G6P to F6P (49). F6P reacts with phosphofructokinase-1 (PFK-1) and ATP to form fructose-1,6-bisphosphate (FBP) (49). Three separate isoenzymes of PFK-1 exist (PFK-L, -M, and –C) and are encoded by three separate genes (80). Muscle primarily expresses PFK-M and liver primarily expresses PFK-L (80, 81). Human PBMCs express all three isoenzymes of PFK, but PFK-L predominates (81).

PFK-1 is an important regulator of glycolytic flux and its activity is controlled by several mechanisms (Figure 1.8) (49). ATP allosterically inhibits

PFK-1, while it is activated by ADP, AMP and fructose-2,6-bisphosphate (F-2,6-P) (49). AKT activates PFK-1 by phosphorylating and activating PFK-2 (82). Active PFK-2 catalyzes the formation of F-2,6-P, thereby stimulating PFK-1 (82). PFK-1 is also regulated on a transcription level by HIF-1α, whose activity increases mRNA levels of PFK-L (74).

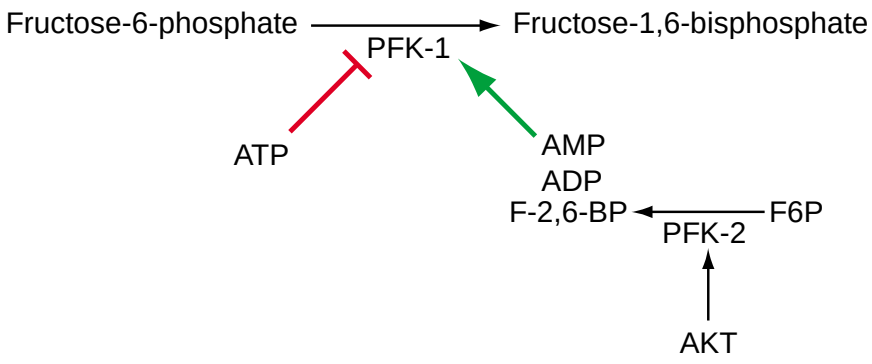

Figure 1.8 Regulation of phosphofructokinase-1. PFK-1 is inhibited allosterically by ATP and stimulated by AMP, ADP and fructose-2,6-bisphosphate (F-2,6-BP). AKT stimulates PFK-1 by phosphorylating and activating phosphofructokinase-2 (PFK-2), which catalyzes the formation of F-2,6-BP. (49, 82).

Lymphocyte stimulation also up-regulates PFK activity. For example, PFK activity increases 10-15-fold following stimulation of thymocytes with conA for 2-3 d (62, 63). Similarly, PFK-L protein levels increase 10-fold following the stimulation of human PBMCs with conA and phorbyl 12-myristate 13-acetate (PMA) for 2 d (64).

Following its formation by PFK-1, FBP is split into two 3-carbon molecules (dihydroxyacetone phosphate (DHAP) and glyceraldehydes-3-phosphate (GAP)) by aldolase (49). There are three types of aldolase, classified as aldolase A, B

and C. Aldolase A is expressed in most mammalian tissues, including muscle, liver, brain and spleen (83). Aldolase B is primarily a liver enzyme (84), while aldolase C is primarily expressed in the brain (85).

Aldolase regulation occurs primarily on a transcriptional level (86, 87). Aldolase B expression is stimulated by ingestion of carbohydrates and insulin signaling (86-88), while aldolase A and C are both induced by HIF-1α (74). The stimulation of thymocytes with conA increases aldolase activity 24-fold (62). While the specific isoforms of aldolase were not analyzed in this study (62), a separate study showed that only aldolase A is detected in conA-stimulated thymocytes (61).

While both DHAP and GAP are generated by aldolase, only GAP can continue along glycolysis (49). Triose phosphate isomerase (TIM) catalyzes the interconversion of GAP and DHAP, which allows carbons from both to continue along the glycolytic pathway. TIM is encoded by a single gene, however several isozymes have been identified based on differences in electrophoretic mobility (89-91). The functional significance of these isozymes isozymes is unclear (89-91). The catalytic activity of TIM is regulated by substrate diffusion (49, 92). TIM activity increases 2-3-fold following PBMC stimulation with PHA and pokeweed mitogen (PWM) (65), which suggests increased TIM expression in activated lymphocytes.

The next step in glycolysis is the oxidation of GAP to 1,3-bisphosphoglycerate (1,3-BPG) by GAP dehydrogenase (GAPDH). This reaction is coupled to the reduction of NAD^+ to NADH, which can be used for oxidative

ATP production or for the conversion of pyruvate to lactate (49). GAPDH is expressed at high levels by all tissues, and thus is considered a “housekeeping gene” (93). However, GAPDH can be regulated on an mRNA level (93), and its activity increases 2-fold in PBMCs stimulated with PHA and PWM (65).

Phosphoglycerate kinase (PGK) catalyzes the conversion of 1,3-BPG to 3-phosphoglycerate (3PG), which generates one molecule of ATP (49). There are two different isoforms of PGK: the ubiquitously expressed PGK-1, and the testes-specific PGK-2 (94). PGK is primarily regulated transcriptionally, and its induction is stimulated by HIF-1α (74). In PBMCs, PGK activity increases 2-fold following stimulation with PHA and PWM (65).

3PG is converted to 2-phosphoglycerate (2PG) by phosphoglycerate mutase (PGM) (49). There are two separate isozymes of PGM, termed PGM-m (muscle-derived) and PGM-b (ubiquitously expressed) (95). Active PGM exists as a dimer composed of b and m subunits. PGM-mm is expressed in skeletal muscle, PGM-mb is primarily expressed in heart, and PGM-bb is expressed in non-muscle tissues (95, 96). PGM is primarily regulated by its transcription (49). In PBMCs, PGM activity increases 3-4-fold following stimulation with PHA and PWM (65).

Enolase catalyzes the formation of phosphoenolpyruvate (PEP) from 2PG (49). Enolase function as a dimer composed of two subunits (97). There are three different isozymes of enolase (α, β, and γ), which combine to form homo- and hetero-dimers (97). The α isozyme of enolase is ubiquitously expressed, the β isozyme is expressed in muscle, and the γ isozyme is primarily expressed in

neural tissue (97). Interestingly, resting PBMCs primarily express the ββ form of enolase, and stimulation with conA and PMA increases protein leves of both ββ and γγ enolase (64). PBMC stimulation with PHA and PWM also increases the activity of enolase by 3-fold (65).

The final enzyme in glycolysis is pyruvate kinase (PK), which catalyzes the conversion of PEP into pyruvate and generates ATP (49). Four different PK isozymes exist in mammals and are classified based on their tissue distribution (98). PK-L is primarily expressed in liver (98). PK-R is expressed in red blood cells from the same gene as PK-L, however it is controlled by a distinct promoter (99). PK-M_1 is expressed by most adult tissues (100), while its splice variant PK-M_2 is expressed in embryonic tissue, proliferating cells, and tumors (98-101). PK is regulated by several mechanisms. PK is allosterically stimulated by its substrate, PEP, and by the upstream glycolytic metabolite FBP (102, 103). PK is also regulated by its quaternary structure. For example, tetrameric PK-M_2 has a high affinity for PEP, while dimeric PK-M_2 has low affinity for PEP (98, 99).

Human PBMCs and rat thymocytes primarily express the PK-M_2 isoform (66, 67). Stimulation of human PBMCs with conA and PMA increases PK-M_2 protein levels (67). Similarly, stimulating rat thymocytes with conA increases both PK-M_2 mRNA and protein (66). Consistent with these results, PK activity is increased 10-30-fold in conA-stimulated rat thymocytes compared to unstimulated controls (62, 63).

Metabolic fates of pyruvate. Once formed, pyruvate has three major metabolic fates (Figure 1.9). It can be converted to lactate by lactate

dehydrogenase (LDH) and secreted from cells through the monocarboxylate transporter (MCT) (49, 104). Alternatively, pyruvate can enter the mitochondria through reactions with pyruvate carboxylase (PC) or pyruvate dehydrogenase (PDH) (105-107).

LDH catalyzes the cytosolic conversion of pyruvate to lactate, which is coupled to the conversion of NADH to NAD^+ (49). Because NAD^+ is required for the GAPDH step of glycolysis, this O_2-independent regeneration of NAD^+ allows hypoxic cells to maintain flux through glycolysis despite the inability to convert NADH to NAD^+ in the mitochondria (49). Lactate dehydrogenase is encoded by two genes, termed *LDH-A* and *LDH-B*. Each gene encodes a separate peptide chain, termed M (muscle) and H (heart) (108, 109). Functional LDH is a homo- or heterotetramer composed of M and H peptides (109). Five isozymes of LDH exist in mammals: LDH-1, which is composed of four H peptides (H_4); LDH-2 (H_3M,); LDH-3 (H_2M_2); LDH-4 (H_1M_3); and LDH-5 (M_4) (110). These isozymes are widely expressed across tissues (108, 109), and all five are present in lymphocytes (64, 67, 111).

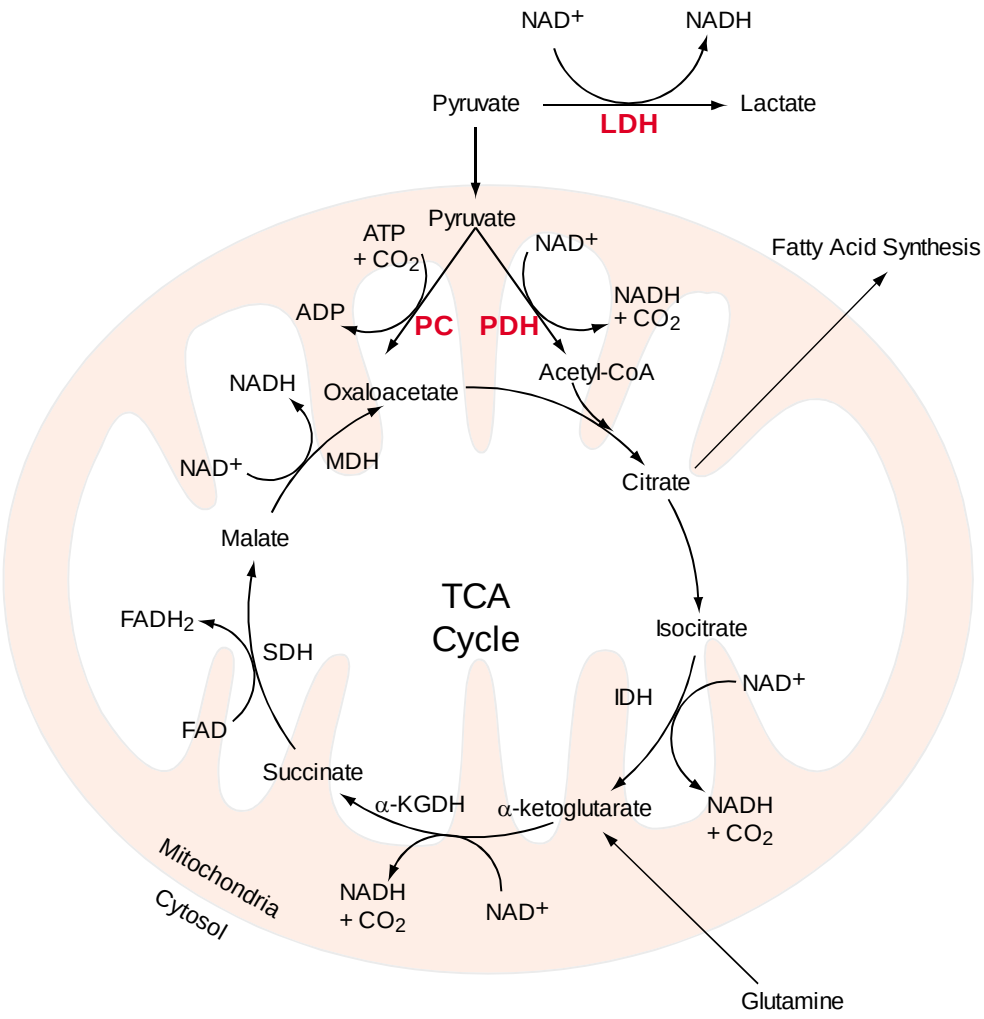

Figure 1.9. Metabolic fates of pyruvate and the TCA cycle. Lactate dehydrogenase (LDH) can convert pyruvate to lactate, which is then secreted from cells. Pyruvate can be converted into oxaloacetate by pyruvate carboxylase (PC) or acetyl-CoA by pyruvate dehydrogenase (PDH). Citrate synthase combines oxaloacetate with acetyl-CoA to form citrate. NADH is generated by isocitrate dehydrogenase (IDH), α-ketoglutarate dehydrogenase (α-KGDH), and malate dehydrogenase (MDH). $FADH_2$ is produced by succinate dehydrogenase (SDH). Carbons leave the cycle as CO_2, but intermediates can also be utilized for biomolecule synthesis. Glutamine-derived carbons enter the cycle as α-ketoglutarate. Adapted from (112, 113).

LDH activity is primarily regulated at the level of gene expression. LDH-A expression increases during hypoxia (114) through stimulation by HIF-1α (74). Importantly, the M chain of LDH has a greater affinity for lactate than the H chain. Thus, the activity an LDH isozyme will vary depending on the number of M subunits it contains (65, 109-111). Stimulation of human lymphocytes with conA and PMA preferentially induces the expression of LDH-5 (M_4) and LDH-4 (M_3H_1), but not LDH-1 (H_4) (64, 67, 111). Consistent with these results, *LDA-A* mRNA increases >10-fold following conA and PMA stimulation of human lymphocytes (111). Furthermore, stimulation of rat thymocytes with conA increases LDH activity 10-fold, and increases lactate production by 35-fold (63).

If pyruvate does not react with LDH, it can enter the mitochondria through the pyruvate transporter (115-117). Once pyruvate is inside the mitochondria, either PDH or PC can catalyze its entry into the TCA cycle, where it can be oxidized to NADH and $FADH_2$ for ATP production or exported for amino acid or fatty acid synthesis (Figure 1.9) (49, 52, 53).

PDH is a multi-enzyme complex that catalyzes the conversion of pyruvate to acetyl coenzyme A (acetyl-CoA), CO_2 and NADH (49, 105). Once converted into acetyl-coA by PDH, pyruvate-derived carbons combine with oxaloacetate and enter the TCA cycle as citrate (118). The PDH complex contains numerous copies of three separate enzymes; pyruvate dehydrogenase (E1, ~ 30 copies per complex), dihydrolipoyl transacylase (E2, ~60 copies per complex) and dihydrolipoyl dehydrogenase (E3, 6 copies per complex) (105). Each E1 subunit is a tetramer composed of 2 α and β subunits, each of which is encoded by a

separate gene (105, 119). E2 and E3 are each encoded by single genes (105). While there is an alternative isoform of E1, it is only expressed in testes (120).

PDH is regulated both by end-product inhibition by NADH and acetyl-CoA and by the phosphorylation status of E1 (Figure 1.10) (105). PDH-kinase (PDH-k) catalyzes the phosphorylation of PDH at three separate serine residues, which inactivates PDH (106). PDH-k is activated by acetyl-coA and NADH, and is inhibited by ADP, pyruvate and NAD^+ (105). The expression of PDH-k is also stimulated by the transcription factor HIF-1α (121, 122). PDH-phosphatase catalyzes the dephosphorylation PDH leading to its activation. PDH-phosphatase is stimulated by both Mg^{2+} and Ca^{2+} (105).

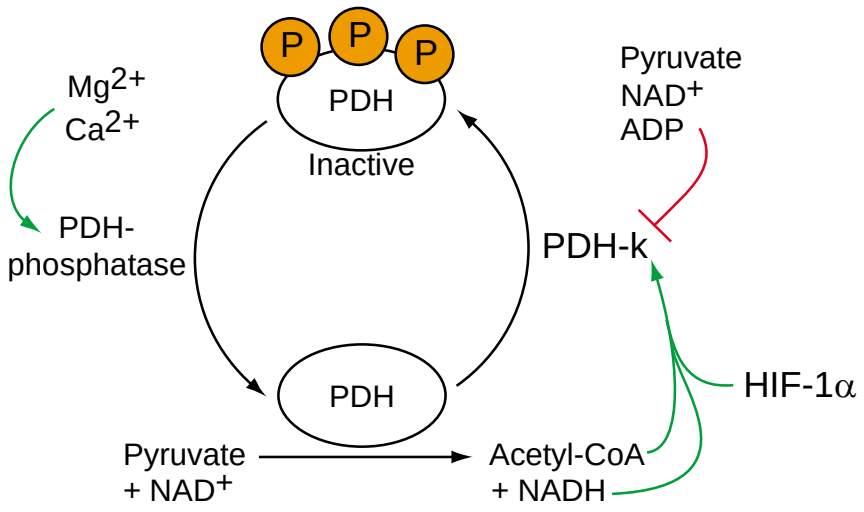

Figure 1.10. Regulation of pyruvate dehydrogenase. PDH is active in its unphosphorylated form. PDH-k dephosphorylates and inactivated PDH. PDH-K is stimulated by acetyl-CoA, NADH and its expression is stimulated by HIF-1α. PDH-K is inhibed by pyruvate, NAD^+ and ADP. PDH-phosphatase, which activates PDH, is stimulated by Ca^{2+} and Mg^{2+}. Adapted from (105).

Stimulation of lymphocytes increases the entry of pyruvate into the TCA cycle through PDH. For example, activation of bulk pig lymphocytes with conA increases PDH activity by 40% within 5 h (123). This PDH stimulation was inhibited by the addition of the Ca^{2+} chelator EGTA, which suggests that lymphocyte stimulation activates PDH-phosphatase in a Ca^{2+}-dependent fashion (123). Consistent with this observation, rat thymocytes stimulated by conA generate 3-fold more CO_2 from pyruvate than unstimulated controls (62).

PC catalyzes the conversion of pyruvate to oxaloacetate, which consumes both CO_2 and ATP (49, 107). PC is encoded by a single gene (124), and is highly expressed in tissues that synthesize glucose such as the liver and the kidney (107). Oxaloacetate synthesis by PC is important to replenish TCA cycle intermediates, which might otherwise be depleted by their utilization in such processes as amino acid synthesis, fatty acid synthesis and gluconeogenesis (107). PC activity is allosterically increased when acetyl-CoA levels are high, which indicates an increased need for TCA cycle intermediates (107, 125). Lymphocytes express PC, and stimulation of human lymphocytes with conA for 1 h increases PC activity by 50% (126).

PC and PDH both catalyze the entry of pyruvate-derived carbons into the TCA cycle (Figure 1.9). The TCA cycle is a series of enzymes that catalyzes the formation of citrate from oxaloacetate and acetyl-CoA and the oxidation of that citrate molecule into oxaloacetate. These oxidation reactions produce CO_2 as well as NADH and $FADH_2$, both of which can be used for oxidative ATP production by the mitochondrial respiratory chain (described below). While the

TCA cycle contains eight enzymes, only three are regulated: citrate synthase, which is inhibited by NADH and citrate; isocitrate dehydrogenase, which is inhibited by ATP and NADH, and stimulated by Ca^{2+} and ADP; and α-ketoglutarate dehydrogenase, which is inhibited by NADH and succinyl-CoA and stimulated by Ca^{2+} (112). In lymphocytes, the activity of the TCA cycle appears to increase following stimulation, possibly due to increased Ca^{2+} (discussed below). For example, rat splenocytes and thymocytes stimulated by conA increase glucose oxidation by 100% and 50%, respectively (62, 127). The TCA cycle can also oxidize glutamine, whose carbons enter the cycle as α-ketoglutarate (Figure 1.9). Rat thymocytes stimulated with conA increase glutamine oxidation 5-fold, again suggesting increased TCA cycle activity in activated lymphocytes (128).

The mitochondrial electron transport chain. The TCA cycle oxidizes carbon substrates and produces high-energy electron carriers NADH and $FADH_2$, but it does not generate large amounts of ATP (112). In actively respiring mitochondria, the energy contained in NADH and $FADH_2$ is used by the electron transport chain (ETC) to form a proton gradient across the inner mitochondrial gradient, and that gradient is then utilized to generate ATP (Figure 1.11).

Electrons carried by NADH or FADH enter the ETC at complex I (NADH-ubiquinone oxidoreductase) or complex II (succinate-ubiquinone oxidoreductase), respectively (49). NADH formed in the TCA cycle is oxidized by the flavin mononucleotide (FMN) located on the matrix face of complex I (Figure 1.11) (129). These electrons are passed along a series of 7 iron-sulfur (Fe-S)

clusters (130) and eventually combine with ubiquinone (Q or CoQ) to form ubiquinol (QH_2 or $CoQH_2$) (129, 131). Complex I also pumps 4 H^+ from the matrix into the intermembrane space for every 2 electrons it transports (Table 1.2) (132, 133). Electrons can also enter the respiratory chain at complex II, which catalyzes the oxidation of succinate into fumarate and transfers the electrons onto flavin adenine dinucleotide (FAD) (134). In a fashion similar to complex I, the reduced flavin of complex II passes its electrons through a series of iron-sulfur clusters leading to the reduction of Q to form QH_2 (134). However, complex II does not pump H^+ into the mitochondrial matrix (135).

Table 1.2. Reactions of the mitochondrial respiratory chain. Q and QH_2 indicate ubiquinone and ubiquinol. H_i^+ indicates a proton in the mitochondrial matrix , while H_o^+ indicates a proton in the intermembrane space. From (136).

Complex	Name	Reaction Catalyzed
I	NADH-Ubiquinone Oxidoreductase	$NADH + Q + 5H_i^+ \rightarrow NAD + QH_2 + 4H_o^+$
II	Succinate dehydrogenase	$Succinate + Q \rightarrow Fumarate + QH_2$
III	Ubiquinone-cytochrome c oxidoreductase	$QH_2 + 2cyt\ c^{3+} + Q + 2H_i^+ \rightarrow 2Q + 2cyt\ c^{2+} + 4H_o^+$
IV	Cytochrome C oxidase	$4cyt\ c^{2+} + 8H_i^+ + O_2 \rightarrow 4cyt\ c^{3+} + 4H_o^+ + 2H_2O$
V	F_1F_o-ATPase	$2\text{-}3\ H_o^+ + ADP + P_i \rightarrow 2\text{-}3\ H_i^+ + ATP$

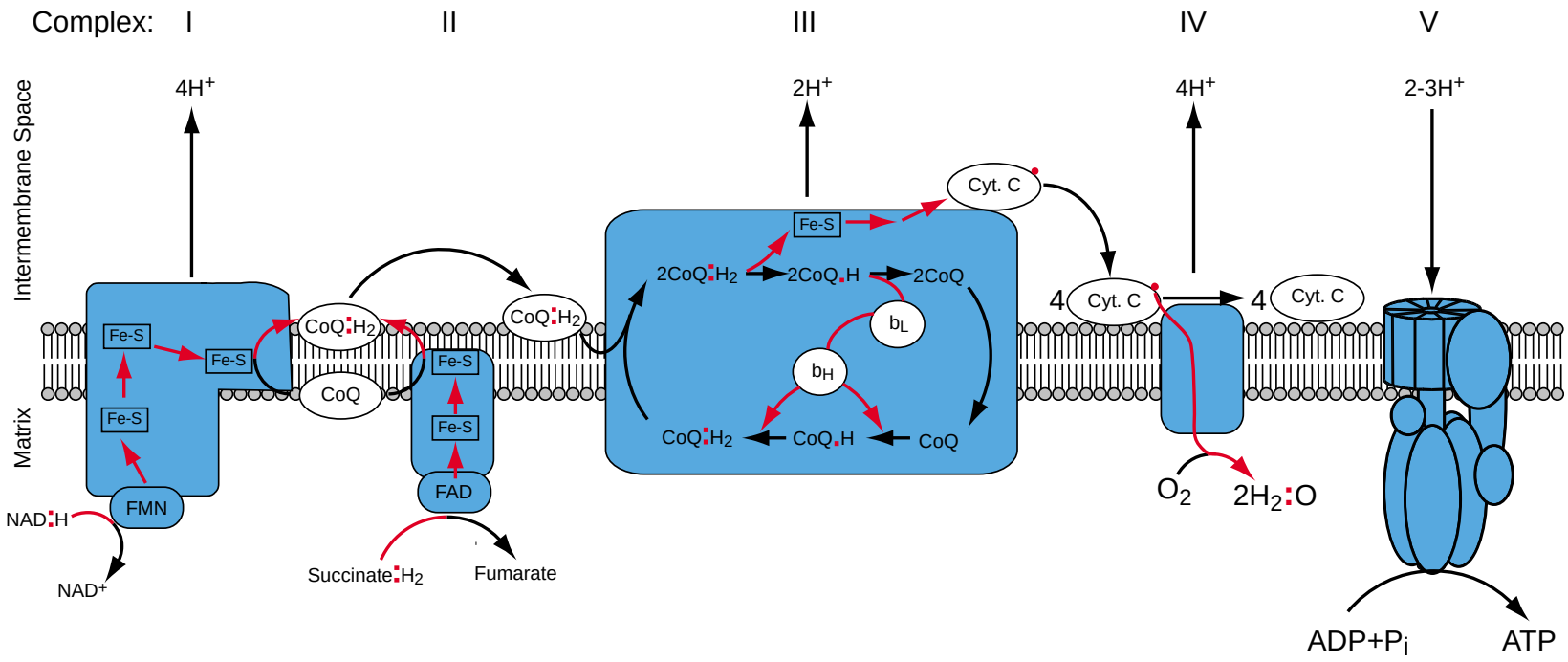

Figure 1.11. Electron transport schematic. Complexes are identified by numbers on top and the flow of electrons is indicated by red arrows. Electrons (red) enter complex I or complex II as NADH or succinate, respectively. Complex I pumps 4 protons (H^+) into the intermembrane space for each NADH. Complex I and II transfer electrons to coenzyme Q (CoQ), which migrates to complex III and transfers electrons to cytochrome c and pumps 2 H^+ for each $CoQH_2$. Reduced cytochrome c migrates to complex IV and passes its electrons to O_2, forming H_2O. Complex IV pumps 4 protons for every 4 cytochrome c oxidized. Complex V synthesizes ATP and allows H^+ to flow into the matrix, but does not transport electrons (130, 134, 135, 137-139).

Complex III (ubiquinone-cytochrome c oxidoreductase) oxidizes QH_2 formed by complex I or complex II and transfers electrons to cytochrome C, while pumping two H^+ into the intermembrane space for every 2 electrons it transports (138). Complex III accomplishes this electron transport and proton pumping through multiple one electron reactions (Figure 1.11). QH_2 first transfers a single electron to an Fe-S cluster and transfers one H^+ into the intermembrane space, thus generating the relatively unstable ubisemiquinone ($QH^{\cdot}$) (139). While the reduced Fe-S cluster passes its electron on towards cytochrome C, ubisemiquinone transfers its free electron to the heme b_L center within complex III. Heme b_L transfers its electron to heme b_H, which resides on the matrix face. Heme b_H adds 2 consecutive electrons to Q, which along with H^+ from the matrix, regenerates QH_2 (138, 139).

The final component of the electron chain is complex IV (cytochrome C oxidase). Complex IV transfers electrons from reduced cytochrome C through a copper center and several heme groups to O_2, which is reduced to H_2O and acts as the final electron acceptor of the ETC (140). For every electron transferred to O_2, a single H^+ is pumped from the matrix to the intermembrane space (141). Because the reactions catalyzed by complex IV lead to a disappearance in O_2, monitoring the consumption of O_2 is often used to assess the activity of the ETC (142, 143).

Complexes I, III and IV pump H^+ into the intermembrane space as they transfer electrons along the ETC (Figure 1.11) (129, 138, 141). This accumulation of H^+ in the intermembrane space creates an electrochemical

gradient (Δp) of 100-200 mV across the inner mitochondrial membrane (144). This gradient is composed of a small pH gradient (~30 mV in actively respiring mitochondria) and a large electric potential (~150 mV in actively respiring mitochondria), termed the mitochondrial membrane potential ($\Delta\psi_m$) (145, 146).

The electrochemical gradient generated by complexes I-IV is counteracted by H^+ flow into the mitochondrial matrix through complex V, also known as the F_1F_o-ATPase (147). Complex V consists of the transmembrane F_o domain, through which protons flow and the F_1 domain, which synthesizes ATP in the mitochondrial matrix (147). These two domains are coupled by a peripheral stalk, which contains the oligomycin sensitivity-conferring protein (OSCP) (148). As protons flow through the F_o region into the mitochondrial matrix, they cause the rotation of the central axis of the F_1 domain and catalyze the synthesis of ATP (149-153). Hence, the generation of $\Delta\psi_m$ by complexes I-IV of the mitochondrial respiratory chain is coupled to ATP production by complex V.

Mitochondrial generation of reactive oxygen species and antioxidants. While most of the O_2 consumed by the mitochondria is converted to H_2O by complex IV, approximately 0.5-3% is converted to superoxide (O_2^-). O_2^- production occurs when single electrons escape from reactive intermediates such as FMN or Fe-S clusters in complex I or ubisemiquinone in complex III and react directly with O_2 (Figure 1.12) (131, 154). O_2^- production by complex I or III increases when the half-lives of reduced reactive intermediates increase (131, 154). This phenomenon has been investigated in complex I using rotenone, a small molecule (Figure 1.12) that inhibits the passage of electrons from the

terminal Fe-S cluster of complex I to ubiquinone (155, 156). Treatment with rotenone causes an accumulation of reduced intermediates proximal to the terminal Fe-S cluster and increases reactive oxygen species (ROS) production into the mitochondrial matrix by 17-fold in actively respiring rat brain mitochondria (131, 154, 157). The site of O_2^- production by complex I is unclear, as both Fe-S clusters (158) and the FMN (157) site have been implicated.

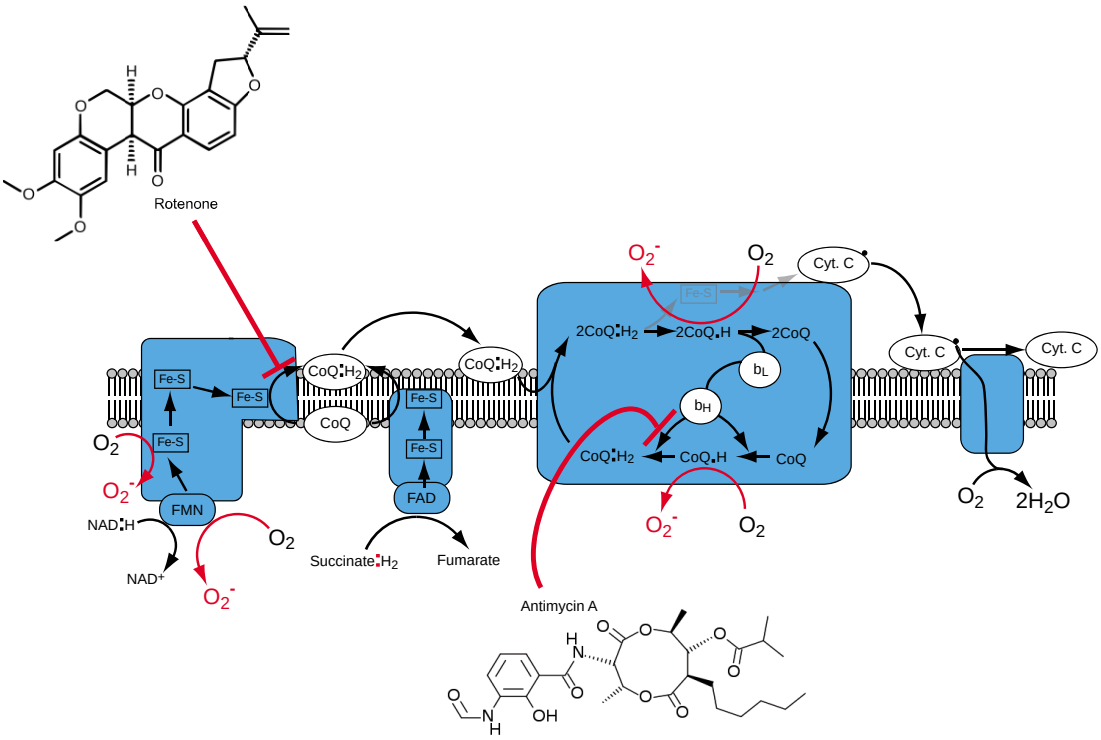

Figure 1.12. O_2^- production by the electron transport chain. O_2^- is formed by single electron reactions with O_2 occuring at complex I and III of the ETC (red arrows). At complex I, O_2 can react with either reduced FMN or iron sulfur clusters, however O_2^- is only released into the matrix. These reactions are increased by the presence of rotenone, which inhibits electron transfer to ubiquinone, thereby increasing the half lives of reduced Fe-S clusters and FMN. At complex III, O_2 reacts with ubisemiquinone (CoQH) to form O_2^-. O_2^- formed at complex III can enter either the matrix or the intermembrane space. O_2^- production at complex III increases in the presence of antimycin A, which inhibits electron transfer from cytochrome b_H to ubisemiquinone, thereby causing ubisemiquinone accumulation (131, 154-156, 159).

The other major site of ROS production in the mitochondria is complex III, which generates O_2^- when ubisemiquinone reacts with O_2 (160). Ubisemiquinone is formed on both the matrix and intermembrane faces of complex III (Figure 1.11), which suggests that complex III can produce O_2^- into both the matrix and intermembrane space (131, 154, 161, 162). Indeed, antimycin A, which inhibits electron flow from cytochrome b_H to ubisemiquinone (Figure 1.12), increases ROS production into both the matrix and intermembrane space by > 10-fold in isolated mouse mitochondria (159).

Mitochondrial ROS production also increases as $\Delta\psi_m$ increases (154). This phenomenon is thought to occur because a large $\Delta\psi_m$ disfavors additional H^+ pumping and extends the half lives of reactive single electron intermediates such as FMN and Fe-S clusters in complex I and ubisemiquinone in complex III (131, 154, 163). The increased lifetimes of these reactive intermediates increases the likelihood that electrons react with O_2 to form O_2^- rather than continuing along the ETC (131, 164-167). In rat heart mitochondria respiring on succinate, increasing $\Delta\psi_m$ by 20% increases H_2O_2 generation by 10-fold (167). In a similar system using rat brain mitochondria and NADH-linked substrates (malate + glutamate or α-ketoglutarate), a 20% change in $\Delta\psi_m$ increases H_2O_2 generation by 3-4-fold (168). In both of these studies, the initial ROS species formed was assumed to be O_2^-, which was then converted to H_2O_2 by superoxide dismutases (167, 168). This relationship between $\Delta\psi_m$ and O_2^- production helps explain why small molecules that inhibit the F_1F_oATPase and increase $\Delta\psi_m$ such

as Bz-423 (169-173), oligomycin (168, 174), PK11195 (175), and farnesol (176) also generate ROS.

Once O_2^- is formed by the mitochondria it has several possible fates (Figure 1.13) (177). O_2^- can oxidize iron present at Fe-S clusters, thereby inactivating enzymes such as aconitase that rely on Fe-S clusters for catalysis (177-179). Alternatively, O_2^- can be converted to hydrogen peroxide (H_2O_2) by a pair of enzymes termed superoxide dismutases (SODs) (177). In the cytosol and mitochondrial intermembrane space, a SOD containing copper and zinc at its active site (Cu,Zn-SOD) catalyzes the following reaction: $2O_2^- + 2\ H^+ \rightarrow O_2 + H_2O_2$ (180). A similar manganese containing-enzyme (MnSOD) catalyzes the same reaction in the mitochondria (180). The importance of these SOD enzymes is evident, as overexpression of Cu,Zn-SOD protects mice from drug-induced Parkinson's disease (181), while mice homozygous for a deletion in MnSOD die within days of birth (182).

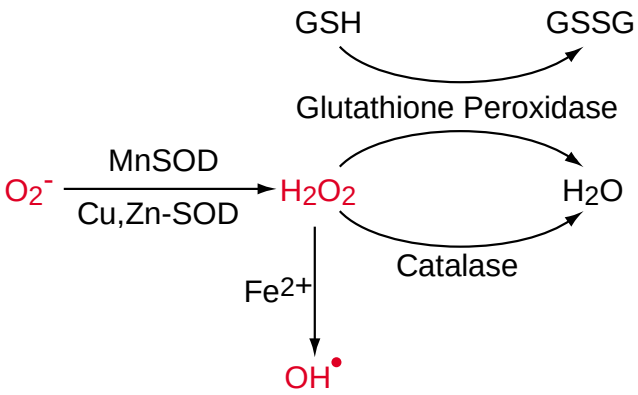

Figure1.13. ROS and antioxidants. O_2^- generated by the ETC is converted to H_2O_2 by SODs. H_2O_2 can either be converted into $OH^\bullet$ by Fenton-like chemistry or detoxified into H_2O by catalase or glutathione peroxidase. Red lettering indicates capability to oxidize cellular substrates. Adapted from (183)

The primary oxidation target of H_2O_2 is the thiol group (-SH) on the amino acid cysteine, which can be oxidized to a sulfenic acid (S-OH) (184). Cysteine oxidation by H_2O_2 can have a variety of biologic effects. H_2O_2 can stimulate cell growth by inhibiting protein tyrosine phosphatases and activating the mitogen-activated protein kinases (MAPKs) extracellular signal-regulated kinase 1 and 2 (ERK1/2) (185-187). Alternatively, H_2O_2 can induce apoptosis by activating the redox sensitive protein apoptosis signal-regulated kinase-1 (ASK-1) (188) and its downstream kinase JNK (187, 189). Whether H_2O_2 stimulates pro-growth or pro-apoptotic pathways may depend on its concentration, as addition of < 0.2 mM H_2O_2 activated ERK1/2 and stimulated proliferation in renal epithelial cells, while concentrations of H_2O_2 > 0.2mM activated JNK and induced apoptosis (187). Importantly, O_2^- is also capable of activating ASK1 (189, 190), which suggests that ASK1 can mediate both O_2^- - and H_2O_2- induced apoptosis. In addition to these specific signaling pathways, H_2O_2 can be converted to hydroxyl radical ($OH^\bullet$) through an iron-catalyzed reaction: $H_2O_2 + Fe^{2+} \rightarrow OH^- + OH^\bullet + Fe^{3+}$ (191). Unlike H_2O_2 and O_2^-, $OH^\bullet$ induces non-specific oxidative damage to DNA, lipids, and proteins, which can lead to apoptosis (192-194).

Cells contain several mechanisms for detoxifying H_2O_2 that limit the production of $OH^\bullet$ and nonspecific oxidative damage (191, 195-197). Catalase, which is only present in the cytosol, catalyzes the iron dependent reduction of H_2O_2 to H_2O (195). Glutathione peroxidase, which is present in both the cytosol and the mitochondrial matrix, can also reduce H_2O_2 to H_2O (198). This reaction is coupled to the oxidation of glutathione (GSH) to its oxidized disulfide form

(GSSG) (196, 197). Pyruvate, a metabolite of glucose, can also detoxify H_2O_2 through a non-enyzmatic decarboxylation reaction (199-204). The role of glutathione and pyruvate as antioxidants are discussed in greater detail in Chapter 3.

The Warburg effect and its etiology. In the presence of O_2, the complete oxidation of glucose to CO_2 generates ~15-fold more ATP than its anaerobic conversion to lactate (78). As such, in the absence of hypoxia many cell types generate their energy through oxidative phosphorylation rather than "wastefully" secreting carbons as lactate (205-207). However, this paradigm does not apply to many types of proliferating cells, which take up glucose at a high rate and, despite the presence of O_2, secrete it as lactate rather than fully metabolizing it through the TCA cycle and oxidative phosphorylation (78). This metabolic phenotype is termed the Warburg effect or aerobic glycolysis. This phenomenon was first demonstrated by Otto Warburg, who showed that cancerous mouse ascites cells produced 60-fold more lactate than non-cancerous kidney or liver cells, but respired only half as fast (205). This observation led to his hypothesis that tumors were characterized by high rates of fermentation. This hypothesis has been confirmed over several decades in numerous cell types (208) and serves as the basis for clinical ^{18}FDG positron emission tomography (PET), an imaging modality in which tumors are identified based on their uptake of a radioactive glucose analog (209).

While numerous studies have shown that increased rates of glycolysis are a general feature of cancers (78, 208, 210-212), the etiology of increased

glycolysis has been more controversial. Warburg suggested that tumor cells depend on glycolysis due to defects in respiration, stating that "The driving force of the increase of fermentation…is the energy deficiency under which the (cancerous) cells operate after destruction of their respiration" (205). However, subsequent studies have shown that, while some cancers show respiratory defects, oxidative metabolism is actually *increased* in numerous tumors compared to normal cells (208, 213). Among the tumor cells with increased respiratory activity are HT29 human colon cancer cells (214), HeLa human cervical cancer cells (215), AS-30D rat hepatoma cells (215), and mouse fibrosarcoma l929 (216). These findings suggest that decreased respiration is not prerequisite for transformation and suggest that aerobic glycolysis is not due to a respiratory defect. Recent studies have begun to elucidate the molecular basis for the Warburg effect, which appears to be controlled by the activation of the transcription factor HIF-1 (217) and the kinase Akt (211).

HIF-1 is a heterodimeric transcription factor composed of HIF-1α and HIF-1β subunits (217). The expression of HIF-1α is regulated by oxygen tension, as HIF-1α protein levels are 20-fold higher during hypoxia (0.5% O_2) than during normoxia (20% O_2) in human HeLa cells (218). This regulation is due to the O_2-dependent hydroxylation of proline residues 402 and 564 on HIF-1α, which allows the von Hippel-Lindau (VHL) protein to bind HIF-1α and target it for proteasomal degradation (Figure 1.14) (219, 220). Hypoxia inhibits proline hydroxylation, resulting in increased HIF-1α levels (221). HIF-1α levels are elevated in a variety of cancers due to local hypoxia, as rapid tumor growth

outpaces blood and O_2 supply (217), and due to mutations in regulators of HIF-1α such as VHL (222). HIF-1 induces glycolysis by increasing the expression of numerous glycolytic genes including GLUT1, GLUT3, HK I and II, PFK-L, aldolase A and C, enolase 1, pyruvate kinase M (PK-M), and LDH-A (74). HIF-1 also induces the transcription of pyruvate dehydrogenase kinase 1 (PDK1), which phosphorylates and inhibits pyruvate dehydrogenase (PDH) (121). This concomitant increase in LDH expression and decrease in PDH activity inhibits the entry of pyruvate into the TCA cycle for oxidation and instead promotes the conversion of pyruvate into lactate and its subsequent secretion from the cell. In addition to decreasing PDH activity, HIF-1 also inhibits oxidative metabolism by decreasing the levels and acitivities of c-myc and its target PGC-1β, a transcription factor that stimulates mitochondrial biogenesis and respiration (223).

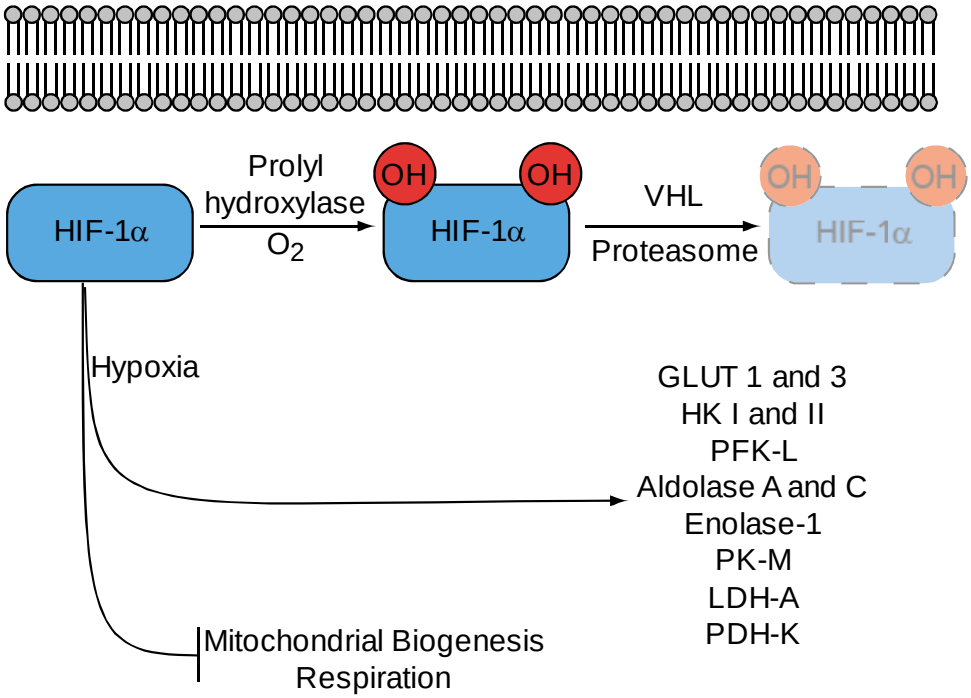

Figure 1.14. Regulation of HIF-1α and its effects on cellular metabolism. HIF-1α is constitutively expressed, and in the presence of O_2 is hydroxylated by O_2-dependent prolyl-hydroxylases. VHL recognizes hydroxylated HIF-1α and targets it for proteasomal degradation. Under hypoxic conditions, HIF-1α induces the expression of numerous glycolytic genes including GLUT1, GLUT3, HK I, HK II, PFK-L, Aldolase A and C, enolase 1, PK-M and LDH-A. HIF-1α also inhibits mitochondrial biogenesis and respiration by inhibiting c-myc acitivity and by inducing PDH-K, which phosphorylates and inhibits pyruvate dehydrogenase (74, 121, 219, 220, 223).

Akt is an evolutionarily conserved kinase that is frequently activated in human cancers (211). In normal tissues, signaling through growth factor

receptors such as the IL-7 receptor (224) or CD28 (59) activate phosphatidylinositol 3-kinase (PI3K), which catalyzes the formation of phosphatidylinositol-triphosphate (PIP_3) (Figure 1.15). PIP_3 interacts with the pleckstrin homology (PH) domain of AKT, and recruits it to the plasma membrane where it is phosphorylated and activated by PI3K-dependent kinase 1 (PDK-1) and mammalian target of rapamycin complex 2 (mTORC2) (211). The activation of AKT is negatively regulated by PTEN, the phosphatase and tensin homolog deleted on chromosome ten, which catalyzes the dephosphorylation of PIP_3 (225).

In cancers, AKT is often constitutively activated due to inactivation of PTEN (226) or activating mutations in PI3K (227, 228). Active AKT promotes the expression and activity of several glucose transporters including GLUT1 and GLUT4 (58, 59, 229). Activated AKT also promotes glycolysis by increasing hexokinase activity (75, 230) and enhacing phosphofructokinase activity by phosphorylating and activating the regulatory enzyme 6-phosphofructo-2-kinase (82, 231). While its role in glycolytic metabolism is well established (59, 75, 231), recent observations suggest that AKT also stimulates oxidative metabolism (232). Mouse embryonic fibroblasts (MEFs) lacking AKT consumed half as much O_2 as wild type MEFs, while MEFs lacking PTEN and Rat1a cells expressing constitutively active AKT consumed 50% more O_2 than wild type controls (232). The ability to increase both glycolysis and OXPHOS is consistent with a role for AKT in cancer metabolism, as many cancers display both increased glycolysis and OXPHOS compared to nontransformed cells (208, 213). AKT also

stimulates fatty acid synthesis in transformed cells through its ability to phosphorylate and activate ATP-citrate lyase (52, 53, 233).

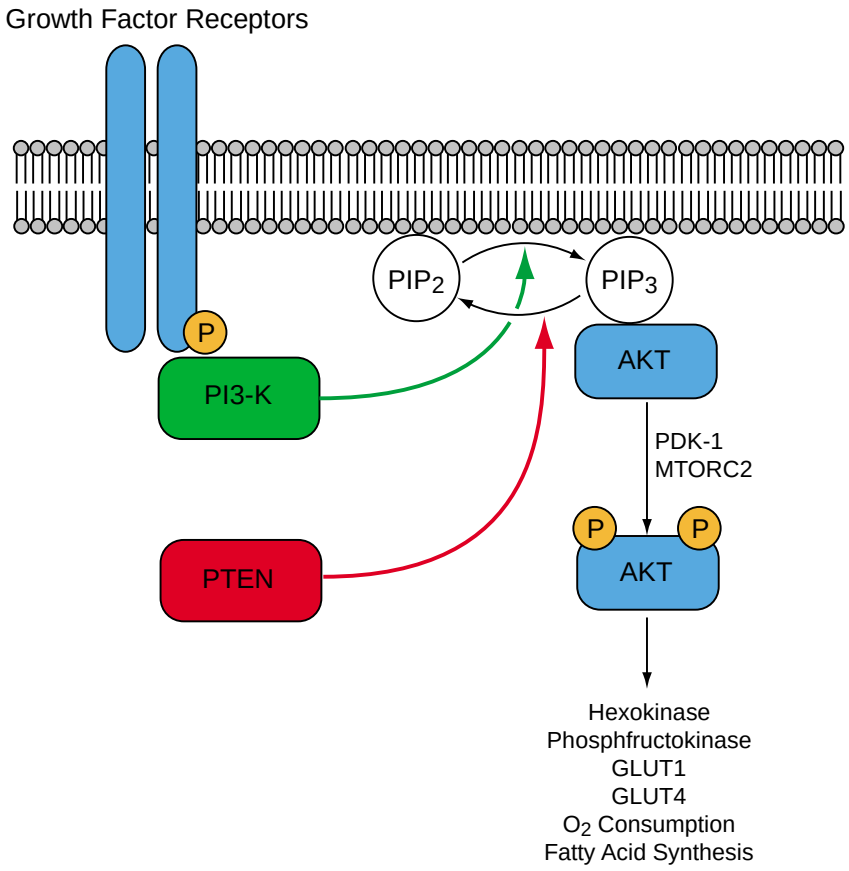

Figure 1.15. Regulation of AKT and its effects on cellular metabolism. Signaling through growth factor receptors activates PI3-K, which catalyzes the conversion of PIP_2 to PIP_3. PIP_3 recruits AKT to the plasma membrane where it is phosphorylated and activated by PDK and MTORC2. Active AKT stimulates O_2 consumption and fatty acid synthesis and stimulates glycolysis by increasing the activities of hexokinase, phosphofructokinase, GLUT1 and GLUT4. PTEN opposes AKT activity by dephosphorylating PIP_3.(211, 232) (58, 59, 75, 82, 229-231)

Utility of the Warburg effect. Increased glycolytic metabolism plays several important roles in cancer cells. The ability to generate energy from anaerobic processes rather than relying on OXPHOS allows cancer cells to survive and grow in areas of hypoxia such as those frequently found in rapidly growing and invasive tumors (234). However, leukemias (235), lymphomas (236) and lung cancers (237) display increased rates of glycolysis, despite being exposed to abundant O_2 in the blood or lungs. These observations suggest that glycolysis may provide benefitis to proliferating tumor cells independent of the ability to survive in hypoxic conditions.

One hypothesis is that increased glycolysis promotes the ability of proliferating tumor cells to synthesize biomolecules such as fatty acids (Figure 1.16) (78). Specifically, increased glycolysis can be used to generate NADPH (through the action of the PPC) and cytosolic acetyl-coA, both of which are required for fatty acid synthesis (78, 238). Several studies support this hypothesis. When the activity of glucose-6-phosphate dehydrogenase (G6PDH), the rate limiting enzyme in the PPC, is decreased using siRNA in A375 melanoma cells, NADPH levels drop by 2.4-fold and cellular proliferation decreases by 30% (239). Similarly, small molecule inhibitors of the pentose phosphate cycle such as oxythiamine (OT) and dehydroepiandrosterone (DHEA), which inhibit transketolase and G6PDH respectively, slow the rate of cancer cell growth (240). Treatment of cultured pancreatic adenocarcinoma cells with OT or DHEA decreases cellular proliferation by 40 or 20% respectively (241), while

injection of OT or DHEA into mice bearing Erlich's ascites tumors decreases tumor cell growth by 80 or 50% respectively (240).

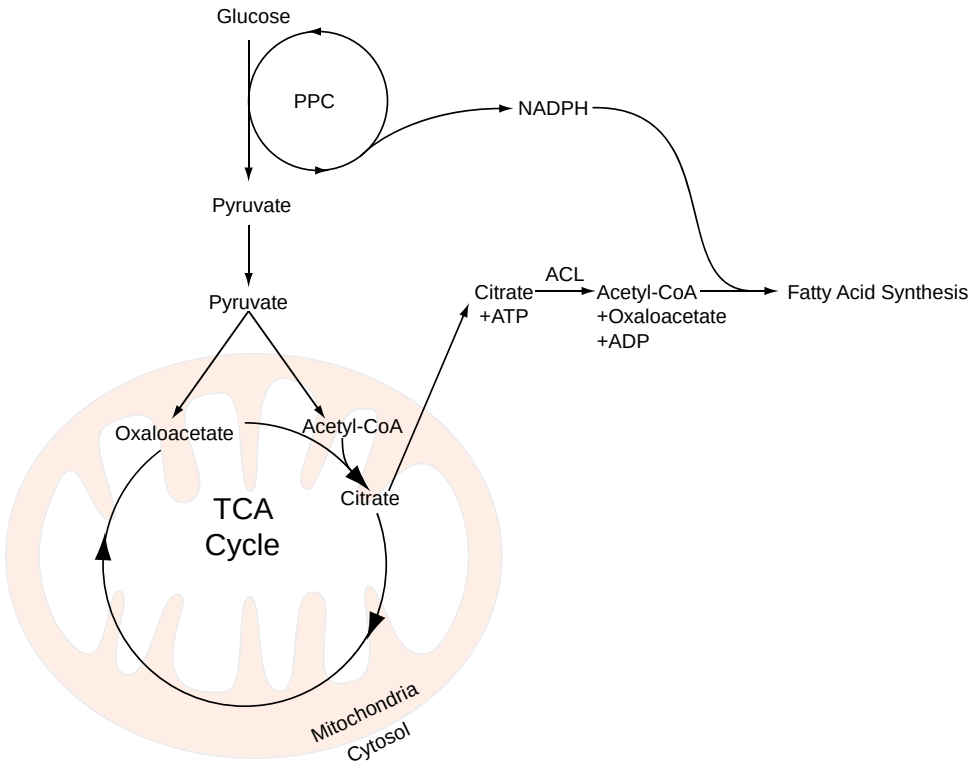

Figure 1.16. Glycolysis and fatty acid synthesis. Glucose metabolism generates NADPH through the pentose phosphate cycle (PPC) and mitochondrial citrate through pyruvate dehydrogenase and pyruvate carboxylase. Citrate is exported to the cytosol where it is converted to acetyl-CoA by ATP-citrate lyase (ACL). Cytosolic acetyl-CoA and NADPH proceed along the fatty acid synthesis pathway (52, 53, 78, 238).

Glycolysis generates cytosolic acetyl-coA by funneling carbons into the mitochondria as pyruvate and forming citrate, which is then exported from the mitochondria to form acetyl-coA through the action of ATP-citrate lyase (ACL) (238). This process is stimulated by AKT, which can phosphorylate and activate ACL (233). Knockdown of ACL using RNA interference inhibits growth of lung cancer cells *in vitro* and *in vivo* (53). ACL knockdown also inhibits the

incorporation of glucose-derived carbons into lipids in activated non-transformed lymphoid cells and inhibits their growth *in vitro (52)*.

Aerobic glycolysis may also promote tumor cell growth and survival by protecting them from ROS production and ROS-mediated damage. Inhibiting glycolysis in human lymphoma cells by using siRNA directed LDH increases oxygen consumption 2.5-fold and increases ROS production as measured by dichlorofluorescein oxidation (242). This decrease in LDH increases apoptosis 3-fold compared to controls. Increased apoptosis is reversed by the antioxidant N-acetyl cysteine (NAC), suggesting that aerobic glycolysis protects cancer cells from ROS-mediated apoptosis (242). A similar study investigating the effects of LDH expression in tumors derived from mammary epithelial cells showed that knockdown of LDH increased respiration by 75% but inhibited rates of proliferation *in vitro* under normoxic (~3-fold inhibition) and hypoxic (~100-fold inhibition) conditions (243). Similarly, mice receiving inoculations of mammary epithelial tumor cells with LDH knocked-down survived 3 times longer than mice inoculated with WT tumor cells, however the role of ROS was not explicitly examined in this study (243). HIF-1 appears to play an important role in the ability of glycolysis to decrease tumor cell ROS production, as it both increases LDH expression and decreases PDH activity (74, 121), thereby funneling glucose-derived carbons away from the mitochondria and lowering ROS production (122).

In a related fashion, glycolysis prevents ROS mediated damage by allowing tumor cells to maintain their antioxidant levels. Inhibiting glycolysis with

the non-metabolizable glucose-analog 2-deoxyglucose (2DG) perturbs antioxidant balance in HeLa cells by decreasing total glutathione levels by 40% and inducing dose- and time- dependent apoptosis (244). This increased apoptosis is reversed by the antioxidant NAC, suggesting that it is due to increased ROS formation (244).

Bioenergetics of unstimulated and stimulated T and B cells. In the absence stimulation through the TCR, T cells are small cells that do not proliferate or secrete cytokines (207). Consistent with their quiescent status, unstimulated T cells have low energetic demands that primarily arise from housekeeping processes such as protein synthesis and ion homeostasis (245). Unstimulated T cells primarily generate ATP by oxidizing carbon substrates. Freshly purified thymocytes take up glucose at a low rate (0.07 nMoles/(min x 10^6 cells), oxidize approximately 15% of it into CO_2 and convert 50% into lactate (63). Resting T cells utilize several other metabolic substrates besides glucose. Freshly purified thymocytes consume glutamine at a rate of 0.03-0.05 nMoles/(min x 10^6 cells), and oxidize 15-20% of into CO_2 (128). Unstimulated lymphocytes also oxidize fatty acids: freshly purified cells from rat lymph nodes metabolize the fatty acid oleate at the same rate as they metabolize glucose (246). However, this study did not distinguish between B and T cells (246).

As discussed above, cells can generate energy either through glycolysis or oxidative phosphorylation (142, 247). By measuring both oxygen consumption and lactate production, Guppy et. al. calculated that freshly purified rat thymocytes generated only 4% of their ATP by producing lactate and 96% by

oxidizing glucose, glutamine and other carbon sources (206). In sum, unstimulated T cells are quiescent cells that meet their minimal energy demands using low rates of oxidative phosphorylation.

Over the past 50 years, it has become apparent that stimulating T cells with mitogens or activating antibodies causes dramatic changes in cellular metabolism (Figure 1.17). In 1963, it was observed that culturing human lymphocytes with PHA for 3 d resulted in glucose depletion and lactate accumulation in the culture media (248). Subsequent studies in the late 1960s and 1970s quantified these changes and showed that PHA stimulation causes a 2-4 increase in lactate production within 4 h of addition to culture, before cells began to grow or divide (249, 250). After 3 d of PHA stimulation, actively proliferating lymphocytes increase glucose consumption and lactate production 10-20-fold compared to unstimulated controls (251). More recent studies have extended these observations and shown that proliferating rat thymocytes stimulated for 2-3 d with conA increase glucose utilization 50-fold and lactate production 36-80-fold compared to unstimulated cells (62, 206, 252). As discussed above, these studies also showed that proliferating thymocytes exhibit a 5-30-fold increase in the activities of glycolytic enzymes such as hexokinase, phosphofructokinase, aldolase, pyruvate kinase and lactate dehydrogenase compared to unstimulated cells (Figure 3.6). Because oxidative metabolism only increases approximately 2-fold following T cell activation, (62, 251), these studies suggest that aerobic glycolysis provides the majority (60-85%) of ATP in activated lymphocytes and that OXPHOS plays a minor role (206, 252).

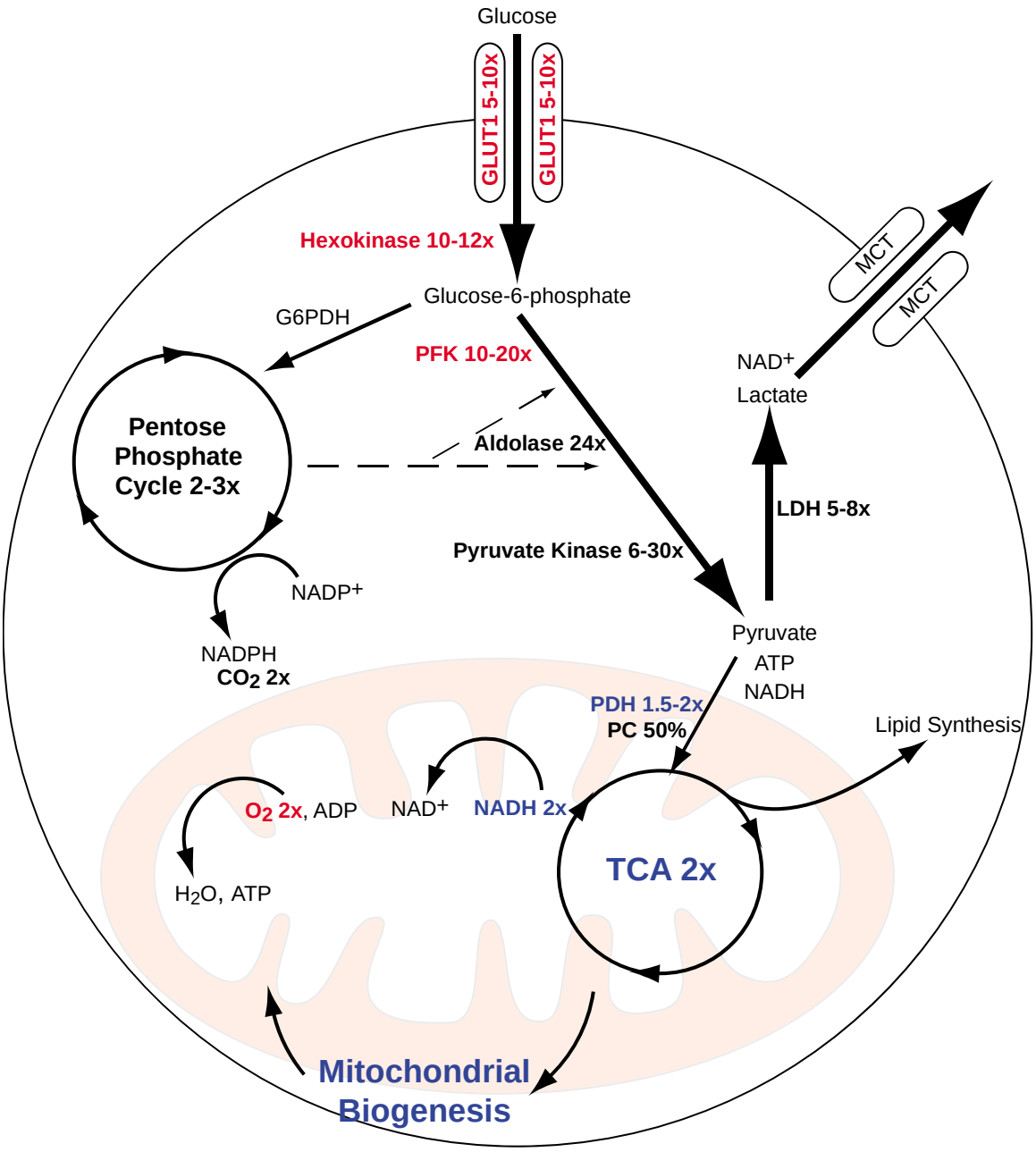

Figure 1.17. Metabolic pathways upregulated in activated T cells. Numbers next to an enzyme or pathway indicate its fold upregulation in activated T cells compared to unactivated controls as described in the text. Enzymes or pathways in red have been directly linked to AKT or costimulatory signaling, while those in blue have been linked to Ca^{2+} signaling (59, 62, 63, 123, 206, 245, 251-254).

Increased aerobic glycolysis in activated T cells is controlled by signaling through CD28 in a PI3-K/AKT-dependent fashion (Figure 1.17, in red). When human $CD4^+$ T cells are stimulated by bead-bound anti-CD3 and anti-CD28 antibodies, they quickly phosphorylate AKT (5-30 min after activation) and later (20 h), upregulate the expression of glucose transporter 1 (GLUT1) and their rates of glycolysis and lactate production by 5-10-fold (59). Increased glucose uptake and glycolysis are inhibited when AKT phosphorylation is blocked by signaling through the inhibitory receptors PD-1 or CTLA4 or by treatment with the PI3-K inhibitor Ly294002, which confirms their dependence on signaling through the PI3-K pathway (59, 255). Similarly, murine $CD4^+$ T cells stimulated through both CD3 and CD28 increase glucose uptake 5-10-fold compared to T cells activated with CD3 alone (58). In addition to regulating GLUT1 expression and activity, activated AKT promotes glycolysis by increasing hexokinase activity through an unkown mechanism (75, 230) and enhacing phosphofructokinase activity by phosphorylating and activating the regulatory enzyme 6-phosphofructo-2-kinase (82, 231).

Lymphocytes also increase oxidative metabolism following activation, although to a lesser magnitude than aerobic glycolysis. Within 30 min of activation with conA, rat thymocytes increase O_2 consumption by 25-30 % (253, 256), and similar changes (30-50% increase) are seen 3-6 h after stimulation of human $CD4^+$ T cells with PMA and ionomycin (257). This increased oxidative metabolism is also seen at later timepoints after activation, when lymphocytes are actively proliferating. 3 d after stimulation with anti-CD3 and anti-CD28

coated microbeads or PHA, human $CD4^+$ T cells or bulk lymphocytes increase O_2 consumption approximately 2-fold compared to unstimulated cells (59, 251).

Early increases in oxidative metabolism following T cell activation are thought to be due to increases in intracellular Ca^{2+} ($[Ca^{2+}]_i$) (Figure 1.17, in blue) (254). Unstimulated T cells have an $[Ca^{2+}]_i$ of 75 nM, which increases to 150 nM within seconds of TCR stimulation (254). This increased $[Ca^{2+}]_i$ enters the mitochondria ($[Ca^{2+}]_m$) through the mitochondrial permeability transition pore (258), where it directly and indirectly activates the dehydrogenases of the TCA cycle. $[Ca^{2}]_m$ stimulates PDH activity by increasing the activity of PDH phosphatase, which dephosphorylates and activates PDH (Figure 1.18) (259). Increased $[Ca^{2}]_m$ also lower the K_m of isocitrate dehydrogenase and alpha-ketoglutarate dehydrogenase activity, thereby increasing their activities (Figure 1.18) (259, 260). Increased TCA cycle activity in activated T cells increases NADH fluorescence 1.5-fold (254). While increased NADH can feed into the electron transport chain and increase O_2 consumption, it appears that NADH-stimulated H^+-transport into the intermembrane space exceeds the rate of rate H^+ flow through the F_oF_1-ATPase, resulting in $\Delta\psi_m$ hyperpolarization and superoxide formation shortly after T cell activation (254). In addition to directly stimulating the TCA cycle, Ca^{2+} also activates the AMP-activated protein kinase (AMPK) at early time points (1-20 min) following TCR stimulation in an [AMP]-independent manner (261). AMPK is an important mediator of cellular energy homeostasis, and its activation promotes both oxidative and glycolytic ATP production by increasing fatty acid oxidation and glycolysis (262, 263).

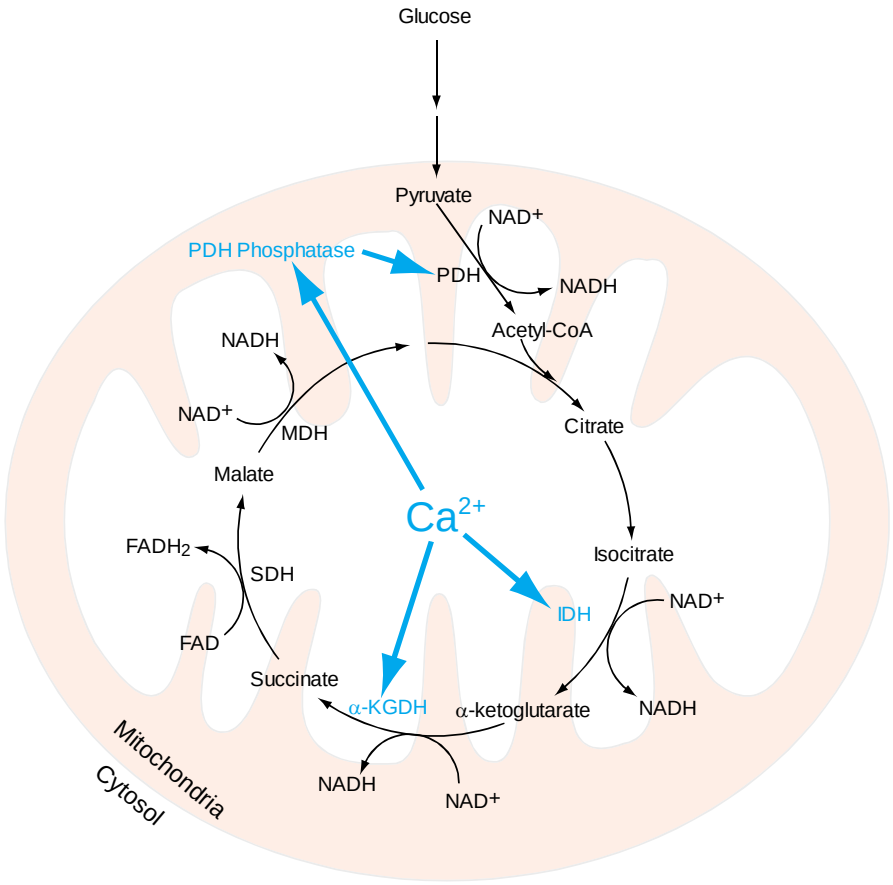

Figure 1.18. $[Ca^{2+}]_m$-mediated stimulation of the TCA cycle. The stimulatory effects of $[Ca^{2+}]_m$ on TCA cycle enzymes are indicated in blue. $[Ca^{+}]_m$ directly stimulates isocitrate dehydrogenase (IDH) and α-ketoglutarate dehydrogenase (α-KGDH) and activates pyruvate dehydrogenase (PDH) phosphatase, which dephosphorylates and activates PDH. Other abbreviations are as follows: succinate dehydrogenase (SDH), malate dehydrogenase (MDH). (123, 259)

Increased $[Ca^{2+}]_m$ may play a role in increased OXPHOS at later timepoints (i.e. 2-3 d) after activation, but these later changes are also likely mediated by an increase in mitochondrial mass. By 24-60 h after stimulation with anti-CD3 and anti-CD28 antibodies or PMA and ionomycin, mouse T cells

increase their mitochondrial mass 5-15 fold as measured by Mitotracker Green fluorescence (264), which is a dye that accumulates in mitochondria independently of $\Delta\psi_m$ (265). Importantly, these changes were not observed in proliferating T cells stimulated by the cytokines IL-2, IL-17 and IL-15, which indicates that increased OXPHOS may not be a feature of all stimulated lymphocytes (264). Ca^{2+}-mediated hyperpolarization may also play a role in increased OXPHOS at these later timepoints, as antibody- or PMA and ionomycin-stimulated T cells also showed a 5-10 increase in Mitotracker Red fluorescence (264), which is a dye that accumulates based on $\Delta\psi_m$ (265).

Although activated T cells increase aerobic glycolysis 10-20-fold while increasing OXPHOS only 2-fold, it is unclear if high rates of glucose uptake and lactate production are necessary for productive T cell activation (i.e. proliferation and cytokine production). Removing glucose from the culture media (but maintaining 2 mM glutamine as a carbon source) results in the complete absence of proliferation and IFN-γ production and a 7-fold decrease in IL-2 production in mouse T cells stimulated for 2 d by anti-CD3 and anti-CD28 (58). Similarly, the number of proliferating human $CD4^+$ cells present 96 h after stimulation by PMA and ionomycin drops by 60% when cells are cultured without glucose (257).

Lowering glucose levels, rather than eliminating glucose entirely, allows T cells to retain their ability to proliferate and synthesize cytokines. Human $CD4^+$ T cells stimulated with anti-CD3 and anti-CD28 antibodies in 0.4 mM glucose (rather than 11 mM), decrease glycolysis 4-fold and increase O_2 consumption by 4-fold, but maintain their ability to proliferate (59). Similarly, murine T cells

stimulated with anti-CD3 and anti-CD28 and cultured in 0.5 mM glucose are identical to T cells in 5 mM glucose with respect to viability, proliferation and IL-2 and IFN-γ production (58). Together, these results show that while low levels of glucose are necessary for activated T cell proliferation and cytokine production, high rates of aerobic glycolysis are not absolutely required, possibly due to the ability of activated T cells to upregulate OXPHOS when glycolysis is restricted. Consistent with this notion, inhibiting OXHPOS with the complex III inhibitor myxothiazol decreases IL-2, TNF-α, IFN-γ and IL-4 production when human $CD4^+$ T cells are stimulated with PMA and ionomycin in restricted glucose conditions (257). However, myxothiazol does not inhibit cytokine production when cells are cultured in 11 mM glucose (257). These results show that activated T cells can proliferate and produce cytokines while relying on OXHPOS as their primary energy source.

While B cell metabolism has not been studied as extensively as that of T cells, it appears that resting and activated B cells share many characteristics with resting and activated T cells. For example, mouse B cells stimulated through the B cell receptor increase glucose uptake and glycolysis 15-20-fold compared to resting B cells (266). Both of these metabolic changes are dependent on the AKT/PI3-K pathway, as PI3-K inhibition with wortmannin or LY294002 abrogated increased glucose uptake and glycolysis in activated B cells (266). These results suggest that, like T cells, B cells increase glucose metabolism in an AKT/PI3-K dependent fashion following stimulation through the antigen receptor.

Statement of purpose. In the setting of autoimmunity (e.g. lupus) or allogeneic transplantation (e.g. GVHD), inappropriately activated lymphocytes mediate disease. Unfortunately, glucocorticoids, a major treatment option for both lupus and GVHD, indiscriminately kill pathogenic and non-pathogenic white blood cells and are therefore associated with high rates of infection. Because dramatic differences in cellular metabolism often exist between cell types (e.g. nontransformed cells vs. cancers, resting vs. activated lymphocytes), an understanding of cellular metabolism in lupus and GVHD could reveal pathways selectively utilized by disease-causing lymphocytes. Such information may be of value for developing therapies that selectively inhibit pathogenic lymphocytes while preserving other aspects of the immune system. This hypothesis is bolstered by studies showing that Bz-423, a novel inhibitor of the mitochondrial ATPase, selectively deletes autoreactive B and T cells in models of lupus without killing bystander lymphocytes.

Therefore, the goal of my research is to determine the metabolic pathways used by pathogenic autoreactive or alloreactive lymphocytes as they mediate disease with the goal of exploiting differential cellular metabolism to selectively kill pathogenic cells. In Chapter 2, lymphocytes from mice with active lupus are shown to rely on oxidative energy production as they mediate disease, and a similar phenotype is observed in chronically-activated human T cells. This oxidative phenotype is contrasted with acutely-activated T cells, which primarily rely on glycolysis for energy production. In Chapter 3, GVHD-causing T cells are shown to increase oxidative metabolism and decrease antioxidants as they

mediate disease. This metabolic phenotype is contrasted with proliferating cells in the bone marrow, which up-regulate glycolysis and maintain antioxidants. In Chapter 4, Bz-423 is shown to selectively kill GVHD-causing T cells without inducing apoptosis in bystander T cells or proliferating cells in the bone marrow. These results lead to a bioenergetic model of Bz-423 sensitivity, in which Bz-423 selectively kills disease-causing lymphocytes with increased oxidative metabolism and depleted antioxidants, but not bystander cells with either low rates of OXPHOS or intact antioxidants.

CHAPTER 2

CHARACTERIZATION OF THE METABOLIC PHENOTYPE OF CHRONICALLY STIMULATED LYMPHOCYTES

Introduction

Systemic lupus erythematosus. Systemic lupus erythematosus (SLE or lupus) is an autoimmune disorder characterized by the inappropriate recognition of self antigens by the immune system (43). According to a 1996 meta-analysis, SLE affects approximately 25 out of every 100,000 residents of the United States, with 90% of those affected being female (267). Symptoms associated with SLE include skin rash, pleuritis, joint pain, nephritis, vasculitis and stroke (268, 269).

SLE is a multifactorial disease whose pathogenesis involves both environmental and genetic factors (270). The importance of genetics in SLE is emphasized by the 24% concordance rate of SLE in monozygotic twins as compared with a 2% rate in dizygotic twins (271). Polymorphisms in several genes are known to contribute to the development of SLE in humans. Expression of the DR2 or DR3 alleles on chromosome 6, which encode MHC class II molecules, is associated with a 2-3-fold increase in SLE incidence in Caucasian populations (268). Similarly, genetic deficiencies in the complement

system components C1q, C2, and C4, which aid in pathogen lysis (31), predispose patients to SLE (268).

Genetic factors also influence the development of lupus-like disease in mice. Studies in the NZM2410 strain of lupus-prone mice have identified three separate genetic regions on chromosomes 1 (*Sle1*), 4 (*Sle2*) and 7 (*Sle3*) linked to the development of lupus-like disease (268). These regions are involved in maintaining B and T cell tolerance, and their functions were determined by transferring individual regions onto non-autoimmune mice. Mice containing *Sle1* produce increased levels of anti-chromatin antibodies (272). B cells from mice containing *Sle2* proliferate 2-fold faster to a variety of stimuli including anti-IgM and LPS in comparison to WT B cells (273). $CD4^+$ T cells from mice containing *Sle3* exhibit increased proliferation in response to anti-CD3 or IL-2 stimulation *in vitro*, and accumulate with an activated phenotype *in vivo* (274). The transfer of any one of these genetic regions onto a non-autoimmune B6 mouse does not result in lupus-like disease (275). However, when all three of these regions are transferred together, mice developed severe nephritis and kidney failure, suggesting that their combined effects are sufficient to cause SLE (275).

While SLE has a strong genetic component that arises from the involvement of numerous genes, environmental factors also play a role in the development of SLE. Several pharmacologic agents are known to induce lupus-like symptoms, termed drug-induced lupus (276). For example, treatment with procainamide, an antiarrythmic, or hydralazine, a vasodilator, is associated with a 7-20% risk of inducing drug-induced lupus (276). The mechanism by which

these compounds induce lupus is thought to involve the inhibition of DNA methylation and subsequent increased inflammatory gene expression (276, 277). Furthermore, the concordance rate of lupus in identical twins is 24% (271). If lupus were solely determined by genetic factors, this value would be closer to 100% (43, 271). Together, these observations suggest that a combination of genetic predisposition and environmental triggers may lead to the development of SLE.

T and B lymphocytes in SLE. The development of SLE is characterized by a loss of tolerance to self-antigen and the expansion of autoreactive B and T lymphocytes. While autoreactive B cells are found in healthy individuals (278, 279), their numbers and activity are increased in patients with lupus (280). For example, the number of B cells actively producing antibodies is increased up to 50-fold in human and murine SLE compared to healthy controls (281-283).

The reasons for autoreactive B cell expansion in SLE are manifold. One contributing factor is increased B cell stimulation through the CD40 receptor (284). B cells express CD40, and costimulatory signals from CD40L can induce B cell proliferation and antibody production (285, 286). B and T cells from patients with lupus express 20-fold more CD40L than do cells from healthy individuals (284), suggesting that stimulation through CD40 may be increased in lupus B cells. Consistent with this hypothesis, inhibiting CD40-CD40L interactions delays lupus development by up to 1 year in lupus-susceptible SNF_1 mice (287). Additionally, reduced inhibitory signaling in lupus B cells may play a role in their hyperactivation. Inhibitory signaling through the FcγRIIB receptor

opposes stimulatory signaling through the B cell receptor by decreasing intracellular levels of phosphatidylinositol (3,4,5) triphosphate (288). B cells from patients with SLE express decreased levels of FcγRIIB (289) and polymorphisms in FcγRIIB are associated with the development of SLE (290, 291). Together, these observations suggest that both increased stimulation through CD40 and decreased inhibitory signaling through FcγRIIB may contribute to the expansion of autoreactive B cells in SLE.

Autoreactive T cells also play a role in SLE pathogenesis (43). T cells that recognize self antigens such as complexes of DNA and histones can be cloned from humans or mice with SLE (292-295). In healthy individuals, autoreactive T cells that have escaped central tolerance are inhibited by a process termed peripheral tolerance (296, 297). Peripheral tolerance is comprised of two major processes, both of which may be defective in lupus T cells. If T cells receive a signal through their T cell receptor (TCR) without accompanying costimulation, they can become anergic, which is a state characterized by inhibited proliferation and decreased IL-2 production (297). The induction of costimulatory molecules on antigen presenting cells (APCs) is associated with Toll-like receptor (TLR) stimulation by pathogen associated molecular patterns such as viral DNA or lipopolysaccharide (LPS) (36). Because self-antigens are not associated with such patterns, the APCs presenting self-antigens are expected to have low levels of costimulatory molecules (35, 298). Thus, in normal individuals, autoreactive T cells receive signaling through the TCR without costimulation and become anergic (35, 297, 298). In SLE, this induction of tolerance to self-antigen appears

to be faulty (299). Compared to T cells from healthy controls, T cells from SLE patients and lupus mice exhibit a 50-100% increase in Ca^{2+} flux following stimulation through the TCR alone (300-302). This increased signal strength in the absence of costimulation could contribute to the ability of SLE T cells to escape tolerance (303).

A second mechanism of maintaining T cell tolerance to self antigens is through activation induced cell death (AICD, Figure 2.1). The repetitive stimulation of T cells increases their surface expression of FAS ligand (FASL) (304-308). FASL then signals through FAS (CD95) on T cells, which activates caspase 8 and induces apoptosis (304). In healthy individuals, this mechanism aids in the deletion of autoreactive T cells, which are continuously exposed to self-antigen (304, 308). However, T cells from mice and patients with lupus exhibit defects in the AICD pathway (299). T cells from MRL-*lpr* and Gld/*gld* mice have defective FAS and FASL, respectively, and both strains develop lupus-like disease (281, 299). While mutations in FAS and FASL in patients with SLE are rare (309), T cells from SLE patients show a 2-3-fold decrease in AICD sensitivity compared to control cells (310, 311). While, the basis for this resistance is unclear, it may be related to alterations in cyclooxygenase (COX) 2 levels in lupus T cells. When lupus T cells are exposed to repetitive TCR stimulation *in vitro*, they increase COX-2 up to 40-fold compared to control T cells (311). This increased COX-2 expression in SLE T cells is associated with increased expression of C-FLIP, which inhibits apoptosis by blocking the activation of caspase 8 (311, 312). However, treating lupus T cells with the

COX-2 inhibitors celecoxib and niflumic acid decreases C-FLIP expression and induces apoptosis (311).

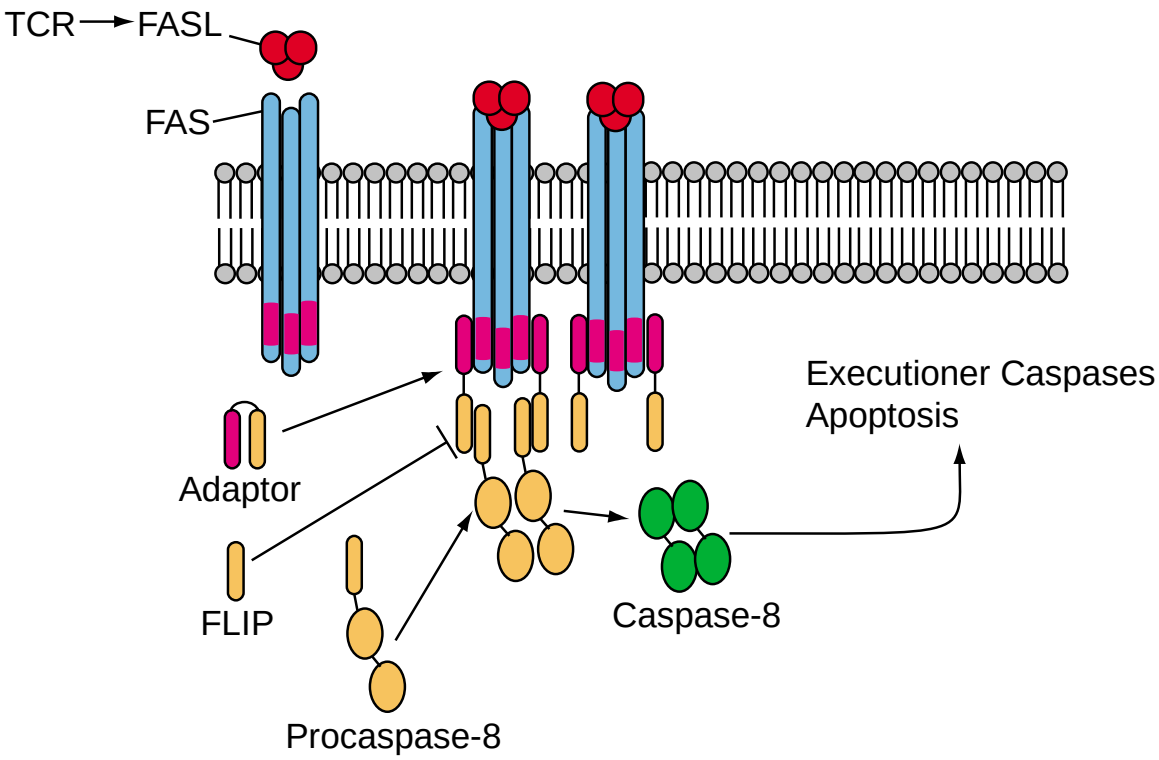

Figure 2.1. AICD in activated T cells. Repetitive stimulation of the TCR induces FASL and FAS expression. Clustering of FAS recruits adaptor proteins such as FADD, which recruit procaspase 8 into a complex termed the death-inducing signaling complex (DISC). Clustering of procaspase 8 stimulates its autoactivation and release from the DISC. Active caspase 8 can activate the executioner caspases-3 and-7, which leads to apoptosis. From (308).

Tissue damage in SLE. Following their stimulation by autoreactive helper T cells, autoreactive B cells in lupus produce antibodies that recognize self antigens (autoantibodies) (43). These autoantibodies are directed against numerous antigens, including double-stranded DNA (dsDNA) (313), nucleosomes (e.g., complexed histones and DNA) (314), and other nuclear

antigens (43). There are two models that explain how autoantibodies mediate the nephritis characteristic of SLE. The first model suggests that autoantibodies bind to nucleosome fragments in the bloodstream and these immune complexes deposit in the glomerular basement membrane of the kidney (315). The presence of these complexes activates complement, recruits white blood cells and induces glomerulonephritis (315). This model is supported by the direct observation that complexes of nucleosomal antigens and anti-nucleosomal antibodies bind to the glomerular basement membrane in rats (316). The second model suggests that anti-nuclear antigens cross-react with proteins present on the glomerular basement membrane such as α-actinin (317), thereby inducing glomerulonephritis. This model is supported by evidence showing that monoclonal anti-DNA antibodies only caused glomerulonephritis in mice when they also cross-reacted with α-actinin (317). The extent to which these two models contribute to tissue damage in human patients with lupus is unresolved (43).

The NZB/W model of SLE. In the early 1960s, New Zealand Black (NZB) and New Zealand White (NZW) mice were mated, yielding lupus-prone offspring (NZB/W), which have since been used as the prototypical mouse model of SLE (318, 319). NZB/W mice display many of the characteristics of human SLE, including the production of autoantibodies to single-stranded and double-stranded DNA, the deposition of autoantibodies in the glomerulus, and the development of fatal nephritis (Figure 2.2) (320). Similarly to humans, the

symptoms of lupus are more frequent and severe in female NZB/W mice than in males (321).

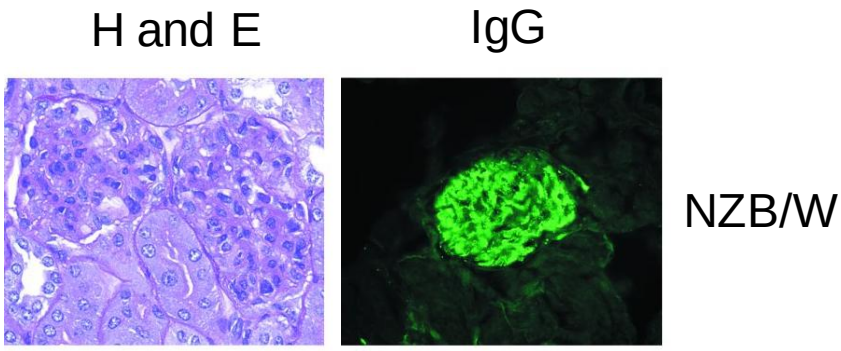

Figure 2.2. Glomerlulonephritis and IgG deposition in the kidneys of NZB/W mice. On the left are hematoxylin and eosin (H and E) stained images showing white blood cell infiltration into the kidneys of NZB/W animals with lupus. On the right, images were stained with a fluorescent antibody against IgG. Green fluorescence indicates IgG deposition in the glomerulus. Images are from 9.5 mo old NZB/W mice with active lupus-like disease (169).

Female NZB/W mice begin to develop anti-DNA antibodies around two months of age, while antibody deposition in the glomerulus and associated glomerulonephritis begin at 3-6 months (313, 322). The severity of the glomerulonephritis increases with age, and leads to a median lifespan of approximately 8.5 months in female NZB/W mice (281, 323).

Both B and T cells are important for the development of disease in NZB/W mice. Three separate studies have documented an improvement in disease when NZB/W mice are treated with antibodies that neutralize or deplete $CD4^+$ T

cells (324-326). Similarly, depleting B cells with an anti-CD20 antibody improves survival in NZB/W mice when the treatment occurs between weeks 12 and 20 (327). Interestingly, B cell depletion beginning at 4 or 8 weeks of age actually *hastens* disease, possibly because of the depletion of regulatory IL-10 producing B cells (327). Hence, both autoreactive T and B cells contribute to lethal lupus-like disease in NZB/W mice.

Lymphocyte metabolism and SLE. Resting lymphocytes, such as those found in the spleens of naïve mice, meet their minimal demand for ATP using low rates of oxidative phosphorylation (OXPHOS) (207). Normal lymphocyte activation is an acute response to signals generated by antigen and costimulatory receptors such as CD28 (34). Once activated, lymphocytes require increased energy to proliferate, produce cytokines and synthesize antibodies. Upon activation, lymphocytes increase oxygen consumption and CO_2 production ~2-fold compared to unactivated controls (127, 206, 251). These changes reflect increased OXPHOS, which in part, results from higher intracellular Ca^{2+} levels (254), stimulating dehydrogenases in the TCA cycle (123, 254, 260).

Despite an ability to increase OXPHOS, acutely activated lymphocytes generate the majority of their ATP by dramatically increasing their rate of glycolysis by taking up large amounts of glucose and converting it to lactate (Discussed in greater detail in Chapter 1). Because acutely activated T cells engage in high rates of glycolysis despite the presence of oxygen, it is termed *aerobic glycolysis* (59, 206, 251). In addition to producing ATP, a high rate of glycolysis helps maintain antioxidant levels in activated cells; e.g., by providing

substrates for the pentose phosphate cycle which produces NADPH, an important intracellular reducing agent (50, 78, 252).

In autoimmune diseases such as SLE, autoreactive lymphocytes are *persistently* stimulated by self-antigen and acquire a *chronically* activated phenotype characterized by sustained proliferation and effector functions (43, 296, 328-333). Although the metabolic pathways used by chronically activated lymphocytes have not been studied directly, several lines of evidence suggest that pathogenic lymphocytes in diseases like lupus, rheumatoid arthritis (RA), psoriasis, and graft-vs-host disease preferentially rely on mitochondrial metabolism (Figure 2.3) (334-337). Indeed, peripheral blood T cells from patients with SLE have a 50% increase in mitochondrial mass compared to control cells from healthy individuals (302). This increase in mitochondrial mass is accompanied by a 20% increase in the mitochondrial membrane potential ($\Delta\psi_m$) as measured by tetramethylrhodamine (TMRM) fluorescence (302). However, the amount of dye used in this study (1 μM), (302) can report on both the plasma membrane potential and $\Delta\psi_m$ (145, 338). Similar results were obtained with two separate potentiometric dyes ($DIOC_6$ and JC-1), however these dyes are also not entirely specific for $\Delta\psi_m$ (145, 302). Despite these limitations, these results are consistent with the interpretation that $\Delta\psi_m$ is hyperpolarized in T cells from lupus patients (339).

This increased $\Delta\psi_m$ in lupus T cells is accompanied by a 40% increase in the fluorescence of dihydroethidium (DHE) (339), a dye whose fluorescence increases following its selective oxidation by O_2^- (340). Hyperpolarization of $\Delta\psi_m$

slows electron transport through the mitochondrial respiratory chain and extends the half lives of reactive intermediates such as flavins, iron-sulfur centers and ubisemiquinone, which leads to increased O_2^- formation (131, 154, 167, 168). Hence, increased O_2^- in lupus T cells could be related to hyperpolarization of $\Delta\psi_m$.

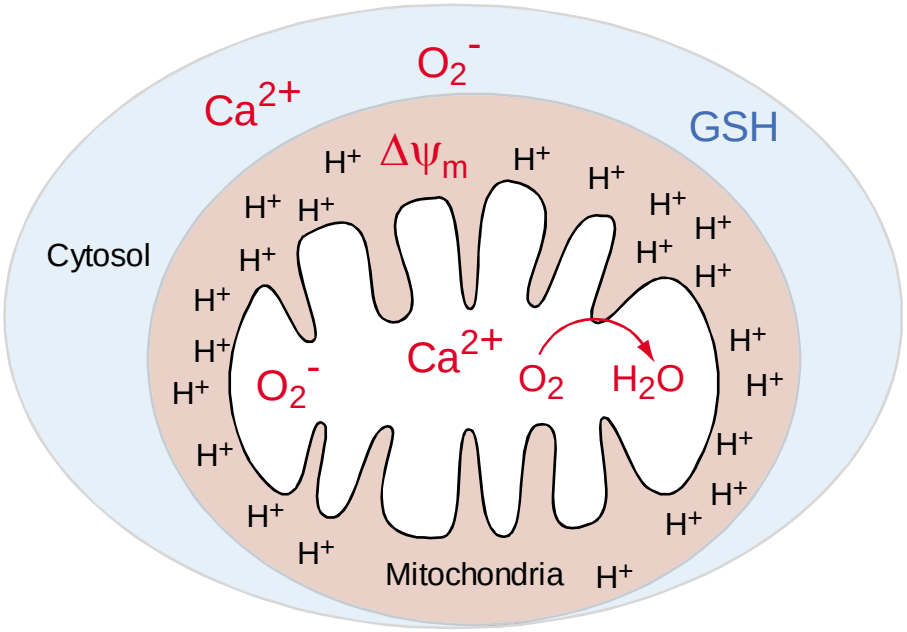

Figure 2.3. Bioenergetic abnormalities of SLE lymphocytes. T cells from patients with lupus display *increased* (red) mitochondrial and cytosolic Ca^{2+}, total cellular O_2^-, O_2 consumption and $\Delta\psi_m$, while total cellular GSH levels are *decreased* (blue) (302, 335, 339, 341).

As discussed above, T cells from patients and mice with lupus show increased $[Ca^{2+}]_i$ flux following stimulation through the TCR (300-302). Additionally, T cells from patients with SLE have a 20-40% increase in *basal* levels of cytosolic and mitochondrial $[Ca^{2+}]$ ($[Ca^{2+}]_m$) compared to control cells, as

measured by the dyes fluo-3 and rhod-2, respectively (302). Increased $[Ca^{2+}]_m$ and $\Delta\psi_m$ hyperpolarization in lupus T cells may be linked, as increased $[Ca^{2+}]_m$ can stimulate the TCA cycle (123, 259, 342) and lead to $\Delta\psi_m$ hyperpolarization (254).

Further evidence of increased mitochondrial metabolism in chronically stimulated lymphocytes comes from the direct measurement of O_2 consumption from lymphocytes of patients with autoimmune disease. A 2003 study showed that peripheral blood mononuclear cells (PBMCs) from 12 patients with active lupus and rheumatoid arthritis consumed 50% more O_2 than cells from healthy controls (335). Together, the observations of increased mitochondrial mass, $\Delta\psi_m$ hyperpolarization, increased $[Ca^{2+}]_m$, and increased respiration suggest an increase in oxidative metabolism in SLE lymphocytes.

In addition to high levels of oxidative metabolism, several studies suggest that lymphocytes from animals and mice with SLE may have *low* rates of glycolysis. T cells from patients with SLE have 30% less total cellular reduced glutathione (GSH) than cells from healthy controls (339). GSH is consumed when glutathione peroxidase catalyzes the formation of H_2O from H_2O_2 (196, 197). Conversely, GSH is formed in an NADPH-dependent fashion by glutathione reductase (196, 197). The NADPH used for GSH formation is generated by the metabolism of glucose through the pentose phosphate cycle (50, 51). Thus, decreased GSH levels could be reflective of inadequate generation of NADPH secondary to insufficient glycolysis (51, 343). Hence, the inability to maintain glutathione at normal levels is consistent with relatively low

rates of glycolysis in lupus T cells. GSH depletion in SLE lymphocytes contrasts with T cells acutely stimulated with mitogens, which increase glutathione levels 2-fold compared to unstimulated cells (344). While mitogen stimulated T cells increase glycolysis 20-40-fold compared to unstimulated cells (206, 252, 253), direct measurements of glycolytic metabolism in lymphocytes from patients or animals with lupus are lacking.

Persistent antigen stimulation in autoimmunity. A successful immune response against an acute infection leads to the clearance of pathogen, which is followed by decreased presentation of foreign antigen by APCs (308). The absence of foreign antigen causes pathogen-specific T cells to cease the production of pro-surivival cytokines such as IL-2. Decreased levels of these growth factors leads to the apoptosis of activated T cells, which is dependent on the BH3-only protein Bim (Figure 2.4) (8-11).

During a chronic viral infection, infectious pathogens cannot be cleared and stimulatory foreign antigen persists (308). Despite this persistence of foreign antigen, pathogen-specific T cells do not proliferate in an unrestrained fashion (9). Indeed, in the setting of chronic mouse γ-herpes virus (MHV), the number of virus-specific T cells peaks after d 14 and then declines, despite the continued presence of antigen. However, when T cells lack both Bim *and* functional FAS, this process is impaired, and pathogen-specific T cells continue to accumulate as MHV persists (308).

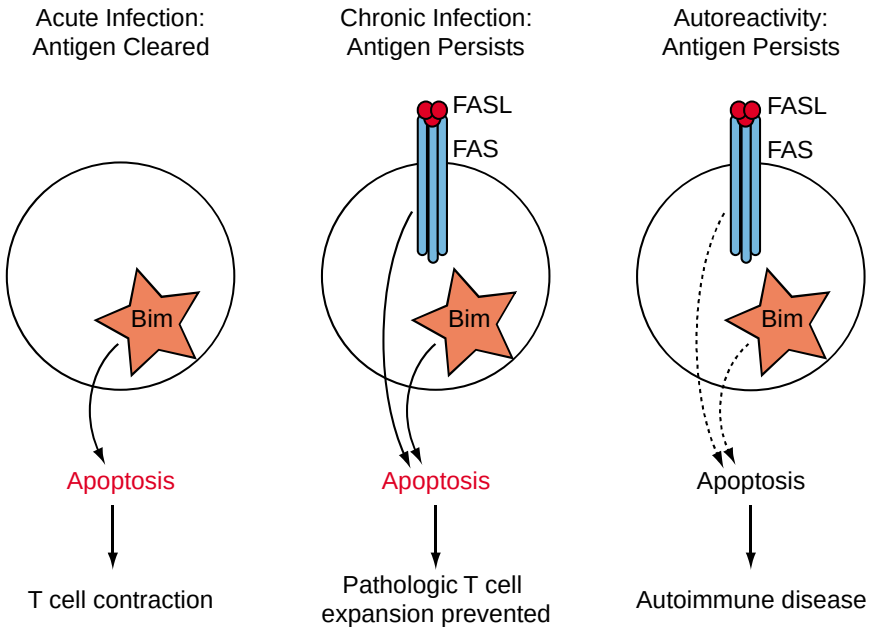

Figure 2.4. T cell apoptosis in the immune response. Following an acute infection, pathogen is cleared, and activated T cells die through a Bim-dependent pathway. During chronic infections, activated T cells are eliminated in a FAS- and Bim-dependent fashion, which prevents their pathologic expansion. In autoimmune diseases, T cells are resistant to FAS-mediated apoptosis and have increased levels of Bcl-2, which inhibits Bim-mediated apoptosis. These abnormalities could contribute to autoreactive T cell expansion and autoimmunity (8-12).

In the setting of lupus, self-antigen is present ubiquitously due to its continual release from dead or dying cells (43, 299, 314-316). However, both pathways that induce apoptosis in activated T cells are defective in T cells from lupus patients. Compared to control T cells, T cells from lupus patients express 5-fold more Bcl-2, which is an antiapoptotic protein that can inhibit Bim-mediated apoptosis (345). Additionally, T cells from lupus patients have increased levels of C-FLIP and are less sensitive to FAS-mediated apoptosis than control cells (299, 310, 311). Thus, persistent stimulation with self-antigen, combined with

defective Bim- and FAS-mediated apoptosis, could relate to the pathologic expansion of autoreactive T cells in lupus.

Persistent antigen stimulation in lupus and other autoimmune diseases has several important consequences. Chronic stimulation of T cells can lead to the increased expression of the Kv1.3 potassium channel, and inhibition of this channel is therapeutic in several models of pathogenic T cell activation, including experimental autoimmune encephalitis (EAE) (328, 333), allograft rejection (333), and rheumatoid arthritis (346). Unstimulated rat T cells express 1-10 Kv1.3 channels, while T cells stimulated 1-2 times with mitogen or antigen express approximately 200 Kv1.3 channels per cell (328). However, when T cells are stimulated > 8 times with antigen, they express approximately 1500 Kv1.3 channels per cell (328). Furthermore, the number of Kv1.3 channels expressed on a T cell clone correlated with its ability to induce EAE, which may explain the efficacy of Kv1.3 inhibition in the treatment of EAE (328). Similarly, myelin-specific T cells isolated from patients with MS express 3-4-fold more Kv1.3 channels than cells from healthy controls (333). Hence, repetitive stimulation can cause changes distinct from acute stimulation that can be exploited therapeutically to treat autoimmune diseases.

Persistent antigen stimulation can also lead to decreased expression of CD28 on T cells (332, 347). In healthy young adults, fewer than 2% of $CD4^+$ and fewer than 25% of $CD8^+$ T cells lack the expression of the costimulatory receptor CD28 (i.e. $CD28^{null}$) (332). When these cells are stimulated *ex vivo* with irradiated allogeneic stimulator cells, they expand and maintain CD28 expression

for the first 2-3 weeks of culture. However, after 4 repetitive stimulations T cells begin to lose CD28, and after 10 stimulations > 70% are $CD28^{null}$ (332). Decreased CD28 expression is due to the inactivation of the transcription factor complex that normally promotes CD28 gene expression (347, 348). Numerous autoimmune diseases, including multiple sclerosis, RA, and lupus are associated with increased frequencies of $CD28^{null}$ T cells, possibly due to persistent stimulation with ubiquitous self antigen (349-351). Indeed, the percentage of T cells lacking CD28 in patients with lupus (29%) is 70% greater than in age-matched healthy controls (17%) (352).

Several observations suggest that $CD28^{null}$ T cells may participate in the pathogenesis of autoimmune diseases. $CD28^{null}$ T cells proliferate in response to autoantigen (353) and produce 2-fold more IFN-γ than $CD28^{+}$ T cells following stimulation with anti-CD3 (354). Furthermore, $CD28^{null}$ T cells from patients with RA express 5-10-fold more perforin and KIR2DL4 (355). Perforin is a pore-forming protein secreted by cytotoxic T cells and natural killer cells that allows granzyme-B-mediated apoptosis (15, 16), while KIR2DL4 is a receptor that activates NK cell cytokine production (356).

Together, these observations suggest that autoreactive $CD28^{null}$ cells arise as a consequence of repetitive TCR stimulation and may play an important role in the pathogenesis of autoimmune diseases such as lupus and rheumatoid arthritis. Importantly, signaling through CD28 increases T cell glucose transporter 1 (GLUT1) expression, glucose uptake and lactate production in a PI3-K/AKT dependent fashion (59, 231). The effects of CD28 extinction on

cellular metabolism are unknown, but may play a role in the metabolic alterations evident in lupus and rheumatoid arthritis (302, 335, 339, 341).

Statement of problem. Little is known regarding cellular metabolism in autoimmune lymphocytes. To characterize the metabolic pathways used by lupus splenocytes, we infused uniformly labeled ^{13}C-glucose into NZB/W mice with active lupus and into non-autoimmune, age-matched Balb/c mice and analyzed tracer-derived ^{13}C redistribution among glucose metabolites using gas chromatography-mass spectrometry (GC-MS) (357). We chose glucose as a tracer because it is the primary energy source for lymphocytes (69) and because its conversion into lactate reflects the rate of aerobic glycolysis while its oxidation into CO_2 occurs during OXPHOS. Additionally, the patterns of tracer distribution into lactate and palmitate indicate relative flux through the pentose phosphate cycle (PPC) (Figure 2.5). Thus, a single tracer allowed the simultaneous interrogation of aerobic glycolysis, PPC activity, and OXPHOS (Figure 2.e). We selected the spleen as the tissue for analysis because it is rich in lymphocytes, many of which are autoreactive in the NZB/W model (358, 359).

Similarly, little is known about the metabolism of chronically activated lymphocytes. To determine if the metabolism of chronically activated lymphocytes differed from acutely activated cells, we conducted studies using a model in which repetitive stimulation of T cells through the T cell receptor (TCR) decreases expression of CD28 over a period of several months (332, 360). These findings were then placed into the context of our studies in the NZB/W mice. Differences in bioenergetics between normal and chronically activated

lymphocytes may ultimately lead to new diagnostic and therapeutic strategies for immune diseases.

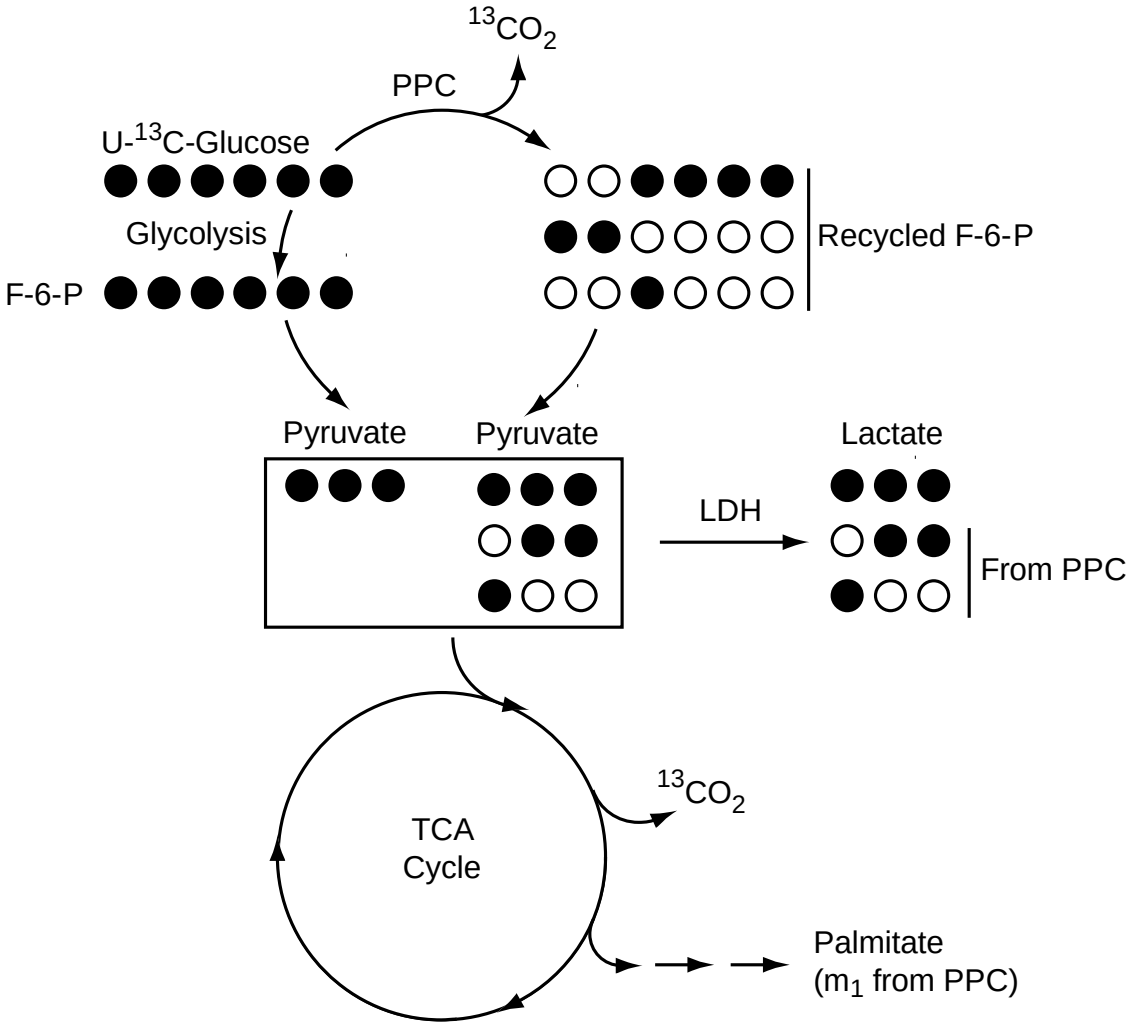

Figure 2.5. Pathways of U-^{13}C-Glucose metabolism through glycolysis and the pentose phosphate cycle. ^{13}C carbon atoms are shown as black circles and ^{12}C carbons are white. Uniformly labeled ^{13}C-glucose (U-^{13}C-Glucose) can be metabolized directly through glycolysis or through the pentose phosphate cycle (PPC). Direct metabolism through glycolysis to fructose-6-phosphate (F-6-P) and pyruvate is shown on the left of their respective boxes. The three major labeled F-6-P products from the PPC and the resulting pyruvate molecules are shown on the right of their respective boxes. PPC products resulting from recombination of 2 separate labeled substrates are likely to be rare and have been omitted. m_3 lactate is formed from either direct glycolysis or the PPC, while m_1 and m_2 lactate are only formed from the PPC. TCA cycle metabolism of tracer-derived pyruvate produces $^{13}CO_2$ and ^{13}C-labeled palmitate, however m_1 palmitate derives only from multiple turns through the PPC.

Results

To investigate glucose metabolism in the setting of SLE, we infused 9-mo old autoimmune female NZB/W (Lupus; n=4) and age-matched healthy female Balb/c (Control; n=2) mice with uniformly labeled ^{13}C-glucose tracer for 6 h. Following tracer administration, we analyzed ^{13}C redistribution into metabolites in the plasma and the spleen.

By 6 h after infusing the $^{13}C_6$-glucose tracer, approximately 7% of plasma glucose contained tracer-derived carbon atoms in both lupus and control mice (Figure 2.6 A, $p>0.5$), indicating that tracer administration from the pump and clearance from the bloodstream were similar in lupus and control mice. The fraction of labeled plasma glucose containing a specific number (x) of tracer-derived carbons ($mx/\Sigma m$) was similar in lupus and control mice for each isotopomer (Figure 2.6 B, $p>0.14$ for all x), indicating that cycling through gluconeogenesis was similar in both groups (361).

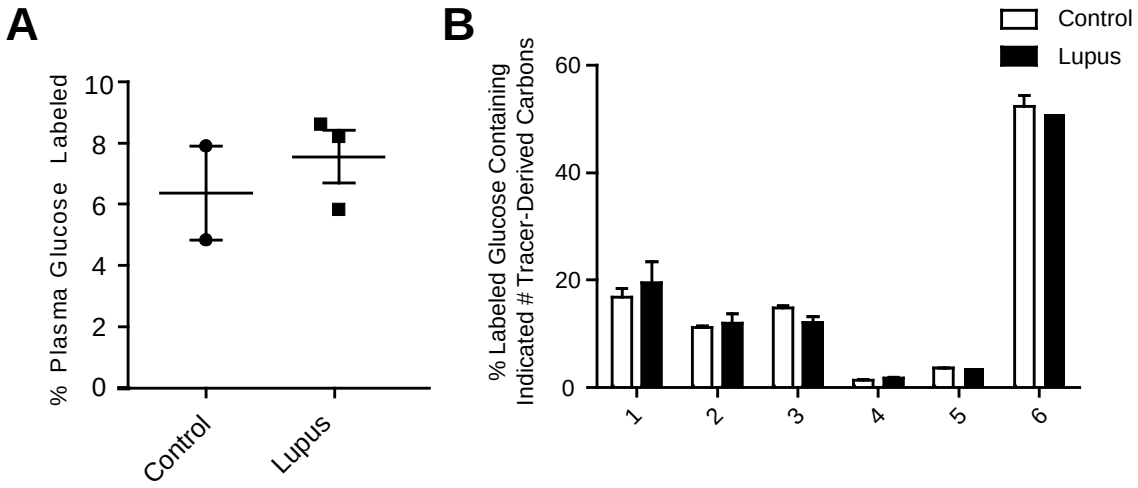

Figure 2.6. Label distribution in plasma glucose. **A**. Fraction of plasma glucose containing tracer-derived ^{13}C. **B.** Percentage of labeled plasma glucose containing the indicated number of tracer-derived ^{13}C atoms. Data are from triplicate samples from two control and three lupus animals.

^{13}C was incorporated into approximately 2% of splenic lactate, 4% of plasma lactate, 1-10% of splenic fatty acids and 4-12% of plasma fatty acids (Table 2.1) indicating that tracer infusion for 6 h is sufficient to allow ^{13}C incorporation into glucose-derived metabolites in both the plasma and the spleen. Only 0.3% of ribose in splenocytes was derived from $^{13}C_6$-glucose tracer in both lupus and control mice, indicating that splenocytes have very slow rates of glucose-derived ribose synthesis, compared to these other metabolites.

Table 2.1. Label distribution in plasma and spleen metabolites. Numbers indicate the percentage of a given metabolite that contains tracer-derived ^{13}C. Data are from triplicate samples from two control and four lupus animals. Numbers in parentheses indicate standard error.

		% Enrichment*	
	Metabolite	Control	Lupus
Plasma	Lactate	4.2 (1.1)	4.3 (0.7)
	Myristate	8.3 (2.5)	11.3 (0.9)
	Palmitate	1.6 (0.1)	1.46 (0.02)
Spleen	Lactate	1.9 (0.4)	1.8 (0.2)
	Myristate	13.0 (0.5)	12.8 (1.2)
	Palmitate	1.2 (0.1)	1.2 (0.1)
	Ribose	0.3 (0.2)	0.3 (0.2)

Splenocyte lactate and CO_2 production. The NZB/W model of lupus is characterized by chronically activated, autoimmune lymphocytes in the spleen (359). If chronically activated lymphocytes selectively increase aerobic glycolysis

and lactate production from glucose (similar to normally activated lymphocytes), ^{13}C enrichment in the lactate pool of lupus splenocytes is expected to be greater than controls. However, the fraction of lactate containing ^{13}C was 1.9% in both groups (Figure 2.7 A, p=0.9), indicating that the relative production of lactate from glucose is the same in lupus and control splenocytes. This finding suggests that lupus and control splenocytes have similar rates of aerobic glycolysis.

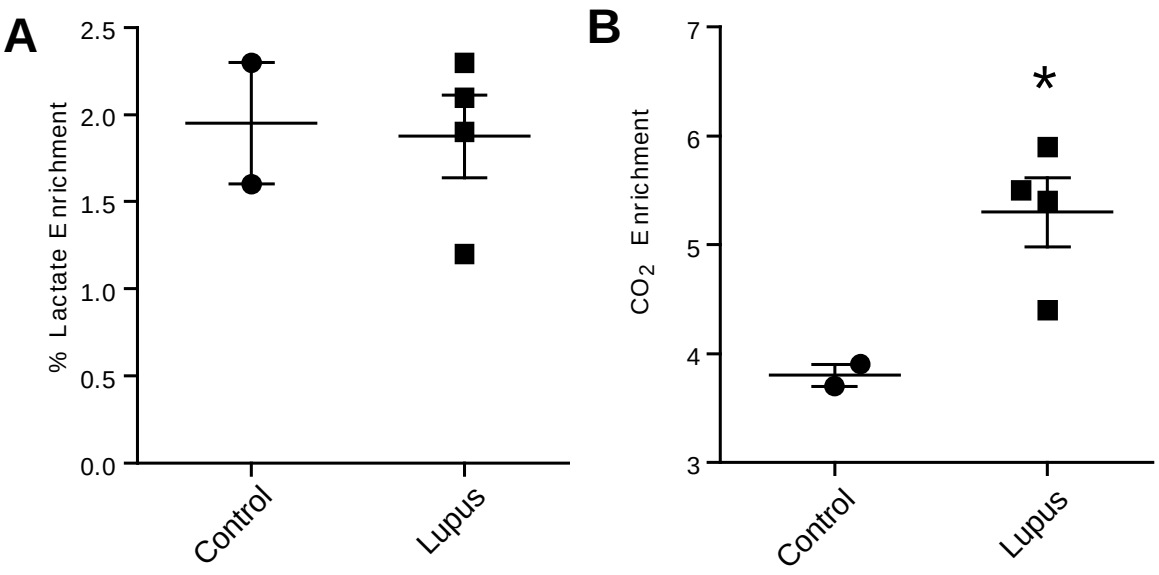

Figure 2.7. Splenic lactate and CO_2 enrichment from lupus and control mice. **A**. Percentage of splenic lactate containing tracer-derived ^{13}C. **B**. Splenic CO_2 containing tracer-derived ^{13}C ($\delta^{13}CO_2$). * $p<0.04$. Measurements were made in triplicate for each mouse and each data point represents the average for a single mouse.

The amount of ^{13}C-label in CO_2 was 40% higher in the spleens of lupus mice compared to controls (Figure 2.7 B, $p<0.04$). This finding indicates that more ^{13}C-labeled glucose tracer is oxidized in the splenocytes of lupus mice than in controls.

Isotopomer distribution of splenic lactate and fatty acids. Glucose oxidation can occur in either the pentose phosphate cycle, where it produces NADPH, or in the TCA cycle, where it drives NADH and ATP production through the electron transport chain (362). We assessed pentose phosphate cycle (PPC) activity by measuring carbon-labeling patterns in both lactate and fatty acids (363-365). The fraction of labeled lactate containing one ($m_1/\Sigma m$) or two ($m_2/\Sigma m$) atoms of ^{13}C indicates cycling through the PPC, while lactate containing 3 atoms ($m_3/\Sigma m$) can be produced from direct glycolysis or the PPC (Figure 2.5, (363-365)). Lactate $m_1/\Sigma m$, $m_2/\Sigma m$ and $m_3/\Sigma m$ do not differ significantly between lupus and control spleens (Figure 2.8 A, $p>0.2$ for each species), arguing that PPC activity is similar in both strains.

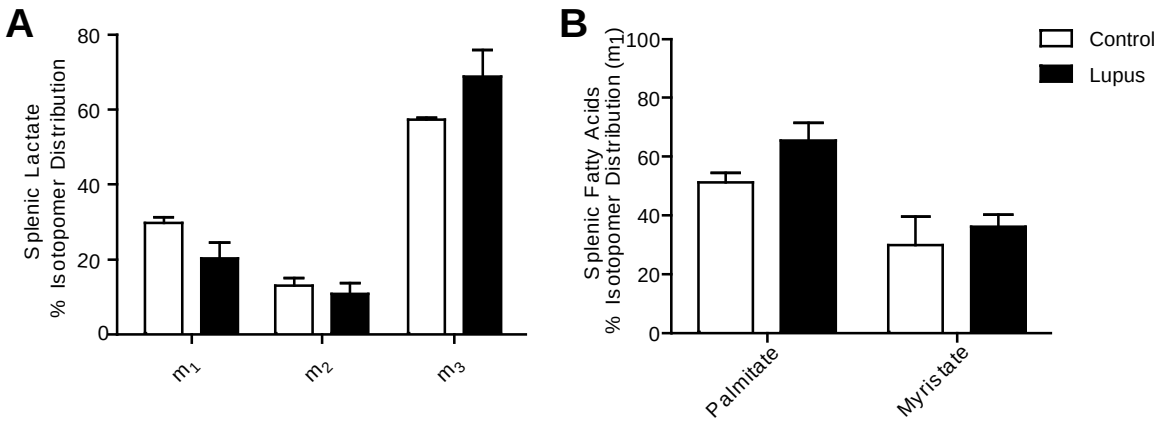

Figure 2.8. Splenic lactate and fatty acid isotopomer patterns reflecting carbon cycling through the pentose phosphate cycle. A. Percentage of labeled splenic lactate containing 1 (m_1), 2 (m_2), or 3 (m_3) tracer-derived ^{13}C atoms. **B**. Percentage of labeled splenic palmitate or myristate containing 1 tracer-derived ^{13}C atom. Data are from triplicate samples from two control and four lupus animals.

The analysis of ^{13}C labeling patterns in fatty acids provides a second, independent measure of PPC activity. Glucose-derived carbons are incorporated into fatty acids when citrate is exported from the mitochondria and converted into acetyl-CoA by ATP-citrate lyase (52). Acetyl-CoA formed in this manner will contain a single tracer-derived ^{13}C only following multiple turns of the PPC (Figure 2.8). Thus, the fraction of a given labeled fatty acid that contains a single tracer-derived ^{13}C ($m_1/\Sigma m$) is indicative of the relative activity of the pentose phosphate cycle. Splenic palmitate and myristate show similar $m_1/\Sigma m$ values in both lupus and control mice, which indicates that the ratio of the pentose phosphate cycle to glycolysis is the same in both strains (Figure 2.8 B, $p>0.2$). Because both lactate and fatty acid labeling patterns suggest that PPC activity is similar in lupus and control splenocytes, the increase in tracer-derived CO_2 in lupus splenocytes likely results from increased glucose oxidation by the TCA cycle.

Metabolic parameters of chronic lymphocyte activation. Chronically activated lupus splenocytes up-regulate oxidative metabolism rather than glycolysis, which is markedly different than the highly glycolytic metabolism characteristic of acutely activated lymphocytes (59, 207, 251, 252). Because chronically activated human lymphocytes lose expression of cell surface receptors that activate aerobic glycolysis (59, 360), we hypothesized that the reliance on OXPHOS observed in lupus splenocytes could result from chronic activation. Recently, a cell culture model of chronic lymphocyte activation was described (360, 366), in which human peripheral blood T cells are acutely

stimulated with PHA and then repetitively stimulated with irradiated allogeneic PBMCs. Cells become chronically activated and lose expression of CD28, a key signaling molecule that is required for activation-induced increased aerobic glycolysis (59). We used this model system to test the hypothesis that, compared to acute stimulation, chronic stimulation decreases aerobic glycolysis. Acutely stimulated $CD8^+$ or $CD4^+$ T cells have rates of lactate production and oxygen consumption (Figures 2.9 and 2.10) higher than rates established for unstimulated mouse (206, 245) or human (251) lymphocytes. However, chronically stimulated T cells have rates of lactate production that are 60% lower than acutely activated controls, while rates of oxygen consumption are equivalent (Figures 2.9 and 2.10). During both acute and chronic activation, $CD8^+$ T cells have higher rates of oxygen consumption and lactate production than $CD4^+$ T cells, which may relate to the increased proliferative capacity observed in antigen-stimulated $CD8^+$ T cells (367-369).

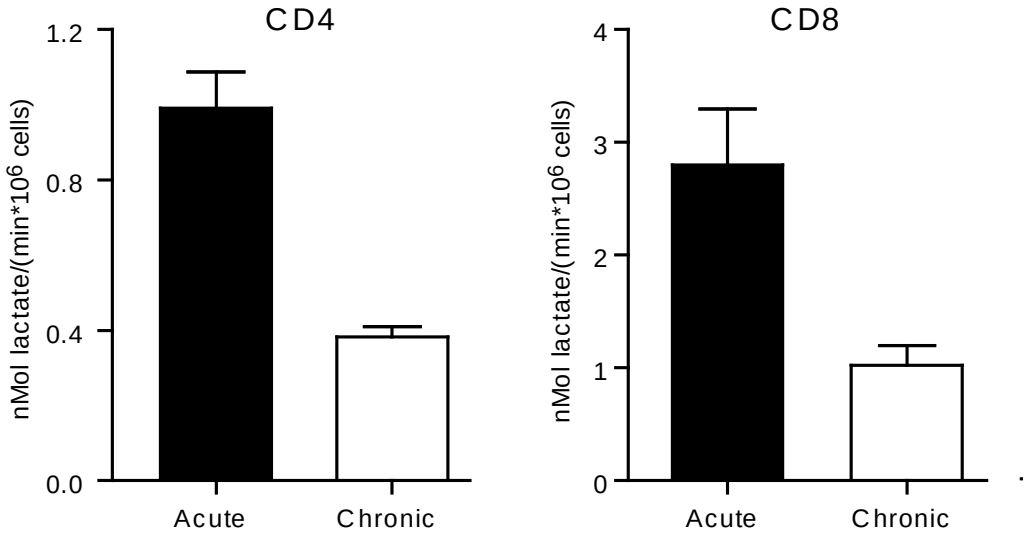

Figure 2.9. Lactate production under conditions of acute and chronic stimulation. CD4 results are from three independent measurements from two separate cultures. CD8 acute is from a single culture. CD8 chronic is from two independent cultures. Error bar reflects standard deviation in the slope of lactate production over time.

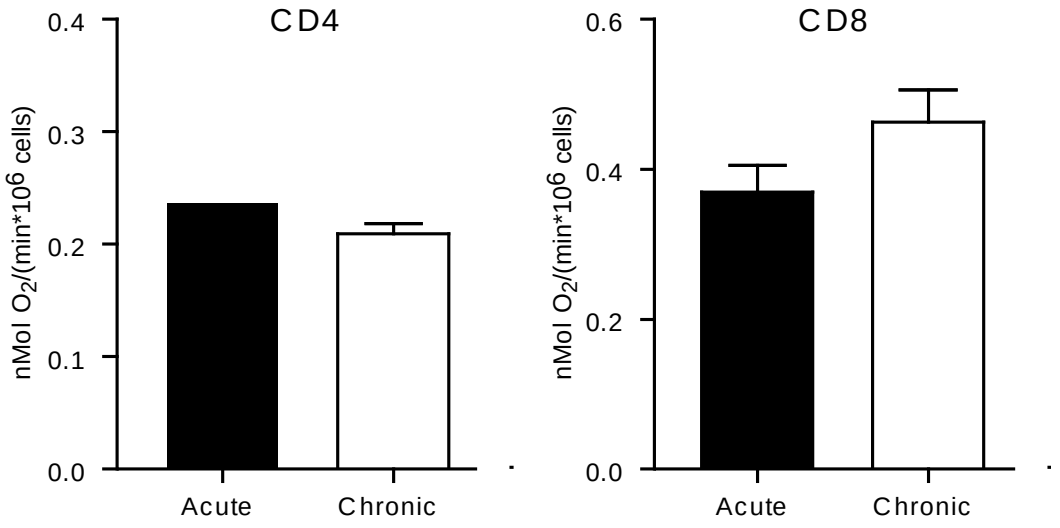

Figure 2.10. Oxygen consumption under conditions of acute and chronic stimulation. CD4 results are from one (acute) or three (chronic) measurements from two separate cultures. CD8 results are from three (acute) or four (chronic) measurements from three separate cultures.

Based on these measurements, ATP production from aerobic glycolysis and OXPHOS was calculated (247). The acutely stimulated T cells meet 50% of their demand for ATP through glycolysis, while chronically stimulated T cells produce only 20-30% of their ATP through this pathway (Figure 2.11). As a result, OXPHOS meets a greater share of the demand for ATP in the chronically stimulated T cells.

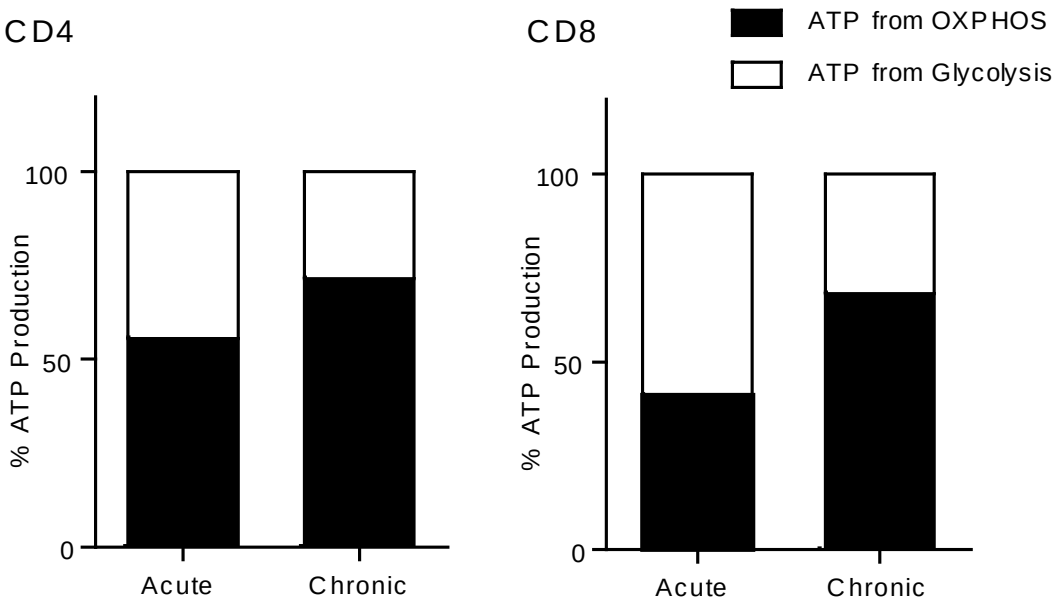

Figure 2.11. ATP production during acute and chronic stimulation. ATP production from OXPHOS and gylcolysis calculated as follows: ATP_{OXPHOS}=5.6 x O_2 consumption (nMoles/(min x 10^6 cells)) and $ATP_{Glycolysis}$=lactate production (nMoles/(min x 10^6 cells))+ 0.4 x O_2 consumption (nMoles/(min x 10^6 cells)) (142).

Discussion

Metabolic changes during acute lymphocyte activation. In the absence of activating signals, quiescent lymphocytes have low rates of oxidative metabolism (207). For example, resting thymocytes take up glucose at a low rate (0.07 nMoles/(min x 10^6 cells)) and oxidize approximately 15% of it into CO_2 (63). ATP generated by resting B and T cells is primarily used for housekeeping functions including ion pumping and protein synthesis (245, 370). When activated, lymphocytes rapidly increase the activity of ATP-requiring processes such as fatty acid and nucleic acid synthesis and calcium signaling (245). In lymphocytes activated by mitogens or stimulatory antibodies, this increased demand for ATP is met by increasing aerobic glycolysis (59, 251, 252, 266). In this pathway, glucose carbons are converted to lactate and secreted from the cell rather than entering the mitochondria for oxidation (207). For example, rat thymocytes stimulated for 2-3 d with concanavalin A (conA) increase glucose utilization 50-fold and lactate production 40-80-fold compared to unstimulated cells (62, 63, 206, 252). In contrast to resting thymocytes, conA–stimulated thymocytes convert only 0.8% of imported glucose into CO_2, while 90% is converted to lactate (63).

T cell activation in response to most infectious pathogens is an acute process initiated by stimulation of TCRs and co-stimulatory receptors such as CD28 (207). Indeed, it is these stimulatory signals through the TCR and CD28 that mediate the metabolic changes observed in acutely activated T cells (69). When human $CD4^+$ T cells are stimulated by bead-bound anti-CD3 and anti-

CD28 antibodies, they phosphorylate AKT and increase the expression of GLUT1 6-7-fold (59). These changes are accompanied by a 15-20-fold increase in glycolysis and lactate production (59). However, increased glycolysis and lactate production are not observed if the CD28 signal is omitted (59).

While the ability of CD28 costimulation to increase glucose metabolism has been attributed to signaling through AKT (59, 207, 255), recent studies in murine $CD4^+$ T cells suggest that AKT-independent processes may also be involved (Figure 2.12) (58). A strong signal (i.e., 5 μg/ml of anti-CD3 antibody) through the TCR alone increases total cellular levels of GLUT1 by 5-fold, but has little effect on cellular glucose uptake (58). When a strong TCR signal is accompanied by either costimulation through CD28 or the expression of a constitutively active form of AKT (myristoylated AKT, myrAKT), GLUT1 expression increases by an additional 30%, but glucose uptake increases 2-3-fold compared to cells stimulated through the TCR alone (58). These results suggest that, when signaling through the TCR is strong, AKT activation and CD28 signaling primarily function to increase the activity or surface localization of GLUT1, rather than increasing its total expression (58). Lowering the strength of stimulus through the TCR (i.e., 1 μg/ml of anti-CD3 antibody) shows that CD28 signaling affects glucose metabolism through both AKT-dependent and AKT-independent pathways. In the context of a low TCR signal, CD28 stimulation can increase total cellular GLUT1, but expression of constitutively active AKT cannot. These observations suggest that AKT-independent signaling downstream of CD28 can increase GLUT1 expression when TCR stimulation is low, while AKT

primarily functions to increase the activity and surface localization of GLUT1 (Figure 2.12) (58). In addition to regulating activity and surface trafficking, activated AKT promotes glycolysis by increasing hexokinase activity (75, 230) and enhancing phosphofructokinase activity by phosphorylating and activating the regulatory enzyme 6-phosphofructo-2-kinase (82, 231).

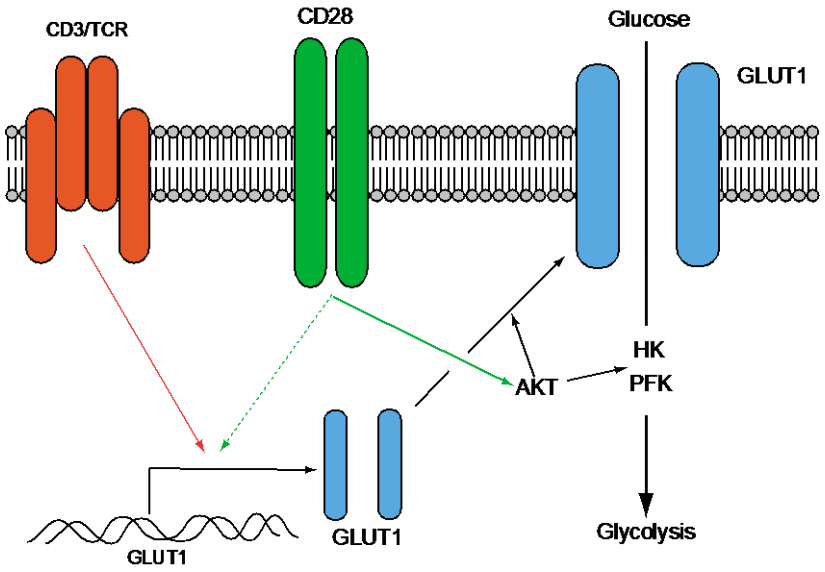

Figure 2.12. Effects of CD3, CD28 and AKT signaling on GLUT1 expression and glycolysis. Signaling through CD3 stimulates GLUT1 expression, but not its surface localization or glucose uptake. AKT-independent signaling through CD28 can augment CD3-mediated increases in GLUT1 expression. AKT functions primarily to increase the activity and surface localization of GLUT1 and stimulate glycolytic enzymes such as hexokinase (HK) and phosphofructokinase (PFK). From (58, 69, 82, 231).

While signaling through CD28 and AKT increases T cell glycolysis, signaling through negative costimulatory receptors such as PD-1 or CTLA-4 inhibits glycolytic metabolism in activated T cells. Signaling through PD-1 decreases T cell glycolysis by inhibiting the activity of PI3-K, thus decreasing

levels of phospho-AKT (255). Similarly, signaling through CTLA-4 decreases T cell glycolysis by increasing the activity of the serine/threonine phosphatase PP2A, which dephosphorylates AKT (255).

Hypoxia-inducible factor 1α (Hif-1α) may also play a role in the glycolytic metabolism of acutely activated T cells (Figure 2.13). Mouse T cells stimulated with anti-CD3 antibodies for 24 h increase HIF-1α expression 5-15 fold at both normoxia (20% O_2) and hypoxia (1% O_2) (371). Studies using Hif-1α deficient T cells suggest that changes in Hif-1α levels regulate the overall rate of glycolysis and determine the fate of glucose-derived carbons in activated T cells. Indeed, murine T cells lacking Hif-1α utilized 2-3-fold less glucose and produced 2-fold more lactate following stimulation with anti-CD3 and anti-CD28 antibodies than did wild type T cells (372). Conversely, Hif-1α deficient T cells converted 5-fold more glucose into lipid than did wild type T cells (372). Because glucose-derived lipid synthesis requires carbons to enter the mitochondria (52, 53, 78), this observation suggests that activated T cells lacking Hif-1α preferentially shuttle glucose-derived carbons into the mitochondria, rather than secreting them as lactate. This hypothesis is supported by studies using FL5.12 cells, a non-transformed IL-3-dependent lymphoid cell line (373). FL5.12 cells lacking Hif-1α produce 10-20-fold less lactate and convert 2-3-fold more glucose into lipid than wild type cells (372). Furthermore, Hif-1α deficient FL5.12 cells showed a 2-3-fold increase in $\Delta\psi_m$ and a 40-80% increase in O_2 consumption compared to wild type cells, both of which are consistent with increased carbon entry into the mitochondria (372). These observations are likely due to the ability of Hif-1α to

increase the transcription of lactate dehydrogenase (LDH) (74, 374) and its ability to inhibit pyruvate dehydrogenase (PDH) by increasing the transcription of PDH-kinase (PDH-k), which phosphoryates and inhibits PDH (Figure 2.13) (121, 375).

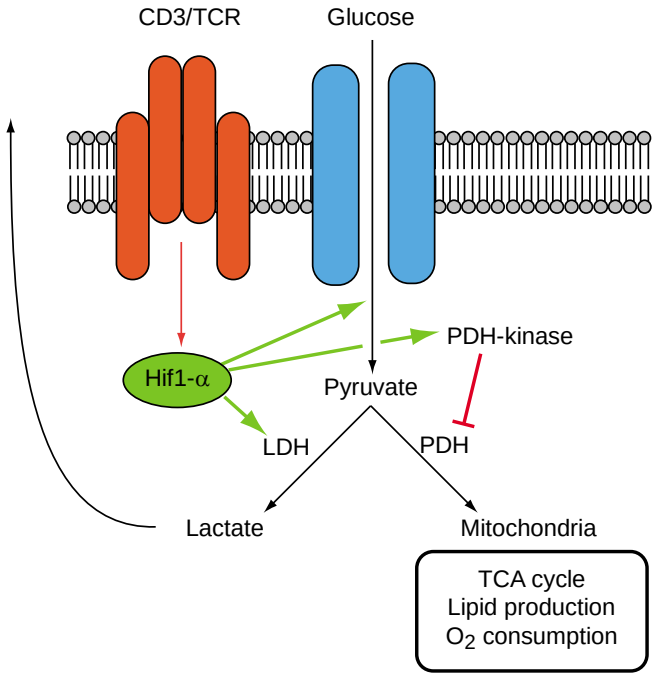

Figure 2.13. Hif-1α signaling in activated T cells. T cells increase Hif1-α levels following stimulation through the TCR. Hif1-α promotes activated T cell glycolysis and lactate production and decreases mitochondrial metabolism. These actions are likely due to the ability of Hif1-α to increase the activity of LDH and inhibit PDH by activating PDH-kinase, which phosphorylates and inhibits PDH (74, 121, 371, 372, 374, 375).

In addition to producing ATP, high rates of aerobic glycolysis supply acutely activated T cells with substrates used by the pentose phosphate cycle to generate NADPH, which maintains the reducing potential of the cellular glutathione pool (50). Indeed, human lymphocytes stimulated with conA in media

containing 11 mM glucose increase glutathione levels by 2-fold over 2-4 d (344). Decreasing glycolysis inhibits the ability of cells to produce glutathione and detoxify reactive oxygen species (ROS). For example, decreasing the concentration of glucose in media from 10 to 1 mM increases ROS production 3-fold in rat thymocytes stimulated by conA as measured by luminal chemiluminescence (376). Similarly, culturing astrocytes in media lacking glucose decreases reduced glutathione levels by 75% within 12 h, while cells grown in media with 5.5 mM glucose maintain glutathione levels within 80-90% of initial levels (343).

Metabolic changes during chronic stimulation. While it is clear that acutely activated lymphocytes dramatically increase glycolysis, the understanding of glucose metabolism in chronically activated lymphocytes in the setting of autoimmunity is limited. However, there is indirect evidence that these cells rely on mitochondrial metabolism rather than aerobic glycolysis as their principle route of ATP synthesis. Increased ROS and markers of oxidative stress have been observed in the serum and tissues of patients with lupus (377), psoriasis (337) and RA (336). For example, the serum of lupus patients contains 30% more hydrogen peroxide (H_2O_2) compared to healthy controls (377). Because ROS are generated during oxidative phosphorylation (378), high levels of ROS and oxidative stress are consistent with an increased dependence on mitochondrial metabolism. However, because these measurements were made in non-lymphoid tissue, they may not directly reflect the metabolism of autoreactive lymphocytes.

Fortunately, several studies have directly measured ROS and antioxidant levels in lymphocytes during SLE. Studies directly analyzing lymphocytes from lupus patients reveal a 20-40% increase in O_2^- levels and $\Delta\psi_m$ compared to healthy controls, both of which are consistent with increased OXPHOS (379). Furthermore, lymphocytes from patients with active RA and lupus consume 25% more oxygen than those from healthy controls (335). Additionally, T cells from patients with SLE have 30% less total cellular reduced glutathione (GSH) than cells from healthy controls (339), while T cells from MRL/*lpr* mice with lupus have 4-fold less GSH than controls (380). These observations suggest that the activity of glycolysis and the pentose phosphate cycle may be insufficient to maintain GSH levels in lupus lymphocytes (50).

To explore the metabolism of chronically activated lymphocytes *in vivo*, we infused uniformly labeled ^{13}C-glucose into NZB/W mice and measured ^{13}C redistribution into products of both aerobic and anaerobic metabolism by GC-MS (363). This technique has been used previously to investigate both oxidative and non-oxidative glucose metabolism (361, 363). Our results indicate that splenocytes from 9 month-old NZB/W mice with active lupus up-regulate glucose oxidation 40% compared to non-autoimmune controls but appear to have similar levels of glucose to lactate conversion and pentose phosphate cycle activity. It is unclear what signaling pathways contribute to increased oxidative metabolism in chronically activated lupus splenocytes. However, T cells from lupus patients have a 40% increase in $[Ca^{2+}]_m$ (302), which is known to stimulate TCA cycle activity leading to NADH production and ROS generation (123, 254, 260). TCA-

induced ROS production is presumed to be a consequence of hyperpolarization of $\Delta\psi_m$ (254, 381), a characteristic identified in lupus lymphocytes (379).

Increased AKT activity could also contribute to increased TCA cycle activity in lupus splenocytes. Splenocytes from both MRL/*lpr* and B6.*Sle1b.lpr* mice with lupus-like disease have 2-6-fold more phospho-AKT than control splenocytes (382, 383). This observation is noteworthy, as active AKT stimulates oxidative metabolism. For example, mouse embryonic fibroblasts (MEFs) that express a constitutively active form of AKT consume 50% more O_2 than do control cells (232). This increased oxidative metabolism could be due to the ability of AKT to stimulate mTORC1, which can increase mitochondrial biogenesis and O_2 consumption (247, 384, 385). Compared to control cells, MEFs with constitutively active AKT also showed a 60% increase in ROS as measured by the dye dichlorofluorescein (DCF) (232), which becomes fluorescent upon its oxidation by a variety of ROS including hydroxyl radicals ($OH\cdot$) and H_2O_2 (386). Thus, increased AKT activity in lupus lymphocytes could contribute to their increased oxidative activity and ROS levels. Interestingly, the expression of constitutively active AKT sensitizes MEFs to apoptosis induced by the addition of exogenous H_2O_2 (232). This observation suggests that lupus lymphocytes might have increased sensitivity to ROS-mediated apoptosis.

While lupus splenocytes up-regulate oxidative glucose metabolism, lymphocytes responding to normal receptor stimulation primarily rely on glycolysis (59, 251, 266). Since, autoimmune B and T cells are chronically activated, we reasoned that the difference in metabolism might arise from

differences in the duration of antigen stimulation and the resulting activation. To investigate this possibility, we repetitively stimulated human T cells *in vitro* to generate a chronically activated phenotype characterized by loss of CD28 expression (366), which mimics the pathologic $CD28^-$ lymphocyte subset found in several chronic inflammatory diseases including RA and lupus (351, 360, 366). These T cells lose CD28 expression due to transcription factor inactivation resulting from chronic stimulation (387). In comparison to the glycolytic phenotype observed in T cells in response to acute stimulation, repetitive stimulation of CD4 and CD8 decreases lactate production and promotes a reliance on oxidative ATP production. These observations suggest that chronic stimulation promotes metabolic adaptations that limit glycolysis and increase OXPHOS, which mirrors the metabolic phenotype found in splenocytes from lupus mice.

Possible explanation for differing bioenergetics of acute and chronic stimulation. These observations raise the question of why glycolysis is restricted during chronic stimulation. Chronic stimulation decreases expression of CD28 and increases the expression PD-1 and CTLA-4 (387-389). Signaling through CD28 activates AKT and increases GLUT1 expression, glucose uptake, and lactate production. Conversely, signaling through PD-1 or CTLA-4 decreases AKT phosphorylation and decreases glucose uptake and glycolysis (59, 255). It is possible that loss of CD28 or increased signaling through PD-1 or CTLA-4 due to chronic stimulation decrease anaerobic metabolism via reduced signaling through this pathway. However, chronically activated lupus lymphocytes display

increased AKT phosphorylation compared to wild type (WT) cells (383, 390, 391), and inhibiting the PI3-K/AKT pathway alleviates disease in the MRL/*lpr* model of lupus (382). Thus, decreased lactate production in chronically activated lymphocytes occurs in the context of an active AKT pathway.

This observation suggests that chronically activated lymphocytes may have low activity of other molecules involved in the regulation of glycolysis. Hif-1α is such a candidate, due to its potent ability to stimulate glucose uptake and lactate secretion in acutely activated T cells (372). Importantly, Hif-1α is not required for autoimmune responses. Indeed, mice lacking Hif-1α in their T and B cells spontaneously develop a lupus-like phenotype characterized by anti-dsDNA antibodies and proteinuria (392). Furthermore, many of the mitochondrial characteristics of lupus lymphocytes, such as increased $\Delta\psi_m$ and O_2 consumption, are recapitulated when siRNA are used to decrease Hif-1α in IL-3-stimulated lymphoid cells (372).

Based on these observations, decreased lactate production in chronically stimulated lymphocytes may be due to low Hif-1α activity rather than low signaling through AKT (Figure 2.14). The activities of both Hif-1α and AKT are low in unstimulated lymphocytes, and these cells have low rates of glucose utilization, lactate production and mitochondrial metabolism (59, 255, 371) (Figure 2.14). Acutely activated lymphocytes have active Hif-1α (371) and AKT (59, 255), which leads to high rates of glucose utilization (59, 231). Most of the pyruvate formed in acutely activated lymphocytes is converted into lactate and secreted (62). However, because so much pyruvate is formed, the *net* entry of

pyruvate into the mitochondria is *increased* in acutely activated lymphocytes compared to unstimulated cells (123). Chronically activated lymphocytes are proposed to have active AKT, but not Hif-1α. This combination of signaling pathways results in a net utilization of glucose that is increased compared to unstimulated cells, but lower than the glucose utilization of acutely activated cells (Figure 2.14). However, the proposed lack of active Hif-1α in chronically stimulated lymphocytes directs the majority of pyruvate into the mitochondria and flux through LDH is low. Confirmation of this model will require the direct assessment of AKT and Hif-1α activity in acutely and chronically stimulated lymphocytes.

This model is consistent with our observations of low lactate production and increased mitochondrial metabolism observed in chronically activated lymphocytes. While it is clear that lupus lymphocytes have increased AKT activity, it is unclear if chronically-activated, $CD28^-$ human T cells have high levels of phospho-AKT. While signaling through CD28 is a well characterized pathway to increase phospho-AKT in T cells (59), several CD28-independent pathways also increase phospho-AKT. Indeed, stimulation with the cytokine IL-2, which is present in chronic-stimulation cell culture conditions, increases AKT phosphorylation in cell lines and primary T cells (393, 394). It is possible that cytokine signaling maintains phospho-AKT levels in $CD28^-$ T cells.

In summary, our data show that splenocytes from autoimmune mice with active disease along with chronically stimulated human T cells, which model pathogenic autoimmune lymphocytes, rely on OXPHOS for a greater share of

ATP synthesis than lymphocytes acutely responding to receptor stimulation. These findings suggest that modulating OXPHOS should have therapeutic effects against autoimmune diseases. In support of this hypothesis, Bz-423, a small molecule that modulates the F_oF_1-ATPase leading to redox-regulated apoptosis, has robust efficacy in models of autoimmune disease with minimal effects on normal immune function (169, 395). Its ability to treat autoimmune disease while sparing normal immune functions may result from differences in the metabolism and redox balance between autoimmune, resting and acutely activated lymphocytes. Thus, measurement and manipulation of glycolytic and oxidative metabolism warrant further investigation as novel diagnostic and therapeutic strategies for immune disorders.

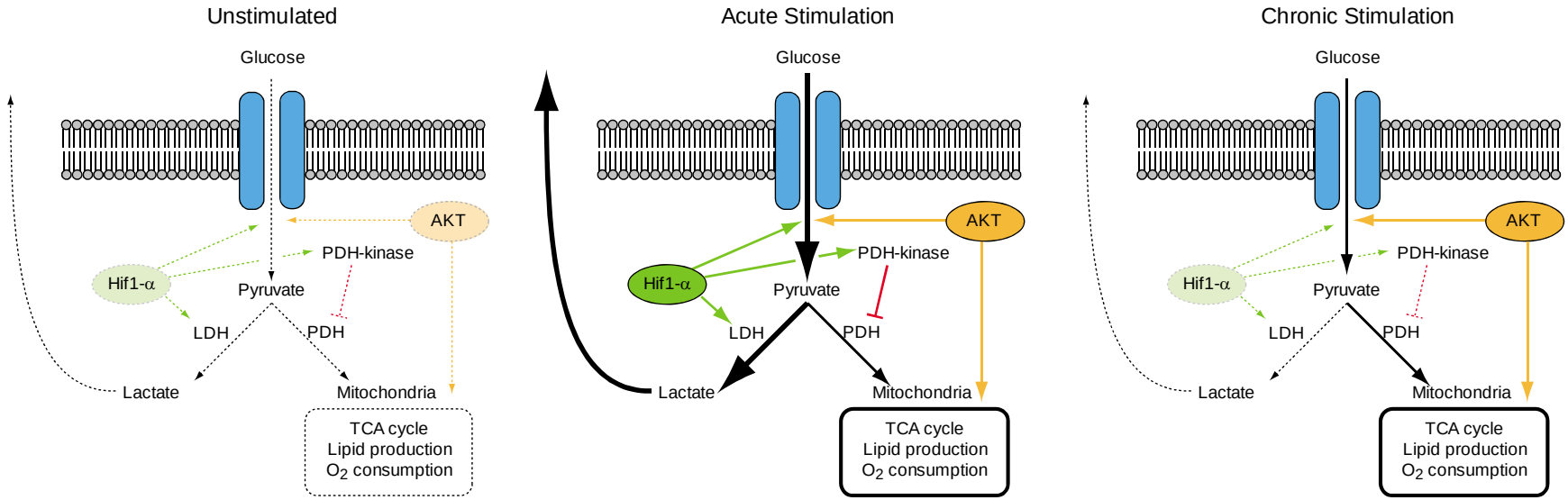

Figure 2.14. Model of AKT and Hif-1α signaling and glucose metabolism in unstimulated, acutely stimulated and chronically stimulated lymphocytes. Details of the model are provided in the text.

Materials and Methods

Lupus mice and tracer administration. 9-mo old autoimmune female NZB/W (Lupus; n=4) and age-matched healthy female Balb/c (Control; n=2) mice were purchased from Jackson Laboratories and cared for according to the Guidelines for Laboratory Animal Medicine at the University of Michigan. The number of mice used is consistent with the literature standard of 3-5 for similar isotopomer studies (357, 396-398). Mice were fasted for 24 hours prior to tracer administration to normalize energy stores. Uniformly labeled ^{13}C-glucose (50 mg, Cambridge Isotope) was dissolved in water (200 μL) and administered as a continuous infusion (8 μL/h) using a subcutaneously implanted Alzet osmotic minipump for 6 h.

Sample preparation. After 6 h tracer administration, animals were euthanized and blood samples were collected by cardiac puncture and spleens were harvested and frozen at -80°C. Samples were shipped to SiDMAP (Los Angeles, CA) and derivitization and gas chromatography-mass spectrometry (GC-MS) were performed as described (399). Lactate was isolated from HCl acidified tissue homogenate or plasma with ethyl acetate and derivatized to its n-propylamide-heptafluorobutyric ester for GC-MS analysis. Fatty acids were extracted from plasma or tissue using petroleum ether and methylated with methanolic-HCl for GC-MS analysis. CO_2 was obtained by adding concentrated HCl to tissue or plasma and directly analyzed by GC-MS.

Gas chromatography/mass spectrometry (GC/MS). A HP5973 mass selective detector and a HP6890 gas chromatograph were used to collect mass spectral data. The settings were as follows: GC inlet 250 °C, transfer line 280 °C, MS source 230 °C, MS Quad 150 °C. An HP-5 capillary column was used for lactate analysis.

Cell Culture. Peripheral blood mononuclear cells (PBMCs) were isolated from healthy donors and $CD4^+$ or $CD8^+$ subsets were isolated using magnetic beads (Miltenyi Biotec, Auburn, CA, USA) according to the manufacturer's protocol yielding purities above 95%. Cells were initially stimulated with phytohemagglutinin (PHA; 1μg/mL) and were cultured in complete RPMI media supplemented with IL-2 (10ng/mL; PeproTech, Rocky Hill, NJ, USA). Cells were restimulated weekly with irradiated allogeneic PBMC at a ratio of 1 stimulator cell to 2.5 responder cells as described (366). For $CD8^+$ and $CD4^+$ cultures, acute stimulation measurements were made 1 and 3 weeks after beginning culture, respectively. Chronic stimulation measurements were made 5 weeks after beginning culture when the cells were typically ~50% $CD28^-$.

Oxygen Consumption and Lactate Production. Cells were resuspended at ~5 x 10^6 cells/mL in complete RPMI media and analyzed at 37 °C using a Clarke electrode. Cells were treated with oligomycin (1-2 μg/ml) to confirm that oxygen was being consumed for ATP synthesis. To measure lactate production, cells were washed and resuspended in DMEM (5-15 x 10^6 cells/mL) and aliquots were quenched at four time points over 2-3 hours using perchloric acid (0.6 M). After removal of cellular debris and neutralization with NaOH, lactate concentrations at

≥3 time points were determined by incubating aliquots of sample (10-20 μL) with lactate dehydrogenase (LDH; 1 μL) and glutamate-pyruvate transaminase (0.375 μL; Sigma Aldrich) in buffer (230-240 μL) containing glutamate (116 mM) and NAD (0.96 mM) at pH 8.9. Lactate levels were determined using a standard curve by monitoring absorption at 340 nM and the rate of lactate production was calculated as a function of time and cell concentration (142). ATP production was calculated as ATP_{OXPHOS}=5.6 x O_2 Consumption and $ATP_{Glycolysis}$=Lactate Production + 0.4 x O_2 Consumption (142)

Data Analysis. GC/MS spectra were analyzed to determine ^{13}C enrichment as described (400). Mass spectral data were generated using three independent injections per animal sample. ^{13}C enrichment in CO_2 was compared to a standard breath and reported as $\delta^{13}CO_2$, which equals [($^{13}C/^{12}C$ sample)/($^{13}C/^{12}C$ standard)-1]x10^3 (401). Enrichment in other metabolites is reported as % enrichment or $m_x/\Sigma m$, where m_x is defined as the fraction of a given metabolite containing x tracer derived carbons and Σm is the sum of all m_x for a given metabolite. Thus, $m_x/\Sigma m$ equals the fraction of total labeled metabolite (Σm) that contains x tracer-derived carbons. The distribution of tracer-derived ^{13}C into glucose-derived metabolites was analyzed according to the schematic diagramed in Figure 2.5. Unless otherwise noted, error bars indicate standard error. Statistical analysis was performed using the Student *t* test for unpaired samples. $p<0.05$ was considered significant.

CHAPTER 3

METABOLISM OF ALLOREACTIVE DONOR T CELLS DURING GVHD

Introduction

Hematopoietic stem cell transplant and immune system reconstitution. Hematopoietic stem cell transplant (HSCT) is a procedure primarily used to treat malignant diseases of the immune system (Figure 3.1) (402). Over 17,000 HSCTs were performed worldwide in 2005, most commonly as a treatment for acute myelogenous leukemia (AML; over 6,000 transplants) or acute lymphoblastic leukemia (ALL; over 3,000 transplants) (402). The steps of a successful HSCT include conditioning of the recipient, transfusion of donor stem cells into the recipient, and post-transplant therapy (47). Together, these steps serve to cure any underlying malignancy, ensure engraftment of the donor immune system within the recipient, and minimize the incidence and severity of any immune-mediated graft-versus-host reaction (47).

Prior to transplantation, HSCT recipients undergo preparative conditioning, which eliminates malignant cells involved in the underlying disease and induces immunosuppression to allow graft acceptance (Figure 3.1) (403). Conditioning regimens involve a combination of total body irradiation (TBI) and cytotoxic chemotherapeutics including etoposide, busulfan, cyclophosphamide

and cytosine arabinoside and are termed myeloablative when given at levels that eradicate the host hematopoietic system (404). Stem cells are harvested either directly from the donor's bone marrow or from the donor's peripheral blood following treatment with granulocyte-colony stimulating factor (G-CSF), which induces stem cells to migrate from the bone marrow to the blood stream, and are then transfused into the conditioned recipient (405).

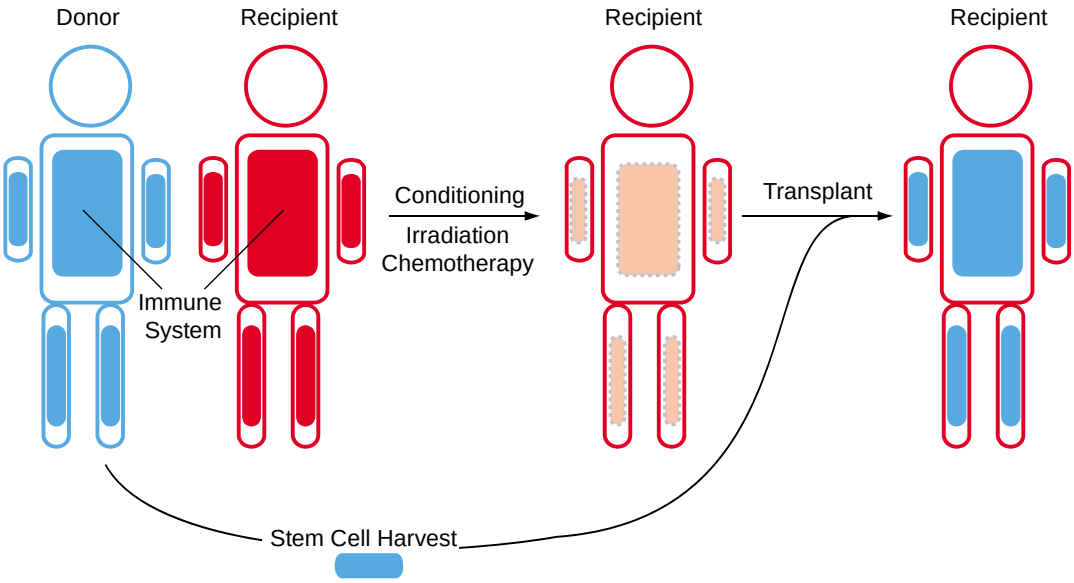

Figure 3.1. Hematopoeitic stem cell transplant. Transplant recipients (red) undergo preparative conditioning, which eliminates the host immune system (solid red). Stem cells harvested from donors (blue) are transplanted into conditioned recipients. The result of the transplant is a recipient (red outline) with a donor-derived immune system (solid blue) (47, 403, 404).

Immediately following myeloablative transplant, recipients undergo a period of severe immunodeficiency during which the host immune system is eliminated while infused donor stem cells proliferate and differentiate to repopulate the host in a process termed engraftment (Table 3.1) (406-409). Neutrophil levels drop from a normal range of 3-6 x 10^9 cells/liter (410) to nearly undetectable levels during this immunosuppressive period, and their recovery is one of the first signs of engraftment (406, 407). The rapid proliferation of neutrophils and neutrophil precursors is stimulated by the cytokine G-CSF (411), and treatment with this cytokine accelerates engraftment following transplant (412). Recipient B and T cell levels also drop as a result of myeloablative conditioning, and their recovery can take 1-2 years (413). T cell repopulation occurs from homeostatic (i.e., antigen-independent) proliferation of mature T cells present in the graft and from maturation of T cells in the thymus following *de novo* generation from the engrafted bone marrow, processes which are both stimulated by the cytokine interleukin 7 (IL-7) (414).

Table 3.1. Immune system recovery following HSCT. From (408, 409).

Cell Type	Estimated Recovery Time
Neutrophils	10-20 d
Monocytes	1 mo
$CD4^+$ T cells	1-2 yr
$CD8^+$ T cells	1 yr
B cells	6 mo
Dendritic cells	6 mo

During the post-transplant period, HSCT patients are at increased risk for infection in part due to their severe leukopenia. Approximately 15-50% of HSCT patients develop bacterial infections within 30 d of transplant (415, 416). Such infections are often caused by gram-positive organisms such as *Streptococcus viridans*, *Staphylococcus aureus, S. epidermidis*, as well as gram-negative organisms such as *Escherichia coli, Klebsiella*, and *Pseudomonas* species (415, 416). Fungal infections are also common early post-transplant (415, 416). A study examining fungal infections post-transplant over a 10 yr period from 1986-96 documented that 12% of pediatric HSCT recipients developed invasive *Candida* or *Aspergillus* infections, which were lethal in 66% of cases (417). Patients treated with high dose methylprednisone (0.25-1 g/day) had a 15-fold increased risk of fungal infection compared to those receiving low doses (2 mg/kg/day), possibly due to the immunosuppressive characteristics of glucocorticoids (417). Viral infections early post-transplant are usually due to the herpes simplex virus (HSV) (415, 416). HSV is typically dormant in immunocompetent individuals, but becomes reactivated in approximately 80% of HSV-positive HSCT patients and typically presents as inflammation of the mouth and gums (gingivostomatitis) (418).

Table 3.2. Common infections at early timepoints post-HSCT. From (415-418)

Type of Infection	Organism		
Gram-positive bacteria	*S. Viridans*	*S. aureus*	*S. epidermidis*
Gram-negative bacteria	*E. coli*	*Klebsiella*	*Pseudomonas*
Fungus	Candida	Aspergillus	
Virus	HSV		

Graft-versus-host disease. In addition to containing stem cells to repopulate the host immune system, HSCT grafts frequently contain donor T cells (47, 48). While the presence of T cells in HSCT grafts decreases infection rates and helps eliminate residual disease (graft-versus-leukemia effect) (419), these cells are also capable of causing graft-versus-host disease (GVHD) (47, 48). The development of GVHD requires mature T cells in the graft, a recipient who cannot reject the T cells, and the expression of antigens in the recipient not present in the donor (48, 420). Donor T cells proliferate in response to foreign recipient peptides in the context of antigen presenting cells (APCs), produce Th_1 cytokines such as IFN-γ, and differentiate into cytotoxic T lymphocytes (CTLs) (Figure 3.2). CTLs mediate tissue damage culminating in clinical GVHD characterized by damage to the skin, liver and gastrointestinal tract (48), and these effects are enhanced by the tissue damage and cytokine release that accompanies recipient conditioning (Figure 3.2) (421). Despite these negative consequences, eliminating T cells from the graft does not improve patient survival following HSCT (422, 423). This observation underscores the beneficial

effects of T cells during HSCT, which include decreased infection rates, improved engraftment, and the elimination of residual disease (422, 423).

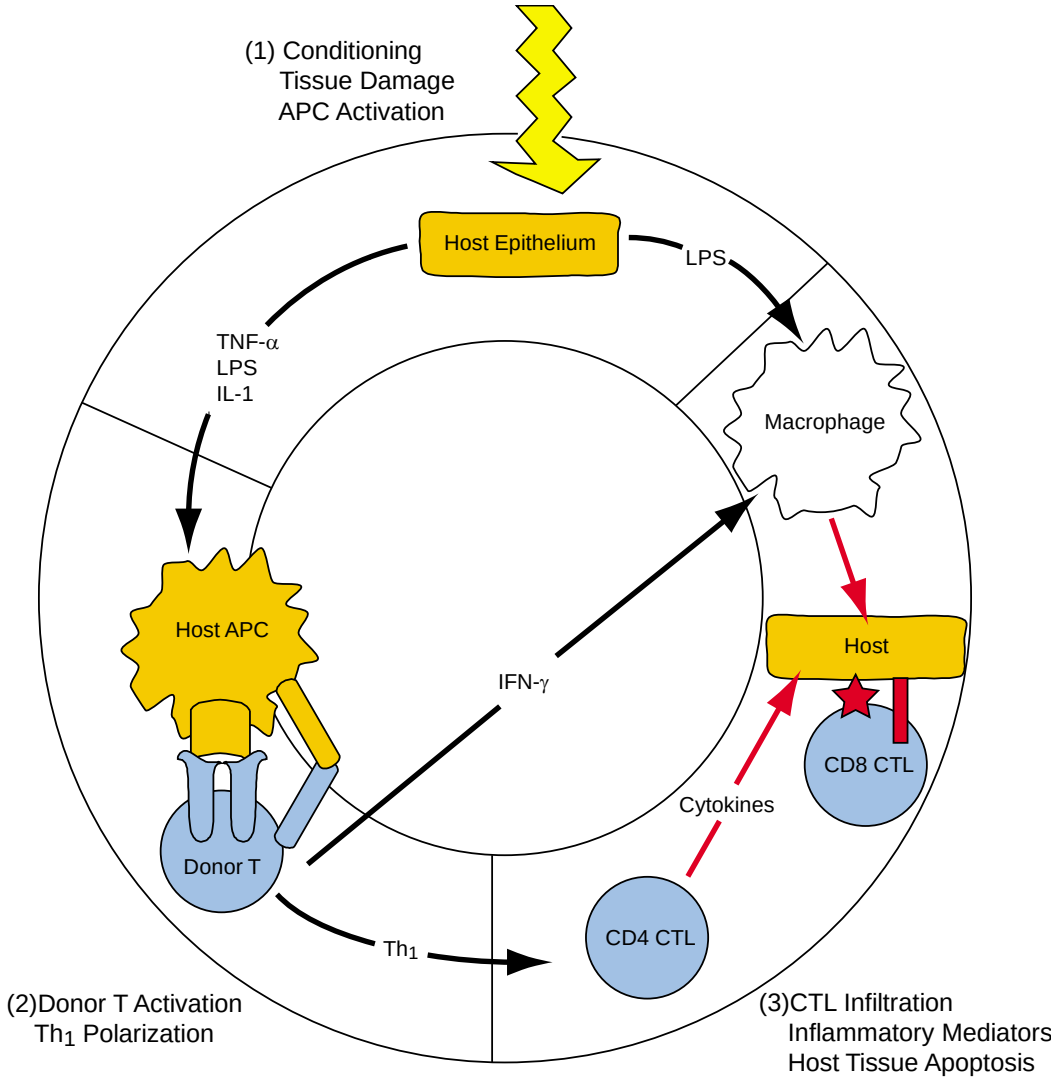

Figure 3.2. GVHD Pathogensis. (1) Conditioning damages host epithelial cells resulting in cytokine production and LPS entry into the bloodstream, which activates host APCs and macrophages. (2) Donor T cells are activated by foreign alloantigen and costimulatory molecules on host APCs and polarize towards a Th_1 cytokine profile. (3) Donor T cells mature into CTLs and, together with activated macrophages, mediate host tissue damage through cyotoxic cytokine production and granzyme B/FASL pathways. Adapted from (48).

Alloantigen recognition. APCs present peptides to T cells in the context of major histocompatibility complex (MHC) molecules on the cell surface (1). Class I MHC molecules are expressed on all nucleated cells and present intracellular antigen to $CD8^+$ T cells, although extracellular antigen can also be presented by class I MHC molecules in a process termed cross presentation (24). Class II MHC molecules are primarily expressed by "professional" APCs (dendritic cells, B cells and macrophages), which sample the extracellular environment and present these peptides to $CD4^+$ T cells on class II MHC molecules (23). GVHD can occur when donor T cells directly recognize MHC molecules as foreign, termed a major histocompatibility mismatch (Figure 3.3) (424). When donor and recipient have identical MHC molecules, donor T cells recognize foreign recipient polymorphic peptide fragments (minor histocompatibility antigens, miHAs) presented on matched MHC molecules. This type of reaction occurs due to genetic diversity between donor and host and is termed a minor histocompatibility mismatch (424).

The type of mismatch present can have a dramatic effect on the overall success of HSCT. A 2007 study showed that of 334 patients undergoing myeloablative transplant between 1993-2003, 54% had developed acute GVHD (grade II or higher) (425). Recipients receiving MHC-matched (6 out of 6 alleles) transplants had a 41% survival rate 3 yr after transplant, while those receiving transplants with > 1 allelic mismatch had only a 23% survival rate (425).

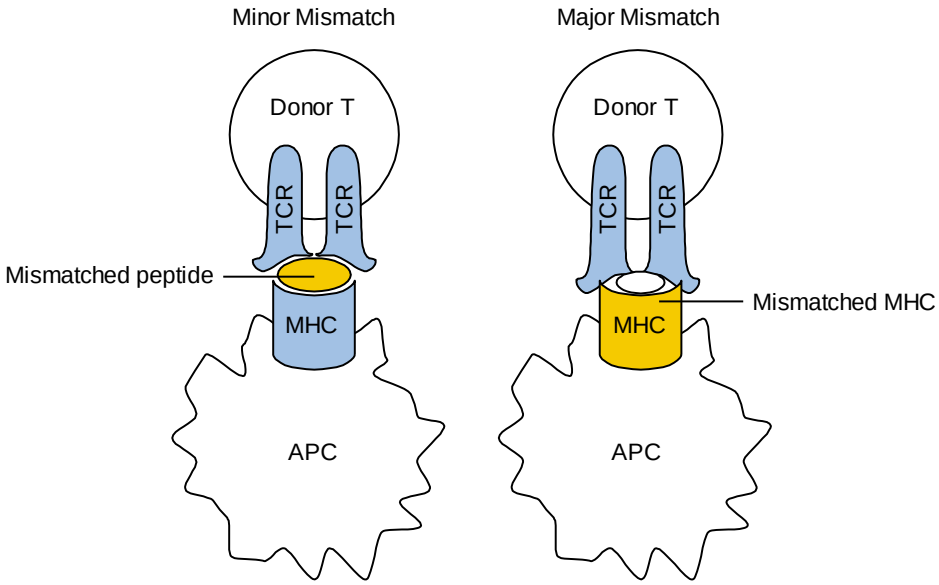

Figure 3.3. Major and minor MHC mismatches. In a minor mismatch (left), the donor and host MHC molecules are matched and donor T cells recognize polymorphic antigens (yellow) in the context of matched MHC (blue). In a major mismatch (right), donor T cells recognize mismatched MHC molecules (yellow). Adapted from (424).

Role of APCs in GVHD. APCs play a critical role in GVHD as they are responsible for the initial activation of donor-reactive T cells (48, 424). When host APCs are eliminated by infusing mismatched NK cells, donor T cells are no longer capable of mediating disease (426). This conclusion is further supported by experiments showing that eliminating host MHC I or MHC II on APCs abrogates CD8 or CD4-mediated GVHD, respectively (427, 428). Interestingly, this study showed that lethal GVHD does not require MHC II expression on host epithelium, indicating that direct T cell receptor (TCR)/MHC II interactions are not necessary during the effector phase of CD4-mediated, MHC class II mismatched

GVHD (428). Of the several types of professional APCs, dendritic cells (DCs) are likely the most important for GVHD initiation, as their infusion (but not that of LPS-activated B cells) is sufficient to induce GVHD in allogeneic transplant recipients that otherwise lacked MHC II on APCs (429).

T cell activation and signaling during (allo)antigen stimulation. During GVHD, signaling through the TCR, costimulatory receptors and cytokine receptors causes T cells to proliferate, secrete proinflammatory cytokines and differentiate into effector T cells (Figure 3.4) (430). TCR signaling causes ζ-chain-associated protein of 70 kDa-(ZAP-70)-mediated linker-of-activated T cells (LAT) and SH2 domain containing leukocyte protein of 76kDa (SLP-76) phosphorylation, which results in phospholipase-C-γ 1 (PLCγ1) activation. PLCγ1 hydrolyzes phosphatidylinositol-3,5-bisphosphate, which causes an increase in diacylglyceride (DAG) and inositol-1,4,5-triphosphate (IP_3) levels (430). DAG activates protein kinase C-θ (PKCθ), an important activator of nuclear factor kappa-light-chain-enhancer of activated B cells (NF-κB), whose deletion reduces GVHD in several models (431). DAG also activates the GTPase Ras, which initiates signaling through the mitogen-activated protein kinase (MAPK) pathway resulting in extracellular signal-regulated kinase 1 (ERK1) and ERK2 activation (430). Activated ERK1 and ERK2 stimulate the activities of activator protein 1 (AP-1) and signal transducer and activator of transcription 3 (STAT3), both of which promote gene transcription in activated T cells (430). ERK1 and ERK2 become phosphorylated during GVHD, and their inhibition with a small molecule results in decreased alloresponses *in vitro* (432).

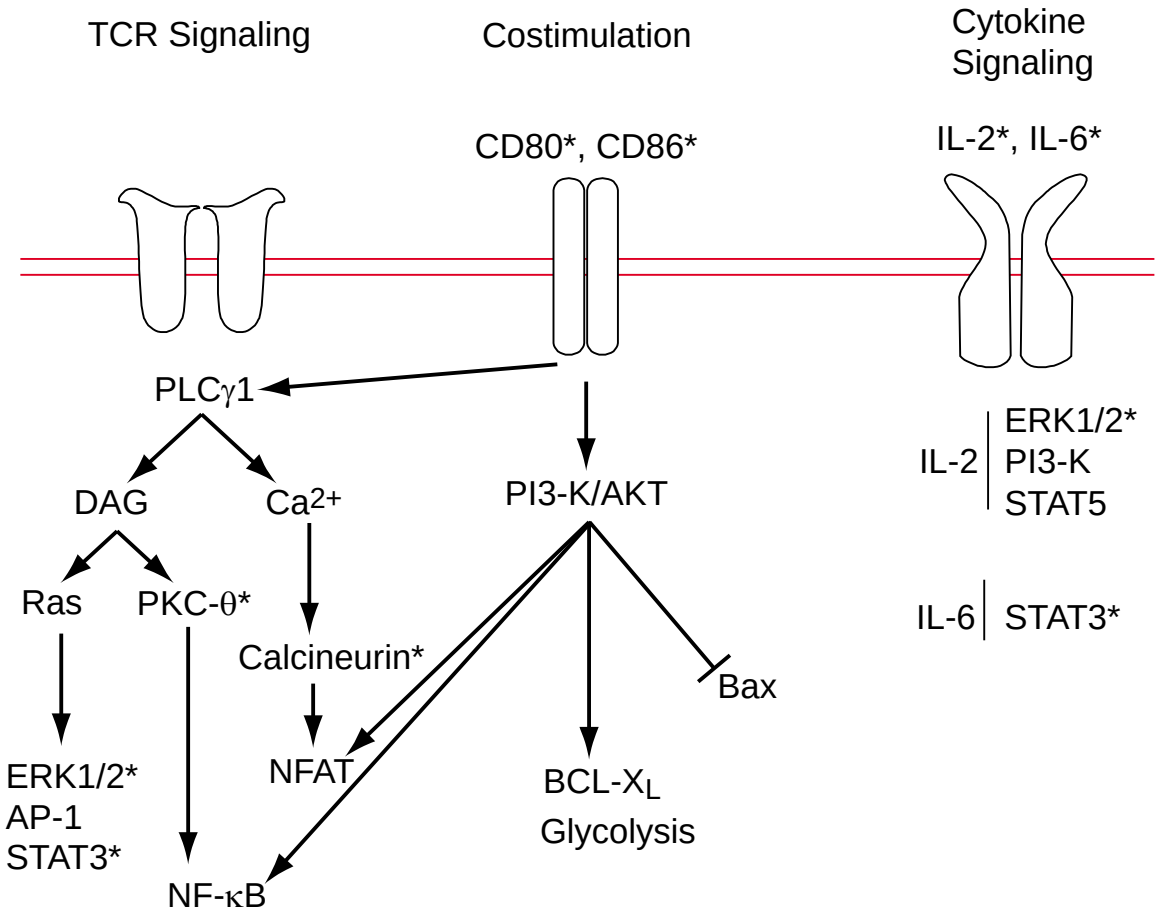

Figure 3.4. Overview of T cell signaling in allo responses. Summary of downstream mediators of TCR, costimulatory and cytokine signaling in donor T cells in GVHD. See text for details. * indicates that inhibition or genetic deletion of the indicated molecule will reduce GVHD according to (431-441).

IP_3 binds to the IP_3 receptor on the endoplasmic reticulum (ER) and causes efflux of Ca^{2+} stores (430). The depletion of ER Ca^{2+} induces the opening of Ca^{2+} release-activated Ca^{2+} (CRAC) channels on the T cell surface and allows the influx of extracellular Ca^{2+} (430). Increased Ca^{2+} levels following TCR stimulation results in calcineurin activation, which dephosphorylates the

transcription factor nuclear factor of activated T cells (NFAT), allowing it to enter the nucleus and, in coordination with AP-1 and NF-κB, promote transcription of genes important in T cell activation such as IL-2 (430). The importance of this pathway in GVHD is emphasized by the fact that calcineuirin inhibition with tacrolimus (FK-506) or cyclosporine is standard treatment for GVHD prophylaxis in patients receiving HSCT (433, 441).

APCs also express Ig-containing costimulatory molecules such as CD80 and CD86, which serve to provide a second stimulatory signal to T cells (442). Ligation of T cell CD28 by CD80 or CD86 phosphorylates the intracellular tail of CD28 and activates the Tec kinases ITK and TEC (34). This kinase activation potentiates TCR-signaling through PLCγ1 (443) and the guanine-nucleotide exchange factor (GEF) VAV1, which increases TCR-dependent activation of NFAT and NF-κB (444). CD28 phosphorylation also recruits PI3K to the plasma membrane through interactions with its p110 subunit (Figure 3.4) (430). The p85 subunit of PI3K catalyzes the formation of PIP_3, which then recruits AKT and its activator PDK-1 to the plasma membrane via their pleckstrin homology (PH) domains (430). Activated AKT has numerous targets and promotes the nuclear localization of NF-κB and NFAT, thereby promoting activated T cell gene transcription (34). In addition to enhancing TCR-mediated gene transcription, costimulation also enhances T cell glycolysis in a PI3K/AKT-dependent fashion (231) and has anti-apoptotic effects mediated by increased BCL-X_L expression and inhibition of Bax activation (75, 445).

When CD80 and CD86 are genetically deleted on host and donor APCs, disease fails to develop in a model of $CD4^+$-dependent MHC-matched GVHD (438). Similarly, blocking costimulatory interactions by using antibodies directed against CD80 and CD86 (439) or blocking CD28 with CTLA4-Ig (440) improves both mortality and weight loss in MHC-mismatched models of GVHD. These data indicate that costimulatory signals through CD28 are critical for GVHD pathogenesis.

Cytokines such as IL-2 and IL-6 also play a role in T cell activation during GVHD (Figure 3.4) (435, 436). IL-2 is produced by activated T cells as a result of NFAT, AP-1 and NF-κB activation (430). IL-2 signals through the heterotrimeric IL-2 receptor (IL-2R), composed of IL-2Rα (CD25), IL-2Rβ (CD122) and the common gamma chain (γc, CD132), which leads to activation of the PI3-K/AKT, MAPK and STAT5 signaling pathways (446). The importance of these signaling pathways in GVHD pathogenesis is emphasized by studies showing that IL-2R blocking antibodies can improve survival, weight loss and skin pathology in a model of MHC-matched GVHD (434). Clinical trials with similar agents have given mixed results in humans (435), likely due to suppressive effects on regulatory T cells, which also express high levels of IL-2R (447). IL-6 is produced by a variety of cell types including epithelial and lymphoid cells, and its levels rise dramatically following recipient conditioning (421, 436, 448) due to increases in pro-inflammatory mediators such as tumor necrosis factor (TNF)-α, IL-1, and lipopolysaccharide (LPS). IL-6 signals through the STAT3 pathway to

induce inflammatory gene transcription (449), and blocking the IL-6 receptor (436) or inhibiting STAT3 directly (432, 437) reduces GVHD.

T cell differentiation and effector functions in nonirradiated GVHD. In specific mouse models of GVHD (parent into F1, P→F1), parental donor cells can induce GVHD in unconditioned F1 recipients (47). In the B6→B6D2F1 model, donor T cells express the $H2^b$ MHC haplotype (450). Because MHC gene expression is codominant (23), the F1 offspring (B6D2F1) of B6 ($H2^b$) and DBA/2 ($H2^d$) parents have the combined $H2^{b/d}$ haplotype. Donor B6 T cells then recognize foreign $H2^d$ expression and react against the mismatched host MHC class I and II molecules (Figure 3.5) (451). Host T cells recognize both $H2^b$ and $H2^d$ as "self" and thus cannot reject the $H2^b$ donor T cells, which eliminates the need for conditioning (451). Because donor T cells lack $H2^d$ MHC class I ($H2K^d$, $H2D^d$) expression, NK-mediated hybrid resistance can be a concern if insufficient numbers of donor T cells are used (452, 453).

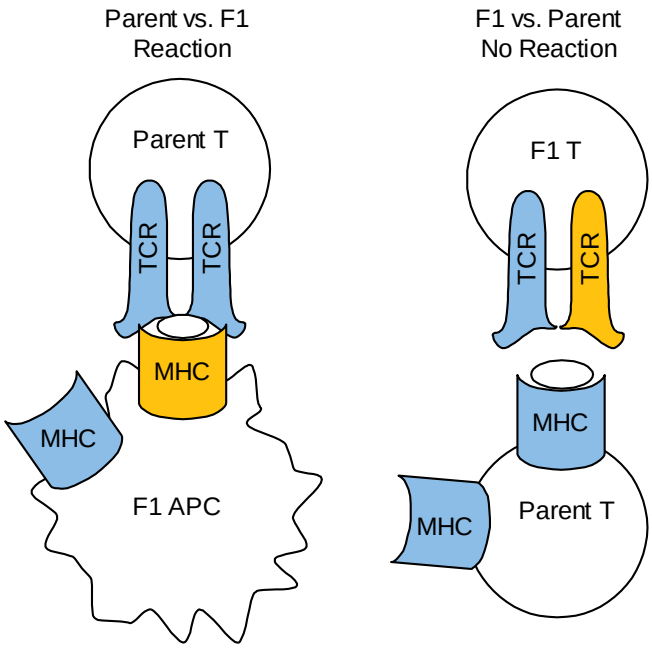

Figure 3.5. Alloantigen recognition in Parent into F1 GVHD models. Parent T cells (left) recognize mismatched MHC molecules on F1 APCs (yellow) that are derived from the second parental strain as foreign. The opposite reaction (right) does not occur, because F1 T cells recognize MHC molecules from both parental strains (i.e, both yellow and blue) as self.

In nonirradiated P→F1 GVHD models, $CD4^+$ and $CD8^+$ donor T cells rapidly proliferate and accumulate in host spleens for 7-10 d after transplant (454-457). This rapid expansion is dependent on costimulatory signaling, as it is significantly reduced by administration of CTLA4-Ig, which blocks signaling through CD28 (458). As donor T cells proliferate in this model, they secrete the proinflammatory cytokines IL-2 and IFN-γ, which promote a Th1-polarized cell-mediated immune response rather than an antibody-mediated Th2 response (457). IFN-γ promotes the differentiation of $CD8^+$ CTLs, which can induce apoptosis in target cells through several pathways (459). For example, CTLs up-

regulate the surface expression of FASL, which ligates FAS receptors on target cells and induce apoptosis through a caspase-8 mediated pathway (460). CTLs can also induce apoptosis through the perforin/granzyme B pathway in which secreted perforin forms pores in target cells allowing secreted granzyme B to enter and induce apoptosis by activating caspase-3 (15). Both of these pathways are important for nonirradiated GHVD pathogenesis as genetically deleting either FASL (461) or perforin (462) in donor T cells significantly reduces lysis of host cells, although the FASL pathway may predominate in other models of GVHD (463). During nonirradiated GVHD, CTLs up-regulate chemokine receptors such as CXCR6, which allow them to traffic to target tissues such as the liver (464) and the bone marrow (461), where they induce liver damage and lethal marrow hypoplasia (453, 461, 464).

Glycolysis and GVHD. During GVHD, donor T cells proliferate, secrete cytokines and differentiate into CTLs. Because these processes require the synthesis of biomolecules and the expenditure of ATP, it is expected that donor T cells will up-regulate their cellular metabolism during GVHD (207). Over the past 40 years, studies on T cells stimulated with mitogens and agonistic antibodies have suggested that activated T cells rely primarily on glycolysis to meet their metabolic needs (207); however, the relative importance of glycolysis and OXPHOS have not been investigated in GVHD or other immune-mediated diseases. Because inhibiting aerobic glycolysis has been suggested as a therapeutic strategy in treating diseases mediated by activated T cells (104, 207),

it is important to determine the extent to which this pathway is used in diseases such as GVHD.

As discussed in Chapter 1, costimulation through CD28 up-regulates glycolysis in activated T cells by activating AKT, and increasing the expression and surface localization of glucose transporter 1 (GLUT1) (58, 59). Costimulatory signaling plays an important role in T cell activation in both irradiated and nonirradiated models of GVHD. In the nonirradiated B6→F1 model, the importance of costimulation was investigated with CTLA4-Ig, which binds CD80 and CD86 thereby preventing signaling through CD28 (458). CTLA4-Ig administration on d2, d5 and d7 decreased donor T cell expansion 4-6 fold and decreased serum IFN-γ 4-fold as measured 14 d after transplant (458). Similarly, genetic deletion of CD80 and CD86 on APCs improved survival and weight loss in an irradiated MHC-matched model of GVHD (438). These findings indicate that signaling through costimulatory pathways are important for donor T cells to mediate GVHD and would suggest that donor T cells might rely on aerobic glycolysis *in vivo*.

While signaling through CD28 increases glycolysis in T cells, signaling through PD-1 or CTLA-4 inhibits glycolysis (59, 255). Both the PD-1 and CTLA-4 signaling pathways are active during GVHD (465-467). For example, GVHD is worsened when PD-1 signaling is blocked by neutralizing antibodies or by using donor T cells that lack the PD-1 receptor (465, 466) or when CTLA-4 signaling is blocked by neutralizing antibodies (467). These findings suggest that inhibitory signals through PD-1 and CTLA-4 help control donor T cells during GVHD.

Together, these observations suggest that the activity of donor T cells in GVHD is influenced by costimulatory signals, which stimulate aerobic glycolysis, and inhibitory signals, which inhibit glycolysis. Hence, it is difficult to determine *a priori* the role of aerobic glycolysis in alloreactive donor T cells.

Evidence for increased aerobic glycolysis in disease-causing T cells *in vivo* comes from studies using positron emission tomography (PET) imaging. Increased uptake of the glucose analog 2-[^{18}F]-Fluoro-2-deoxy-D-glucose (FDG) has been detected in the lymph nodes of patients with lupus (468), the spinal cord of mice with experimental autoimmune encephalitis (469), and the intestine of mice and patients with GVHD (470). However, these studies cannot identify which cells at sites of inflammation are taking up the tracer. Furthermore, the FDG tracer used in PET studies cannot be metabolized past the proximal (hexokinase) step of glycolysis (209). Therefore, FDG-PET does not distinguish between the oxidative (i.e. OXPHOS) or nonoxidative (i.e., glycolysis) breakdown of glucose in those cells (Figure 3.5). Due to the ambiguities of FDG-PET data, direct measurements of OXPHOS and glycolysis in alloreactive donor T cells are necessary to understand the metabolic pathways used by these cells as they mediate GVHD.

OXPHOS and GVHD. T cells activated *in vitro* primarily rely on high rates of aerobic glycolysis, but maintain their ability to proliferative and synthesize cytokines when glycolysis is inhibited by using oxidative phosphorylation (OXPHOS) as their primary energy source (Chapter 1) (58, 59, 257). This flexibility is problematic when attempting to predict the extent to which

alloreactive donor T cells use OXPHOS *in vivo*. Furthermore, the little data that exists regarding oxidative metabolism in activated T cells *in vivo* is indirect. Antigen-specific $CD8^+$ T cells responding to lymphocytic choriomeningitis virus (LCMV) 5 d after infection increase their mitochondrial membrane potential ($\Delta\psi_m$) 5-fold as measured by the potentiometric dye $DiOC_6$. $\Delta\psi_m$ returns to baseline levels by d 8, when virus has been cleared (471) but remains elevated when a chronic strain of the virus is used, suggesting that this increase is due to antigen stimulation of the TCR receptor, possibly due to Ca^{2+}-mediated activation of the TCA cycle (254). While an increase in $\Delta\psi_m$ LCMV-specific T cells also showed a 3-fold increase in dihydroethidium (DHE) fluorescence 5 d after infection with LCMV, suggesting increased O_2^- levels in responding T cells (471). Similar increases in $\Delta\psi_m$ and reactive oxygen species (ROS) production are seen in autoimmune T cells in lupus (Chapter 2) (472), again suggesting that activated T cells can increase OXPHOS *in vivo*. In other work, it was found that peripheral blood mononuclear cells (PBMCs) from patients with active rheumatic disease consume O_2 25% faster than healthy controls, while PBMCs from patients with active infectious disease show a 30% increase in respiration (335). However, none of these studies investigated glycolytic metabolism in conjunction with their measurements of $\Delta\psi_m$, ROS levels or respiration. Without such measurements, it is difficult to determine the relative importance of OXPHOS and glycolysis in these different settings. Indeed, in pancreatic β cells, increased glucose metabolism is associated with an increased $\Delta\psi_m$ (362). However, in mammary tumor cells, decreased glucose metabolism (achieved by siRNA-mediated

inhibition of lactate dehydrogenase) is associated with *decreased* $\Delta\psi_m$ (243). Regardless of the relative utilization of glycolysis and OXPHOS, these data suggest that OXPHOS may play a role in fueling alloreactive donor T cell responses *in vivo* (433).

Further evidence suggesting increased OXPHOS in alloreactive donor T cells comes from the importance of Ca^{2+} signaling in T cells during GVHD. Inhibiting Ca^{2+} signaling with tacrolimus or cyclosporine is frequently used for GVHD prophylaxis (discussed further in Chapter 4) and suggests that alloreactive donor T cells may exhibit increased Ca^{2+} signaling during GVHD (441, 473). Because Ca^{2+} signaling in activated lymphocytes activates pyruvate dehydrogenase (123) and increases NADH production (254), these observations suggest that alloreactive donor T cells may up-regulate OXPHOS.

Recent data suggest that cytokine signaling might also be related to OXPHOS in activated T cells. STAT3 activation is important for GVHD pathogenesis (Figure 3.4) (432, 437), and activated STAT3 was recently discovered to play an important role in OXPHOS by interacting with and stimulating complex I of the mitochondrial respiratory chain (474). This finding suggests that oxidative metabolism in GVHD-causing donor T cells could be related to cytokine stimulation as well as Ca^{2+} signaling. Thus, while existing data suggest that mitochondrial metabolism will be increased in alloreactive donor T cells, direct experimental measurements are needed to explore the importance of this pathway in GVHD.

Energy production of non-T cells in the immune system. While evidence exists for both OXPHOS and glycolytic energy production in antigen-stimulated T cells, hematopoietic stem cells (475), granulocytes such as neutrophils (476), and T cells proliferating in response to cytokine-stimulation (224, 477) primarily rely on increased glycolysis to generate their energy. Proteomic analysis of primitive Lin^- c-Kit^+ $Sca\text{-}1^+$ (LSK^+) stem cells shows increased levels of glycolytic enzymes such as glyceraldehydes-3-reductase, pyruvate kinase, and lactate dehydrogenase compared to less primitive Lin^- c-Kit^- $Sca\text{-}1^-$ cells (475). Furthermore, these primitive LSK^+ cells have a 5-fold increase in GLUT1 as determined by fluorescence microscopy and produce 5-fold more lactate when cultured *ex vivo* compared to LSK^- cells (475). A reliance on glycolytic energy production is important for stem cell function, as activating mitochondrial biogenesis and ROS production by deleting tuberous sclerosis complex 1 (TSC1) and activating the mTOR pathway results in reduced hematopoietic function (478).

In the absence of antigen stimulation, T cells can proliferate when stimulated by cytokines. IL-7 is an important mediator of T cell differentiation and proliferation in the thymus and it is the major factor governing homeostatic proliferation of mature T cells in the periphery (224, 414, 477). IL-7 stimulation activates AKT through the STAT5 pathway and causes a 2-fold increase in surface GLUT1 expression and glucose uptake in naïve and activated T cells (224, 477). Unlike TCR stimulation, IL-7-mediated stimulation has not been linked to Ca^{2+} signaling and IL-7-related changes in oxidative metabolism have

not been investigated. Additionally, stimulation of T cells with other cytokines (IL-2, IL-17 or IL-15) does not increase mitochondrial mass or cause $\Delta\psi_m$ hyperpolarization (264), suggesting that cytokine stimulation in the absence of TCR activation may lead selectively to increased glycolysis.

Neutrophils cultured directly *ex vivo* or stimulated to induce phagocytosis produce lactate at a fast rate (1.3 nMoles lactate/(min x 10^6 cells)), and this correlates with a high rate of glucose uptake (0.84 nMoles glucose/(min x 10^6 cells)) (479). Both of these values are > 10-fold higher than rates reported in resting thymocytes (62, 206). In human neutrophils, complexes I, III and IV of the respiratory chain do not associate into the higher order supercomplexes that are characteristic of mitochondria from tissues such as the heart or PBMCs (480, 481). Treatment with rotenone or sodium azide, which inhibit complexes I and IV of the mitochondria respectively, have no effect on neutrophil ATP levels, while the glycolytic inhibitor sodium iodoacetate reduces neutrophil ATP levels by more than 90% following 6 h of treatment (476). Thus, high rates of glycolysis in neutrophils may result from an inability to synthesize ATP through their mitochondria. Together, these data show that a high rate of OXPHOS is not a uniform characteristic of all activated cells of the immune system and suggest that repopulating granulocytes and homeostatically proliferating T cells may rely on glycolysis in the setting of HSCT.

ROS, antioxidants and GVHD. ROS are formed from numerous sources including complexes I and III of the mitochondrial respiratory chain (131, 154), cytosolic peroxisomes (482), and neutrophils and macrophages during the

respiratory burst (483). While ROS can oxidize cellular proteins, lipids and nucleotides, such reactions are inhibited by antioxidants such as glutathione, catalase, manganese superoxide dismutase (MnSOD), copper/zinc-superoxide dismutase (Cu, Zn-SOD) and pyruvate (177, 180, 191, 193, 195, 197, 200). Hence, accumulation of ROS and markers of ROS oxidation, termed oxidative stress, can indicate an imbalance between ROS production and their detoxification by antioxidants (191, 193).

Following allogeneic HSCT, patients have a 2-fold and 1.5-fold increase in plasma malondialdehyde (MDA) and nitric oxide, respectively, two markers of oxidative stress (484, 485). Compared to healthy controls, transplant recipients also have significantly decreased activities of important plasma antioxidant enzymes, including total superoxide dismutase (65% decrease), catalase (CAT, 30% decrease) and glutathione peroxidase (20% decrease) (485). However, no relationship was observed between decreased antioxidant activity and the development of GVHD (485).

Increased oxidative stress is also observed in mice suffering from GVHD. The lungs of mice with GVHD have increased MDA and a decreased ratio of reduced to oxidized glutathione (486). Additionally, the livers of mice with GVHD have decreased total levels of glutathione (486). However, this study did not include conditioned animals transplanted with syngeneic T cells, so increased oxidative stress may result from the conditioning regimen rather than from the presence of alloreactive donor T cells. Furthermore, these measurements were made in plasma, liver and lung, but not in lymphocytes (484-486). Hence, these

studies suggest an imbalance between ROS production and ROS detoxification during GVHD, but offer limited information on the redox environment within alloreactive donor T cells.

In a different mouse model, the intracellular ROS and glutathione levels of various blood cells during MHC-mismatched GVHD were measured using the dye 2′-7′-dichlorofluorescein diacetate (DCF), which fluoresces when it reacts with a variety of ROS including hydrogen peroxide (H_2O_2) and hydroxyl radicals ($OH\cdot$) (386). Lymphocytes, neutrophils and red blood cells (RBCs) from mice 5 weeks after GVHD induction have 3-fold increased levels of ROS and 3-fold depleted levels of reduced glutathione compared to untreated control mice (487). Additionally, ROS levels in RBCs are greater in mice with GVHD than in control mice transplanted with syngeneic lymphocytes, which suggests that increased oxidative stress is due to the presence of alloreactive donor T cells rather than the conditioning regimen. Because ROS production and oxidative stress are associated with high levels of oxidative metabolism (378), the presence of increased ROS and oxidative stress during GVHD is consistent with increased activity of OXPHOS in pathogenic donor T cells.

Glutathione and pyruvate. Glutathione (Figure 3.6) is the primary antioxidant in mammalian cells, at concentrations between 1 and 10 mM in most tissues (196). Glutathione peroxidase detoxifies H_2O_2 to water by converting reduced glutathione (GSH) to its oxidized form (GSSG) (Figure 3.7) (197). Hence, glutathione limits the apoptosis and non-specific oxidation of DNA, proteins and lipids that can accompany the production of ROS (187, 189, 192-

194). The antioxidant function of glutathione is emphasized by studies showing that inhibiting glutathione synthesis sensitizes lymphoma cells to ROS-mediated apoptosis (488, 489). Similarly, treatment with exogenous glutathione protects the mitochondrial DNA of human lymphocytes from oxidative damage induced by the pro-oxidant t-butyl hydroperoxide (490).

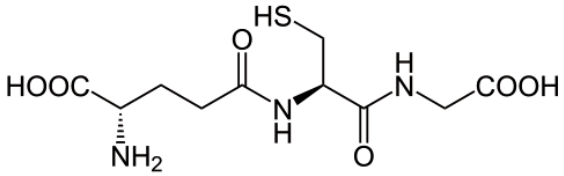

Glutathione

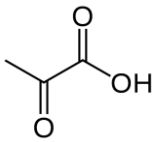

Pyruvate

Figure 3.6. Structures of glutathione and pyruvate. From (49, 196).

The regeneration of GSH from oxidized GSSG is catalyzed by glutathione reductase (Figure 3.7) (196). This reaction requires NADPH, the majority of which is formed from glucose metabolism through the pentose phosphate cycle (PPC) (49). Hence, a deficiency in glucose metabolism could impair NADPH production in the PPC and therefore inhibit the regeneration of reduced glutathione. The importance of the PPC for maintaining glutathione levels has primarily been investigated in cells of the nervous system. In astrocytes and neurons, increasing oxidative stress by adding H_2O_2 to cultures stimulates the PPC by 70% (51). However, when the glutathione redox system is inhibited by depleting glutathione or inhibiting glutathione peroxidase, H_2O_2 no longer stimulates the PPC. These observations suggest that H_2O_2 stimulates PPC

activity by increasing the need for reduced glutathione and NADPH (51). Similarly, inhibiting glucose entry into the PPC with the glucose-6-phosphate dehydrogenase (G6PDH) inhibitors dehydroepiandrosterone or 6-anicotinamide increases ROS levels as measured by DCF fluorescence, which is consistent with decreased glutathione levels (50).

Yeast cells also rely on aerobic glycolysis to maintain GSH levels and minimize ROS production. When *Saccharomyces cerevisiae* are switched from a media supporting glycolysis (2% glucose) to a media supporting respiration (2% glycerol) ROS levels increase 2-3 fold as measured by DHE oxidation (491). When proliferating glycolytic yeast cells are transferred into respiratory media nearly 100% die; however, only 40% die when these cells are treated with reduced glutathione. Hence, these observations indicate that high rates of glycolysis are important for maintaining glutathione levels and minimizing oxidative stress in a variety of cell types.

These results suggest that decreased levels of glutathione and increased ROS levels in lymphocytes during GVHD could be a consequence of low glycolytic metabolism and PPC flux. This hypothesis is supported by studies showing that high rates of glycolysis limit ROS production in lymphocytes. Indeed, concanavalin A (conA)-stimulated thymocytes cultured in media with low glucose (1.2 mM) increase ROS levels 2-3 fold compared to cells cultured in media with high glucose (10 mM), as measured by luminol chemiluminescence or DCF oxidation (376). However, this study did not specifically address glutathione levels or PPC activity (376).

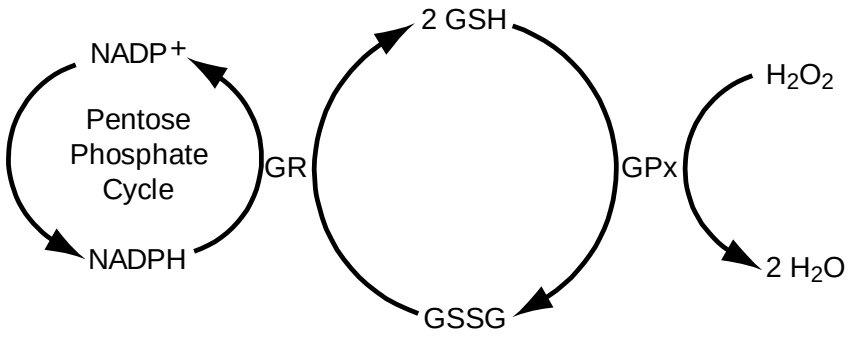

Figure 3.7. Glutathione regeneration and detoxification of hydrogen peroxide. Reduced glutathione (GSH) becomes oxidized to GSSG as it converts hydrogen peroxide (H_2O_2) to water in a reaction catalyzed by glutathione peroxidase (GPx). GSH is regenerated from GSSG in a reaction catalyzed by glutathione reductase (GR). The GR reaction requires NADPH, which is generated when glucose is metabolized in the pentose phosphate cycle (197).

Pyruvate is a metabolite of glucose and is another antioxidant closely tied to glycolytic metabolism. Pyruvate is formed in the cytoplasm when pyruvate kinase dephosphorylates phosphoenolpyruvate (49). Its antioxidant properties are thought to be related to its ability to eliminate H_2O_2 (Figure 3.8) and possibly its ability to reduce O_2^- production in mitochondria (203). Addition of pyruvate (0.1-2 mM) to culture media reduces H_2O_2-induced apoptosis and ROS production in a neuroblastoma cell line (203). Pyruvate also reduces ROS formation due to ischemia-reperfusion injury in perfused guinea pig hearts, although this could be due to its ability to inhibit NADH oxidase rather than direct ROS scavenging (492). The ROS-protective effects of pyruvate have proven beneficial in preclinical models, where administration of pyruvate reduces tissue damage and ROS production in rat ischemia-reperfusion models of the small intestine (202) and liver (201). Ethyl pyruvate, a stable derivative of pyruvate (493), also reduces tissue damage in rat models of hemorrhagic shock (494) and

stroke (495) and mouse models of sepsis (496). These protective effects are also seen in lymphoid cells, as adding pyruvate to culture media inhibits ROS production in cultured thymocytes and HL-60 leukemia cells (252). Like glutathione, pyruvate is an antioxidant formed by the metabolism of glucose. Thus, the increased ROS levels and altered antioxidant balance in lymphocytes during GVHD could be due, in part, to abnormally low levels of pyruvate, secondary to low rates of aerobic glycolysis.

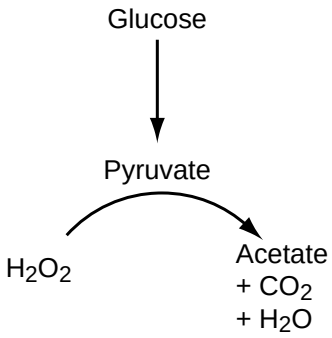

Figure 3.8. Pyruvate formation and degradation by H_2O_2. Glucose generates pyruvate through the cytosolic steps of glycolysis. Pyruvate can directly react with ROS such as hydrogen peroxide yielding acetate, CO_2 and H_2O (200).

Statement of problem. GVHD is the major morbidity associated with hematopoietic stem cell transplantation, and current treatments are lacking. Alloreactive donor T cells perform numerous metabolically active functions, but how they meet these energetic demands is unknown. Literature reports of increased oxidative stress suggest that these T cells may rely on OXPHOS rather than glycolysis. Identifying the metabolic pathways used by alloreactive donor T cells could identify novel therapeutic targets for the treatment of GVHD.

RESULTS

Prolfiling the metabolism of splenocytes from mice with GVHD. The non-irradiated B6→F1 model of GVHD is characterized by rapid proliferation of donor $CD4^+$ and $CD8^+$ T cells 7-10 d following transplant (expansion phase) followed by CTL-mediated apoptosis of host and donor lymphoid cells (contraction phase), which leads to high levels of mortality by 21 d after transplant (451). During the graft-versus-host reaction, donor T cells produce Th1 cytokines such as IFN-γ, which promote the differentiation of CTLs and the development of anti-host cytotoxicity (459). To confirm that our transplant system behaved as previously reported, we infused congenic B6-Ly5.2 cells into unirradiated F1 (allogeneic) or B6 (syngeneic) recipients and enumerated donor T cells and measured their expression of CTL-related molecules following transplant. Hematopoietic cells from the B6-Ly5.2 mice express the CD45.1 protein tyrosine phosphatase isoform on their cell surface, while cells from B6 or F1 mice express CD45.2 (497, 498). This distinction allowed the discrimination of donor and host lymphocytes. By 8 d after infusion into allogeneic recipients, donor $CD4^+$ and $CD8^+$ had expanded 18- and 39-fold, respectively, compared to donor T cells infused into syngeneic B6 recipients (Figure 3.9, $p<0.002$ for both comparisons). The number of donor T cells peaked after d 8 and had decreased by 25% by 14 d after transplant. During this expansion, alloreactive donor T cells increased their expression of IFN-γ 5-10-fold over syngeneic T cells (Figure 3.10 A, $p<0.02$) and granzyme B 7-fold over syngeneic T cells (Figure 3.10 B, $p<0.01$), both of which are important effector molecules for CTL activity (16).

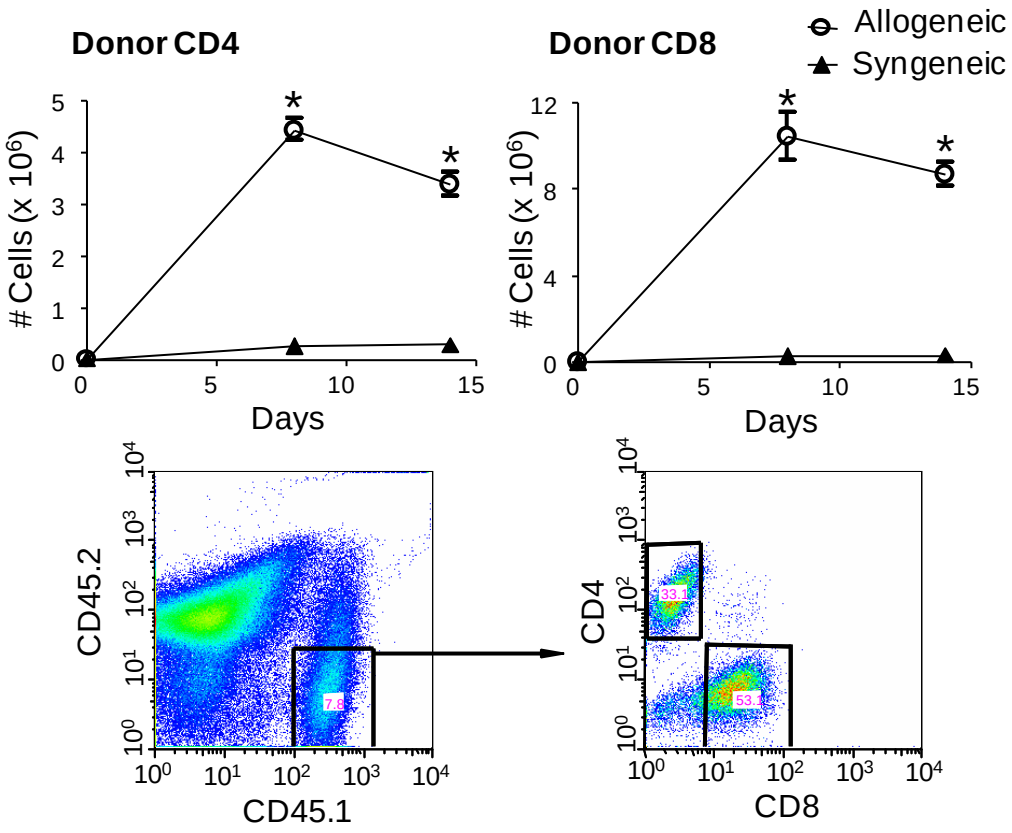

Figure 3.9. Donor T cell expansion during non-irradiated GVHD. F1 (allogeneic, white circles) or B6 (syngeneic, black triangles) mice were injected i.v. with B6-Ly5.2 splenocytes (35 x 10^6). On d 8 or 14 after transplant, recipient splenocytes were counted and stained for CD4, CD8, CD45.1 (donor) and CD45.2 (host) expression. Donor T cells were gated as indicated (right panels) and enumerated. Data are from 4 (allogeneic) or 2 (syngeneic) mice per timepoint and error bars indicate standard error. * $p < 0.002$.

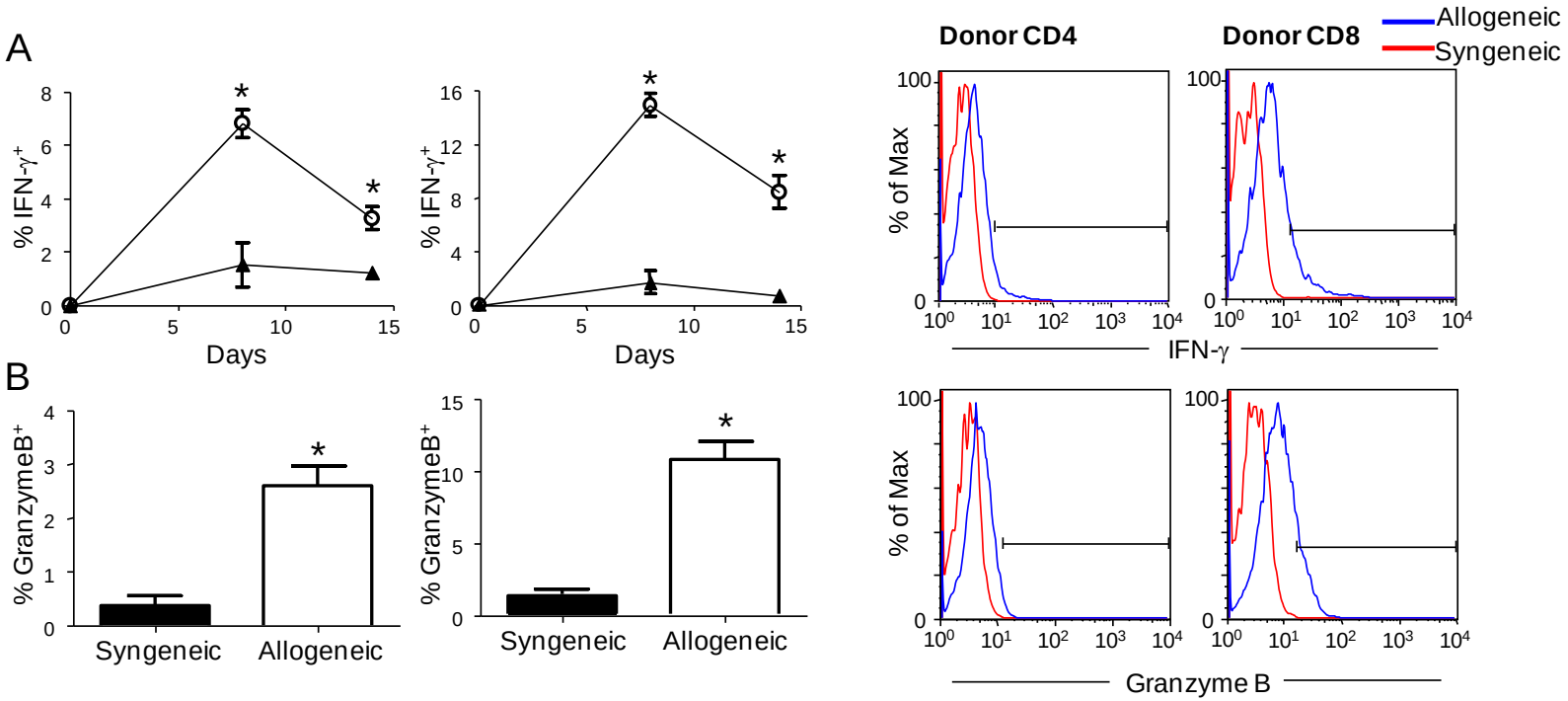

Figure 3.10. Donor T cell effector molecule expression during non-irradiated GVHD. A and B. F1 (allogeneic, white circles) or B6 (syngeneic, black triangles) mice were injected i.v. with B6-Ly5.2 splenocytes (35 x 10^6). Splenocytes were fixed and permeabilized without restimulation to measure IFN-γ and Granzyme B expression. Granzyme B was measured 8 d after transplant. Histograms are gated on CD45.1$^+$ CD45.2$^-$ CD4$^+$ or CD45.1$^+$ CD45.2$^-$ CD8$^+$ as in A and show IFN-γ or Granzyme B staining 8 d after transplant in allogeneic (blue) or syngeneic (red) splenocytes. Data are from 4 (allogeneic) or 2 (syngeneic) mice per timepoint and error bars indicate standard error. * $p < 0.02$.

Proliferation and effector molecule production require the *de novo* biosynthesis of cellular membranes and pro-inflammatory proteins, both of which are energetically demanding processes (207). For example, the synthesis of a single palmitate molecule, a major component of cellular membranes, requires 7 molecules of ATP, while protein synthesis requires a single GTP (equivalent to one ATP (49)) for each amino acid incorporated (49, 78, 499). Because alloreactive donor T cells have increased proliferation and effector molecule production, we hypothesized that splenocytes from mice receiving allogeneic infusions would have increased ATP production compared to splenocytes from mice receiving syngeneic infusions.

The two major routes of ATP production are glycolysis and OXPHOS, which can be assessed by lactate production and O_2 consumption respectively (78, 142, 143, 207, 247). Two days after GVHD induction, splenocytes from mice receiving allogeneic or syngeneic infusions had similar rates of O_2 consumption (0.44 vs. 0.38 nMoles O_2/min x 10^6 cells, p=0.16) and lactate production (0.37 vs. 0.28 nMoles lactate/min x 10^6 cells, p=0.24) (Figure 3.11 A-B). However, by d 7-14 after GVHD induction, splenocytes from mice receiving allogeneic infusions increased O_2 consumption 60-80% and lactate production 50% compared to mice receiving syngeneic infusions (Figure 3.11 A-B, Table 3.3). Lactate production and O_2 consumption were not analyzed after d 14 because nonirradiated GVHD induces severe lymphopenia at these time points (453, 461, 500). These results suggest that splenocytes from mice receiving

allogeneic infusions increase both oxidative and glycolytic metabolism compared to syngeneic controls.

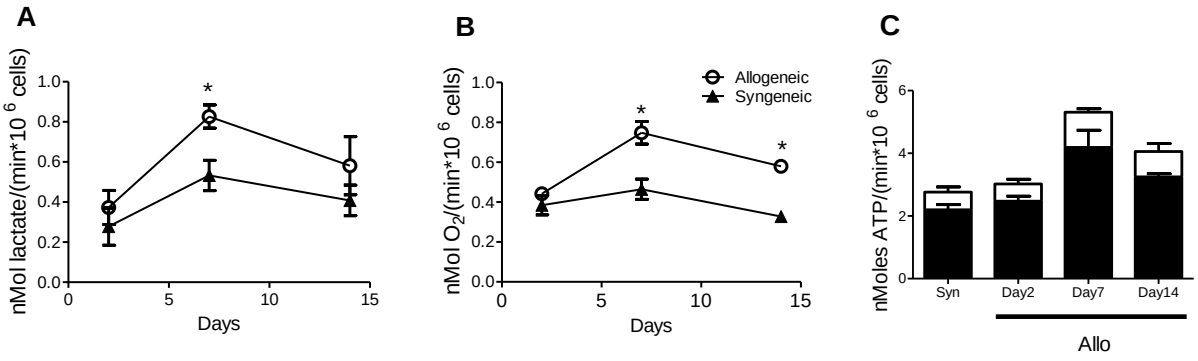

Figure 3.11. Lactate Production, O_2 Consumption and ATP production of splenocytes from mice with GVHD. F1 (allogeneic) or B6 (syngeneic) mice were injected i.v. with B6-Ly5.2 splenocytes (50 x 10^6). **A and B.** On d 2-14 after transplant, recipient splenocytes were RBC-lysed and analyzed for O_2 consumption and lactate production. Data are averaged from 3 mice per condition and error bars indicate standard error. **C.** ATP production was calculated as ATP_{OXPHOS}(Black)=5.6 x O_2 Consumption and $ATP_{Glycolysis}$(White)=Lactate Production + 0.4 x O_2 Consumption. Syngeneic results were pooled (n=9). * $p < 0.05$ compared to syngeneic.

Table 3.3. Lactate production and O_2 consumption of GVHD and control splenocytes. Data are averaged from 3 mice per group and numbers in parentheses indicate standard error. p values compare Syn and Allo groups from the same day and are unpaired and 1 tailed.

	Lactate Production			**O_2 Consumption**		
	nMoles Lactate/(min x 10^6 cells)			nMoles O_2/(min x 10^6 cells)		
	Syn	**Allo**	**p**	**Syn**	**Allo**	**p**
Day 2	0.28 (.09)	0.37 (.09)	0.24	0.38 (.05)	0.44 (.02)	0.16
Day 7	0.53 (.08)	0.87 (.06)	0.018	0.47 (.05)	0.75 (.06)	0.01
Day 14	0.41 (.08)	0.58 (.15)	0.16	0.33 (.03)	0.58 (.01)	0.001

Using the rates of O_2 consumption and lactate production, it is possible to calculate the amount of ATP cells produce through oxidative phosphorylation and glycolysis (142, 247, 501). The metabolism of one glucose molecule through aerobic glycolysis produces 2 molecules of ATP and 2 molecules of lactate, thus each lactate produced indicates a single molecule of ATP produced through glycolysis (78). The amount of ATP produced per O_2 consumed varies depending on the substrate oxidized (502). For NADH-linked substrates such as malate and pyruvate, 4.6 ATP are theoretically generated per O_2 consumed based on calculations from studies in isolated mitochondria (502). However, a ratio of 5.6 ATP per O_2 consumed is frequently used for mammalian cells (142, 247, 501). This value is used because it was determined empirically in intact renal tubular cells (143), although this study did not take proton leak into account. Such a consideration is important, as protons returning to the mitochondrial matrix through a path independent of the F_1F_o-ATPase do not catalyze ATP production (502). Hence, a calculation of mitochondrial ATP production that does not account for proton leak will overestimate the amount of ATP synthesized per O_2 (502).

The complete oxidation of glucose generates 2 ATP from glycolysis and 30-34 ATP from OXPHOS (49, 78). Using an ATP/O_2 ratio of 5.6, this suggests that the complete oxidation of one glucose molecule requires 5.3-6 molecules of O_2 (i.e. 30 ATP/5.6 (ATP/O_2)). Thus, if glucose is the only substrate oxidized, each molecule of O_2 consumed will correspond to approximately 0.2 molecules of glucose metabolized (142). Because a single glucose molecule generates 2

molecules of ATP as it is converted into pyruvate, each O_2 consumed indicates an additional 0.4 ATP produced through glycolysis (142). Thus, ATP production from glycolysis is calculated as lactate production + 0.4 x O_2 consumption, while ATP production from OXPHOS is calculated as 5.6 x O_2 consumption (142, 247, 501). Using these equations, OXPHOS was estimated to provide 80% of the ATP for each splenocyte group analyzed (Figure 3.11 C, Table 3.4).

Table 3.4. ATP production of GVHD and control splenocytes. ATP production was calculated as described in the text and in Figure 3.11. Data are averaged from 3 (Allo) or 9 (Syn) mice per group, and numbers in parentheses indicate standard error.

		ATP Production		% ATP Production	
		nMoles ATP/(min x 10^6 cells)			
		OXPHOS	**Glycolysis**	**OXPHOS**	**Glycolysis**
Syn	**combined**	2.2 (0.1)	0.56 (0.06)	80	20
Allo	**Day 2**	2.5 (0.1)	0.55 (0.09)	82	18
Allo	**Day 7**	4.2 (0.3)	1.13 (0.06)	79	21
Allo	**Day 14**	3.2 (0.1)	0.81 (0.15)	80	20

To determine the amount of O_2 consumption used for ATP synthesis, we treated splenocytes with the F_1F_o-ATPase inhibitor oligomycin, using concentrations (1-2 μg/mL) that are 100-200x greater than the apparent K_i for inhibition of ATP synthesis (171). The difference between routine respiration (i.e., without any inhibitors present) and oligomycin-inhibited respiration indicates the amount of O_2 consumption used for ATP synthesis (Figure 3.12, “OXPHOS”)

(503, 504). Oligomycin treatment reduced O_2 consumption by 54-68% in nearly all splenocyte groups (Table 3.5), indicating that the majority of O_2 consumed under routine conditions is used for ATP synthesis, with the rest being used for other processes such as proton leak (Table 3.5, “Leak”) (503). However, oligomycin only inhibited 45% of respiration in syngeneic splenocytes on d 2 after transplant, which was different than the 57-62% inhibition seen in syngeneic cells on d 7 and d 14. The reason for this variation is unclear.

We next treated cells with carbonylcyanide-p-trifluoromethoxyphenylhydrazone (FCCP, 6-12 μM), a protonophore that increases respiration by uncoupling O_2 consumption and ATP synthesis (503). The difference between routine respiration and FCCP-stimulated respiration is termed the reserve capacity (Figure 3.12), and cells may use it to generate additional ATP when energetic demands increase (504). FCCP increased splenocyte respiration rates approximately 2-fold over routine rates in all mice analyzed, indicating an equivalent fraction of reserve capacity in all groups (Table 3.5).

Splenocytes from mice 7 or 14 d after infusion of allogeneic cells increased routine, oligomycin-inhibited and FCCP-stimulated O_2 consumption rates compared to splenocytes from mice receiving syngeneic splenocytes (Table 3.5, $p<0.05$ for each comparison). These results show that the increase in routine respiration rates in allogeneic splenocytes is accompanied by an increase of similar magnitude in total respiratory capacity. In addition, splenocytes from mice receiving allogeneic infusions increased the percentage of routine

respiration used for ATP synthesis by 14% 7 d after transfusion as compared to pooled syngeneic controls (68% vs. 54%, $p<0.05$). Similar changes were seen in the percent utilization of the total respiratory capacity; 36% of total respiratory capacity was used for ATP synthesis in d 7 allogeneic splenocytes vs. 28% for pooled syngeneic controls, although these changes were not significant (Table 3.5, $p=0.09$). These data suggest that splenocytes from mice with GVHD increase oxidative ATP production compared to syngeneic splenocytes by increasing total respiratory capacity and may increase the percentage of respiration used for ATP synthesis. These results are summarized graphically in Figure 3.13.

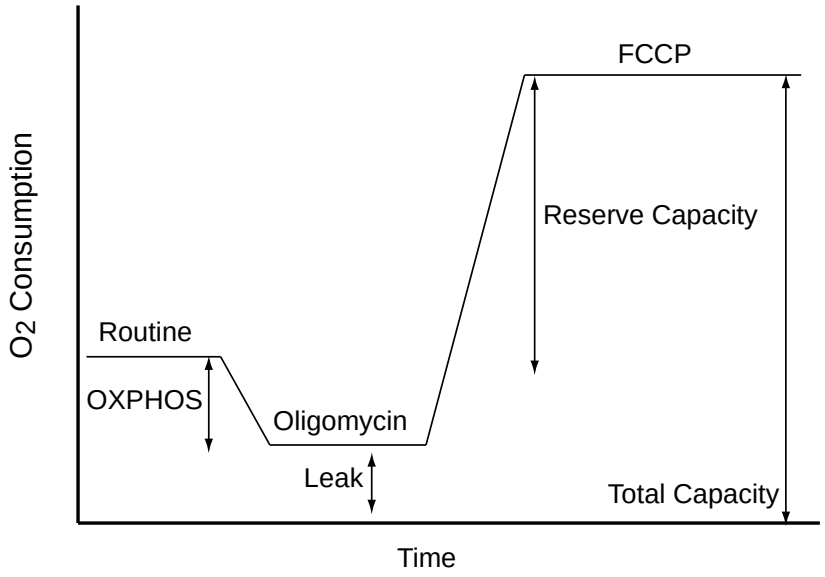

Figure 3.12. Schematic of O_2 consumption parameters. Routine is the O_2 consumption rate of unmanipulated cells. Oligomycin is the O_2 consumption rate following addition of oligomycin (1-2μg/mL). FCCP is the O_2 consumption rate following addition of FCCP (10-12 μM). OXPHOS, LEAK, Reserve Capacity and Total Capacity are described in the text and are indicated by two-headed arrows.

	nMoles O_2/(min x 10^6 cells)				% of Routine		% of Total Capacity		
	Routine	**Oligo**	**FCCP**	**OXPHOS**	**OXPHOS**	**Leak**	**OXPHOS**	**Leak**	**Reserve**
Syn d2	0.38 (0.05)	0.22 (0.04)	0.76 (0.10)	0.16 (0.06)	43 (7)	57 (7)	22 (2)	29 (4)	49 (2)
Syn d7	0.46 (0.05)	0.17 (0.02)	0.83 (0.05)	0.29 (0.05)	62 (3)	38 (3)	36 (7)	21 (1)	43 (8)
Syn d14	0.33 (0.03)	0.14 (0.02)	0.7 (0.07)	0.19 (0.03)	57 (4)	42 (4)	27 (1)	20 (3)	53 (2)
Syn Combined	0.39 (0.03)	0.18 (0.02)	0.76 (0.04)	0.22 (0.03)	54 (4)	46 (4)	28 (3)	24 (2)	48 (3)
Allo d2	0.44 (0.02)	0.18 (0.02)	0.9 (0.03)	0.26 (0.03)	59 (3)	41 (3)	29 (1)	21 (3)	50 (4)
Allo d7	0.75 (0.06)*	0.24 (0.03)*	1.43 (0.15)*	0.51 (0.06)*	68 (2)**	32 (2)**	36 (2)	17 (1)**	47 (2)
Allo d14	0.58 (0.01)*	0.22 (0.03)*	1.1 (0.03)*	0.36 (0.04)*	62 (5)	38 (2)	33 (2)	20 (3)	47 (1)

Table 3.5. O_2 consumption parameters of GVHD splenocytes. O_2 consumption measurements were made as in Figure 3.11. Routine, Oligo and FCCP rates were collected as described in the text and methods. Calculations for OXPHOS and percentages were made as described in the methods. Numbers in parentheses indicate standard error. 3 mice per group were analyzed. Syn combined is averaged over all 9 syngeneic mice. * $p<0.05$ compared syngeneic controls collected on the same day. ** $p<0.05$ compared to pooled syngeneic controls. Extramitochondrial oxygen consumption was ignored in these experiments.

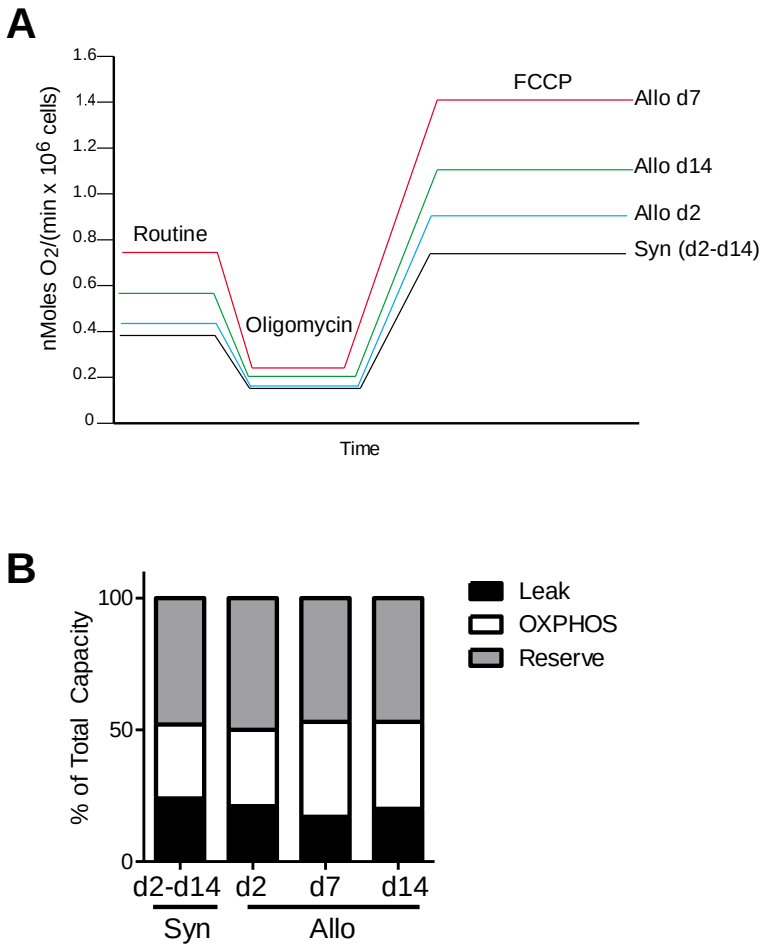

Figure 3.13. O_2 consumption parameters of GVHD splenocytes. Data are from table 3.5. **A.** Routine, Oligo and FCCP rates of O_2 consumption. **B.** The percentage of total respiratory capacity used for proton leak (black), OXPHOS (white) and kept in reserve (gray).

Oxidative and glycolytic metabolism of purified donor T cells from mice with GVHD. In the non-irradiated B6→F1 model of GVHD, disease-causing donor T cells comprise < 10% of splenic lymphocytes 7-8 d after transplant (Figure 3.14). Hence the metabolic characteristics of bulk splenocytes likely reflect the metabolism of a combined population of host T and B cells in addition to GVHD-causing donor T cells.

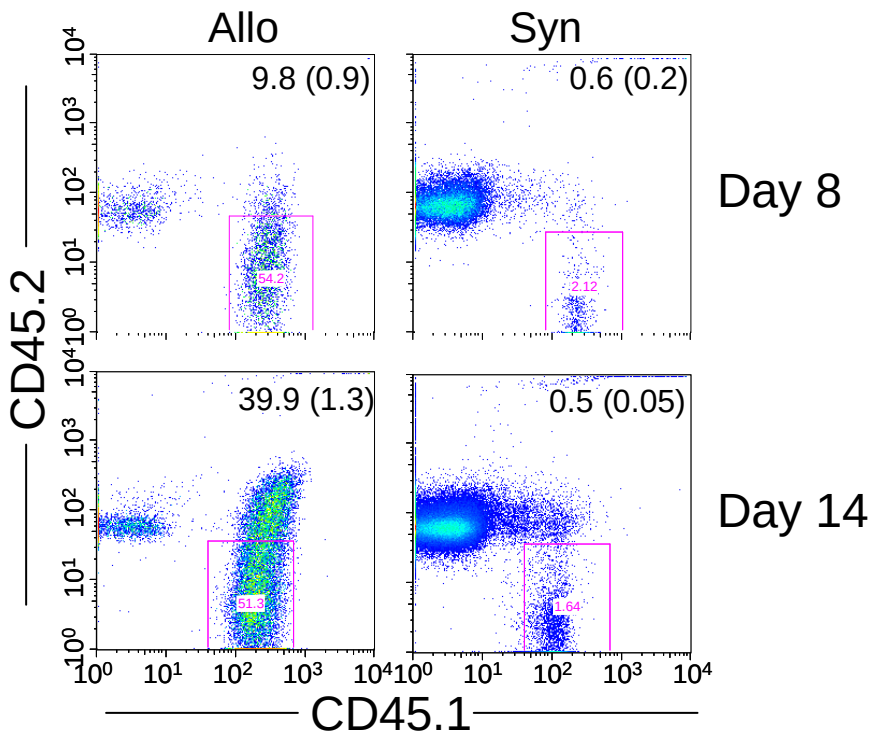

Figure 3.14. Percentage of splenocytes that are donor T cells. Donor splenocytes (B6-Ly5.2, 35 x 10^6) were infused into F1 (Allo, n=4) or B6 (Syn, n=4) mice. At the indicated times, splenocytes were analyzed and donor T cells were identified as CD45.1$^+$ CD45.2$^-$ and either CD4$^+$ or CD8$^+$. Numbers in the upper right of each plot indicate the percentage of splenocytes that were CD45.1$^+$ CD45.2$^-$ CD4$^+$ CD8$^-$ or CD45.1$^+$ CD45.2$^-$ CD4$^-$ CD8$^+$ (i.e. the percentage of splenocytes that are donor T cells), while numbers in parentheses indicate standard error. Flow plots were gated on cells that were CD4$^+$ or CD8$^+$ and then plotted as shown. Pink numbers inside boxes indicate the percentage of T cells that are CD45.1$^+$ CD45.2$^-$.

To specifically characterize the metabolism of alloreactive donor T cells, donor T cells were purified from spleens of animals with GVHD by positive magnetic selection using the Thy1.1 (d 5 or d 7) or CD45.1 (d 14) marker. Thy1.1 is a congenic marker expressed only on T cells, while CD45.1 is expressed on all hematopoietic cells (498, 505, 506). Magnetic purification was chosen over flow-cytometry-based sorting because its speed and cell yield were

more compatible with the high cell numbers (i.e. 5 x 10^6) required for O_2 consumption and lactate production analysis (142, 247).

Purification of donor T cells over two subsequent ferromagnetic columns yielded purities over 85% (Figure 3.15). Spleens from mice contained approximately 200 x 10^6 cells on d 7 after transplant, and donor T cells were pooled from 1-2 mice per data point. Approximately 4-5 x 10^6 donor T cells were obtained per spleen used. Control unstimulated T cells were purified by Thy1.2 positive selection from naïve B6-Ly5.2 mice (Unstim) or from F1 mice 7 d after GVHD induction (Host). As a positive control, we stimulated T cells from B6-Ly5.2 mice for 48 h with anti-CD3 and anti-CD28 antibodies, which is known to increase both O_2 consumption and lactate production (59).

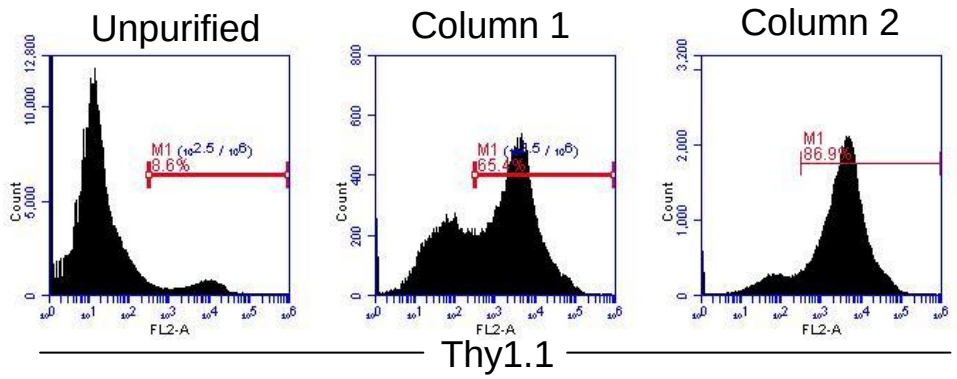

Figure 3.15. Purification of donor T cells. Donor splenocytes (50 x 10^6 B6-Thy1.1) were transfused into F1 recipients. On d 7 post-transfusions, splenocytes were stained with PE-anti-Thy1.1 and donor T cells were purified using magnetic anti-PE microbeads. Plots show the percentage of cells staining positive for PE-Thy1.1 without magnetic separation (unpurified), with purification over a single LS column (Column 1) or purification over one LS and one MS column (Column 2).

Alloreactive donor T cells consumed O_2 at rates of 0.45 and 0.48 nMoles O_2/(min x 10^6 cells) on d 5 and d 7 after transplant, respectively (Figure 3.16 and Table 3.6). These O_2 consumption rates were 2.2- and 2.4-fold greater than control unstimulated T cells, respectively (Table 3.6, $p<0.0001$ for each comparison). Host T cells from mice with GVHD served as a second control and consumed O_2 at a rate of 0.24 nMoles O_2/(min x 10^6 cells), which was not significantly different than unstimulated T cells (Figure 3.16, Table 3.6). The increase in O_2 consumption observed in alloreactive donor T cells was similar to that seen in control T cells stimulated *in vitro* with anti-CD3/28 antibodies, which consumed 0.54 nMoles O_2/(min x 10^6 cells) (Figure 3.16, Table 3.6). By d 14 after transplant, the rate of donor T cell O_2 consumption had decreased to 0.28 nMoles O_2/(min x 10^6 cells), which is 40% greater than unstimulated cells (Figure 3.16, Table 3.6). This finding indicates that donor T cell OXPHOS may peak after d 7, suggesting that increased OXPHOS may coincide with the expansion phase of GVHD (Figure 3.16).

Alloreactive donor T cells produced lactate at rates of 0.18, 0.53, and 0.23 nMoles lactate/(min x 10^6 cells) on d 5, 7, and 14 after transplant, respectively. These rates were 1.5-4-fold higher than those seen in unstimulated T cells, which produced 0.11 nMoles lactate/(min x 10^6 cells) (Table 3.6). However, donor T cells did not produce lactate significantly faster than host T cells, which produced 0.46 nMoles lactate/(min x 10^6 cells) (Table 3.6). T cells stimulated with anti-CD3/28 antibodies produced 3.4 nMoles lactate/(min x 10^6 cells), which is 30-fold

higher than the lactate production of unstimulated T cells ($p<0.0001$) and 6.5-fold higher than d 7 donor T cells ($p=0.004$).

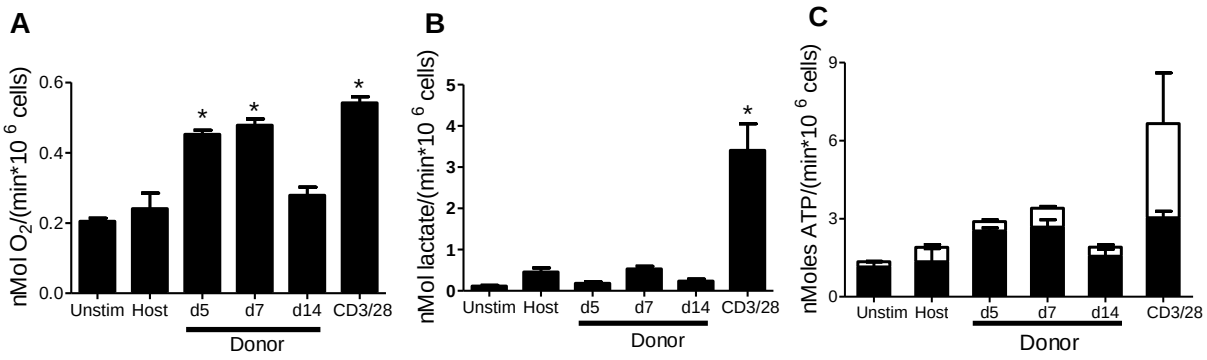

Figure 3.16. O_2 consumption, lactate production and ATP production of donor T cells during GVHD. A and B. O_2 consumption and lactate production from freshly purified CD90.2 T cells from naïve B6-Ly5.2 mice (Unstim), CD90.2 purified host T cells from F1 mice 7 d after GVHD induction (Host), Thy1.1 purified donor T cells from F1 mice 5 or 7 d after GVHD induction with 50 x 10^6 B6-Thy1.1 splenocytes (Donor d5, d7), CD45.1 purified donor T cells from F1 mice 14 d after GVHD induction with 50 x 10^6 B6-Ly5.2 splenocytes (Donor d14) or CD90.2 purified T cells stimulated for 48 h with anti-CD3 and anti-CD28 antibodies (0.5 μg/mL, soluble; CD3/28). Purity of cells was > 85% by flow cytometry. O_2 consumption and lactate production replicates are as follows: Unstim (15 O_2, 12 lactate), Host (4 O_2, 4 lactate), Donor d5 (3 O_2, 3 lactate), Donor d7 (8 O_2, 5 lactate), Donor d14 (4 O_2, 3 lactate), CD3/28 (7 O_2, 9 lactate). * $p<0.02$ compared to Host. **C**. ATP from OXPHOS is in black and ATP from glycolysis is in white. ATP production was calculated as $ATP_{OXPHOS}=5.6 \times O_2$ Consumption and $ATP_{Glycolysis}$ = Lactate Production + 0.4 x O_2 Consumption. Error bars indicate standard error.

			p values				p values	
O_2 Consumption	**n**	**vs. Unstim**	**vs. Host**	**Lactate Production**	**n**	**vs. Unstim**	**vs. Host**
nMoles O_2/(min x 10^6 cells)				nMoles Lactate/(min x 10^6 cells)			
Unstim	0.20 (0.01)	15	-	1×10^{-1}	0.11 (0.02)	12	-	6×10^{-5}
Host	0.24 (0.04)	4	1×10^{-1}	-	0.46 (0.10)	4	6×10^{-5}	-
Donor d5	0.45 (0.01)	3	2×10^{-9}	6×10^{-3}	0.18 (0.04)	3	1×10^{-1}	4×10^{-2}
Donor d7	0.48 (0.02)	8	3×10^{-13}	6×10^{-5}	0.53 (0.07)	5	6×10^{-7}	3×10^{-1}
Donor d14	0.28 (0.02)	4	1×10^{-3}	2×10^{-1}	0.23 (0.05)	3	2×10^{-2}	7×10^{-2}
CD3/28	0.54 (0.02)	7	1×10^{-14}	1×10^{-5}	3.40 (0.65)	9	5×10^{-6}	6×10^{-3}

Table 3.6. O_2 consumption and lactate production of T cells during GVHD. Numbers are averaged from the indicated n measurements and numbers in parentheses indicate standard error. p values are one tailed.

Although donor T cells purified on d 7 after transplant and control stimulated T cells both increase O_2 consumption 2-3-fold over unstimulated cells (Table 3.6), donor T cells only increased lactate production 4-fold, while control stimulated T cells increased lactate production 30-fold (Table 3.6). These disparate rates of lactate production suggested different routes of energy production in donor and control stimulated T cells. Indeed, OXPHOS provided 79% of ATP in donor T cells, but only 46% in T cells stimulated with anti-CD3/28 antibodies (Figure 3.16, Table 3.7, $p<0.05$).

Table 3.7. ATP production of T cells during GVHD. Data are from Figure 3.16. ATP production was calculated as $ATP_{OXPHOS}=5.6 \times O_2$ Consumption and $ATP_{Glycolysis}$=Lactate Production + $0.4 \times O_2$ Consumption. Numbers in parentheses indicate standard error.

	ATP Production nMoles ATP/(min x 10^6 cells)		**% ATP Production**	
	OXPHOS	**Glycolysis**	**OXPHOS**	**Glycolysis**
Unstim	1.1 (0.1)	0.20 (0.01)	85	15
Host	1.3 (0.3)	0.55 (0.05)	71	29
Donor d5	2.5 (0.1)	0.36 (0.04)	88	12
Donor d7	2.7 (0.1)	0.72 (0.03)	79	21
Donor d14	1.6 (0.1)	0.34 (0.05)	82	18
CD3/28	3.0 (0.1)	3.62 (0.74)	46	54

Oligomycin decreased O_2 consumption by 60-66% in all T cells (Table 3.8). This finding indicates that 30-40% of basal respiration is used for processes other than ATP production such as proton leak (503). FCCP

increased respiration rates approximately 2-fold, which defines the reserve respiratory capacity in these cells (503). While the percentage of routine respiration used for OXPHOS (i.e., that which was inhibited by oligomycin) did not change between the T cell groups, the *magnitude* of routine, oligomycin-inhibited and FCCP-stimulated respiration rates were increased in alloreactive donor T cells and control stimulated cells as compared to unstimulated T cells (Table 3.8).

Donor T cells also differed from unstimulated T cells with regard to the percentage of respiratory capacity used for OXPHOS and kept in reserve (Figure 3.12). Donor T cells isolated 7 d after transplant had a 10% increase in the fraction of total capacity used for OXPHOS and a 10% decrease in the fraction of capacity in reserve as compared to unstimulated T cells. These data suggest that alloreactive donor T cells increase ATP synthesis compared to unstimulated T cells both by increasing total respiratory capacity, and also by increasing the fraction of that capacity that is directed towards ATP synthesis (Table 3.8). These results are summarized graphically in Figure 3.17.

	nMoles O_2/(min x 10^6 cells)				% of Routine		% of Total Capacity		
	Routine	Oligo	FCCP	OXPHOS	OXPHOS	Leak	OXPHOS	Leak	Reserve
Unstim (n=15)	0.20 (0.01)	0.08 (0.01)	0.52 (0.04)	0.13 (0.01)	62 (2)	38 (2)	26 (2)	15 (1)	58 (3)
Host (n=4)	0.24 (0.04)	0.08 (0.01)	0.45 (0.12)	0.16 (0.04)	66 (3)	34 (3)	37 (1)*	20 (4)	43 (5)*
Donor d5 (n=3)	0.45 (0.01)*	0.18 (0.02)*	0.91 (0.07)*	0.27 (0.03)*	60 (4)	40 (4)	30 (2)	20 (3)	50 (4)*
Donor d7 (n=8)	0.48 (0.02)*	0.17 (0.01)*	0.93 (0.07)*	0.31 (0.01)*	65 (1)	35 (1)	35 (3)*	19 (1)*	47 (3)*
Donor d14 (n=4)	0.28 (0.02)*	0.10 (0.01)	0.56 (0.08)	0.18 (0.02)*	66 (1)	34 (1)	34 (4)	18 (2)	48 (6)
CD3/28 (n=7)	0.54 (0.02)*	0.21 (0.01)*	1.14 (0.07)*	0.36 (0.04)*	66 (6)	34 (6)	32 (2)	17 (3)	51 (3)

Table 3.8. O_2 consumption parameters of control and alloreactive donor T cells. O_2 consumption measurements were made as in Figure 3.16. Routine, Oligo and FCCP rates were collected as described in the text and methods. Calculations for OXPHOS and percentages were made as described in the methods. Numbers in parentheses indicate standard error. * $p<0.05$ compared to Unstim. Extramitochondrial O_2 consumption was ignored in these experiments.

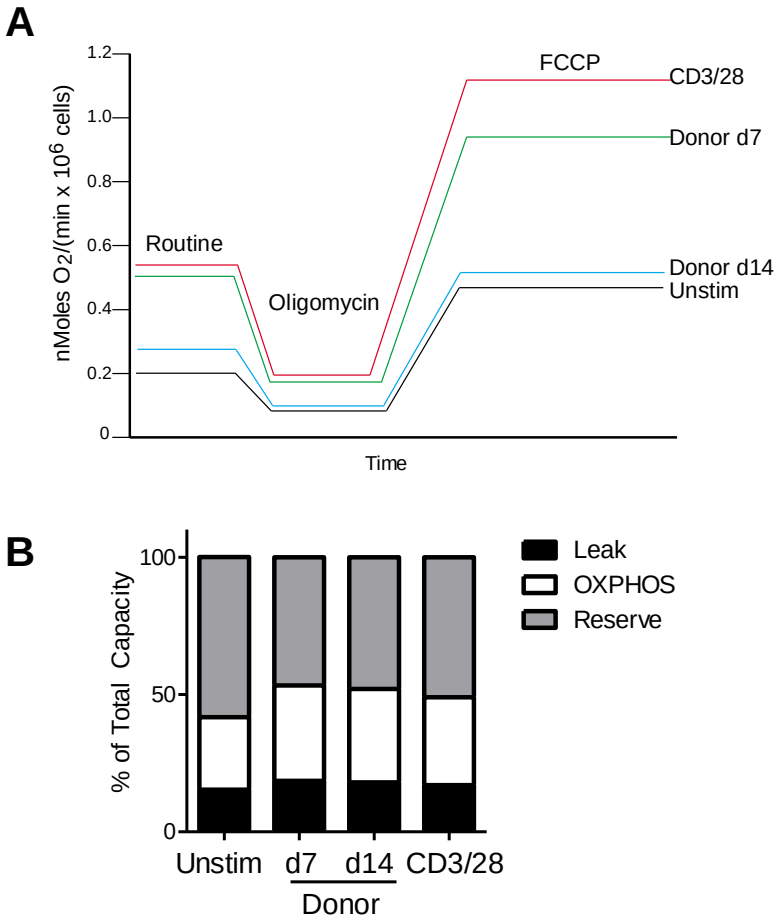

Figure 3.17. O_2 consumption parameters of control and alloreactive donor T cells. Data are from table 3.8. **A.** Routine, Oligo and FCCP rates of O_2 consumption. **B.** The percentage of total respiratory capacity used for proton leak (black), OXPHOS (white) and kept in reserve (gray).

Alloreactive donor T cells from mice with GVHD produce lactate 7-fold slower than T cells stimulated with anti-CD3/28 antibodies (Figure 3.16 B). One possible explanation for this difference is that stimulation with anti-CD3/28 antibodies activates all T cells regardless of their TCR specificity (507) while stimulation with MHC-mismatched alloantigen is estimated to activate only 1-10% of T cells (508). Hence, low rates of lactate production by donor T cells on d 7

could be due to the presence of large numbers of unactivated T cells in this population. To exclude this possibility, we analyzed the expression of the CD44 and CD62L on donor T cells on d 8 after transplant. Naïve T cells express low levels of CD44 and high levels of CD62L, while antigen-experienced effector or memory T cells express high levels of CD44 and low levels of CD62L (13, 509). We further analyzed the division status of donor T cells on d 2-7 after transplant using the cytoplasmic dye carboxyfluorescein diacetate succinimidyl ester (CFSE). The amount of CFSE in a cell decreases by half following each division, which causes a 2-fold decrease in fluorescence for each cell division (510, 511)

Approximately 80% of donor $CD4^+$ and donor $CD8^+$ T cells were $CD44^{hi}CD62L^{lo}$ by d 8 after transplant, consistent with an activated effector/effector memory phenotype (Figure 3.18 A) (512, 513). This finding contrasts with donor T cells from syngeneic transplants, of which fewer than 20% were $CD44^{hi}CD62L^{lo}$ (Figure 3.18 A). Similarly, 80-95% of donor T cells had divided 4 d after allogeneic transplant, while fewer than 10% of donor T cells divided after syngeneic transplant (Figure 3.18 B-C). These results show that by 7-8 d post-transplant, over 80% of donor T cells are activated. Hence, the relatively low lactate production in these cells is unlikely to be due to the presence of unactivated donor T cells.

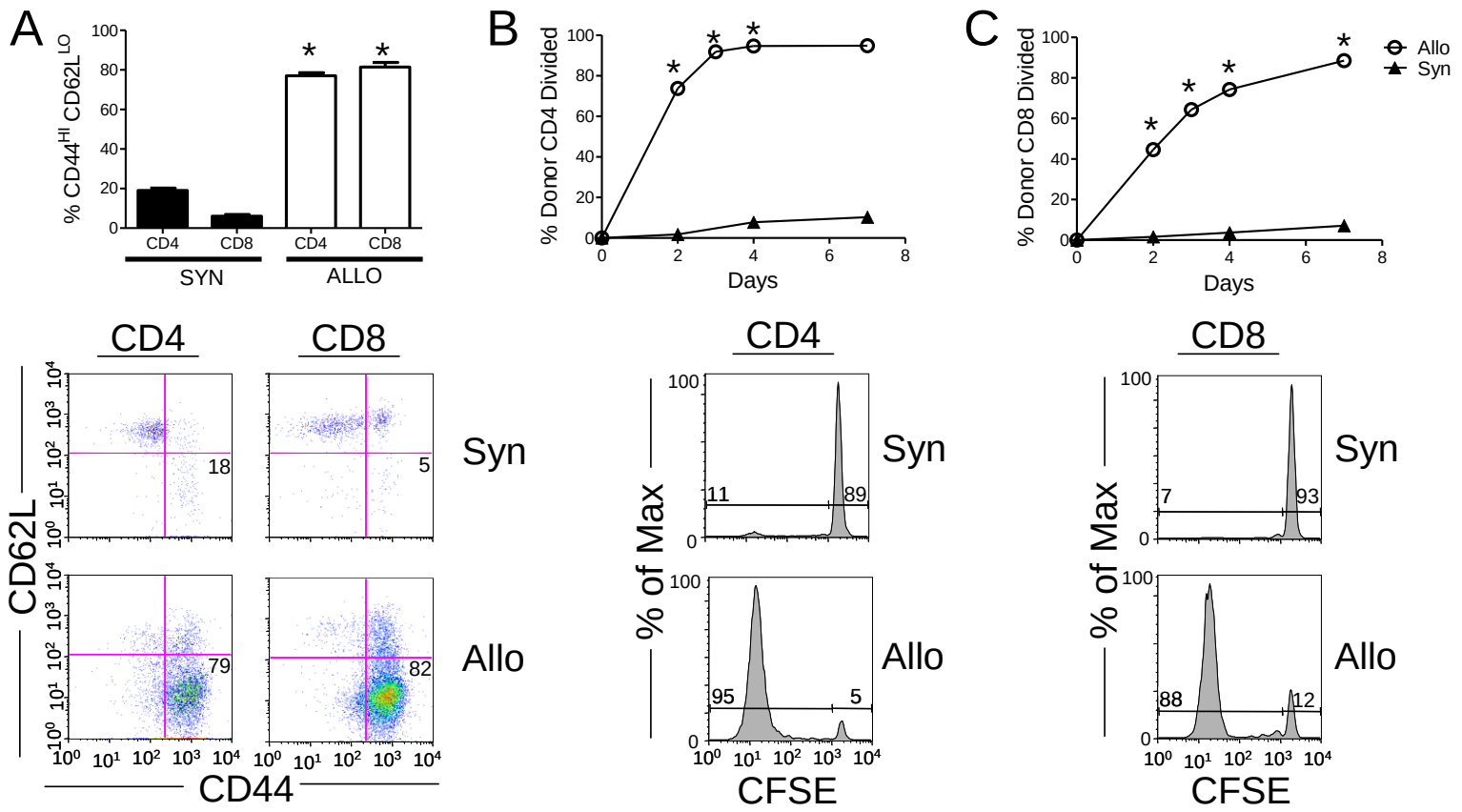

Figure 3.18. Activation marker expression and division status of donor T cells. A. Splenocytes (50 x 10^6) from nonirradiated allogeneic (B6-Ly5.2→F1, n=4) or syngeneic (B6-Ly5.2→B6, n=2) were analyzed 8 d after transplant. Donor T cells were identified and gated based on CD45.1$^+$ CD4$^+$ or CD45.1$^+$ CD8$^+$ expression and then analyzed for CD44 and CD62L expression as shown in flow cytometry plots. * p<0.0001 vs. syn. **B and C.** CFSE-labled splenocytes (50 x 10^6) from nonirradiated allogeneic (white circles, B6-Ly5.2→F1, n=3 per timepoint) or syngeneic (black triangles, B6-Ly5.2→B6, 1 per timepoint) were analyzed 2-7 d after transplant. Donor T cells were identified and gated based on CD45.1$^+$ CD4$^+$ or CD45.1$^+$ CD8$^+$ expression and the percentage of cells that had undgergone ≥1 division by CFSE was quantified as shown in flow cytometry histograms, which are from mice analyzed on day 7. * p<0.0001 vs. combined syn.

Glycolytic rate and GLUT1 expression of alloreactive donor T cells.

Aerobic glycolysis occurs when glucose-derived carbons are converted to lactate by lactate dehydrogenase (LDH) and secreted (59, 252). Several other possible fates exist for glucose-derived carbons, including oxidation in the TCA cycle and incorporation into biomolecules such as fatty acids (Figure 3.19) (52, 78, 207). Thus, lower rates of lactate production in alloreactive donor T cells compared to control stimulated T cells do not necessarily indicate lower glucose utilization, as high rates of glucose oxidation or glucose-derived biomolecule synthesis could occur concurrently with lower rates of lactate production.

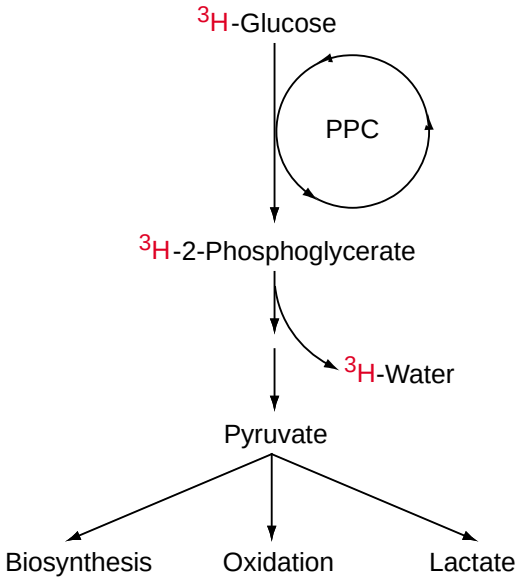

Figure 3.19. Glycolytic rate assay principle and fates of pyruvate. Glucose containing a 5-^{3}H label is metabolized by cells to ^{3}H-2-phosphoglycerate through the first eight steps of glycolysis. Enolase catalyzes the conversion of ^{3}H-2-phosphoglycerate to phosphoenolpyruvate and forms $^{3}H_2O$, which is analyzed following evaporation. Determination of the glycolytic rate in this manner indicates the amount of glucose metabolized for biosynthesis, oxidation and lactate production, but gives no information on pentose phosphate cycle activity (68, 373).

To determine the absolute rate of glycolysis in alloreactive donor T cells, we analyzed the conversion of 5-[^{3}H]-glucose to ^3H_2O, which occurs during the enolase-catalyzed penultimate step in glycolysis (49, 68). The amount of ^3H_2O formed reflects the total amount of glucose that will be oxidized in the TCA cycle, secreted as lactate, or converted into other biomolecules (Figure 3.19) (68). Alloreactive donor T cells were purified from the spleens of F1 mice 7 d after induction of nonirradiated GVHD as in O_2 consumption and lactate production experiments. Unstimulated T cells and T cells that had been stimulated with anti-CD3/28 antibodies were used as controls and display low and high rates of glycolysis respectively (58, 59).

Alloreactive donor T cells increased glycolysis 4-fold compared to unstimulated T cells (Figure 3.20 A). Further elevations in glycolysis were observed in T cells stimulated with anti-CD3/28 antibodies, which increased their glycolytic rate 30- and 7-fold compared to unstimulated and alloreactive donor T cells, respectively (Figure 3.20 A). These differences in glycolytic rate are consistent with differences observed in lactate production (Figure 3.16 B) and suggest that the decreased rate of lactate production in alloreactive donor T cells compared to T cells stimulated by anti-CD3/28 antibodies reflects lower total glycolytic metabolism.

Following activation through the TCR and CD28, T cells increase glycolysis in part by increasing their expression and plasma membrane localization of glucose transporter 1 (GLUT1) in a PI3-K/AKT-dependent fashion (Chapter 1) (58, 59, 68, 69). This regulatory mechanism suggests that

decreased rates of glycolysis in donor T cells as compared to T cells stimulated by anti-CD3/28 antibodies could be due to decreased levels of GLUT1 expression. To test this hypothesis, total cellular GLUT1 expression in purified donor T cells was evaluated by western blot (68). This method does not discriminate between plasma membrane (i.e., active) and intracellular (i.e., inactive) GLUT1 (58, 68). However, this distinction requires methods incompatible with the limiting number of primary cells available in our studies. Such methods include physically separating the plasma membrane from other cellular components, which requires 15 x 10^6 cells per analysis, (75) or using cells that express a GLUT1 molecule genetically designed to contain an extracellular FLAG or Myc tag (58, 68, 224, 514). However, mice do not currently exist that express FLAG- or Myc- tagged GLUT1.

Donor T cells purified 7 d after induction of GVHD expressed approximately 2-fold more GLUT1 compared to unstimulated T cells (Figure 3.20 B). This increased GLUT1 expression is similar to the increased lactate production and glycolytic rate in alloreactive donor T cells (Figure 3.16 B, Figure 3.20 A). However, unstimulated T cells, host T cells and alloreactive donor T cells all expressed approximately 5-fold less GLUT1 than T cells stimulated with anti-CD3/28 antibodies (Figure 3.20, B). This low GLUT1 expression in alloreactive donor T cells compared to control stimulated T cells may account for the disparate rates of lactate production and glycolysis between these two groups.

However, without direct measurements of cell surface GLUT1, we cannot exclude the possibility that *surface* GLUT1 levels are equivalent between alloreactive donor T cells and T cells stimulated with anti-CD3/28 antibodies (i.e., that most of the GLUT1 in CD3/28 cells is intracellular). This possibility is unlikely because stimulation with anti-CD3/28 antibodies increases the surface localization of GLUT1 (58, 69) and most GLUT1 expressed by mitogen-stimulated T cells is located in the plasma membrane (60). If surface GLUT1 levels were equivalent in alloreactive donor T cells and T cells stimulated with anti-CD3/28 antibodies, it would suggest other glycolytic enzymes such as hexokinase or phosphofructokinase as possible mediators of the different glycolytic rates between these two cell types (231).

While alloreactive donor T cells on d 7 after transplant have a decreased glycolytic rate and GLUT1 expression compared to control stimulated T cells, these observations do not preclude higher rates of glycolysis earlier during donor T cell expansion. Purification of donor T cells earlier than d 5 is not an ideal strategy for analyzing metabolic paramaters because 30-50% of donor T cells have not yet divided by 2 d after transplant (Figure 3.18). Thus, measurements of O_2 consumption, lactate production or GLUT1 expression would reflect both alloreactive and non-reactive donor T cells and make interpretation difficult. To separately analyze divided and undivided cells, we labeled donor T cells with CFSE and measured total cellular GLUT1 by flow cytometry (Figure 3.21) (59, 510).

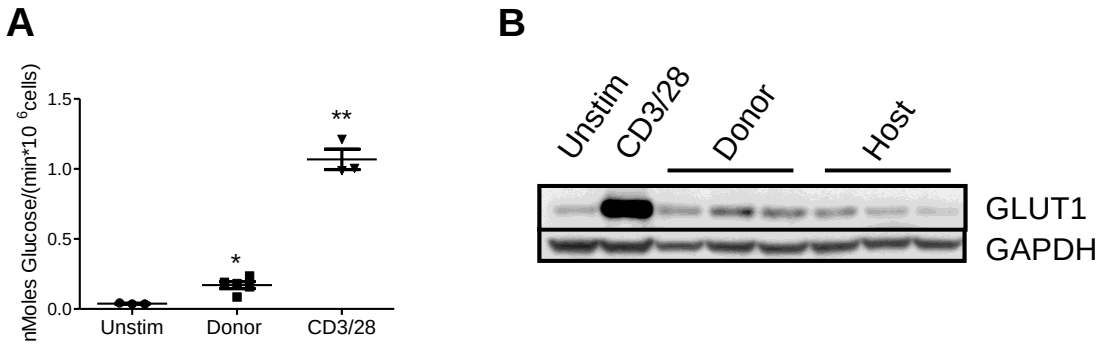

Figure 3.20. Glycolytic rate and GLUT1 expression of alloreactive donor T cells. Donor (Thy1.1^{+}) T cells were purified from F1 animals 7 d after i.v. injection of allogeneic B6-Thy1.1 splenocytes (50 x 10^{6}). T cells were purified from naïve B6 or B6-Ly5.2 mice based on Thy1.2 expression immediately before analysis (Unstim) or stimulated for 48 h with anti-CD3 and anti-CD28 antibodies (0.5 μg/mL, soluble; CD3/28). All populations were ≥ 85% pure. **A**. Unstim and CD3/28 T cells are from 3 independent mice or cultures. Donor T cells were from 10 mice with GVHD (2 mice/data point). T cells were incubated with 5-^{3}H-glucose for 1 h and the glycolytic rate was normalized to the cell number. * p=0.01 vs. Unstim. ** p<0.0001 vs. Unstim or Donor. **B.** Donor and Host T cells were purified from 3-4 independent mice 7 d after transplant. Lysates were deglycosylated prior to gel electrophoresis and analysis in order to prevent GLUT1 smearing. The GLUT1 band appeared at 45 kD as expected (58).

Both CD4 and CD8 divided donor T cells had approximately 2-fold more GLUT1 staining than undivided T cells on d2, d4 and d7 after transplant (Figure 3.21 A, Table 3.9). These increases are consistent with the 2-4-fold increase in GLUT1 expression and glycolytic rate observed in purified donor T cells on d 7 compared to unstimulated T cells (Figure 3.21). This 2-fold increase in GLUT1 expression contrasts with the 10-fold increase observed in control T cells stimulated *in vitro* with anti-CD3/28 antibodies (CD4: 120 vs. 14, CD8: 154 vs. 14)) or allogeneic stimulator cells (CD4: 166 vs. 16, CD8: 192 vs. 20) (Figure 3.21 B). These results indicate that alloreactive donor T cells have 2-fold more GLUT1 than undivided controls up to d7 during GVHD, but have 5-fold less GLUT1 than T cells stimulated *in vitro* with anti-CD3/28 antibodies or alloantigen. These results suggest that the lactate production and glycolytic rate of alloreactive donor T cells will be increased in comparison to unstimulated T cells, but decreased in comparison to control-stimulated T cells, even at early time points during expansion (58, 69).

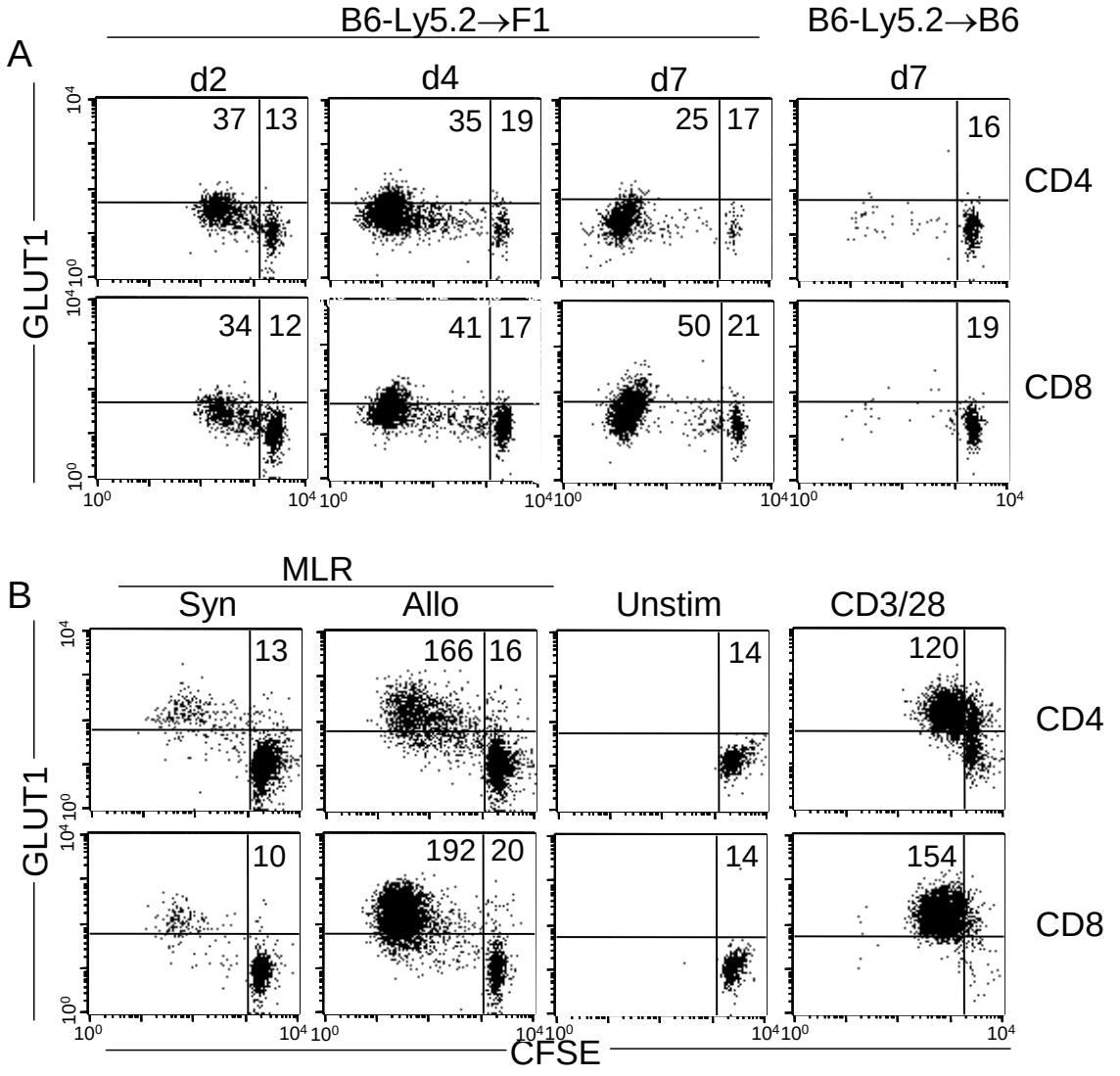

Figure 3.21. GLUT1 expression of alloreactive donor T cells during *in vivo* expansion. Numbers in the upper left quandrant indicate the GLUT1 MFI of divided cells and numbers in the upper right quadrant indicate the GLUT1 MFI of undivided cells. **A**. Donor splenocytes (B6-Ly5.2, 50 x 10^6) were labeled with CFSE and injected into F1 or B6 recipients. At the indicated timepoint, splenocytes were stained for surface markers and total cellular GLUT1. Donor T cells were identified as CD45.1$^+$ and CD4$^+$ or CD8$^+$. Flow plots are representive of 3 animals analyzed per timepoint. For B6-Ly5.2→F1, numbers are averaged from three mice, SEM values are in table 3.9. **B**. T cells (B6-Ly5.2) were labeled with CFSE and cultured with syngeneic (Syn, B6) or allogeneic (Allo, F1) splenocytes for 4 d and stained as in A. Alternatively, CFSE-labeled T cells were stained and fixed prior to culture (Unstim) or following 48 h culture with anti-CD3/28 antibodies (0.5 μg/mL).

Table 3.9. GLUT1 expression of alloreactive donor T cells during *in vivo* expansion. Donor splenocytes (B6-Ly5.2, 50 x 10^6) were labeled with CFSE and injected into F1 or B6 recipients. At the indicated timepoint, splenocytes were stained for surface markers and total cellular GLUT1. Donor T cells were identified as CD45.1$^+$ and CD4$^+$ or CD8$^+$. Data are averaged from 3 mice per timepoint and numbers in parentheses indicate SEM. * $p<0.001$ for divided vs. undivided within a given timepoint and cell type.

	Day 2		Day 4		Day 7	
	Undivided	Divided	Undivided	Divided	Undivided	Divided
CD4	13 (1)	37 (1)*	19 (2)	35 (2)*	16.9 (0.2)	25.2 (0.3)*
CD8	12.5 (0.3)	34 (2)*	17 (1)	41 (1)*	21 (1)	50 (1)*

Donor T cell size during GVHD. In addition to its role in ATP production, glycolysis provides carbon atoms and NADPH for biomolecule synthesis in proliferating cells (78). Because alloreactive donor T cells have a relatively low rate of glycolysis, one might expect their rate of proliferation to be similarly low due to an inability to synthesize biomolecules. However, CFSE profiles analyzed on d 2 after stimulation suggest that donor T cells proliferate at least as fast as T cells stimulated by anti-CD3/28 antibodies (Figure 3.21). An alternative hypothesis is that donor T cells compensate for low rates of glycolysis and biomolecule production by limiting their size, rather than their rate of proliferation.

To address this possibility, we measured the forward light scatter (FSC) of dividing donor T cells as they mediated GVHD. The FSC of a cell changes in proportion to its diameter, and is thus representative of cell size (515). As controls, we used unstimulated T cells and T cells stimulated for 48 h by CD3/28

antibodies, which have low and high rates of glycolysis, respectively (Figure 3.20). Donor T cells purified on d 7 of GVHD had greater FSC values 50% greater than unstimulated T cells ($p<0.0001$). T cells stimulated with anti-CD3/28 antibodies further increased their cell size, as they had FSC values 30% higher than donor T cells ($p=0.0003$). Together, these results suggest that, while donor T cells increase their size as they mediate GVHD, they are smaller than control T cells stimulated with anti-CD3/28 antibodies.

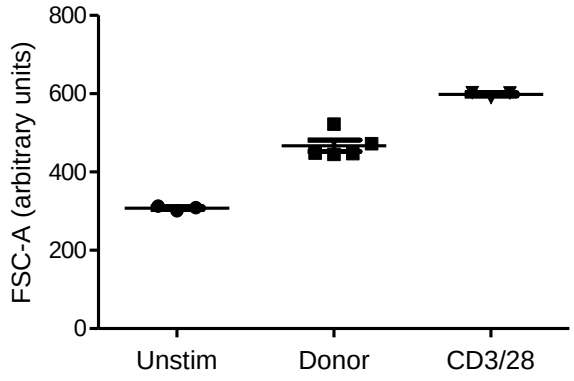

Figure 3.22. FSC-A analysis of donor T cells. Aliquots of cells purified for glycolytic rate analysis (Figure 3.20) were set aside and analyzed by flow cytometry. FSC-A indicates the area of the Forward Light Scatter parameter. Unstim and CD3/28 T cells are from 3 independent mice or cultures. Donor T cells are from 10 mice with GVHD (2 mice/data point).

Characterization of CD28, PD-1, CTLA-4 and phospho-AKT expression in alloreactive donor T cells. In activated T cells, aerobic glycolysis is stimulated by signaling through CD28, which activates PI3K and AKT, and leads to increased GLUT1 expression, glycolysis and lactate production (Chapter 1) (58, 59, 207). This pro-glycolytic signaling is opposed by signaling through the inhibitory receptors PD-1 and CTLA-4 (59, 255). Because alloreactive donor T cells have relatively low levels of aerobic glycolysis, we hypothesized that increased signaling through PD-1 and CTLA-4 and/or decreased signaling through CD28 could contribute to this phenomenon.

We first addressed this question by comparing the expression of CD28, CTLA-4 and PD-1 on unstimulated T cells and alloreactive donor T cells mediating GVHD. Unstimulated T cells expressed CD28, but had low levels of PD-1 and CTLA-4 (Figure 3.23 A). Similarly, donor T cells analyzed on d 7 after infusion into F1 hosts expressed CD28 (Figure 3.23 B). However, donor T cells increased their expression of both CTLA-4 and PD-1 (Figure 3.23 B). This observation suggests that increased signaling through CTLA-4 or PD-1 could restrict glycolysis in donor T cells as they mediate GVHD.

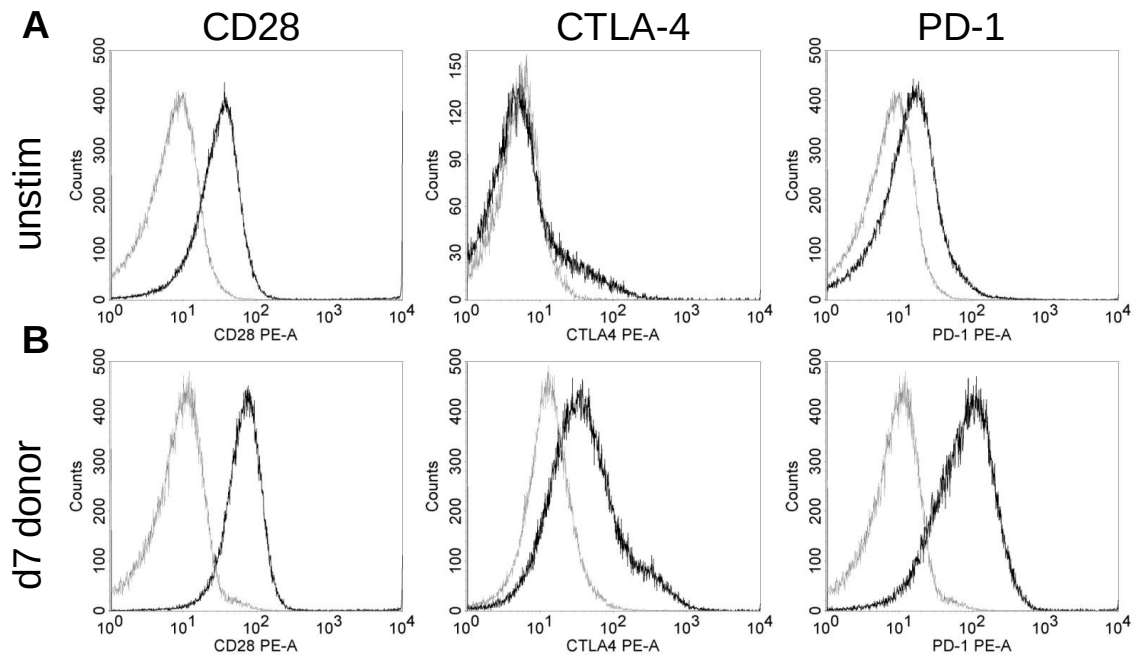

Figure 3.23. CD28, CTLA-4 and PD-1 expression in alloreactive donor T cells. A. Unstimulated T cells (unstim) from naïve B6-Ly5.2 mice (n=3) were identified on the basis of CD45.1, CD4 and CD8 expression. **B.** B6-Ly5.2 splenocytes (50 x 10^6) were injected into B6D2F1 recipients (n=3) and splenocytes were analyzed on d 7 after transplant. Donor T cells were identified on the basis of CD45.1, CD4 and CD8 expression. **A and B.** Gray histograms are isotype controls while black histograms are of the indicated protein. Cell surface CD28 and PD-1 and total cellular CTLA-4 were analyzed. Similar results were obtained from 3 mice in each group.

Signaling through CTLA-4 and PD-1 inhibits glycolysis by decreasing levels of phospho-AKT (255). Therefore, if low glycolysis in donor T cells is due to increased signaling through CTLA-4 and PD-1, we would expect these cells to have relatively low levels of phospho-AKT. To test this hypothesis, we purified alloreactive donor T cells 7 d after GVHD induction and compared phospho-AKT expression to unstimulated cells and to T cells stimulated with anti-CD3/28

antibodies. Alloreactive donor T cells had increased phospho-AKT compared to unstimulated control T cells (Figure 3.24 A). However, phospho-AKT was undetectable in control-stimulated T cells, likely because this phosphorylation peaks early after stimulation (i.e. within 1 h) and then decreases in *in vitro* models of T cell activation (516-518).

We then assessed phospho-AKT levels in CFSE-labeled donor T cells using flow cytometry, which allowed us to specifically analyze undivided and divided $CD4^+$ and $CD8^+$ donor T cells. AKT phosphorylation was observed in divided (i.e., $CFSE^{lo}$) donor $CD4^+$ and $CD8^+$ T cells on d 7 after transplant, suggesting an association with activation (Figure 3.24 B). These results show that alloreactive donor T cells can increase AKT phosphorylation *in vivo* as compared to unstimulated T cells, which is consistent with the modest increase in GLUT1 expression, lactate production and glycolytic rate compared to unstimulated T cells (Figure 3.16 B, Figure 3.20 A). However, the ability of alloreactive donor T cells to phosphorylate AKT suggests that other molecules that stimulate glycolysis such as HIF-1α (217, 372) or other molecules downstream of CD28 such as the TEC kinases or Vav1 (58) may have decreased activity in alloreactive donor T cells as compared to T cells stimulated with anti-CD3/28 antibodies and may be responsible for the differing levels of glycolysis in these two cell types.

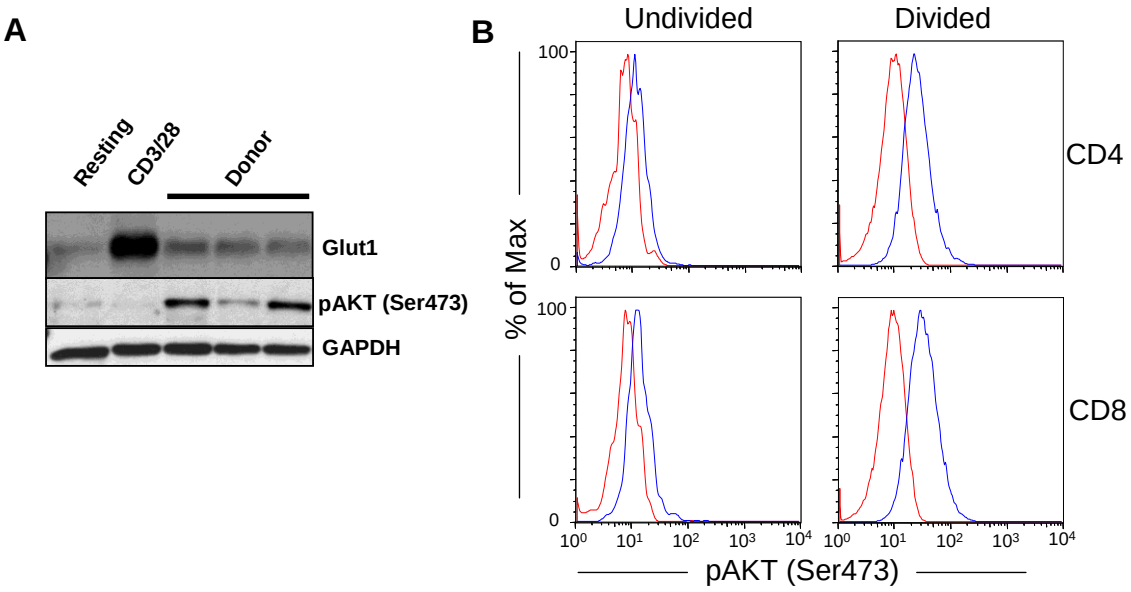

Figure 3.24. Phospho-AKT expression in alloreactive donor T cells. A. Donor (Thy1.1$^+$) T cells were purified from F1 animals 7 d after i.v. injection of allogeneic B6-Thy1.1 splenocytes (50 x 10^6). Control T cells were purified from naïve B6-Ly5.2 mice based on Thy1.2 expression immediately before analysis (Resting) or stimulated for 48 h with anti-CD3 and anti-CD28 antibodies (0.5 μg/mL, soluble; CD3/28). Cellular lysates were immunoblotted with antibodies specific for phosphor-AKT, GLUT1 or GAPDH. **B.** GVHD splenocytes were analyzed 7 d after the infusion of CFSE-labeled allogeneic B6 splenocytes (50 x 10^6) into F1 recipients. Donor cells were identified based on the absence of H-2k^d and gated as either CD4$^+$ or CD8$^+$. Cells were further classified as undivided or divided based on their CFSE status as in Figure 3.18. Red histograms are isotype control samples while blue histograms are stained for phospho-AKT.

$\Delta\psi_m$ and ROS levels in alloreactive donor T cells. In addition to generating ATP, OXPHOS produces ROS as a byproduct when electrons escape from the electron transport chain (252, 378). O_2^-, and in the presence of superoxide dismutases, H_2O_2 production increases as the voltage across the

mitochondrial inner membrane becomes increasingly negative (i.e., a greater accumulation of protons in the intermembrane space), a state termed $\Delta\psi_m$ hyperpolarization (131, 168, 381). $\Delta\psi_m$ hyperpolarization disfavors additional proton pumping, thus increasing the half-lives of reactive iron-sulfur clusters and ubisemiquinone, which undergo single electron reactions with O_2 to form O_2^- (131, 154, 167).

T cells activated *in vitro* increase their intracellular [Ca^{2+}] levels from 75 nM to 150 nM within minutes of anti-CD3 stimulation, which activates the TCA cycle and leads to a 2-fold increase in NADH that hyperpolarizes $\Delta\psi_m$ (254). Because the increased O_2 consumption observed in donor T cells suggests similar increases in TCA cycle activity, we hypothesized that alloreactive donor T cells might have a hyperpolarized $\Delta\psi_m$ compared to unstimulated T cells, which could coinincide with increased O_2^- levels.

To test this hypothesis, donor T cells were identified and distinguished into activated ($CFSE^{lo}$) or unactivated ($CFSE^{hi}$) subsets (Figure 3.26) 4 d after transplant into F1 (allo) or B6 (syn) hosts and $\Delta\psi_m$ was evaluated using tetramethylrhodamine methyl ester (TMRM). TMRM is a cationic lipophilic fluorescent dye (Figure 3.25) that accumulates in membranes as the voltage across that membrane increases (145, 519). This property has led to the frequent use of TMRM to assess $\Delta\psi_m$ in whole cells. However, TMRM can accumulate in both the plasma and the mitochondrial membranes, which often complicates interpretation (145, 338, 519).

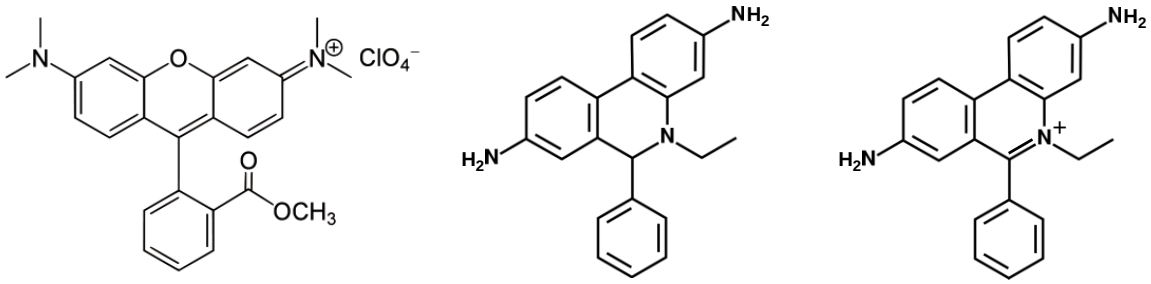

TMRM DHE E^+

Figure 3.25. Structures of TMRM, DHE and Ethidium. From (520, 521).

Divided donor T cells had a 60% increase in TMRM fluorescence compared to unactivated donor T cells ($CFSE^{hi}$) in allo or syn recipients or unactivated host T cells (Figure 3.26 A). This finding could result from either an increased plasma or mitochondrial membrane potential (145, 338). However, there is disagreement as to whether T cells increase the potential of the plasma membrane following activation (522). The studies in which plasma membrane hyperpolarization was observed suggest that it is small in magnitude (~ 5 mV) and lasts less than 5 min after activation (523-525). Although effects due to changes in plasma membrane potential cannot be discounted, our results are consistent with an interpretation in which $\Delta\psi_m$ is hyperpolarized in divided donor T cells.

To measure ROS levels in alloreactive donor T cells, we stained CFSE-labeled donor T cells with DHE (Figure 3.25). The weakly fluorescent DHE is

oxidized to form the highly fluorescent ethidium (E^+) by O_2^-, but not by other oxidants such H_2O_2 or $HNOO^-$ (526). These properties make DHE fluorescence a selective marker of O_2^- levels (340). However, due to the ability of DHE to dismutate O_2^- to H_2O_2, DHE fluorescence is considered a qualitative, rather than quantitative, marker of O_2^- levels (340, 520).

Dividing donor T cells showed a 2-fold increase in DHE staining compared to control unactivated T cells (Figure 3.26 B). This result suggests that alloreactive donor T cells have increased levels of O_2^-, which coincides with the increased TMRM staining observed in these cells (Figure 3.26 A).

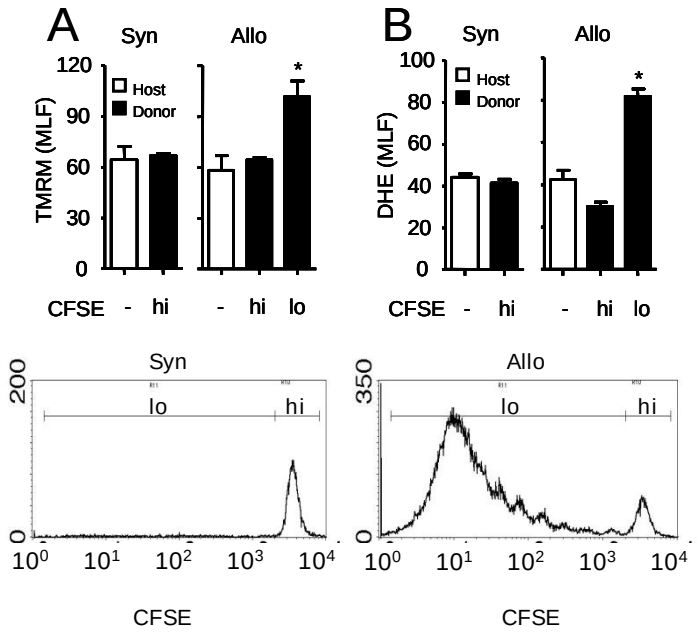

Figure 3.26. TMRM and DHE staining of alloreactive donor T cells. B6-Ly5.2 splenocytes (50 x 10^6, CFSE-labeled) were injected i.v. into F1 (allo) or B6 (syn) recipients. On d 4 following transplant, splenocytes were analyzed for TMRM (**A**, n=8/group) or DHE (**B,** n=6/group) staining. For each mouse, the mean log fluorescence (MLF) from a sample without DHE or TMRM dye was subtracted from the MLF value for the stained samples. CFSE gating strategy is shown below. * indicates $p<0.05$.

Glutathione and pyruvate levels of alloreactive donor T cells. Cells utilize a variety of antioxidants to scavenge ROS and prevent oxidative damage to biomolecules (527). Among these antixodants are pyruvate and glutathione, both of which are consumed as they detoxify ROS (Figure 3.7, Figure 3.8) (196, 200, 528). Because alloreactive donor T cells have increased O_2^- levels compared to unstimulated T cells (Figure 3.26 B), we hypothesized that they may also have lower levels of antioxidants.

We measured intracellular pyruvate levels using an enzymatic kit based on the generation of H_2O_2 following the reaction of pyruvate and pyruvate oxidase (529). Alloreactive donor T cells purified 7 d after transplant had nearly undetectable levels of pyruvate, while unstimulated T cells from naïve mice or host T cells from d 7 GVHD mice had 6-10 pMoles pyruvate/μg protein (Figure 3.27 A). We next measured total intracellular glutathione levels using an assay that generates color as 5,5'-dithiobis-(2-nitrobenzoic acid) reacts with glutathione (530). Alloreactive donor T cells purified 7 d after transplant into F1 hosts had 16 pMoles glutathione/μg protein, which is 25% less compared to or host T cells (Figure 3.27 B). Together, these results show that alloreactive donor T cells have decreased antioxidant levels compared to unstimulated and host T cells, perhaps due to their increased O_2^- levels.

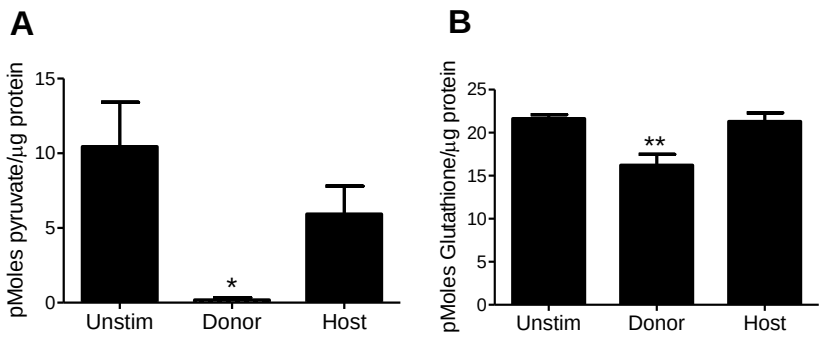

Figure 3.27. Pyruvate and glutathione levels of alloreactive donor T cells. Donor (Thy1.1$^+$) or Host (Thy1.2$^+$) T cells were purified from F1 animals 7 d after i.v. injection of allogeneic B6-Thy1.1 splenocytes (50 x 10^6). Unstimulated T cells were purified from naïve B6 or B6-Ly5.2 mice based on Thy1.2 expression immediately before analysis (Unstim)**. A**. Pyruvate levels from Unstim (n=5), Donor (n=5) or Host (n=3) T cells were determined using the Biovision assay kit. Results are combined from 3 independent experiments. * p<0.01. **B**. Total glutathione levels from Unstim (n=2), Donor (n=8) or Host (n=5) T cells. Results are combined from 2 independent experiments. ** p=0.01 Donor vs. Host, p=0.04 Donor vs. Unstim.

O_2 consumption, lactate production and GLUT1 expression of proliferating bone marrow cells after transplant. Following myeloablative bone marrow transplantation, numerous cell types proliferate within the recipient (48, 406, 412, 424, 531). Donor-derived myeloid and lymphoid precursors rapidly proliferate in the bone marrow to regenerate the host immune system (406, 408, 412), while mature donor T cells in the periphery can proliferate in response to alloantigen and mediate GVHD (48, 424). Alloreactive donor T cells increase OXPHOS compared to unstimulated cells and use this pathway to generate 80-90% of their ATP (Figure 3.16). However, the metabolic pathways used by proliferating bone marrow cells post-transplant unknown (406).

Mature peripheral granulocytes have mitochondria that inefficiently synthesize ATP, possibly because complexes I, III and IV do not associate into the higher order supercomplexes that are characteristic of mitochondria from tissues such as the heart (discussed further below) (480, 481). Because granulocytes are amongst the first cells to be generated by post-transplant bone marrow (408, 409), this observation suggests that proliferating bone marrow cells may increase glycolysis rather than OXPHOS post-transplant.

To test this hypothesis, we transfused donor (B6) bone marrow into lethally irradiated syngeneic recipients (1100 cGy, B6-Ly5.2) to induce rapid proliferation in the bone marrow. We first analyzed the surface expression of lineage markers of naïve and post-transplant bone marrow to determine the cell types present. Naïve and post-transplant bone marrow cells primarily (40-50%) stained for the granulocyte lineage marker GR-1, rather than for the B cell or T cell markers B220 (10-25%) or Thy1.2 (< 5%) (Figure 3.28 A and B). We next assessed cellular proliferation in naïve and post-transplant bone marrow by injecting mice with 5-bromo-2-deoxyuridine (BrdU), a nucleoside analog whose incorporation indicates active DNA synthesis, and measuring its incorporation by flow cytometry (532). After transplant, 80% of bone marrow cells stained positively for BrdU, as compared to 55% of bone marrow cells from naïve mice

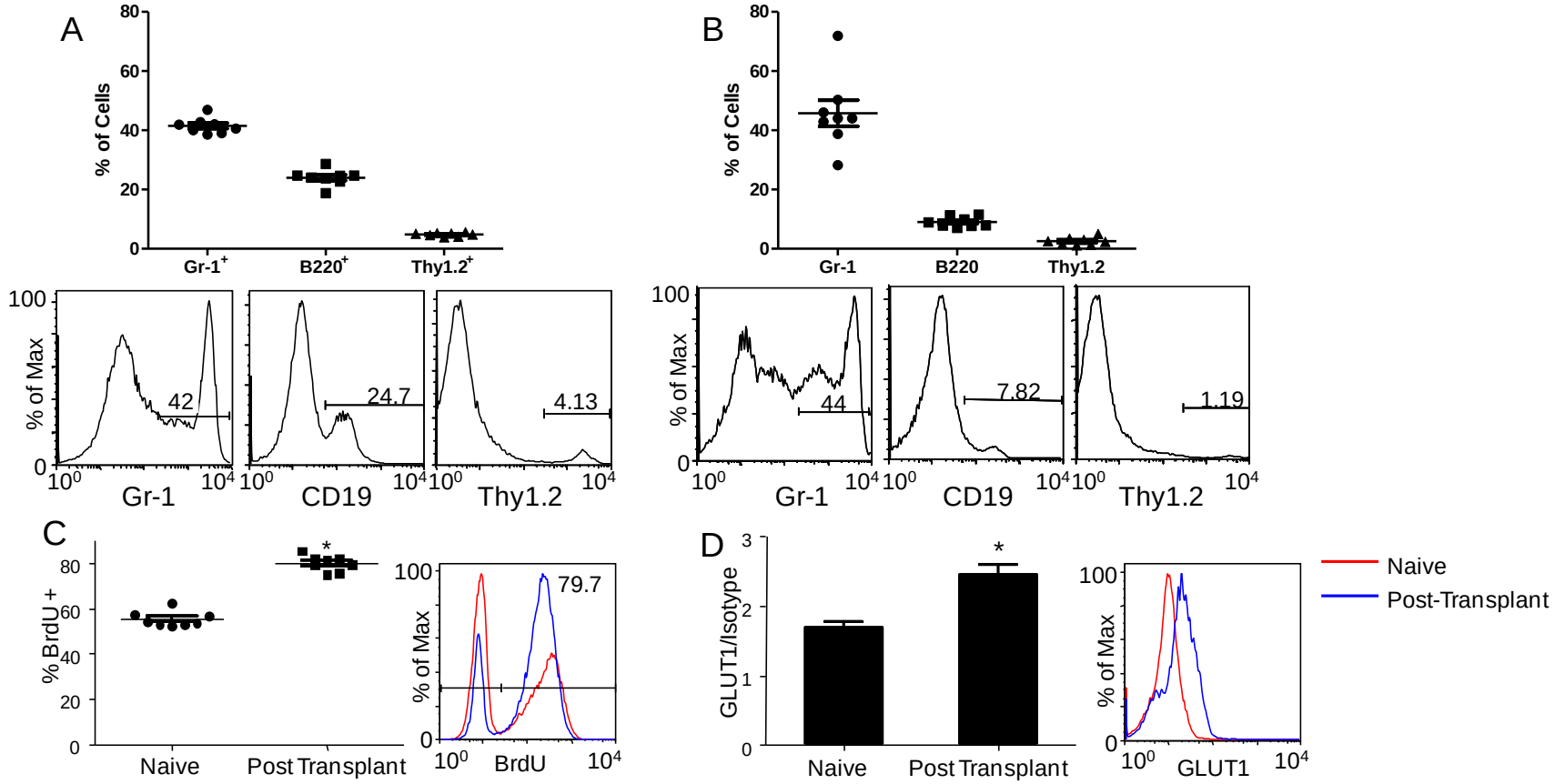

Figure 3.28. Lineage marker expression, BrdU incorporation and GLUT1 expression in naïve and post-transplant bone marrow. Lethally irradiated (1100 cGy) B6-Ly5.2 mice were transplanted with B6 bone marrow cells (5 x 10^6). **A and B**. Bone marrow from naive B6 (A, n=8) and d 8 post-transplant (B, n=8) mice were analyzed for lineage markers by flow cytometry as indicated. **C**. Naïve B6 (n=8) or d 7 post-transplant mice (n=8) were injected with BrdU (100mg/kg) and given BrdU drinking water (1mg/mL). 24 h later, bone marrow was harvested and analyzed for BrdU incorporation. **D.** Bone marrow cells from naïve B6 (n=10) or d 8 post-transplant mice (n=10) were analyzed for GLUT1 expression by flow cytometry. * $p<0.001$

(Figure 3.28 C, $p<0.001$). Together, these results show that post-transplant bone marrow cells are primarily granulocytes and that they have increased proliferation compared to bone marrow cells from naïve mice.

To determine the metabolic changes that accompany this increased proliferation, we measured GLUT1 expression, lactate production and O_2 consumption in bone marrow cells from post-transplant and naïve animals. Post-transplant bone marrow cells increased GLUT1 expression by 50% over naïve bone marrow (Figure 3.28 D), which suggests an increased glycolytic metabolism in post-transplant cells. Consistent with this hypothesis, post-transplant bone marrow cells increased lactate production 2.8-fold compared to naïve bone marrow (Figure 3.29 A).

Unlike GLUT1 expression and lactate production, rates of O_2 consumption were not statistically different between post-transplant and naïve bone marrow (Figure 3.29 B). This finding suggests that metabolic demands associated with increased proliferation in post-transplant bone marrow cells (Figure 3.28) are met by increased glycolysis rather than increased OXPHOS. In support of this hypothesis, post-transplant bone marrow cells did not increase oxidative ATP production compared to naïve cells (1.3 ± 0.1 vs. 1.4 ± 0.2 nMoles ATP/(min x 10^6 cells), $p=0.2$), but increased glycolytic ATP production 2.5-fold (0.98 ± 0.11 vs. 0.39 ± 0.06 nMoles ATP/(min x 10^6 cells), $p=0.0002$). Thus, post-transplant bone marrow cells produced 43% of their ATP through glycolysis and 57% through OXPHOS (Figure 3.29 C). These results indicate that bone marrow cells increase glycolysis but do not increase OXPHOS following transplant.

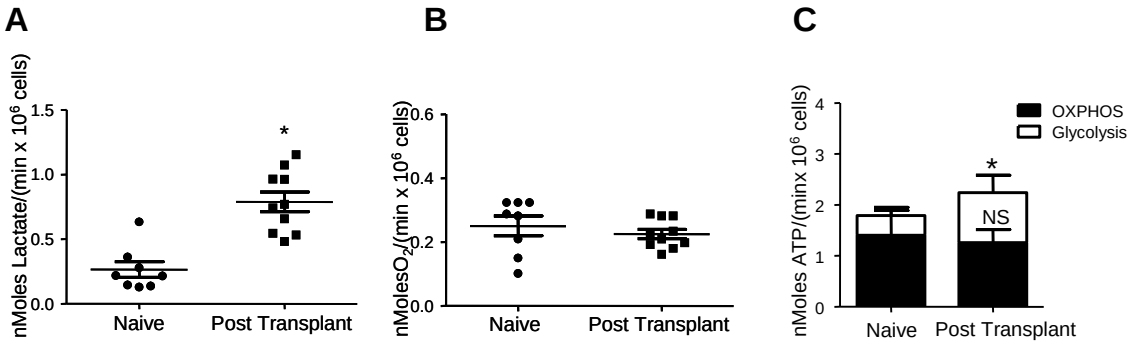

Figure 3.29. Lactate production, O_2 consumption and ATP production of naïve and post-transplant bone marrow. A and B. Bone marrow from naïve B6 (n=8) or d 8 or d 9 post-transplant (n=10) mice was harvested, RBC-lysed and analyzed for lactate production and O_2 consumption. **C**. ATP production was calculated from A and B as ATP_{OXPHOS}=5.6 x O_2 Consumption and $ATP_{Glycolysis}$=Lactate Production + 0.4 x O_2 Consumption. Error bars indicate standard error. * $p<0.001$

Treatment of bone marrow cells with oligomycin reduced respiration rates by 62-64% in naïve and post-transplant bone marrow cells (Table 3.10). This finding indicates that, like T cells (Table 3.10), bone marrow cells use ~65% of their basal respiratory rates to synthesize ATP. FCCP treatment of bone marrow cells showed that post-transplant cells had a small but significant (20% increase, $p=0.03$) increase in total respiratory capacity (Table 3.10). This finding suggests that post-transplant bone marrow cells may have a greater ability to increase oxidative ATP synthesis than naïve bone marrow cells, if energetic demands increase (503). These data are shown graphically in Figure 3.30.

	nMoles O_2/(min x 10^6 cells)				% of Routine		% of Total Capacity		
	Routine	**Oligo**	**FCCP**	**OXPHOS**	**OXPHOS**	**Leak**	**OXPHOS**	**Leak**	**Reserve**
Naïve (n=8)	0.26 (0.03)	0.10 (0.01)	0.53 (0.04)	0.16 (0.02)	62 (2)	38 (2)	30 (2)	18 (2)	52 (3)
Post-Transplant (n=7)	0.23 (0.02)	0.08 (0.01)	0.65 (0.05)*	0.15 (0.01)	64 (3)	36 (3)	23 (1)*	13 (1)*	64 (1)*

Table 3.10. O_2 consumption parameters of naïve and post-transplant bone marrow. O_2 consumption measurements were made as in Figure 3.29. Routine, Oligo and FCCP rates were collected as described in the text and methods. Calculations for OXPHOS and percentages were made as described in the methods. Numbers in parentheses indicate standard error. * $p<0.05$ compared to Naïve bone marrow. Treatment with myxothiazol showed that extramitochondrial O_2 consumption was less than 5% of routine rates and was ignored.

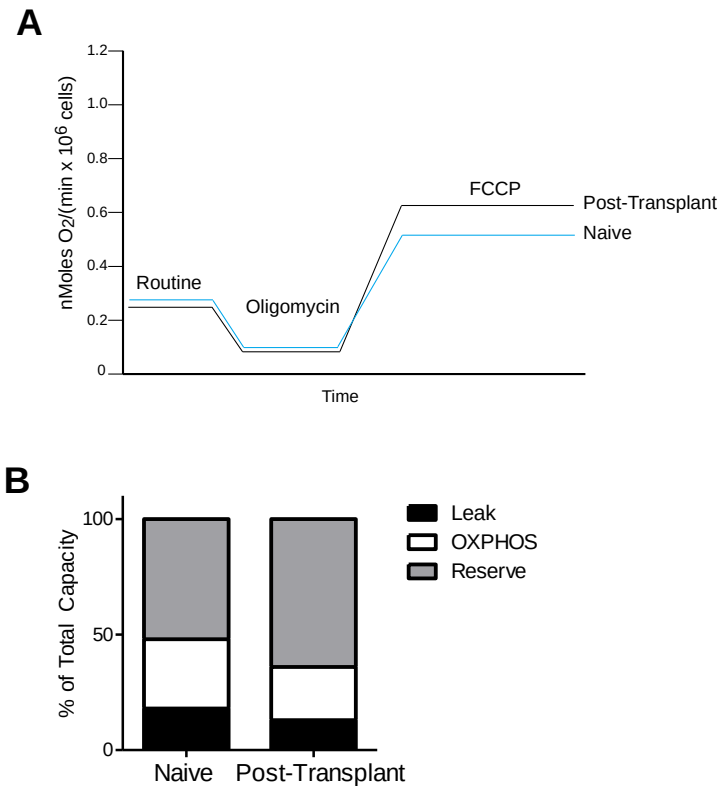

Figure 3.30. O_2 consumption parameters of naïve and post-transplant bone marrow. Data are from table 3.8. **A.** Routine, Oligo and FCCP rates of O_2 consumption. **B.** The percentage of total respiratory capacity used for proton leak (black), OXPHOS (white) and kept in reserve (gray).

Following transplant, bone marrow cells do not increase oxidative ATP production compared to naïve bone marrow cells, but increase lactate production 3-fold (Figure 3.29). This finding contrasts with alloreactive donor T cells, which increase both OXPHOS and lactate production compared to unstimulated T cells (Figure 3.16). On an absolute level, proliferating bone marrow cells generate less ATP than alloreactive donor T cells (Figure 3.16, Figure 3.29, $p<0.0001$), which suggests that they may have lower overall bioenergetic demands (207).

Because proliferation requires large amounts of energy (78, 207), post-transplant bone marrow cells could have lower energetic demands than alloreactive donor T cells due to slower rates of proliferation.

To test this hypothesis, we measured the proliferative index of alloreactive donor T cells and post-transplant bone marrow granulocytes. The proliferative index is defined as the average number of divisions undergone by dividing cells (533) and was calculated using FlowJo software (Figure 3.31). The proliferation index of donor bone marrow granulocytes post-transplant was 2-fold lower than that of alloreactive donor T cells (Figure 3.31). These observations suggest that alloreactive donor T cells may have increased energetic demands compared to post-transplant bone marrow cells due to their higher rates of proliferation.

While donor T cells transplanted into nonirradiated syngeneic recipients do not proliferate (Figure 3.18, Figure 3.26), donor T cells transplanted into *irradiated* syngeneic recipients proliferate to fill the empty immune system (534). This antigen-independent expansion is termed homeostatic proliferation (534). Homeostatically proliferating syngeneic T cells also had lower rates of proliferation than alloreactive donor T cells (Figure 3.31, 1.7 vs. 3.5, $p<0.0001$), suggesting that T cells proliferating in response to alloantigen may have increased energetic demands compared to T cells proliferating to fill an empty niche.

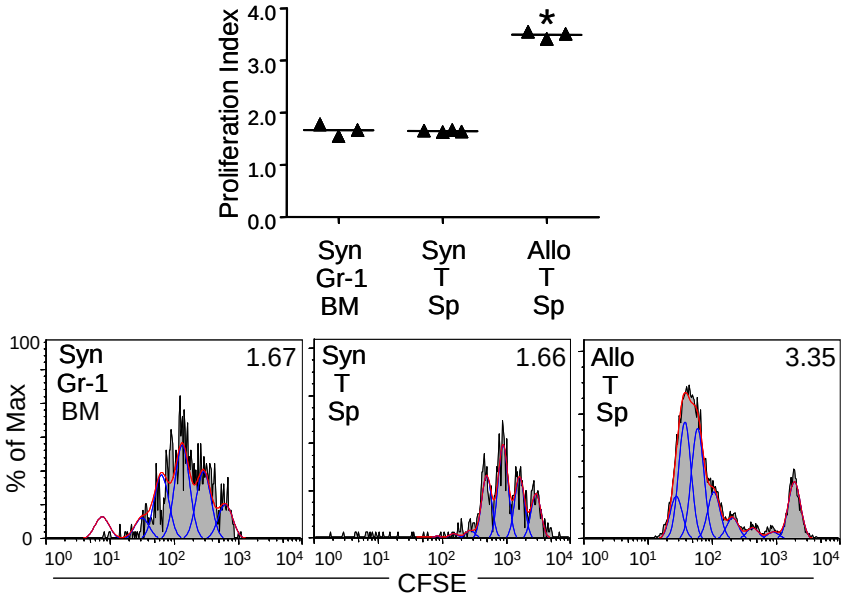

Figure 3.31. Proliferation indices of post-transplant bone marrow cells, syngeneic T cells and alloreactive T cells. Syn: CFSE-labeld bone marrow (B6, 5-50 x 10^6) was transplanted into congenic (B6-Ly5.2) recipients conditioned with 1100 cGy. Allo: CFSE-labeled splenocytes (B6-Ly5.2, 50 x 10^6) were transplanted into F1 recipients. Donor cells were identified based on CD45.1 and CD45.2 expression 72 h post transplant in the bone marrow (BM) or spleen (Sp) and gated as Gr-1^+ (Gr-1) or CD4/8^+ (T). Proliferation index is indicated in the upper right corner of histograms and was calculated using FlowJo software as shown for representative mice. Data are combined from 3 separate experiments. * $p < 0.001$.

Pyruvate levels of post-transplant bone marrow cells. While alloreactive donor T cells increase OXPHOS 2-fold over unstimulated T cells and use glycolysis to generate only 10-20% of their ATP (Figure 3.29, Table 3.8), post-transplant bone marrow cells do not increase OXPHOS following transplant compared to naïve bone marrow cells and use glycolysis to generate 40% of

their ATP (Figure 3.29, Table 3.10). Post-transplant bone marrow cells also produce lactate 70% faster compared to alloreactive donor T cells purified 7 d after transplant (0.9 vs. 0.5 nMoles lactate/(min x 10^6 cells), p=0.02). This increased glycolysis could help post-transplant bone marrow cells maintain their levels of antioxidants while they proliferate (252, 376, 535). To test this hypothesis, we measured intracellular pyruvate in bone marrow cells from naïve and post-transplant mice. Pyruvate levels in naïve and post-transplant bone marrow were nearly identical (Figure 3.32). This finding indicates that, unlike alloreactive donor T cells, repopulating bone marrow cells do not have decreased levels of pyruvate compared to unstimulated or naïve controls. Because pyruvate functions as an antioxidant (203, 493, 495), this finding suggests that alloreactive donor T cells may be more sensitive to ROS-mediated cell death than post-transplant bone marrow cells.

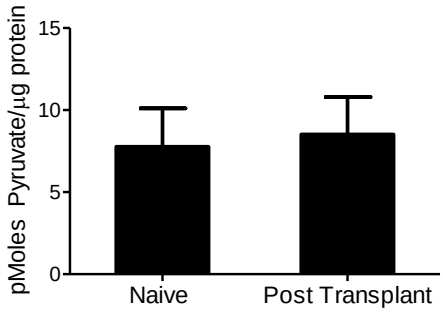

Figure 3.32. Pyruvate levels of naïve and post-transplant bone marrow cells. Lethally irradiated (1100 cGy) B6-Ly5.2 mice were transplanted with B6 bone marrow cells (5 x 10^6). Bone marrow was harvested from naïve B6 (n=8) or d7/d8 post-transplant (n=9) mice and RBC-lysed. Pyruvate levels were measured using the pyruvate assay kit from Biovision.

Discussion

The experiments reported in this chapter demonstrate that alloreactive donor T cells possess bioenergetic characteristics that distinguish them from unstimulated T cells, control-stimulated T cells and proliferating cells in the bone marrow. During the development of disease in the B6→F1 model of nonirradiated GVHD, alloreactive donor T cells have high rates of OXPHOS than glycolysis and depleted glutathione and pyruvate levels. This bioenergetic phenotype is distinct from the "Warburg effect", which was recently hypothesized to characterize *all* proliferating cells (78). The following sections will (1) discuss the potential carbon sources used to support OXPHOS in alloreactive donor T cells; (2) contrast the bioenegetics of alloreactive donor T cells with the bioenergetics of control-stimulated T cells, which utilize high rates of aerobic glycolysis; (3) contrast alloreactive donor T cell metabolism with that of proliferating post-transplant bone marrow cells; and (4) discuss the role that cytokine signaling and conditioning may play in regulating metabolism during GVHD.

Potential carbon sources for alloreactive donor T cells. Unlike acutely stimulated T cells (Figure 3.16) (207, 250-252, 536) or proliferating bone marrow cells (Figure 3.29), alloreactive donor T cells generate 80-90% of their energy using OXPHOS. OXPHOS is driven by the electron carriers NADH and $FADH_2$ (502). Electrons from these molecules generate a proton gradient across the inner mitochondrial membrane as they are passed along complexes I-IV (CI-CIV) of the electron transport chain to O_2, the terminal electron acceptor (138, 140,

145, 381). Protons flow back down this gradient through complex V (the F_1F_o-ATPase) to generate ATP (153). Hence, the oxidation of NADH and $FADH_2$ drive O_2 consumption and oxidative ATP production (OXPHOS). Because NADH and $FADH_2$ are formed during the oxidation of glucose (502), amino acids (113) and fatty acids (537), it is possible that any of these carbon sources could contribute to increased OXPHOS in alloreactive donor T cells.

Glycolysis is increased 4-fold in alloreactive donor T cells compared to unstimulated cells (Figure 3.20), which suggests that increased glucose oxidation in the TCA cycle may play a role in providing the NADH for donor T cell OXPHOS. While some glucose-derived carbons are apparently used for lactate production in alloreactive donor T cells (Figure 3.16), some may enter the mitochondria for oxidation or for biomolecule synthesis (Figure 3.33) (78, 207). The rapid proliferation of donor T cells suggests a need for newly synthesized biomolecules and an increase in glucose-derived fatty acid synthesis, rather than complete oxidation of glucose into CO_2 (372). However, glucose-derived fatty acid synthesis requires glucose-derived pyruvate to pass through either pyruvate carboxylase (PC) or pyruvate dehydrogenase (PDH), before forming citrate and being exported to the cytosol for conversion into fatty acids (Figure 3.33). Because PDH generates NADH (105, 123), increased flux through PDH could contribute to increased OXPHOS in alloreactive donor T cells. In support of this hypothesis, increased glucose-derived fatty acid synthesis contributes to increased OXPHOS in an IL-3 dependent lymphoid cell line (372). In these experiments, fatty acid synthesis was increased by lowering HIF-1α levels, which

otherwise inhibits glucose-derived carbon entry into the mitochondria by inhibiting PDH (121, 122, 372). Cells with decreased levels of HIF-1α increased glucose-derived lipid synthesis by 2-3-fold despite lower overall glucose uptake. This increased lipid synthesis was accompanied by a 1.5-2-fold increase in O_2 consumption, presumably due to increased NADH formation by pyruvate dehydrogenase (372).

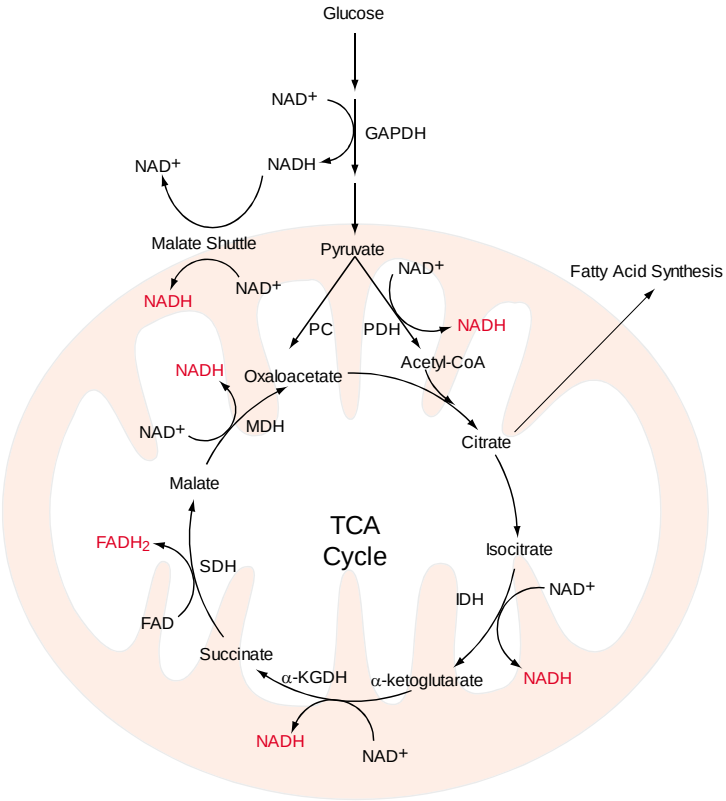

Figure 3.33. NADH and $FADH_2$ generation from glucose. Glucose can generate NADH and $FADH_2$ through the indicated reactions. Substrates in red can be used for oxidative ATP production. Abbreviations are as follows: glyceraldehydes-3-phosphate dehydrogenase (GAPDH), pyruvate dehydrogenase (PDH), pyruvate carboxylase (PC), isocitrate dehydrogenase (IDH), α-ketoglutarate dehydrogenase (α-KDH), succinate dehydrogenase (SDH), malate dehydrogenase (MDH). Other steps have been omitted for clarity. Adapted from (49).

Another potential fuel source to support increased OXPHOS in alloreactive donor T cells is amino acid oxidation. Glutamine is the most abundant amino acid in the plasma, with a concentration around 0.6 mM in healthy human subjects (538), and its metabolism is important for proliferating cells, including lymphocytes (62, 113, 206, 538-543). Glutamine enters cells through neutral amino acid transporters such as SN2, ASCT2 and SLC1A5 (113, 541). Mitochondrial glutaminase cleaves glutamine into ammonia and glutamate, which can be used for numerous metabolic functions including oxidative ATP production and NADPH generation (Figure 3.34) (113, 544, 545). Following this reaction, glutamate transaminase catalyzes the formation of the TCA-cycle intermediate α-ketoglutarate. Glutamine-derived α-ketoglutarate is either oxidized by the TCA cycle, resulting in NADH production, or is exported from the mitochondria as malate in order to generate NADPH and pyruvate through the action of malic enzyme (113). Glutamine metabolism is regulated by the oncogene c-Myc, which promotes glutaminase expression by regulating microRNA transcription (542) and increases the expression of glutamine transporters such as SN2 and ASCT2 by directly inducing their transcription (541).

T cells stimulated with phorbyl 12-myristate 13-acetate (PMA) and ionomycin increase c-Myc RNA levels > 10-fold compared to unstimulated cells (546). Similarly, T cells responding to immunization with hen egg lysozyme up-regulate c-Myc expression *in vivo* (547). Because c-Myc promotes glutamine uptake and utilization (541, 542), these observations suggest that activated T cells might up-regulate glutamine metabolism. Indeed, rat thymocytes stimulated with conA consume 8-fold more glutamine and produce 4-fold more glutamine-derived CO_2 than resting thymocytes (62). This increased glutamine metabolism is important for lymphocyte proliferation, as reducing glutamine levels in culture media from 0.6 to 0.01 mM decreases conA-stimulated PBMC proliferation by 10-fold (538). Similar experiments indicate that glutamine restriction inhibits conA-stimulated proliferation 5-10-fold in rat (539) or mouse lymphocytes (540). Glutamine is also important for lymphocyte cytokine production, as human PBMCs stimulated with conA in media without glutamine produce 2-5-fold less IL-2, IFN-γ and IL-10 compared to cells stimulated with 0.6 mM glutamine (548).

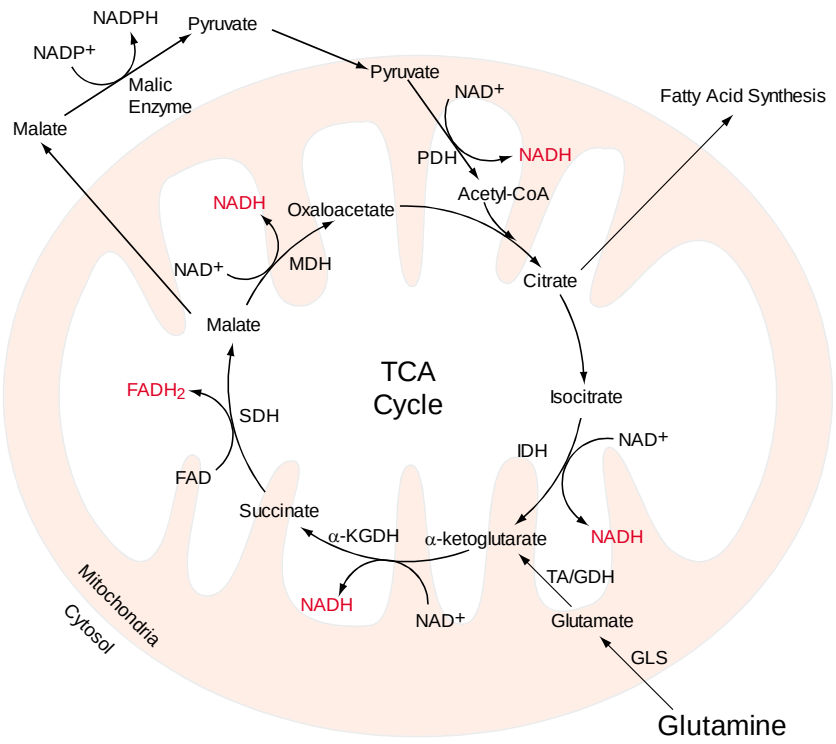

Figure 3.34. Mitochondrial glutamine metabolism. Glutamine enters mitochondria and is converted to glutamate by glutaminase (GLS). Glutamate is converted into α-ketoglutarate by transaminases (TA) or glutamate dehydrogenase (GDH). Malate can be exported from the mitochondria to generate pyruvate and NADPH by malic enzyme. Red text indicates potential for OXPHOS utilization. Other abbreviations are as follows: pyruvate dehydrogenase (PDH), isocitrate dehydrogenase (IDH), α-ketoglutarate dehydrogenase (α-KDH), succinate dehydrogenase (SDH), malate dehydrogenase (MDH). Other steps have been omitted for clarity. Adapted from (49) and (113).

Glutamine metabolism also appears to play a role in immune responses *in vivo*. Lymphocytes from rats (549) or mice (550) fed glutamine-enriched diets proliferate 2-5-fold faster in response to conA than lymphocytes from control animals. In humans, decreased plasma glutamine levels in burn victims is correlated with profound immunosuppression (538). Conversely, glutamine supplementation decreases by 20% the incidence of sepsis in newborns with low

birth weights (551) and decreases the incidence of pneumonia and bacteremia by 28-35% in trauma patients (552).

Together, these studies document the importance of glutamine metabolism for T cell proliferation and cytokine production and suggest that increased OXPHOS in alloreactive donor T cells may be fueled by glutamine oxidation. However, a recent microarray analysis revealed that $CD8^+$ effector T cells in an irradiated model of murine GVHD have *decreased* levels of c-Myc mRNA compared to naïve T cells (553). Because c-Myc stimulates glutamine uptake and utilization (541, 542), this observation suggests that glutamine may play a limited role in fueling OXPHOS in alloreactive donor T cells. Studies in human allogeneic HSCT patients support this hypothesis (554, 555). Supplementing the diets of post-transplant patients with glutamine reduced infection rates and increased the number of circulating lymphocytes; however, glutamine supplementation did not increase the incidence of GVHD (554, 555). Although the relationship between glutamine supplementation and GVHD severity was not analyzed, these studies suggest that glutamine metabolism may play less of a role in alloreactive donor T cells than it does in other lymphocyte populations.

Fatty acids are another potential fuel source whose oxidation could drive increased OXPHOS in alloreactive donor T cells (Figure 3.35). Fatty acids travel through the blood stream complexed with albumin or as part of triglycerides (556) and are imported into cells through fatty acid transport proteins (FATPs) (557). Once inside cells, fatty acids are conjugated to coenzyme A in the cytosol by

fatty acyl CoA synthetase to form acyl CoA esters (558). Carnitine palmitoyltransferase (CPT) 1, which is the rate limiting step in fatty acid oxidation (FAO) catalyzes the converstion of acyl CoA esters into acylcarnitines in the intermembrane space (559, 560). Acylcarnitines then enter the mitochondrial matrix through carnitine:acylcarnitine translocase (560). Once inside the matrix, acylcarnitines are converted back into acyl CoA esters by CPT2, which liberates free carnitine for export and reuse in the cytosol (560). Acyl CoA molecules can then enter the β-oxidation pathway, where an acyl chain consisting of 2n carbons generates n acetyl coA, NADH and $FADH_2$ molecules (560).

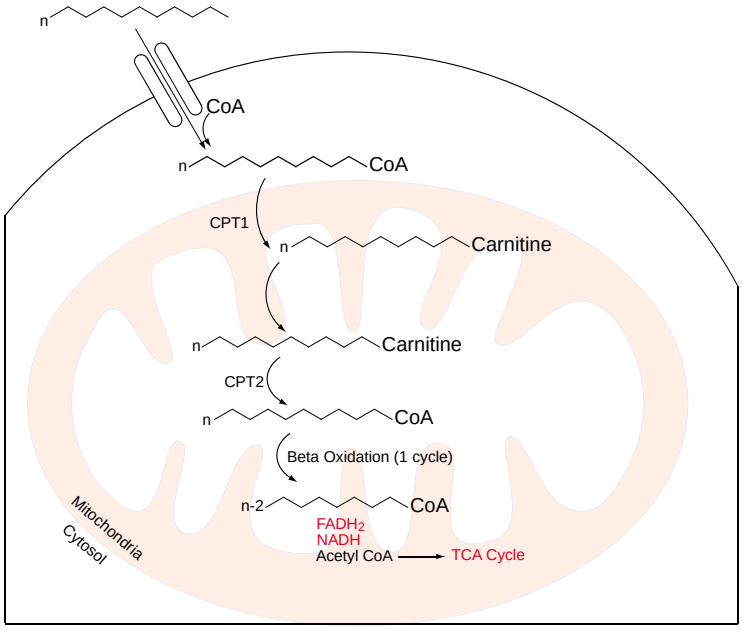

Figure 3.35. Fatty acid oxidation. Fatty acids (containing n carbons) are imported through fatty acid transport proteins and conjugated to coenzyme A by fatty acyl coA synthetase. Carnitine palmitoyltransferase (CPT) 1 catalyzes the formation of acylcarnitines, which enter the mitochondria through the carnitine:acylcarnitine translocase. CPT2 catalyzes the regeneration of acyl-CoA, which can then enter the beta oxidation pathway. Each cycle of beta oxidation shortens the acyl-CoA by two carbons and yields one $FADH_2$, one NADH and once acetyl CoA, which can enter the TCA cycle. Red text indicates potential utilization by OXPHOS. Adapted from (49) and (560).

FAO generates large amounts of ATP (100-130 ATP per palmitate oxidized (502)); however, its role in lymphocyte metabolism is not well understood. One of the important regulators of FAO in mammalian cells is the AMP-activated kinase (AMPK), which activates β-oxidation by phosphorylating and inhibiting acetyl coA carboxylase (ACC) (Figure 3.36) (561, 562). Inhibition of ACC leads to decreased levels of malonyl-CoA, an inhibitor of CPT1 (563). Thus AMPK activity increases CPT1 activity by reducing malonyl-CoA levels (560).

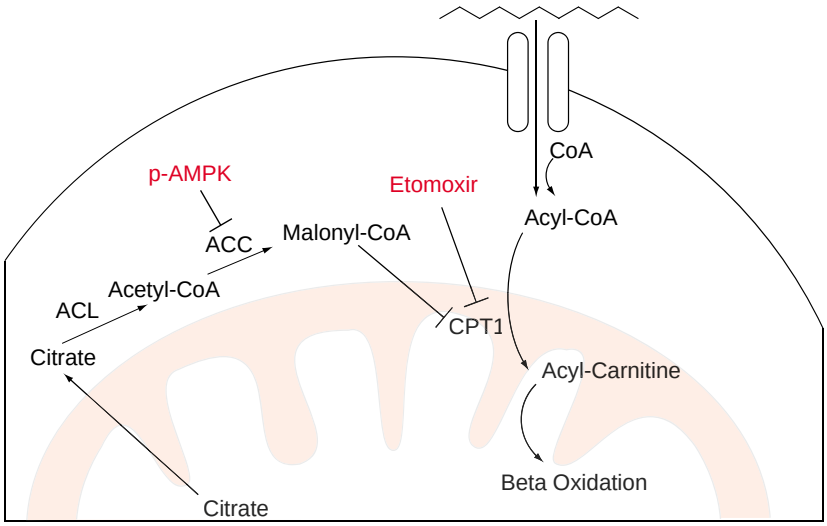

Figure 3.36. Regulation of FAO by p-AMPK and etomoxir. p-AMPK phosphorylates and inhibits acetyl CoA carboxylase (ACC), which decreases the concentration of malonyl-CoA. Because manonyl-CoA is an allosteric inhibitor of CPT1, the actions of p-AMPK stimulate fatty acid oxidation. Etomoxir inhibits fatty acid oxidation through its irreversible inhibition of CPT1. From (560, 563-565).

Stimulation of human or mouse T cells with ionomycin or anti-CD3 activates AMPK within minutes (261). This TCR-mediated AMPK activation may

be important for activated lymphocytes to increase energy production in anticipation of the energy demands of proliferation. However, a more recent study suggests that AMPK is dispensible for many T cell responses (566). For example, mouse T cells lacking the catalytic subunit of AMPK (AMPKα1 in lymphocytes (261, 566)) proliferate and produce IFN-γ and IL-4 equally well as compared to wild type T cells in response to anti-CD3 stimulation (566). Similarly, wild type mice lacking AMPKα1 generate equivalent antibody titers following primary and secondary (d 14) Keyhole limpet hemocyanin (KLH) immunization, and OVA-specific wild-type or AMPKα1 deficient T cells proliferate identically in response to OVA immunization and cause identical amounts of swelling in antigen-specific delayed-type hypersensitivity (DTH) tests (566).

While these results suggest that T cells do not require active AMPK to mediate immune responses, they do not rule out a role for FAO in lymphocyte activation, as signaling molecules other than AMPK may stimulate FAO. Muscle cells expressing a kinase dead (KD) isoform of AMPKα2 cannot increase AMPK activity when stimulated to contract (567). Despite this lack of AMPK activity, AMPKα2 KD muscle cells phosphorylate acetyl coA carboxylase and oxidize palmitate as efficiently as wild-type cells during contractions(567). The existence of AMPK-independent pathways that activate fatty oxidation indicates that simply measuring AMPK activity is insufficient to assess the activity of FAO in lymphocytes.

The role of β-oxidation in lymphocytes has been investigated by the direct measurement of fatty acid oxidation and by using genetic models with defects in FAO (246, 568-570). Rat lymphocytes stimulated for 1 h with conA do not increase their rate of oleate metabolism compared to control cells (246), while mouse T cells stimulated for 4 d with IL-2 and anti-CD3 and anti-CD28 antibodies *decrease* palmitate oxidation 2-fold compared to unstimulated T cells (570). These observations suggest that FAO is not important for acute T cell responses. Recent studies in mice support this hypothesis. $CD8^+$ T cells lacking TNF receptor-associated factor 6 (TRAF6 KO T cells) have decreased levels of genes involved in fatty acid oxidation compared to wild type T, however this study did not report the specific genes analyzed (568). TRAF6 KO T cells accumulate identically to wild type cells out to d 6 following immunization with an OVA-expressing strain of LCMV (568). Together, these observations suggest that FAO is not important for acute T cell responses *in vitro* or *in vivo*.

Despite their identical expansion in response to LCMV, TRAF6 KO T cells decline faster than WT cells and fail to convert into memory cells (568). Unlike activated WT T cells, which increase FAO 5-fold following IL-2 withdrawal, TRAF6 deficient T cells do not increase FAO. These observations suggest that increasing β-oxidation may be important for activated T cells to transition into memory cells when cytokine levels become limiting *in vivo* (568, 569). Consistent with this hypothesis, treatment with metformin, which activates AMPK and increases T cell FAO *in vitro*, improves memory T cell generation *in vivo* following LCMV infection for both WT and TRAF6 KO T cells (568, 569).

While $CD4^+$ or $CD8^+$ memory T cells ($CD44^+$ and or $CD62L^-$) from naïve mice do not cause GVHD (571, 572), *alloreactive* memory T cells mediate severe GVHD (573). These experiments were performed by first transferring T cells from naïve mice into allogeneic recipients to induce GVHD. Donor $CD4^+$ or $CD8^+$ memory T cells isolated from these primary recipients were then transferred into secondary recipients, where they caused severe GVHD (573). While the role of memory T cells has not been investigated in the nonirradiated P→F1 model, the donor T cells we analyzed were 80% $CD44^+$ $CD62L^-$, consistent with an effector/effector memory phenotype. Because FAO is an important aspect of memory T cell metabolism (568, 569), it is possible that this pathway contributes to increased OXPHOS in alloreactive donor T cells during nonirradiated GVHD.

Further evidence for FAO as the fuel source for alloreactive donor T cells comes from a study of the nutritional status of 13 patients with chronic GVHD (574). Patients with chronic GVHD oxidize fatty acids 2-fold faster than healthy controls, however, both groups oxidized carbohydrates at the same rate (574). While these observations were based on whole body measurements and does not specifically reflect lymphocyte metabolism, they are consistent with increased FAO contributing to increased OXPHOS in alloreactive donor T cells.

Preliminary evidence from this laboratory also suggests that FAO contributes to increased OXPHOS in alloreactive donor T cells. A recent screen of intracellular metabolites revealed that alloreactive donor T cells increase the levels of several acyl-carnitine species (C8, C14:1-OH, C16:1, C18:1, C18:2) by 10-20-fold compared to unstimulated T cells. Because acyl-carnitines are

intermediates that shuttle fatty acids into the mitochondria for β-oxidation (Figure 3.35), they likely support increased FAO in alloreactive donor T cells (575).

Increased FAO in alloreactive donor T cells would have several implications for the management of GVHD. Donor T cells lacking TRAF6 should mediate less severe GVHD than WT T cells, due to their inability to increase β-oxidation (568). Conversely, drugs that increase FAO such as metformin may increase GVHD severity (568). Furthermore, drugs that inhibit FAO may have beneficial effects in the setting of GVHD. One such agent is etomoxir, which inhibits β-oxidation by inhibiting CPT1 (Figure 3.36) (559). While clinical studies using etomoxir have focused on its therapeutic effects in heart failure (565, 576-578), the importance of β-oxidation in memory T cells (568, 569) suggests that etomoxir should be investigated in T cell-mediated diseases where memory cells play a role, such as GVHD (573) and multiple sclerosis (45).

These observations suggest a model in which alloreactive donor T cells use glucose to synthesis biomass and fatty acids to generate ATP (Figure 3.37). The modestly increased glucose utilized by alloreactive donor T cells is preferentially used to synthesize the new fatty acids necessary for rapid proliferation (78) (Figure 3.37). While alloreactive donor T cells likely metabolize glucose primarily for biomass, they may increase the oxidation of fatty acids to drive oxidative ATP synthesis (Figure 3.37). This phenotype would allow alloreactive donor T cells to proliferate and generate ATP without using large amounts of glucose or secreting large amount of lactate, however it results in an impaired antioxidant balance (discussed below).

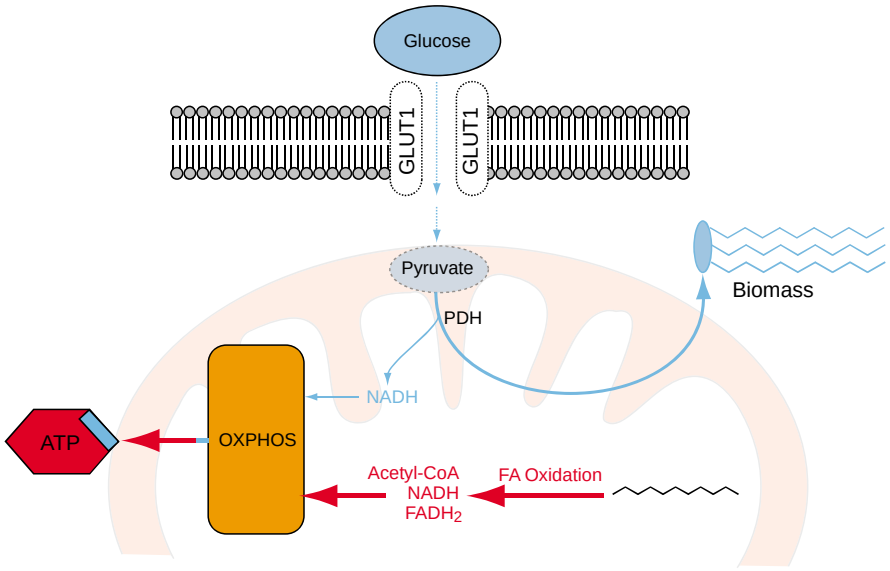

Figure 3.37. Proposed model for increased OXPHOS in alloreactive donor T cells. Alloreactive donor T cells are proposed to primarily use glucose for biomolecule synthesis (blue). As glucose-derived carbons enter the mitochondria, a modest amount of NADH is formed through pyruvate dehydrogenase (PDH). Fatty acid oxidation (red) is proposed to generate the majority of ATP in alloreactive donor T cells by fueling OXPHOS.

Comparison of alloreactive donor T cells to control-stimulated T cells.

Both alloreactive donor T cells and T cells stimulated with anti-CD3 and anti-CD28 antibodies (control-stimulated T cells) increase OXPHOS 2-3-fold compared to unstimulated T cells. However, control-stimulated T cells increase lactate production, glycolysis and GLUT1 expression up to 30-fold compared to unstimulated T cells. This high rate of aerobic glycolysis is similar to the metabolic phenotype found in many cancers (the Warburg effect), but is distinct from alloreactive donor T cells, which exhibit relatively low levels of GLUT1, glycolysis and lactate production. The possible etiology of this difference and its consequences are discussed below.

Similar to cancer cells (Chapter 1), aerobic glycolysis in activated T cells is primarily controlled by signaling through phosphatidylinositol 3-kinase (PI3-K)/AKT and HIF-1α (59, 207, 231, 372). When human $CD4^+$ T cells are stimulated by bead-bound anti-CD3 and anti-CD28 antibodies, they activate PI3-K, phosphorylate AKT and increase the expression of GLUT1 (59). These changes are accompanied by a 15-20-fold increase in glycolysis and lactate production, which is not observed if the CD28 signal is omitted (59). Similarly, GLUT1 expression does not increase in mouse and human T cells activated by anti-CD3 and anti-CD28 if PI3-K signaling is inhibited with the small molecule Ly294002 (58, 59). These observations suggest that the PI3-K/AKT pathway is involved in mediating the glycolytic phenotype of acutely activated T cells. Indeed, active AKT promotes the surface expression of GLUT1 (58), increases the activity of hexokinase (HK) (75, 230, 579) and increases the activity of phospho-fructokinase-1 (PFK-1) (82). AKT also phosphorylates and activates ATP-citrate lyase (ACL), which stimulates the conversion of glucose into the fatty acids necessary for proliferation (52, 53, 233).

These observations suggest that the relatively low levels of glucose metabolism in alloreactive donor T cells could be due to low levels of AKT phosphorylation. In activated T cells, increased signaling through negative costimulatory receptors such as PD-1 or CTLA-4 can decrease AKT phosphorylation and restrict glycolytic metabolism (59, 255). Signaling through PD-1 decreases T cell glycolysis by inhibiting the activity of PI3-K, thus decreasing levels of phospho-AKT (Figure 3.38) (255). Similarly, signaling

through CTLA-4 decreases T cell glycolysis by increasing the activity of the serine/threonine phosphatase PP2A, which dephosphorylates AKT (255). Alloreactive donor T cells increase both PD-1 and CTLA-4 expression on d 7 after GVHD induction (Figure 3.23). These observations suggests that negative signaling through these pathways may be lead to low levels of AKT phosphorylation and low rates of glycolysis in alloreactive donor T cells. However, we observed *increased* levels of phospho-AKT in alloreactive donor T cells as compared to both unstimulated cells and control-stimulated T cells (Figure 3.24), suggesting that low glycolysis in alloreactive donor T cells occurs *despite* increased AKT phosphorylation.

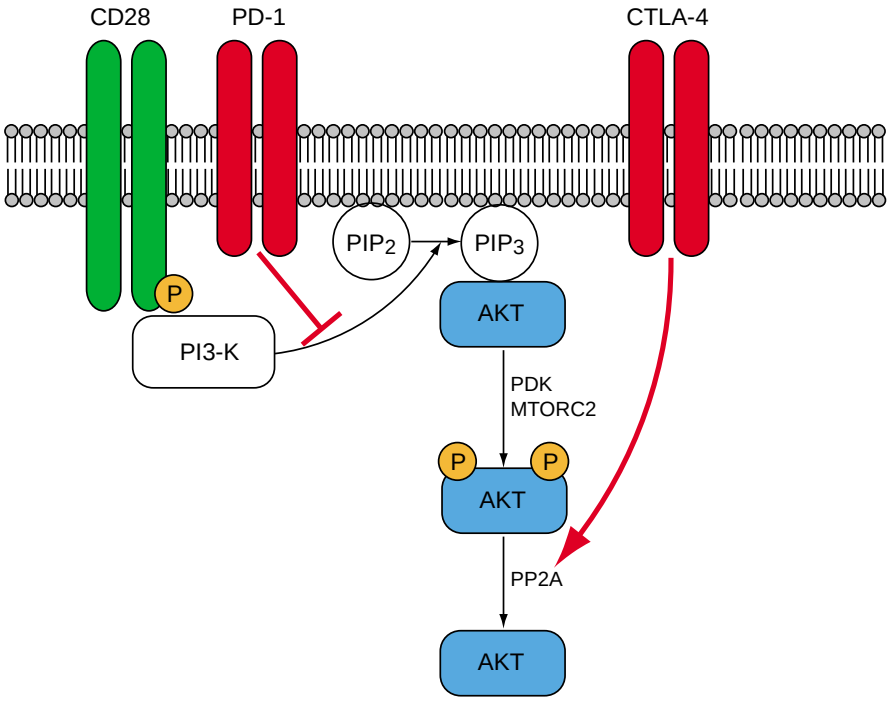

Figure 3.38. Regulation of AKT phosphorylation by CD28, PD-1 and CTLA-4. CD28 stimulation activates PI3-K to form PIP_3, which recruits AKT to the plasma membrane allowing its phosphorylation by PDK and MTORC2. PD-1 signaling decreases AKT phosphorylation by inhibiting PI3-K activity. CTLA-4 decreases AKT phosphorylation by activating the phosphatase PP2A (255).

Because low rates of glycolysis in alloreactive donor T cells are not accompanied by low levels of AKT phosphorylation, decreased activity in other pro-glycolytic signaling pathways may be responsible decreased glycolysis. HIF-1α expression increases the expression of numerous enzymes involved in glycolysis, including GLUT1, HK, PFK-1, aldolase, enolase and lactate dehydrogenase (LDH) (74). Hence, decreased glycolysis in alloreactive donor T cells could be due to decreased HIF-1α activity as compared to control-stimulated T cells.

In mouse T cells, HIF-1α mRNA increases 15-fold following stimulation for 24 h with anti-CD3 and anti-CD28 antibodies (371). Increased mRNA expression is accompanied by a similar increase in HIF-1α protein in activated T cells (371). T cells lacking HIF-1α consume 3-fold less glucose and produce 2-fold less lactate compared to wild type T cells following stimulation with anti-CD3 and anti-CD28 antibodies (372). These observations indicate that the induction of HIF-1α expression is important for increased glycolytic metabolism in antibody-stimulated T cells. Hence, low rates of glycolysis in alloreactive donor T cells could be explained by low expression of HIF-1α. While there is little data regarding the role of HIF-1α in GVHD, a recent microarray analysis showed that effector $CD8^+$ T cells in a model of irradiated GVHD have 3-fold more HIF-1α mRNA than naïve T cells (553). This increase is modest compared to the 15-fold increase in HIF-1α mRNA reported in T cells stimulated by anti-CD3 and anti-CD28 antibodies (371). While the importance of O_2-dependent HIF-1α protein

degradation cautions against the over-interpretation of mRNA levels (218, 221), these studies are consistent with an interpretation in which alloreactive donor T cells have decreased HIF-1α activity compared to control-stimulated T cells (Figure 3.39). In this model, both alloreactive donor T cells and control-stimulated T cells have active AKT, which promotes glucose uptake, glycolysis and fatty acid synthesis. However, increased HIF-1α in control-stimulated cells leads to higher rates of glucose uptake, glycolysis and lactate production compared to alloreactive donor T cells. A direct comparison of HIF-1α *protein* levels in alloreactive donor T cells and control-stimulated T cells is necessary to test the validity of this model.

Another important difference between alloreactive donor T cells and control-stimulated cells is the environment in which they expand. Control-stimulated T cells were grown in cell culture containing 10% fetal bovine serum (FBS), which typically has a fatty acid concentration of 21-28 μM (580, 581). Alloreactive donor T cells expand *in vivo*, where plasma fatty acid concentrations range from 400-600 μM (557). These observations suggest that control-stimulated T cells may be forced to rely on glycolysis as their primary energy source because they do not have access to substrates for fatty acid oxidation. In support of this hypothesis, inhibition of fatty acid oxidation with etomoxir causes a 10-20-fold increase in lactate production in leukemia cells cultured *in vitro* (564). If fatty acid oxidation is similarly limited in control-stimulated T cells *in vitro* as a result of low fatty acid levels, increasing the fatty acid concentration in culture

could reduce the lactate production of control-stimulated T cells to levels similar to those observed in alloreactive donor T cells.

Decreased glycolytic metabolism in alloreactive donor T cells compared to control-stimulated T cells has important functional implications for these two cell types. As discussed in Chapter 1, high rates of glycolytic metabolism are used by proliferating cancer cells to produce ATP, to provide carbon for biomolecule synthesis, and to generate antioxidants that protect from ROS-mediated damage (50, 78, 121, 208, 217, 223, 242, 491). Recent studies suggest that glycolysis plays similar roles in non-cancerous proliferating cells such as lymphocytes (78, 207, 252, 372). Because alloreactive donor T cells exhibit 7-fold lower rates of glycolytic metabolism compared to control-stimulated cells, it is important to consider how these three functions differ in these two cell types.

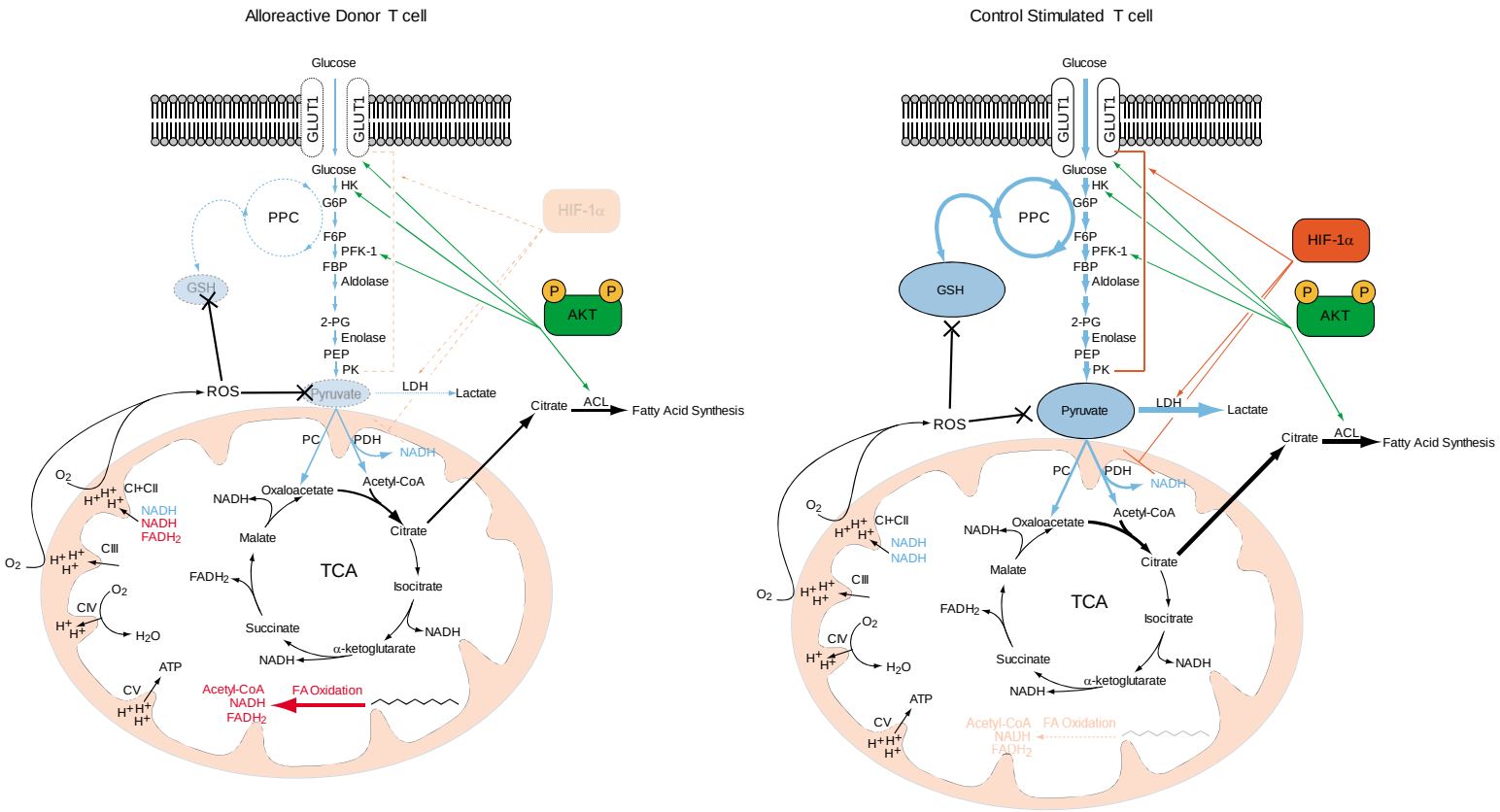

Figure 3.39. Model of the bioenergetic differences between alloreactive donor T cells and control-stimulated T cells. Control stimulated T cells (right) have both active HIF-1α and AKT, which stimulated high rates of glucose uptake, glycolysis and lactate production (blue). OXPHOS in these cells is primarily due to NADH from the PDH reaction, as fatty acid oxidation is restricted. Because flux through glycolysis is high, pyruvate and glutathione formation is increased, and these metabolites are not depleted through reactions with ROS. Alloreactive donor T cells (left) have active AKT, but their HIF-1α activity is proposed to be lower than control-stimulated T cells. Low HIF-1α activity leads to low rates of glucose metabolism, which is primarily used for fatty acid synthesis. Low flux through glycolysis prevents the regeneration of pyruvate and glutathione, leading to their depletion from reactions with ROS. The majority of ATP in these cells is proposed to be generated through fatty acid oxidation (red).

Unlike proliferating cancer cells that display a "respiratory defect" (205), oxidative metabolism is increased 2.5-fold in alloreactive donor T cells compared to unstimulated controls. Hence, alloreactive donor T cells compensate for low rates of glycolysis by increasing oxidative ATP production. Unlike alloreactive donor T cells, control-stimulated T cells generate large amounts of ATP through both glycolysis and OXPHOS. While rates of O_2 consumption in alloreactive donor T cells and control-stimulated T cells are similar, the carbon substrates used to support this OXPHOS likely differ. Indeed, alloreactive donor T cells appear to increase FAO (discussed above), while antibody-stimulated T cells *decrease* palmitate oxidation 2-fold compared to unstimulated cells (570). However, the high rate of glucose-derived lipid synthesis in antibody-stimulated T cells suggests that NADH from pyruvate dehydrogenase may be responsible for increased OXPHOS in these cells (372) (Figure 3.39).

The second major role of aerobic glycolysis in proliferating cells is to provide carbons for biomolecule synthesis (78). Because alloreactive donor T cells have low rates of glycolysis compared to control-stimulated cells, they might be expected to have decreased rates of glucose-derived lipid synthesis and thus lower rates of proliferation than control-stimulated T cells (Figure 3.39). However, CFSE staining indicates that both cell types proliferate at similar rates (Figure 3.21). This observation suggests that alloreactive donor T cells may preferentially use glucose-derived carbons to synthesize fatty acids and other molecules, rather than secreting them as lactate or oxidizing them to form CO_2 (Figure 3.38, Figure 3.39) (52, 372). An alternative explanation is that, in

response to low rates of glycolysis, alloreactive donor T cells limit their size rather than their rate of proliferation, thus requiring less biosynthetic carbon per division (373, 582, 583). In support of this hypothesis, donor T cells are significantly smaller than control-stimulated T cells (Figure 3.22).

Another important function of aerobic glycolytic is to protect cells from ROS production and subsequent oxidative damage (50, 252, 491). Glycolysis accomplishes this function by generating NADPH to maintain the reduced glutathione pool (50, 196, 197, 343) and by keeping pyruvate levels high (56-59). Both of these aspects of ROS protection appear to be compromised in alloreactive donor T cells.

Synthesis of the tripeptide antioxidant glutathione is catalyzed by γ-glutamylcysteine synthetase (GCS) and glutathione synthetase (197). Following oxidation by peroxides, glutathione is either reduced back to GSH by glutathione reductase and NADPH (197) or is exported from cells through ATP-dependent (MDRPs) (Figure 3.40) (584). Total glutathione levels are decreased 25% in alloreactive donor T cells compared to unstimulated T cells. This decrease suggests either increased export of oxidized glutathione or decreased glutathione synthesis. Human PBMCs activated with conA *in vitro* increase glutathione levels by 2-fold over 2-4 d, suggesting that glutathione synthesis does not decrease in activated T cells (344). Similarly, PI3-K/AKT signaling increases transcription of GCS (585), again suggesting that glutathione synthesis may not be decreased in alloreactive donor T cells, which contain phosphorylated AKT (Figure 3.24). These observations suggest that decreased glutathione levels in

alloreactive donor T cells might be due to increased export rather than decreased synthesis. However, a direct examination of GCS expression and activity in alloreactive donor T cells would be needed to rule out decreased GSH synthesis in these cells.

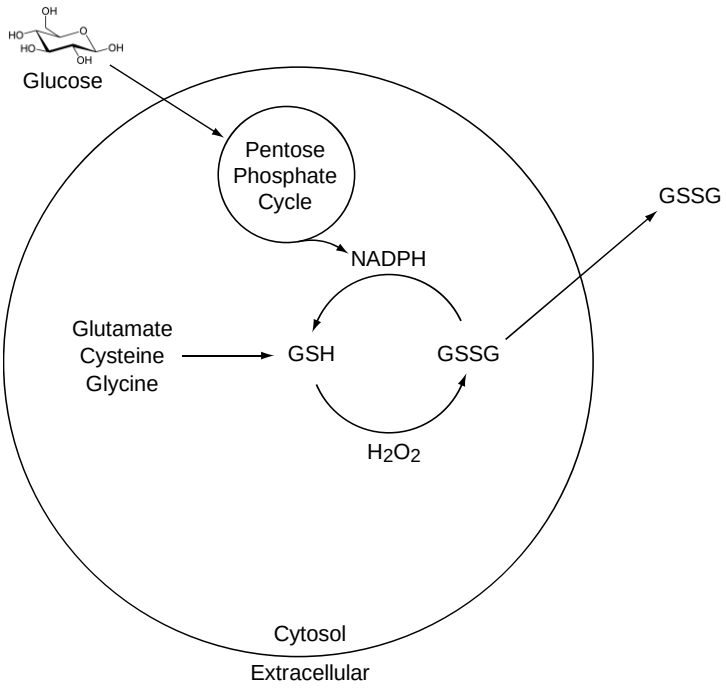

Figure 3.40. Glutathione synthesis, oxidation, reduction and export. Glutamylcysteine synthetase, the rate limiting step in glutathione synthesis, conjugates glutamate with cysteine. Glycine is added by glutathione synthetase which forms reduced glutathione (GSH). GSH is oxidized to GSSG by H_2O_2 in the presence of glutathione peroxidase. GSSG is reduced to GSH by glutathione reductase using NADPH generated from the pentose phosphate cycle. During periods of oxidative stress, GSSG is exported from cells through MDRPs. (51, 196, 197, 584)

If GSH synthesis is not decreased in alloreactive donor T cells compared to unstimulated controls, it suggests that the low levels of glutathione in these cells results from increased oxidation to GSSG and subsequent export. Glutathione is oxidized by H_2O_2 (196, 197), which is formed by the reaction of O_2^- with superoxide dismutases (SODs) (527). Elevated DHE staining in alloreactive donor T cells (Figure 3.26) indicates increased O_2^- in these cells and suggests increased H_2O_2, as T cells express both Mn and Cu/Zn SOD (586, 587). These observations suggest that GSH oxidation in alloreactive donor T cells will be increased in comparison to unstimulated controls. Such increased GSH oxidation to GSSG could be countered by increased NADPH-dependent regeneration of GSH (Figure 3.40) (196, 197). While the glycolytic rate of alloreactive donor T cells is increased 4-fold compared to unstimualted cells (Figure 3.20), it appears that the pentose phosphate cycle activity of alloreactive donor T cells may not generate sufficient NADPH to prevent the export of oxidized glutathione (584). This interpretation suggests that increasing glycolytic rates in alloreactive donor T cells (to the levels observed in control-stimulated cells) may prevent glutathione depletion. Evidence for this relationship between glycolysis and glutathione levels has been observed in primary mouse astrocytes (343). Culturing these cells in media lacking glucose decreases reduced glutathione by 75% within 12 h, whereas cells grown in media with 5.5 mM glucose maintain glutathione levels within 80-90% of initial levels (19.7 nMoles glutathione/mg protein) (343).

Glycolysis also allows cells to maintain high levels of pyruvate. Increasing the glucose concentration of cell culture media from 2.5 mM to 12 mM causes a pancreatic β-cell line to increase intracellular pyruvate levels by greater than 10-fold (15 vs. 180 nMoles pyruvate/mg protein) (535). This association between glucose metabolism and pyruvate levels likely occurs because pyruvate is a direct metabolite of glucose (Figure 3.41) (200, 252). Pyruvate levels in alloreactive donor T cells are nearly undetectable, while unstimulated cells have 6-10 pMoles pyruvate/μg protein (Figure 3.27). However, glycolytic rates are increased 4-fold in donor T cells compared to unstimulated cells, which suggests a 4-fold *increase* in pyruvate formation (Figure 3.20). For depletion of the pyruvate pool to occur under such a situation, the consumption of pyruvate must outpace its increased production.

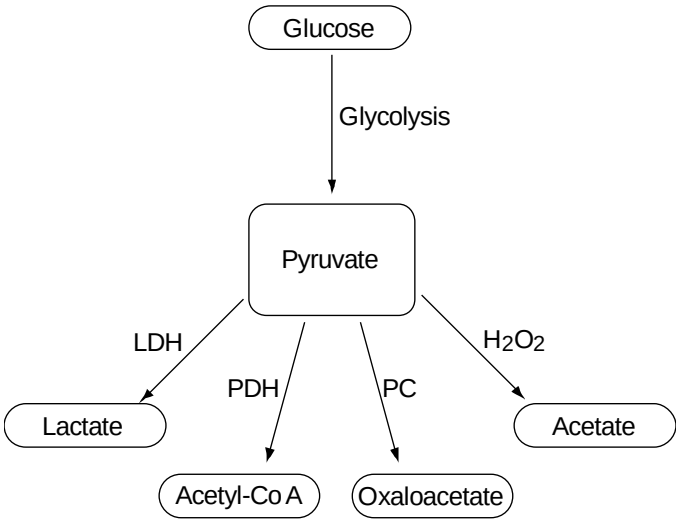

3.41. Formation and consumption of pyruvate. Pyruvate is primarily formed through glycolysis. Lactate dehydrogenase (LDH) converts pyruvate into lactate. Pyruvate dehydrogenase (PDH) converts pyruvate into acetyl-coA. Pyruvate carboxylase (PC) converts pyruvate into oxaloacetate. Nonenzymatic reactions with H_2O_2 convert pyruvate into acetate. (123, 200, 252, 588, 589)

Pyruvate can be consumed by pyruvate dehyrogenase (123), pyruvate carboxylase (589), lactate dehyrdogenase (223, 243) or through direct reactions with hydrogen peroxide (Figure 3.40) (200, 203). Mitogen-stimulated lymphocytes increase PDH and PC activity by 50% within 1 h of stimulation (123, 246), suggesting that activated lymphocytes increase their utilization of pyruvate through both of these pathways. Our data are consistent with increased flux through PDH in alloreactive donor T cells, as this reaction allows glucose-derived carbons to be used for fatty acid synthesis, which is necessary for proliferation (Figure 3.39) (52, 53). Alloreactive donor T cells also have increased rates of lactate production and ROS levels as compared to unstimulated T cells (Figure 3.16, Figure 3.26), both of which could contribute to pyruvate depletion in these cells.

These observations suggest that rates of glycolysis in alloreactive donor T cells, while modestly increased over unstimulated cells, are not sufficient to maintain glutathione and pyruvate levels in these cells. Unlike alloreactive donor T cells, control-stimulated T cells engage in high rates of glycolysis that could allow them to maintain high levels of both glutathione and pyruvate (Figure 3.39). Indeed, PBMCs stimulated with conA for 2-4 d *double* their glutathione levels compared to unstimulated cells (344). While the role of glycolysis was not addressed in this study, conA stimulation increases glucose utilization and lactate production by 20-40-fold in rat thymocytes, which suggests that increased glutathione levels could relate to increased glycolysis (62, 206). Similarly, rat

thymocytes stimulated with conA increase glucose-derived pyruvate levels 10-fold compared to resting cells (252).

These observations suggest that control-stimulated T cells, which have high rates of glycolysis, will have increased levels of glutathione and pyruvate compared to alloreactive donor T cells and may therefore be resistant to ROS-mediated apoptosis. Furthermore, if the high glycolysis observed in control-stimulated T cells faithfully models the metabolism of acutely-stimulated T cells *in vivo*, it would suggest that T cells responding to an acute viral infection or immunization may be able to maintain their intracellular pyruvate and glutathione levels in a manner that alloreactive donor T cells do not (Figure 3.39). Such differences in intracellular antioxidants would predict that acutely-stimulated lymphocytes might be resistant to apoptosis induced by pro-oxidant compounds such as arsenic trioxide (ATO) or Bz-423 (169, 172, 380, 488, 489).

Implications of bone marrow metabolism for GVHD treatment. Following myeloablative conditioning, recipients undergo a several week period of profound immunodeficiency (590) during which the host immune system dies and infused donor stem cells migrate to the bone marrow and begin to repopulate the immune system (591). During this time period, peripheral blood immune cells drop to nearly undetectable levels (407, 408). This leukopenia is counteracted by the rapid proliferation of precursor cells in the bone marrow, which regenerates the innate and adaptive immune system in the host (408, 411, 592).

This rapid proliferation of cells in the bone marrow complicates the treatment of GVHD. The current standard for treatment of acute GVHD is a

course of glucocortoids, aimed at inducing apoptosis in and inhibiting the function of alloreactive donor T cells (discussed in detail in Chapter 4) (593-595). However, glucocorticoids are non-specifically immunotoxic (594), and inhibit reconstitution of NK cells and interferon α/β-producing plasmacytoid DCs following transplant (596, 597). This lack of specificity is a problem clinically, as delayed reconstitution is associated with an increased frequency of cytomegalovirus (CMV), adenovirus and herpes zoster virus in the post-transplant period (596). Because of these issues with glucocorticoids, there is currently a large effort to develop improved treatments for GVHD (598).

Work over the past 40 years has documented that activated lymphocytes increase glycolytic and oxidative metabolism compared to unactivated lymphocytes. (59, 206, 250-252, 264, 471). These changes have generated interest in inhibiting activated lymphocyte metabolism in an attempt to treat lymphocyte-mediated diseases (207). Because glycolysis provides the majority of energy for activated T cells in culture models (59, 63, 206), current studies have focused on inhibiting enzymes important for glycolysis, such as the monocarboxylate transporter (MCT)1, which transports lactate out of cells (599). Inhibitors of MCT1 decrease PMA and ionomycin-stimulated T cell proliferation *in vitro* and reduce disease severity in a model of collagen-induced arthritis *in vivo* (104). While such compounds may preferentially affect activated lymphocytes due to their increased rates of lactate production compared to unactivated lymphocytes, they may have limited utility in the treatment of GVHD.

Whereas a treatment for GVHD might inhibit the growth of or kill proliferating alloreactive donor T cells, it should at the same time spare proliferating cells in the bone marrow. Both alloreactive donor T cells and post-transplant bone marrow cells have rates of lactate production that are increased 3-4-fold compared to naïve cells (Figure 3.16, Figure 3.29). This observation suggests that agents that inhibit glycolysis may inhibit the reconstitution of the host immune system in addition to inhibiting alloreactive donor T cells and may lead to an increased incidence of opportunistic infections post-transplant.

While inhibiting glycolysis may not be an ideal strategy to treat GVHD, our studies suggest that modulating OXPHOS may allow the selective inhibition of alloreactive donor T cell function without affecting proliferating cells in the bone marrow. Donor T cells consume O_2 twice as fast and have decreased pyruvate levels compared to post-transplant bone marrow cells (Figures 3.16, 3.27, 3.29, and 3.32). Increased oxidative metabolism in donor T cells suggests that they may be more sensitive to inhibition of this pathway than post-transplant bone marrow cells. Similar differential sensitivity to OXPHOS inhibition has been observed in leukemia cell lines with respect to cytovaricin and apoptolidin, which inhibit the mitochondrial ATPase (600). Sensitivity to cytovaricin correlates with expression of enzymes important for oxidative phosphorylation such as aspartate aminotransferase, which is used by the malate-aspartate shuttle to transfer cytosolic NADH into the mitochondria for oxidative ATP production (600, 601). This correlation suggests that cell lines with increased oxidative activity are more sensitive to apoptosis induced by inhibition of the mitochondrial ATPase. In

support of this hypothesis, forcing cells to rely on OXPHOS by inhibiting glycolysis with 2-deoxyglucose or the LDH inhibitor oxamate increased the amount of apoptosis induced by apoptolidin by 3-10-fold in 8 different cell lines (600). While reports documenting apoptolidin or cytovaricin use *in vivo* are lacking, the selectivity of these agents for cells with increased OXPHOS suggests that they might be able to kill alloreactive donor T cells while sparing unstimulated T cells or proliferating bone marrow cells.

Intracellular pyruvate levels are > 10-fold decreased in alloreactive donor T cells compared to post-transplant bone marrow cells (Figure 3.27, Figure 3.32). Pyruvate plays an important role as an intracellular antioxidant due to its ability to detoxify both H_2O_2 (200) and O_2^- (203, 602). Pyruvate's role as an antioxidant has been primarily investigated in the setting of ischemia-reperfusion injury (201, 495, 588). Ischemia reperfusion injury occurs when occluded vessels, such as those responsible for stroke or myocardial infarction, are reopened allowing the return of blood flow to the affected organ (603). The reintroduction of O_2 to the ischemic tissue causes increased production of O_2^- and H_2O_2 within minutes and leads to additional apoptosis and tissue damage (603, 604). Pyruvate treatment of ischemic rat small intestine tissue reduces reperfusion-induced ROS production 5-fold as measured by luminol chemiluminescence, and decreases histological evidence of tissue damage compared to control treated tissue (202). Similarly, treatment with increasing concentrations of pyruvate decreases ROS production in post-ischemic guinea pig hearts by 80% as measured using a 1-hydroxy-3-carboxy-pyrrolidine spin trap (492). Pyruvate can also decrease ROS

production in settings independent of ischemia-reperfusion, as pyruvate treatment reduces rotenone- and antimycin A-induced O_2^- production by 50% in isolated submitochondrial particles (203).

The antioxidant properties of pyruvate and its reduction in alloreactive donor T cells compared to post-transplant bone marrow cells suggests that these cells types may have differing sensitivities to ROS-mediated apoptosis. Several therapeutic agents mediate their beneficial affects by killing cells in an ROS-dependent fashion. ATO is one such agent that induces apoptosis in leukemia cells through an ROS-mediated mechanism (488, 489, 605). Sensitivity to ATO-induced apoptosis is inversely correlated to intracellular glutathione levels across multiple leukemia cell lines (488). Furthermore, increasing intracellular glutathione levels with the glutathione precursor N-acetyl-cysteine decreases ATO-induced apoptosis, while lowering glutathione levels with the γ-glutamylcysteine synthetase inhibitor buthionine sulfoxide increases ATO-induced apoptosis (488, 489). A similar phenomenon is observed with the pro-oxidant chemotherapeutic agent paclitaxel (606). The IC_{50} of paclitaxel positively correlates with total antioxidant capacity (TAC) across 16 different cell lines (606) and lowering a cell line's TAC using BSO increases paclitaxel sensitivity (606). Although these studies did not investigate pyruvate levels specifically, they suggest that alloreactive donor T cells, with depleted pyruvate and glutathione levels, may be more sensitive to ATO- and paclitaxel-induced apoptosis than will post-transplant bone marrow cells. Such selectivity would be useful therapeutically, as inducing selective apoptosis in alloreactive donor T cells may

reduce GVHD without slowing engraftment. ATO is especially promising as a potential treatment for GVHD because, in addition to its anti-leukemia effects (607), it has recently been shown to reduce disease in the MRL/*lpr* model of lupus by eliminating autoreactive T cells with depleted glutathione levels (380).

It is unclear why proliferating bone marrow cells use such a different metabolic program than proliferating alloreactive donor T cells. Gr-1$^+$ granulocytes are the most abundant cell type in the bone marrow of naïve and post-transplant mice (Figure 3.28), suggesting that the metabolism of proliferating bone marrow cells may reflect the metabolic activity of granulocytes such as neutrophils. Bone marrow-derived donor granulocytes proliferate significantly slower than alloreactive donor T cells (Figure 3.31). Because proliferation is an ATP-demanding process (207), the slower rate of proliferation of bone marrow cells may indicate a decreased demand for ATP compared to alloreactive donor T cells. While the basis for these disparate rates of proliferation is unclear, they are supported by precedent in the literature. Granulocyte progenitor cells require approximately 24 h to synthesize DNA and generate a mature granulocyte (608), while CD4$^+$ or CD8$^+$ T cells responding to antigen divide approximately every 10-12 h (511, 609, 610). Hence, OXPHOS may be lower in proliferating bone marrow cells in part because their ATP requirements are lower than alloreactive donor T cells.

Another factor that may contribute to the lack of increased OXPHOS in proliferating bone marrow granulocytes is the inability of mature neutrophil mitochodnria to synthesize ATP. Neutrophils have a 10-fold decrease in

mitochondrial DNA copy number compared to PBMCs (476) and components I, III and IV of their respiratory chains are not organized into the higher-order supercomplexes that are characteristic of mitochondria from heart or lymphocytes (480, 481). These observations suggest that the respiratory complexes of mature neutrophil mitochondria might not be able to generate large amounts of ATP. Indeed, inhibitors of the electron transport chain (ETC) such as rotenone (complex I), antimycin A (complex III), aurevertin B (complex V) and KCN (complex IV) do not deplete ATP in mature neutrophils, although they deplete the ATP of PBMCs by more than 75% within 2 h (481). Conversely, inhibiting neutrophil glycolysis with sodium iodoacetate completely depletes ATP levels following 6 h of treatment (476). These observations suggest that granulocyte mitochondria may not be able to increase oxidative ATP synthesis and that the increased ATP demands that accompany proliferation in the post-transplant setting must be met by glycolysis instead.

Role of cytokines and irradiation on alloreactive donor T cell metabolism. The studies performed in this chapter characterized the bioenergetics of alloreactive donor T cells in the context of a *nonirradiated* model of GVHD. This model shares many features with irradiated GVHD models, including the development of anti-host CTLs and the production of pro-inflammatory cytokines such as IL-2, IFN-γ, and TNF-α (451, 455, 457, 611, 612). However, there are several important differences between irradiated and nonirradiated GVHD. Irradiation causes damage to the epithelium of the gut, which exposes the immune system to bacterial-derived products such as LPS that can activate

TLRs on various cells of the immune system (47, 48, 421). This tissue damage and TLR activation induces the production of IL-1 and TNF-α, termed the "cytokine storm" (47, 48, 421). While TNF-α also plays a role in nonirradiated GVHD pathogenesis (611), it is likely that TNF-α and IL-1 levels vary between models of irradiated and nonirradiated GVHD. Importantly, TNF-α and IL-1 increase HIF-1α DNA binding activity in human hepatoma cells (613) and rat alveolar epithelial cells (Figure 3.42) (614). Although the ability of TNF-α and IL-1 to increase HIF-1α activity in T cells has not been investigated, these observations suggest that the irradiation-induced cytokine storm may increase HIF-1α levels in GVHD-causing T cells, and as a consequence, induce glycolysis (74, 217, 372). Hence, it will be important for future studies to investigate donor T cell metabolism in irradiated models of GVHD.

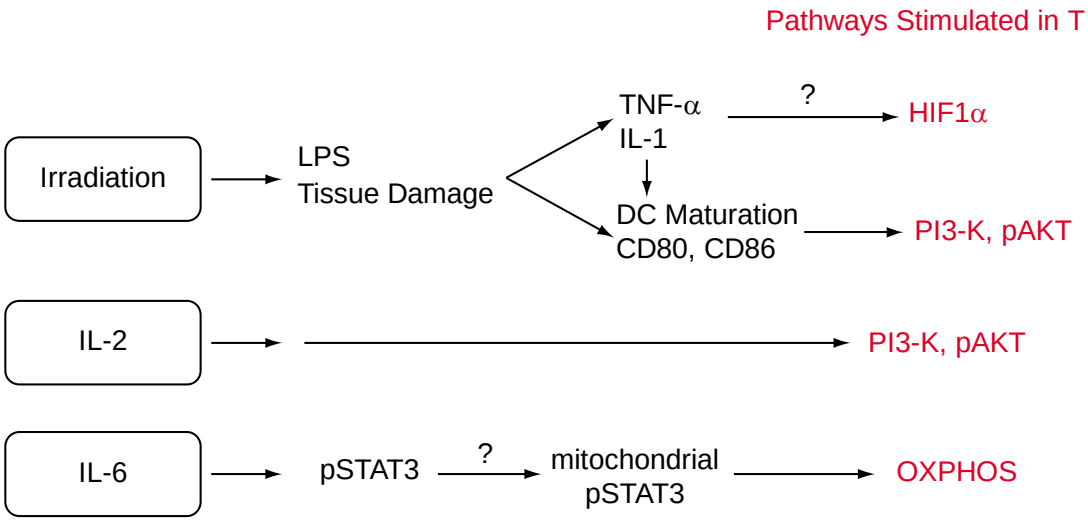

Figure 3.42. Potential roles of irradiation and cytokine signaling in alloreactive donor T cell metabolism. Irradiation causes tissue damage and allows bacterial LPS to enter the recipient . Tissue damage and LPS causes a "cytokine storm" characterized by high levels of TNF-α and IL-1 (47, 48, 421). While these cytokines activate HIF-1α in liver and epithelial cells, their ability to activate T cell HIF-1α is unclear, as indicated by "?" (613, 614). LPS, TNFα and IL-1 activate dendritic cells (DCs) and increase their expression of the B7 molecules (CD80 and CD86), which stimulate T cells through CD28 and induce PI3-K/AKT activation (36, 58, 59). IL-2 signaling may contribute to PI3-K/pAKT activation and glycolysis in alloreactive donor T cells during nonirradiated GVHD (615). IL-6 signaling phosphorylates STAT3, however it is unclear if this signaling causes pSTAT3 to enter the mitochondria, where it could stimulated OXPHOS (474, 616).

Lethal irradiation and the subsequent cytokine production may also affect cellular metabolism by increasing the expression of costimulatory molecules on DCs (27, 32, 36, 617, 618). Indeed, TNF-α (617), LPS (619) and IL-1 (620) all increase DC expression of B7 molecules, which stimulate T cells through the

CD28 receptor (36). While costimulation is important in the pathogenesis of nonirradiated GVHD (458), these observations suggest that DCs in nonirradiated hosts may express decreased levels of costimulatory molecules compared to DCs in irradiated hosts. Because signaling through CD28 regulates T cell glycolysis (58, 59), irradiation-induced increases in DC B7 molecule expression could enhance glycolysis in alloreactive T cells (Figure 3.42). These observations further emphasize the need to extend the metabolic analysis performed in this work to irradiated models of GVHD.

While the traditional "cytokine storm" is absent in this nonirradiated model of GVHD, plasma levels of several cytokines are elevated in mice suffering from nonirradiated GVHD compared to naïve mice, including IFN-γ (4000-fold increase), TNF-α (4-fold increase), IL-2 (6-fold increase), IL-4 (9-fold-increase) and IL-6 (10-fold increase) (611). As discussed above, TNF-α may affect T cell metabolism by activating HIF-1α (613, 614). Furthermore, IL-2 has direct effects on T cell metabolism (615), while aspects of IL-6 (474, 621) signaling suggests that it may also modulate T cell metabolism. Hence, changes in the cytokine environment during nonirradiated GVHD could contribute to the bioenergetic phenotype of alloreactive donor T cells.

IL-2 is produced by activated T cell and signals through the heterotrimeric IL-2 receptor (IL-2R), composed of IL-2Rα (CD25), IL-2Rβ (CD122) and the common gamma chain (γc, CD132). Because activation of the IL-2 receptor stimulates the PI3-K/AKT pathway (394), IL-2 signaling is expected to increase cellular glucose metabolism. Indeed, incubating primary human T cells with IL-2

for 4 h increases glycolysis by 40% (615). IL-2-stimulation also increases T cell size (615), which suggests that IL-2-stimulated glucose utilization is directed towards fatty acid synthesis (Figure 3.42). Serum levels of IL-2 are increased 6-fold on d 6 following nonirradiated GVHD induction, which suggests that the metabolic changes in alloreactive donor T cells could be related to increased IL-2 signaling (457, 611). Indeed, alloreactive donor T cells express increased levels of phospho-AKT and have increased cell size compared to unstimulated cells, both of which are consistent with increased IL-2 signaling (394, 615).

IL-6 is produced by a variety of cells including activated macrophages and T cells and has pleiotropic effects, which include inducing the proliferation and differentiation of cytotoxic T cells (622, 623). Binding of IL-6 to its receptor induces the phosphorylation and dimerization of the signaling molecule STAT3, which can then traffic to the nucleus and alter gene transcription (622-624). In addition to its canonical role as a modulator of transcription, phosphorylated STAT3 was recently discovered to traffic to the mitochondria, where it directly interacts with complexes I and II of the mitochondrial respiratory chain (474, 616). Mouse heart mitochondria lacking STAT3 consume O_2 50% slower than wild type mitochondria, suggesting that STAT3 plays a role in OXPHOS (474). IL-6 levels are increased 10-fold in mice with nonirradiated GVHD (611), and IL-6 and STAT3 signaling are important for the pathogensis of GVHD in several irradiated models (432, 436, 437). Thus, it is tempting to speculate that IL-6 signaling could contribute to increased OXPHOS in alloreactive donor T cells by increasing the phosphorylation and mitochondrial localization of STAT3 (Figure

3.42). Future studies should address this issue by analyzing the mitochondrial localization of STAT3 in unstimulated and alloreactive donor T cells.

Although both IL-2 and IL-6 may contribute to the bioenergetic phenotype of alloreactive donor T cells, it is important to note that host T cells purified from animals suffering from GVHD have similar metabolic characteristics as unstimulated T cells from naïve mice (low OXPHOS, low glycolysis), despite being exposed to the same systemic cytokines as alloreactive donor T cells. While these results do not preclude a role for cytokine signaling in determining the metabolism of GVHD-causing T cells, they suggest that cytokine signaling alone does not give rise to the metabolic phenotype observed in alloreactive donor T cells.

In summary, alloreactive donor T cells increase OXPHOS as they mediate nonirradiated GVHD, likely due to increased fatty acid oxidation. Alloreactive donor T cells have decreased glycolysis compared to control-stimulated T cells, perhaps due to increased fatty acid oxidation and decreased HIF-1α activity. High rates of OXPHOS in alloreactive donor T cells contrasts with the metabolism of proliferating bone marrow cells, which only increase glycolysis following transplantation. These metabolic alterations are associated with depleted antioxidants in alloreactive donor T cells, which suggests that treatment with pro-oxidant compounds could have therapeutic utility in models of GVHD and may spare T cells whose antioxidants are intact.

Materials and Methods

Reagents. Dihydroethidium (DHE), 5-(and-6)-chloromethyl-2',7'dichlorodihydrofluorescein diacetate, acetyl ester (DCFDA) and tetramethylrhodamine methyl ester (TMRM) were purchased from Invitrogen. DMEM media was purchased from Gibco and contained 10% heat-inactivated fetal bovine serum (FBS: Gibco), glucose (25 mM), glutamine (4 mM), HEPES (1 mM), penicillin (100 units/ml), streptomycin (100 μg/ml), minimal non-essential amino acids (1x), sodium pyruvate (1 mM) and 2-mercaptoethanol (0.05 mM). Unless indicated, all other reagents were purchased from Sigma.

Mice. Female C57Bl/6 (B6; H-2^b, CD45.2^+Thy1.2^+) and B6.Ly-5a (B6-Ly5.2; H-2^b, CD45.1^+Thy1.2^+) were purchased from Charles River Laboratories or Jackson Laboratories. Female B6.PL-Thy1a (B6-Thy1.1; H-2^b, CD45.2^+Thy1.1^+) and C3H.SW (H-2^b, CD45.2^+) were purchased from the Jackson Laboratory (Bar Harbor, ME). B6D2F1 (F1) mice were purchased from Charles River Laboratories or Taconic Laboratories. Mice were housed in specific pathogen free conditions and cared for according to the Guidelines for Laboratory Animal Medicine at the University of Michigan. All mice were at least seven weeks old prior to use.

T cell purification and splenocyte preparation. T cells were purified from the spleens of B6 or B6-Ly5.2 mice by $CD90^+$ positive selection according to the manufacturer's protocol. Mice were anesthetized with isoflurane and euthanized by CO_2 asphyxiation. Spleens were harvested and placed into sterile MACS

running buffer (PBS, 0.5% BSA (w/v, Fischer), 2 mM EDTA). Spleens were dissociated using sterile frosted microscope slides and strained over a 40 μM filter (BD Falcon) into 50 ml conical vials. Dishes and filters were then rinsed once with MACS running buffer. Cells were pelleted at 1400 RPM and resuspended in 50 μl anti-CD90 microbeads and 950 μl MACS running buffer per spleen and placed on ice for 15 min. Greater than 10x excess MACS running buffer was added and cells were pelleted at 1400 RPM and resuspended in MACS running buffer (500 μl) and up to 3 spleens were applied to a single LS magnetic column in a MidiMACS magnetic. After three rinses with MACS running buffer, the column was removed from the magnetic field and the positively labeled cells were flushed out using 5 ml of buffer. Cells were washed once with DMEM media, counted, stained for purity and placed on ice until use. T cells were typically >85% TCR-β positive.

Splenocytes were processed as for T cells, with DMEM media replacing MACS running buffer. After centrifugation, cells were resuspended in RBC lysis buffer (4 ml; Sigma) for 4 min at room temperature. Splenocytes were washed twice with DMEM media. Splenocytes were either used immediately for O_2 consumption and lactate production assays, or placed on ice until used for mixed lymphocyte reactions.

CFSE labeling. Vybrant CFDA SE Cell Tracer Kit was purchased from Invitrogen. Cells were suspended in L-15 media or MACS running buffer consisting of PBS, 0.5% BSA (w/v, Fischer) and 2 mM EDTA at a concentration < 20×10^6 cells/ml. 5(6)-carboxyfluorescein diacetate, succinimidyl ester (CFSE)

was dissolved in DMSO and added to cells at a final concentration of 5 μM and cells were incubated at 37 °C for 15-30 minutes. After two washes with DMEM media, cells were placed on ice until use.

Bone marrow transplantation. To induce GVHD in non-irradiated recipients, syngeneic (B6) and allogeneic (F1) recipient mice were infused through the tail vein with $50.0x10^6$ bulk splenocytes from B6-Ly5.2 or B6-Thy1.1 donor mice in L-15 media (250 μl, Cellgro). In irradiated models, B6-Ly5.2 mice were conditioned with a single dose of 900 cGy TBI (^{137}Cs source), followed by tail vein infusion of $5.0x10^6$ bone marrow (BM) cells plus either $4.0x10^6$ or $0.2\text{-}0.5x10^6$ positively-selected $CD90^+$ or $CD8^+$ T cells as indicated, from allogeneic (C3H.SW) or syngeneic (B6) donor mice in L-15 media (250 μl). After transplant, animals were kept in specific pathogen free housing and given hyperchlorinated (pH=3.0) drinking water for 3 weeks.

T cell antibody stimulations and mixed lymphocyte reactions (MLRs). For antibody stimulation, T cells from B6-Ly5.2 mice were resuspended at 1×10^6 TCR-β^+ cells/ml in DMEM media. Functional grade anti-CD3 (clone 145-2C11; eBioscience) and anti-CD28 (clone 37.51; eBioscience) were added to cells at a final concentration of 0.5 μg/ml or left unstimulated as controls. 200 μL of cells (0.2×10^6 cells) were cultured in flat-bottomed 96 well plates at 37 °C. For MLRs, T cells from B6-Ly5.2 mice (0.4 or $0.5x10^6$ TCR-β^+) were cultured at a 2:1 ratio with splenocytes (0.2 or 0.25×10^6 splenocytes) from B6 mice (syngeneic cultures) or B6D2F1 mice (allogeneic cultures) in 200 μL of media in flat-bottomed 96 well plates at 37 °C.

Flow cytometry. Cells (1 x 10^6) in single cell suspension were resuspended in Fc Block buffer composed of PBS, FBS (2% v/v) and anti-mouse CD16/CD32 Fc III/II receptor (1:250 dilution; BD Biosciences) for 10 min at 4 °C to minimize non-specific binding. Cells were spun (1400 RPM, 5 min) and resuspended in PBS containing 2% fetal bovine serum (FACS wash, 100 μl) with antibodies against cell surface antigens (1:200 dilution) for 20 min at 4 °C. Cells were then washed twice with FACS wash and either analyzed immediately or fixed and analyzed 1-2 days later. The mitochondrial membrane potential ($\Delta\Psi_m$) was measured by labeling cells with TMRM (50nM; Invitrogen) and antibodies to cell surface antigens for 30 minutes at 37°C in pre-warmed FACS wash. Stained cells were washed once prior to analysis. Carbonyl cyanide 4-(trifluoromethoxy) phenylhydrazone (FCCP; 30μM; Sigma-Aldrich) was used as a positive control for disruption of $\Delta\Psi_m$. To detect O_2^-, cells were stained for cell surface markers for 15 min at 37°C in pre-warmed FACS wash followed by incubation with DHE (4μM; Invitrogen) for 30 min at 37°C.

Intracellular IFN-γ and CTLA4 were assessed by permeabilizing fixed cells with eBioscience permeabilization buffer. Following permeabilization, cells were incubated with antibodies recognizing IFN- γ or CTLA4 in permeabilization buffer (1:200 dilution, 45 min at 4 °C). Following this incubation, cells were washed twice with permeabilization buffer, resuspended in staining buffer and analyzed.

For GLUT1 analysis, CFSE-labeled cells were surface stained as described above and fixed. 1-2 d later, cells were permeabilized by washing with permeabilization buffer (eBioscience) and incubated for 20 minutes with 10%

normal mouse serum at 4°C. Cells were then incubated with rabbit anti-GLUT1 (Abcam, 1:800 dilution) or isotype control for 45 minutes at 4°C, washed twice, incubated with APC-labeled anti-Rabbit Fab (Jackson ImmunoResearch) for 45 min at 4°C, and washed twice more. All samples were analyzed using either a BD FACS Calibur cytometer or a BD FACS Canto cytometer and CellQuest or FlowJo software. GLUT1 results are reported as either MFI or the fold increase in GLUT1 MFI over isotype MFI as indicated, and reflect total cellular levels of GLUT1. The following antibodies and their isotype controls were used: anti-mouse CD4 (FITC, PerCP-Cy5.5, APC, PE, Pacific Blue, Pacific Orange clone RM4-5, Rat IgG2a), CD8a (FITC, APC, PerCP-Cy5.5, APC-Cy7 and Pacific Blue, clone 53-6.7, Rat IgG2a), CD45.1 (FITC, PE, APC, PerCP-Cy5.5, APC-Alexa750 clone A20, Ms IgG2a), CD45.2 (FITC, PE, PerCP-Cy5.5 and APC-eFluor780 clone 104, Ms IgG2a), CD90.1 (FITC and PE, clone HIS51, Rat IgG2a), IFN-γ (PE, clone XMG1.2, Rat IgG1), CD44 (FITC, PE, APC, clone IM7, Rat IgG2b), CD62L (FITC, PE, APC, clone MEL-14, Rat IgG2a), Gr-1 (eFluor450, clone RB6-8C5, Rat IgG2b), CD19 (FITC, PE, APC, clone 1D3, Rat IgG2a), PD-1 (PE, clone J43, Hamster IgG), CTLA-4 (PE, clone UC10-4B9, hamster IgG) and B220 (APC, clone RA3-6B2, Rat IgG2a) (BD Biosciences and eBioscience).

Donor T cell purification. GVHD was induced by injecting 50 x 10^6 B6-Thy1.1 splenocytes into unirradiated F1 recipients. 7 d after GVHD induction, mice were euthanized and spleens were harvested into dishes containing MACS running buffer, disrupted using frosted microscope slides (Fisher) and passed through 40 μM filters (BD) to form single cell suspensions. Anti-mouse

CD16/CD32 Fc III/II receptor (Fc Block) was added to cells (1:400 dilution) to prevent non-specific antibody binding. After 10 min, PE-anti-Thy1.1 (BD; 1:800 dilution) was added to splenocytes for 15 min at room temperature. Cells were washed once with MACS running buffer and resuspended with anti-PE microbeads (100-200 μL; Miltenyi Biotec) and MACS running buffer (800-900 μL) for 15 minutes at room temperature. Cells were washed once with MACS running buffer, resuspended in MACS running buffer (1 ml) and applied to an LS magnetic column (Miltenyi Biotec). After 3 washes, the column was removed from the magnetic field and the positively labeled cells were collected. The positively collected cells were spun, resuspended in MACS running buffer (500 μL) and applied to an MS magnetic column (Miltenyi Biotec). After 3 washes, the positive fraction was collected, analyzed for PE-Thy1.1 fluorescence and used immediately. 2-5 x 10^6 donor T cells were typically obtained per spleen.

O_2 consumption. Cells were resuspended in DMEM media at 2-5 x 10^6 cells/ml, placed into a sealed 2 ml chamber and O_2 consumption was analyzed on an Oxygraph-2k O_2 electrode (Oroboros Instruments). After a stable rate of O_2 consumption was seen, oligomycin (1-2 μg/ml) was added to inhibit ATP-synthesis coupled respiration. Carbonyl cyanide 4-(trifluoromethoxy) phenylhydrazone (FCCP) was then added in 2 μM increments to measure total respiratory capacity. In some experiments, myxothiazole (1 μM) was then added to fully inhibit mitochondrial respiration. Oligomycin, FCCP and myxothiazole were all prepared at 10-20x stocks in ethanol and stored at -20 °C.

"Routine" indicates O_2 consumption without any additions to media. "Oligo" indicates O_2 consumption in the presence of 1-2 μg/ml oligomycin. "FCCP" indicates maximal O_2 consumption following a titration of FCCP (typically 6-12 μM FCCP). "OXPHOS" is calculated as the rate of O_2 consumption that is inhibitable by oligomycin (Routine-Oligo). The % of the routine rate used for OXPHOS is calculated as (Routine-Oligo)/Routine, while the % of the routine rate used for proton leak is calculated as (Oligo/Routine). The % of capacity used for OXPHOS is calculated as (Routine-Oligo)/FCCP, the % of capacity used for Leak is calculated as (Oligo/FCCP), and the % of capacity in reserve is calculated as (FCCP-Routine)/FCCP.

Lactate production. Cells were washed and resuspended in DMEM (5-15x10^6 cells/mL) and aliquots (50 or 100 μL) were quenched at four time points over 2-3 hours using perchloric acid (0.6 M, 25 or 50 μL). After removal of cellular debris and neutralization with NaOH, lactate concentrations at ≥ 3 time points were determined by incubating aliquots of sample (10-20 μL) with lactate dehydrogenase (LDH; 1 μL) and glutamate-pyruvate transaminase (0.375 μL; Sigma Aldrich) in buffer (230-240 μL) containing glutamate (116 mM) and NAD (0.96 mM) at pH 8.9. Lactate levels were determined using a standard curve by monitoring absorption at 340 nM and the rate of lactate production was calculated as a function of time and cell concentration. ATP production was calculated as ATP_{OXPHOS}=5.6 x O_2 Consumption and $ATP_{Glycolysis}$=Lactate Production + 0.4 x O_2 Consumption.

Glycolytic rate. Cells (~4 x 10^6) were washed in PBS and resuspended in Krebs buffer (1 mL; 115 mM NaCl, 2 mM KCl, 25 mM $NaHCO_3$, 1 mM $MgCl_2$, 2 mM $CaCl_2$, 0.25% FBS, pH 7.4) for 30 min at 37 °C. During this incubation, cells were recounted to determine the exact concentration. Cells were spun down and resuspended in Krebs buffer (500 μL) containing 10 mM glucose and 10 μCi 5-^{3}H-glucose tracer (PerkinElmer) and placed into a 24 well plate for 1 h at 37 °C. HCL (100 μl of 0.2 M) was then added to each well and mixed in order to lyse cells and stop the reaction. Lysate (180 μl, in triplicate per condition) was placed into a 0.6 ml centrifute tube, which was placed inside a 1.5 ml centrifuge tube with its lid removed. This combination of tubes was placed inside a large scintillation vial containing 0.5 ml water and sealed to allow tracer-derived ^3H_2O in the 0.6 ml tube to equilibrate with H_2O in the bottom of the scintillation vial. After 72 h, the 0.6 ml tube was removed and placed into a separate scintillation vial. Scintillation fluid (5ml) was added to the vial containing the 0.6 ml tube (tube) and the vial containing 0.5 ml H_2O and the 1.5 ml tube (vial) and samples were analyzed on a scintillation counter (Beckman LS 6500). The fraction of glucose metabolized was calculated as: $(CPM_{Vial}*180/500+ CPM_{vial})/(CPM_{tube} + CPM_{vial})$.

GLUT1 western blot. Cells (~5 x 10^6) were washed once with PBS and resuspended in lysis buffer (~ 50 μl) containing 1% Triton X-100, 0.1% SDS and protease inhibitors (Roche, Complete EDTA-free) for 1 h on ice. Lysates were centrifuged for 10 min (14,000 RPM, 4 °C) and protein containing supernatant was separated from cellular debris. Protein levels were determined using the

Bradford protein assay (Bio-Rad) using BSA as a standard. Immediately prior to gel electrophoresis, lysates were deglycosylated using the PNGaseF kit (New England Biosciences). Proteins (10 μg) were diluted to a total of 9 μl with water and denaturing buffer (1 μl) was added and the mixture was incubated at room temperature for 30 min. Water (4 μl), NP-40 (2 μl), G7 reaction buffer (2 μl) and PNGaseF (2μl) were then added and the mixture was incubated at 37 °C for 1 h. Gel loading buffer (5 ul of 5x stock) was added to deglycosylated lysates for 30 min at room temperature. Proteins were separated by SDS-polyacrylamide gel electrophoresis and transferred to polyvinylidene difluoride membranes. Membranes were blocked using skim milk powder (5% w/v) in PBS containing Tween (0.05% v/v) for 1 h and then probed with rabbit-anti GLUT1 antbody (Abcam, 1:1000 dilution). Primary antibodies were detected with horseradish peroxidase-linked donkey anti-rabbit IgG (GE Healthcare, Piscataway, NJ) and visualized with a chemiluminescence detection system (GE Healthcare).

Phospho-AKT determination. pAKT levels in cell lysates were determined by western blot using a rabbit monoclonal antibody directed against phosphorylated serine 473 (Cell Signaling, catalog # 193H12). This procedure was identical to the determination of GLUT1 by western blot, however lysates were not deglycosylated and membranes were blocked with 3% BSA rather than skim milk. Determination of pAKT levels by flow cytometry was identical to GLUT1 staining by flow cytometry, however a 1:200 dilution of rabbit-anti-pSer473 was used instead of the anti-GLUT1 antibody

Pyruvate measurements. Pyruvate levels were determined in using the pyruvate assay kit (BioVision, Mountain View, CA). Cells (~10 x 10^6) were washed once with PBS and then incubated with detergent-containing pyruvate assay buffer (50-100 μl) for 15 min at 4 °C on a rotator to lyse cells. Cellular debris was pelleted and supernatant was isolated following a high speed spin (14,000 RPM, 20 min, 4 °C). Pyruvate levels in the supernatant were determined using the pyruvate oxidase-linked colorimetric kit (BioVision) and normalized to protein levels as determined using the Bio-Rad protein assay.

Glutathione measurements. Cells (5-10 x 10^6) were washed with PBS (10 ml) and resuspended in lysis buffer (50 μl) composed of potassium phosphate (0.1 M), EDTA (5 mM), Triton X-100 (0.1%, v/v) and sulfosalicylic acid (0.6% w/v) at pH 7.5 and placed on a low speed rotator (15 min, 4 °C). Cellular debris was pelleted and supernatant was isolated following a high speed spin (14,000 RPM, 20 min, 4 °C) and stored at -80 °C until analysis. Sulfosalicylic acid (10% w/v, 20 μl) was added to lysate (20 μl) mixed and placed on ice for 15 min to precipitate proteins. Protein-free supernatant was isolated following centrifugation (5,000 RPM, 15 min 4 °C). Glutathione standards (Sigma) were prepared in 5% (w/v) sulfosalicylic acid. Glutathione standards or lysate samples (10 μl) were added to wells of a 96 well plate (standard range: 50-1500 pMoles glutathione/well) and mixed with buffer (40 μl) containing potassium phosphate (0.1 M) and EDTA (5 mM) at pH 7.5. The assay was started by adding activation buffer (150 μl) containing 5,5′-Dithiobis(2-nitrobenzoic acid) (59.4 μg/ml), glutathione reductase (1 unit/ml) and NADPH (168 μg/ml). Absorbance (412 nM) was measured

kinetically over 10 minutes on an automated plate reader. Glutathione levels of lysates were normalized to protein levels as determined using the Bio-Rad protein assay.

BrdU staining. 24 h prior to analysis, mice were injected with BrdU (Sigma, 100mg/kg in PBS) and placed on drinking water containing BrdU (1 mg/ml). One mouse per group received no BrdU as a negative control. BrdU staining was performed using the FITC-BrdU kit (BD Biosciences). After Fc receptor blockade and surface staining, cells (~1 x 10^6) were resuspended in Cytofix/Cytoperm Buffer (15 min, room temperature) to fix cells and resuspended in FACS wash at 4 °C overnight. The next day, cells were washed with Perm/Wash buffer (200 μl) and resuspended in Cytoperm Plus Buffer (100 μl, 4 °C). After 10 min, cells were washed and refixed in Cytofix/Cytoperm Buffer (5 min, room temperature). Cells were resuspended with DNase (30 μg, 1 h, 37 °C) to expose BrdU epitopes. Cells were washed with Perm/Wash buffer and then resuspended with FITC-anti-BrdU (1:50 dilution, 20 min, room temperature). Cells were washed twice with Perm/Wash buffer, refixed in Cytofix/Cytoperm buffer and analyzed in FACS wash buffer.

CHAPTER 4

EFFECTS OF BZ-423 IN MODELS OF ALLOGENEIC AND SYNGENEIC BONE MARROW TRANSPLANTATION

Introduction

Graft-versus-host disease prophylaxis. Following allogeneic bone marrow transplantation, patients are at significant risk of developing graft-versus-host disease (GVHD), which is characterized by damage to the skin, liver and gastrointestinal tract (48). The cornerstone of GVHD management is prophylaxis with immunosuppressive compounds such as calcineurin inhibitors (i.e., cyclosporine A and tacrolimus), antiproliferative agents (methotrexate and mycophenolate mofetil) and rapamycin (Figure 4.1) (441, 625).

Cyclosporine A (CsA) is a non-ribosomal peptide synthesized by the fungus *Hypocladium inflatum* (626). CsA inhibits T cell activation by binding to cyclophilin A and inhibiting the phosphatase calcineurin (627). Because calcineurin activates the transcription factor NFAT in a Ca^{2+}-dependent fashion following TCR stimulation (430), CsA treatment potently inhibits T cell proliferation and cytokine synthesis (626). Tacrolimus (FK506) is a macrolide that was isolated from the bacteria *Streptomyces tsukubaensis* (628). Tacrolimus functions similarly to CsA, in that it inhibits calcineuirin. However, tacrolimus

binds to the FK506 binding protein (FK506BP) and this complex inhibits calcineurin (629).

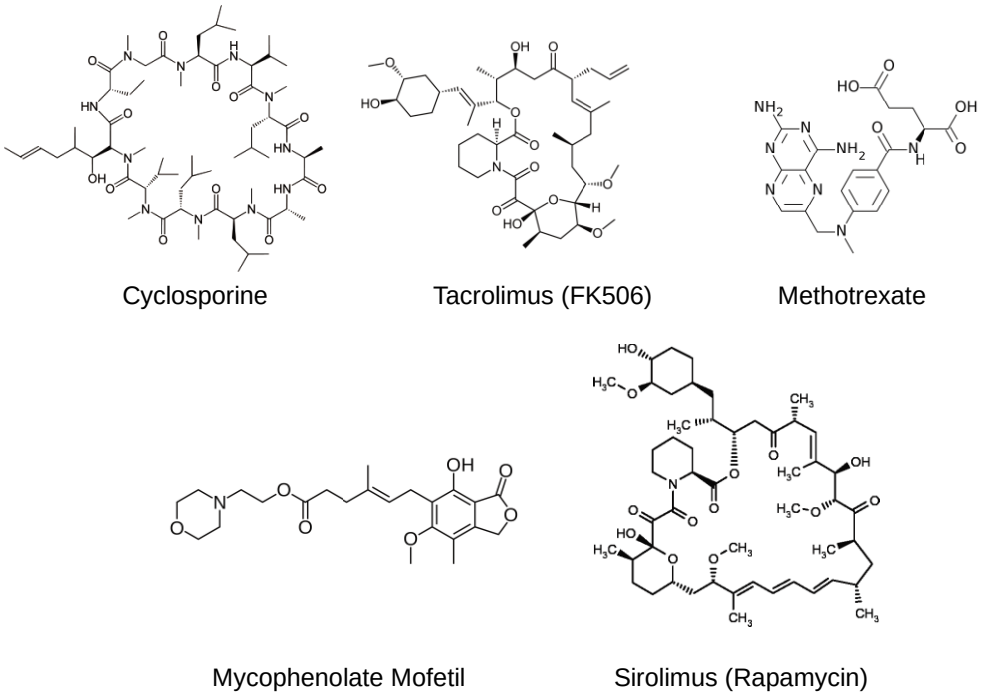

Figure 4.1. Structures of selected drugs used for GVHD prophylaxis. (44, 626, 627, 630)

Standard GVHD prophylaxis involves a calcineurin inhibitor combined with methotrexate (Figure 4.1), an inhibitor of dihydrofolate reductase (DHFR) (631). DHFR is an enzyme important in thymidine biosynthesis (632), and its inhibition with methotrexate (50 nM) completely inhibits phytohemagglutinin (PHA)-stimulated T cell proliferation (633). When combined with a calcineurin inhibitor, methotrexate helps prevent GVHD. According to a recent meta analysis of 5 separate randomized trials, 45% of patients receiving a calcineurin inhibitor without methotrexate developed GVHD (634). However, when methotrexate was

added to the prophylactic regimen, the percentage of patients developing GVHD dropped to 22% (634).

Rapamycin, which is also known as sirolimus, is a macrolide isolated from the bacteria *Streptomyces hygroscopicus* (625). Like the calcineurin inhibitors, rapamycin is also used as a prophylactic agent for GVHD (625). Rapamycin inhibits mTORC1, a kinase downstream of AKT that is involved in cell growth and proliferation (635). A 2007 study of 83 transplant recipient showed that using rapamycin and tacrolimus as prophylactic agents leads to an GVHD incidence of 20.5%, which suggests that rapamycin might have utility as an alternative to methotrexate (636)**.**

Mycophenolate mofetil (MMF, Figure 4.1) is a precursor of mycophenolic acid, which inhibits inosine monophosphate dehydrogenase, an important enzyme in guanosine nucleotide synthesis (630). MMF inhibits mitogen-stimulated T cell proliferation (630) and Staphylococcus aureus enterotoxin A-induced IL-2, IFN-γ and TNF-α production (637). These immunosuppressive properties have lead to the use of MMF in combination with a calcineurin inhibitor as a prophylactic strategy for GVHD (638). However, MMF treatment decreases neutrophil engraftment by 40% in a mouse model of allogeneic bone marrow transplantation (BMT) (639) and its utility in preventing GVHD is unclear; a 2004 study of 34 patients suggested that MMF does not decrease GVHD incidence in the setting of reduced intensity transplantation (640).

Treatment of GVHD. Despite these various prophylactic measures, many transplant patients develop GVHD. A 2008 study showed that 35% of patients

(n=1960) undergoing myeloablative human leukocyte antigen (HLA)-matched transplants from sibling donors developed GVHD (641). Similarly, a 2002 study showed that of *all* patients receiving allogeneic transplants at the University of Minnesota between 1990 and 1999 (n=1181), 63% developed GVHD (642). When patients fail prophylaxis and develop GVHD, they are typically treated with glucocorticoids (GCs) such as methylprednisolone (Figure 4.2) (473).

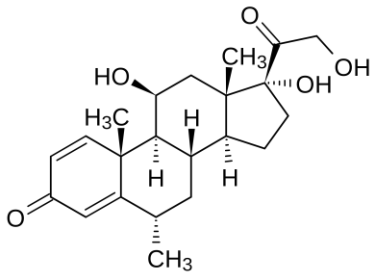

Figure 4.2. Structure of methylprednisolone. From (643).

GCs are steroid hormones produced endogenously by the adrenal gland (644). In addition to their role in the whole body stress response (645), endogenous GCs negatively regulate the function of the immune system (644). Decreasing endogenous GC production by removing adrenal glands from adult rats increases thymus size by 50-80% (646). Endogenous GC production is stimulated by adrenocorticotropic hormone (ACTH), which is produced by the pituitary gland (647). Administering exogenous ACTH stimulates endogenous GC production and decreases the size of both the thymus and lymph nodes (648). Additionally, patients with Cushing's Disease have abnormally elevated

GC levels and are at increased risk for opportunistic infections such as cryptococcosis and candidiasis (647).

GCs achieve their immunosuppressive effects by binding to the cytosolic glucocorticoid receptor, which allows this complex to enter the nucleus and affect gene transcription (644). GCs decrease the activity of transcription factors important for T cell activation such as AP-1 and NF-κB (644, 649-652) and reduce the production of proinflammatory cytokines such as IL-2, IL-6 and IFN-γ (473, 595). Additionally, GCs induce apoptosis in various cells of the immune system, including thymocytes, splenic T cells, and dendritic cells (594, 653-655). These pro-apoptotic effects can significantly affect circulating lymphocyte numbers *in vivo* following GC treatment. For example, a single dose of the GC methylprednisolone (25 mg/kg) lowers peripheral blood lymphocyte counts by > 50% 4 h after injection into healthy mice (656). The precise signaling pathways involved in GC-mediated apoptosis are unclear (644). However, GC-mediated apoptosis in thymocytes is inhibited by Bcl-2 or Bcl-x_L overexpression, which suggests the involvement of the mitochondrial pathway of apoptosis (657-659).

Because of these immunosuppressive properties, GCs have been used since the late 1940s to treat a variety of immune-mediated diseases, including rheumatoid arthritis (660), systemic lupus erythematosus (644, 661), and GVHD (441). When BMT recipients fail prophylaxis and develop GVHD, they are typically treated with high dose methylprednisone (i.e., 2 mg/kg per day). However, GC treatment fails to induce durable responses in more than half of patients with GVHD (598, 642). This deficiency is reflected in the high mortality

observed in patients with GVHD. Of 443 patients with GVHD at the University of Minnesota between 1990 and 1999, 47% died within 1 yr of transplant, despite treatment with high dose GCs. Similarly, a 1998 Italian study of 97 patients showed that treatment with standard (2 mg/kg) or higher (10 mg/kg) doses of methylprednisolone therapy resulted in only 60% overall survival 3 yr after development of GVHD (593).

In addition to their limited efficacy, GCs have numerous side effects that detract from their clinical utility. One of the most important complications of GC treatment is increased rates of infection (662). In the general population, the risk of tuberculosis infection increases 5-fold with GC treatment (663). Similarly, a case-control study of 228 renal transplantation patients showed that the likelihood of invasive aspergillosis infection correlated with the average daily intake of prednisone (664). An additional complication associated with chronic GC treatment is Cushing's syndrome, which is characterized by hypertension, bone loss, muscle wasting, weight gain and fat accumulation in the face and upper back (665).

In the BMT setting, GC treatment is associated with delayed reconstitution of several cell types. By d 60 after BMT, patients receiving GC treatment had fewer plasmacytoid dendritic cells and fewer monocytes compared to those not receiving GCs, although this study did not indicate the magnitude of these decreases (596). Similarly, a 2005 study of 77 transplant recipients showed that patients treated with prophylactic prednisolone had 2-fold fewer NK cells than patients receiving only prophylactic cyclosporine and methotrexate (597).

When treatment with GCs fails to reverse GVHD, several secondary treatment options exist. A frequent treatment strategy involves antibody-mediated T cell depletion. Several agents exist for this purpose (Table 4.1), including alemtuzumab, which recognizes CD52 expressed on mature leukocytes (666, 667). Visilizumab and OKT3 achieve a similar result by binding to CD3 on T cells leading to their depletion (668, 669). While not a monoclonal antibody, anti-thymocyte globulin (ATG) is another agent that depletes T cells (670). ATG is produced from the antiserum of horses or rabbits immunized with human T cells (670). Thus, ATG contains a variety of antibodies that recognize and deplete human T cells when infused into patients suffering from GVHD (670).

Unfortunately, these depletion strategies are directed against antigens expressed on all T cells, and thus do not distinguish between T cells mediating GVHD and bystander cells that may be important in anti-pathogen immunity. Possibly because of this lack of specificity, T cell-depletion strategies are associated with high rates of life-threatening infections (Table 4.1) (666-670). For example, a 2008 study of alemtuzumab treatment for steroid-refractory GVHD showed that 33% of patients receiving alemtuzumab developed neutropenia, and 78% developed infections, including cytomegalovirus (CMV), pneumonia and tuberculosis (667).

Table 4.1. Leokocyte depletion agents for steroid-refractory GVHD. From (666-670).

Agent	Antigen Recognized	Expression	Adverse Effects
Alemtuzumab (666, 667)	CD52	Mature Leukocytes	Delayed reconstitution Neutropenia Infection
Visilizumab (668)	CD3	T Cells	Infection
OKT3 (669)	CD3	T Cells	Infection
ATG (670)	Polyclonal	T Cells	Infection Poor Outcome

Several strategies besides T cell depletion exist for the treatment of steroid-refractory GVHD. One such strategy is the neutralization of tumor necrosis factor (TNF)-α, an inflammatory cytokine produced by activated macrophages and T cells (671, 672). Infliximab and etanercept are monoclonal antibodies that neutralize TNF-α, and kill cells that produce TNF-α (421, 671, 673). This activity has led to the use of anti-TNF-α therapy as an addition to GC treatment and as a treatment for steroid-refractory GVHD (674, 675). As in cellular depletion strategies, infection is a common side effect of anti-TNF-α therapy. A 2004 Italian study documented that 72% of patients receiving infliximab as a treatment for steroid-refractory GVHD developed infections,

including septicemia, bacterial pneumonia, cytomegalovirus (CMV), and invasive fungal infections (674).

Extracorporeal photopheresis (ECP) is another strategy used to treat GVHD (676). ECP involves the isolation of a patient's peripheral blood mononuclear cells and their treatment with 8-methoxypsoralen (8-MOP) and ultraviolet A (UVA) radiation (676). UVA photoactivates 8-MOP thereby inducing DNA cross-linking and apoptosis. Treated cells are then transfused back into GVHD patients. A 2006 Austrian study showed that ECP-treatment for steroid-refractory GVHD yielded a response rate of 60%; however, rates of infectious complications were not reported (677). Currently, many of the details of ECP's mechanism are unknown. However, ECP treatment increases regulatory T cell numbers in both mice and humans, which may be related to its ability to attenuate GVHD (678, 679).

The limited efficacy of therapies for GHVD combined with the increased rates of infection that accompany such therapies highlight the need for novel GVHD treatments. One such avenue of investigation involves the modulation of cellular redox status. As discussed in Chapter 3, patients with GVHD exhibit increased oxidative stress in both plasma and white and red blood cells (487, 680). Investigators have used this knowledge in an attempt to treat GVHD by restoring antioxidant balance. However, treatment with *N*-acetylcysteine (NAC), a precursor of glutathione (681) had no effect on disease in a mouse model of GVHD (487). Similarly, in a small clinical study (n=8), 75% of patients with GVHD who were treated with NAC died of GVHD or transplant complications

within 100 days of GVHD development (680). However, this study did not include patients not receiving NAC, so its results are difficult to interpret (680). While these studies suggest that increasing antioxidant levels has little benefit in GVHD, an alternative strategy is to use the depleted antioxidant status of alloreactive donor T cells to target these cells for deletion with pro-oxidant therapeutics such as arsenic trioxide (380, 489) or Bz-423 (169, 172, 395).

Bz-423. Bz-423 is a non-anxiolytic 1,4-benzodiazepine with proapoptotic and immunomodulatory properties (Figure 4.3) (169). Bz-423 was identified by screening a library of 1,4-benzodiazepines for lymphotoxicity using Ramos B cells, which are derived from Burkitt's lymphoma and resemble activated, germinal center B cells (682). Bz-423 treatment for 24 h induces dose-dependent apoptosis in Ramos B cells with an EC_{50} of 6-8 μM (169, 683). However, structural analogs of Bz-423 that lack the 4'-phenolic hydroxyl or the 3-position naphthalene groups induce limited apoptosis at concentrations up to 60 μM (169).

These structural and pro-apoptotic characteristics distinguish Bz-423 from prototypical 1,4-benzodiazepines such as diazepam, clonazepam and lorazepam (Figure 4.3), which exert their biologic effects by binding to the central benzodiazepine receptor (CBR) within the γ-aminobutyric acid (GABA) receptor complex on post-synaptic neurons (684). Unlike prototypical benzodiazepines, Bz-423 does not bind the CBR and does not cause neurologic effects in mice, indicating that its proapoptotic effects likely stem from a mechanism distinct from interactions with GABA receptors (169, 395).

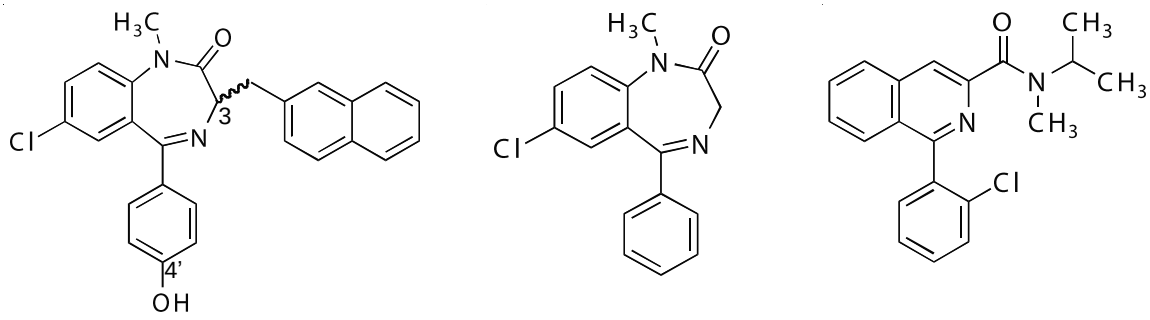

Bz-423 Diazepam PK11195

Figure 4.3. Structure of Bz-423, diazepam and PK11195. Bz-423 contains a naphthalene group at the 3 carbon and a phenolic OH at the 4' position. These structural features distinguish it from ligands of the central benzodiazepine receptor, such as diazepam, and ligands of the peripheral benzodiazepine receptor, such as PK11195 (169, 175, 685).

Benzodiazepines can also bind a receptor localized on the mitochondrial outer membrane, termed the peripheral benzodiazepine receptor (PBR) (686). Unlike the CBR, the PBR has a wide tissue distribution that includes cells of the immune system (686, 687). Although the precise function of the PBR is uncertain, it has been implicated in cellular proliferation, porphyrin and heme biosynthesis and steroidogenesis (688). PK11195, a ligand of the PBR, does not induce apoptosis in primary thymocytes or in CEM-C7 leukemia cells (Figure 1.3) (689). However, PK11195 can sensitize cells to apoptosis induced by other agents, such as etoposide and dexamethasone (689). Furthermore, PK11195 has anti-inflammatory effects in several mouse models, including autoimmune arthritis (690, 691).

Several lines of evidence suggest that Bz-423 exerts its pro-apoptotic effects by binding a cellular target distinct from the PBR. While Bz-423 is capable of binding to the PBR, it does so with a 10-50-fold lower affinity than the prototypical PBR ligands 4-chlorodiazepam (4-ClDz) and PK11195, as measured by the ability to displace radiolabeled PK1195 from the PBR (692, 693). Despite their tighter binding to the PBR, PK11195 and 4-ClDz only induce apoptosis in Ramos B cells at high concentrations, with EC_{50} values 15-20-fold higher than Bz-423 (90 and 130 μM respectively vs. 6.3 μM). Furthermore, preincubation of Ramos B cells with PK11195 (20 μM) does not inhibit Bz-423-induced apoptosis (169). Together, these observations suggest that Bz-423 induces apoptosis through a mechanism independent of binding to the PBR.

Effects of Bz-423 in models of lupus. Because of its potent ability to induce apoptosis in a germinal center-like B cell line, Bz-423 was administered to NZB/W mice, which suffer from a lupus-like disease characterized by the pathologic expansion of germinal center B cells (169, 694). A short (1 week) course of Bz-423 treatment increases B cell apoptosis in the spleens of NZB/W mice (169). Similarly, a 12-week course of Bz-423 reduces germinal center numbers by 40%, increases germinal center TUNEL staining (a marker of apoptosis), and reduces the incidence of nephritis by 60% (169). Importantly, Bz-423 does not broadly induce lymphocyte apoptosis or affect the number of T cells in treated mice, indicating that its effects might be specific for disease-causing lymphocytes.

Bz-423 shows similar efficacy when used to treat MLR-*lpr* mice, which develop a T cell dependent lupus-like disease (395). A short (1 week) course of Bz-423 treatment reduces the number of pathogenic $CD4^+$ T cells in MLR-*lpr* mice without significantly depleting the number of B cells (395). This observation again suggests that Bz-423 specifically induces apoptosis in disease-causing lymphocytes rather than being broadly lymphotoxic. In support of this hypothesis, 7 d of Bz-423 treatment does not reduce the number of T or B cells in the spleens of healthy Balb/c mice (395).

Longer term Bz-423 treatment (14 weeks) improves renal function and decreases histologic manifestations of nephritis and arthritis in MLR-*lpr* mice (395). This same study showed that Bz-423 treatment does not significantly affect the cell mediated immune response to a foreign antigen, as measured by hind paw swelling in response to a delayed-type hypersensitivity (DTH) test. Similarly, Bz-423 treatment does not decrease antibody production following immunization with keyhole limpet hemocyanin (KLH) (395). Both of these results suggest that Bz-423 does not broadly impair lymphocyte function.

Anti-proliferative and anti-psoriatic effects of Bz-423. In addition to its ability to induce apoptosis in lymphoid cells, Bz-423 can induce cell cycle arrest and inhibit proliferation without inducing apoptosis (692, 695). These experiments were carried out in media with 10% fetal bovine serum (FBS), in which nearly 99% of Bz-423 is bound to bovine serum albumin (BSA). Under these conditions, 20 μM Bz-423 inhibited Ramos cell proliferation by 6-fold and nearly doubled the percentage of cells arrested in the G_0/G_1 stage of the cell

cycle (692). These anti-proliferative effects stem from the ability of Bz-423 to induce proteosomal degradation of the transcription factor c-myc (695). Treating Ramos cells with Bz-423 (15 μM) for 24 h decreased c-myc levels by > 90% and significantly decreased the expression of cyclins (D3 and E), and cyclin-dependent kinases (CDK 2, 4 and 6), all of which are transcriptionally activated by c-myc (695, 696). These changes were associated with decreased pRb phosphorylation, which is the primary substrate of the CDKs (695, 697). Because dephosphorylated pRb prevents the transcription of E2F-regulated genes and cell cycle entry (697), these changes are likely responsible for the anti-proliferative effects of Bz-423. Indeed, when c-myc degradation was blocked by inhibiting the proteosome, Bz-423 was no longer able to decrease cyclin D3 expression (695). Furthermore, transfecting Ramos cells with c-myc mutants resistant to proteosomal degradation abrogated the ability of Bz-423 to induce cell cycle arrest (695).

The antiproliferative effects of Bz-423 are not limited to lymphoid cells. Bz-423 also inhibits cellular proliferation in the setting of psoriasis, a disease characterized by excessive proliferation of keratinocytes that results in epidermal hyperplasia (698). Bz-423 inhibits the growth of proliferating keratinocytes *in vitro* at concentrations < 2 μM (699). Similarly, treatment with 1 μM Bz-423 completely reverses retinoic acid-induced epidermal thickening in an organ culture model of epidermal hyperplasia (699). However, when normal skin tissue is cultured without retinoic acid (i.e., no hyperplasia), Bz-423 treatment has no effect on epidermal thickness (699). These observations suggest that Bz-423

may selectively inhibit psoriatic keratinocyte proliferation without affecting normal skin.

In addition to these *in vitro* effects, Bz-423 has potent anti-psoriatic effects in animal models, in which psoriatic human skin is transplanted onto severe-combined-immunodeficient (SCID) mice (700). Treatment with corticosteroids or Bz-423 decreases epidermal thickness by 2-3-fold compared to vehicle treatment. However, unlike corticosteroids, Bz-423 treatment did not induce atrophy of the normal mouse skin surrounding the transplanted psoriatic lesion (700). These results support *in vitro* observations that Bz-423 selectively inhibits the growth of psoriatic skin tissue without affecting normal skin (699).

Bz-423 production of ROS. Because Bz-423 induces apoptosis in pathogenic germinal center B cells and reduces the number of pathogenic cells in two separate models of lupus, studies were undertaken to investigate its apoptotic signaling mechanism. Treating T or B cell lines or mouse embryonic fibroblasts (MEFs) for 1-2 h with Bz-423 results in a dose-dependent increase in the fluorescence of dihydroethidium (DHE) (169, 172, 173), a redox sensitive dye that fluoresces due to selective oxidation by superoxide (O_2^-) (340). This O_2^- signal precedes the collapse of the mitochondrial membrane potential ($\Delta\psi_m$), caspase activation and cytochrome C release, which suggests that it might be a cause rather than a consequence of apoptosis (169, 173). Bz-423 also generates reactive oxygen species (ROS) in the spleens of NZB/W mice 2 h after i.p. injection, suggesting that O_2^- generation may be important for its therapeutic effects *in vivo* (169). This O_2^- signal is required for Bz-423-induced apoptosis

because its inhibition with antioxidants such as vitamin E or the superoxide dismutase (SOD) mimetic manganese(III)*meso*-tetrakis(4-benzoic acid) porphyrin (MnTBAP), significantly reduces caspase activation, cyctochrome c release and cell death in MEFs and B and T cell lines (169, 173, 175). PEG-catalase, which converts hydrogen peroxide to water (701), does not protect against Bz-423-induced apoptosis, which suggests that superoxide rather than hydrogen peroxide is the ROS species important for induction of apoptosis (172).

Studies in isolated mitochondria show that Bz-423 generates ROS when mitochondria are actively respiring (i.e., in the presence of succinate and ADP, state 3 respiration), but not when mitochondria are inactive (i.e., in the presence of succinate and oligomycin and without ADP, state 4 respiration) (169). Similarly, co-treatment with sodium azide, an inhibitor of respiration, completely abolishes Bz-423 induced ROS production in Ramos B cells (169). This observation supports the hypothesis that active respiration may be necessary for Bz-423 activity in intact cells.

ROS production is also important for the anti-proliferative effects of Bz-423. Anti-proliferative concentrations (e.g., 20 μM in media with 10% FBS) of Bz-423 increase dichlorofluorescein (DCF) fluorescence in Ramos B cells, which indicates increased ROS levels (386, 692). This DCF fluorescence was reduced when cells were co-treatment with MnTBAP, which suggests that it was caused by O_2^- formation. MnTBAP treatment also decreases Bz-423-induced c-myc degradation (695) and increases the GI_{50} of Bz-423 by 2-fold (692). Together, these observations suggest that O_2^- is an important mediator of Bz-423's

antiproliferative effects in Ramos B cells (692). Anti-proliferative concentrations of Bz-423 also increase both DHE and DCF fluorescence in keratinocytes (699, 700). Blocking this ROS production with vitamin E abrogates Bz-423's ability to inhibit keratinocyte proliferation *in vitro*, which suggests that O_2^- may also mediate Bz-423's anti-psoriatic effects (700).

Molecular target of Bz-423. The molecular target of Bz-423 was discovered based on phage-display screens. These experiments demonstrated a direct interaction between Bz-423 and the oligomycin sensitivity conferring protein (OSCP), a component of the mitochondrial F_1F_o-ATPase (170). Bz-423 inhibits ATP synthesis and hydrolysis in submitochondrial particles (SMPs), but this inhibition is lost when OSCP is removed from SMPs. Bz-423 also inhibits ATP synthesis and O_2 consumption in Ramos B cells, and causes an increase in $\Delta\psi_m$ shortly (1 hr) after treatment (170). Together, these data suggest that Bz-423 causes a respiratory transition from state 3 (active ATP synthesis) to state 4 (inhibited ATP synthesis) and slows the rate of H^+ flow through the F_1F_o-ATPase. This slowed H^+ flow causes H^+ accumulation in the intermembrane space, thereby increasing $\Delta\psi_m$ (Figure 4.4). Increased $\Delta\psi_m$ slows electron transport through the mitochondrial respiratory chain (MRC) and increases the half-life of reduced flavins, Fe-S clusters, and ubisemiquinone, which favors electron escape and superoxide formation (167).

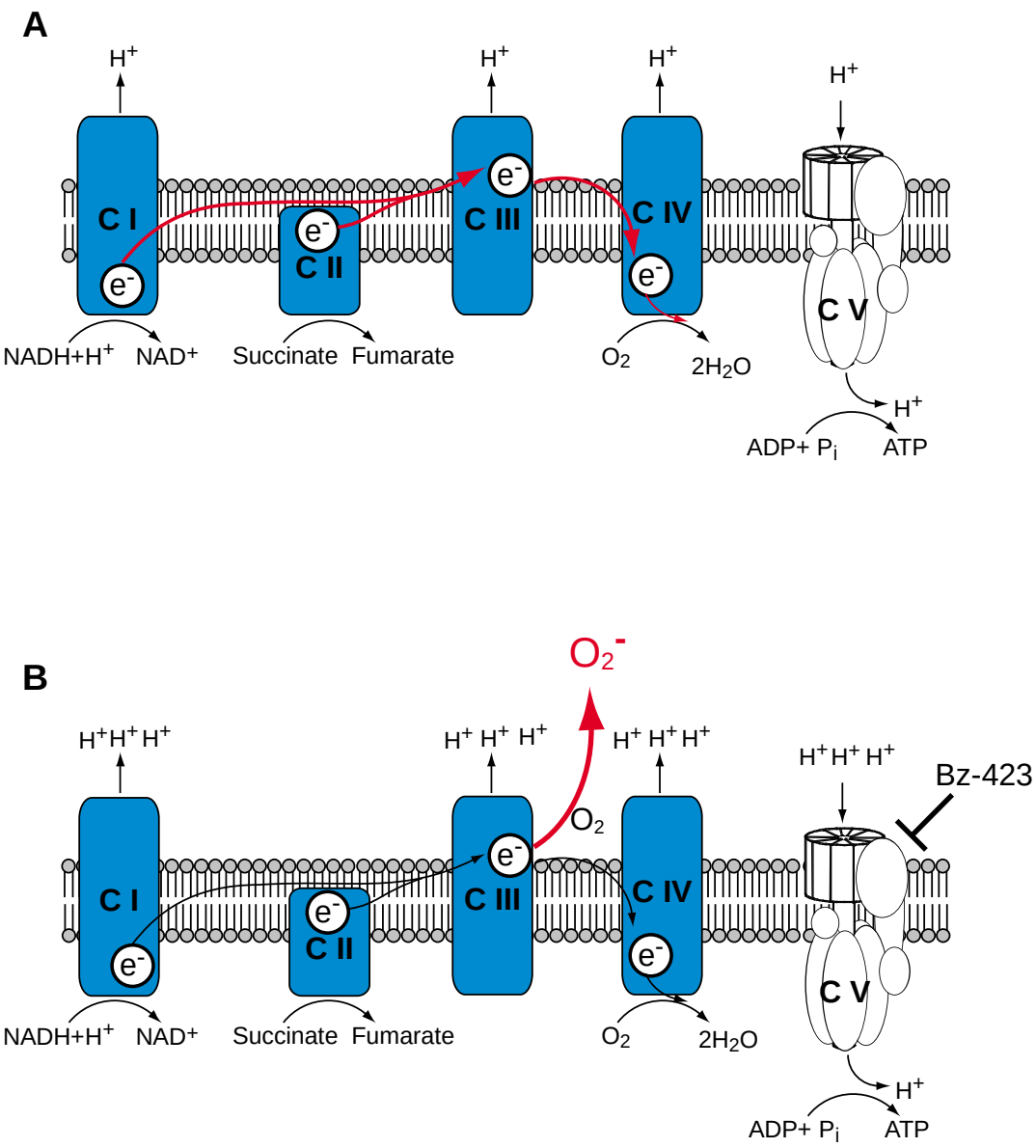

Figure 4.4. Electron transport, ATP synthesis and Bz-423-induced ROS formation. **A**. In state 3 respiration, electrons are transferred along the MRC (in red) and protons (H^+) are pumped into the intermembrane space. Protons then flow through the F_1F_o-ATPase catalyzing the synthesis of ATP. **B**. Bz-423 modulates the F_1F_o-ATPase, slowing proton flow through the enzyme and resulting in H^+ accumulation in the intermembrane space. This transition to state 4 respiration disfavors the flow of electrons from complex to complex and causes the buildup of reactive intermediates resulting the escape of electrons from complex III (in red) and the formation of superoxide.

While superoxide can be formed at complex I or complex III in the MRC (154), Bz-423 forms substantial superoxide even when rotenone is present (170). This observation suggests that Bz-423 produces superoxide at complex III because rotenone blocks reverse electron flow to the active flavin and iron-sulfur centers of complex I (154). The OSCP is important for Bz-423-induced O_2^- production in intact Ramos cells, as decreasing OSCP levels using small inhibitory RNA (siRNA) decreases ROS production and apoptosis following Bz-423 treatment (170).

Transduction of Bz-423-induced O_2^- into apoptosis. In intact cells, Bz-423 generates O_2^- and leads to biochemical changes characteristic of apoptosis, including the collapse of $\Delta\psi_m$, and the translocation of cytochrome C from the intermembrane space to the cytosol (169, 172, 683). However, in isolated mitochondria, Bz-423 produces O_2^- but does not cause $\Delta\psi_m$ collapse or cytochrome C translocation (169, 172). These observations suggest that O_2^- produced by Bz-423 must signal through cytosolic factors in order to induce apoptosis.

The mitochondrial pathway of apoptosis is regulated by numerous cytosolic proteins (Figure 4.5). Bax and Bak are effector proteins that, when activated, begin the apoptotic signaling cascade by permeabilizing the mitochondrial outer membrane (702). In the absence of pro-apoptotic signals, Bak is localized in the mitochondrial membrane, but is kept inactive by interactions with anti-apoptotic proteins such as Mcl-1 and Bcl-x_L (703). Bax is a cytosolic protein that becomes phosphorylated in response to pro-apoptotic

signals and translocates to the mitochondria (704). Like Bak, the ability of mitochondrial Bax to permeabilize the mitochondrial membrane is blocked by interactions with anti-apoptotic proteins such as Bcl-2, Mcl-1 and Bcl-x_L (702). Cell death occurs when apoptotic stimuli activate pro-apoptotic "BH3-only" proteins such as Bad, Bim, tBid, Puma and Noxa (702). Active BH3-only proteins activate Bax and Bak and induce their dissociation from constraining anti-apoptotic proteins, leading to permeabilization of the mitochondrial outer membrane and apoptosis (702).

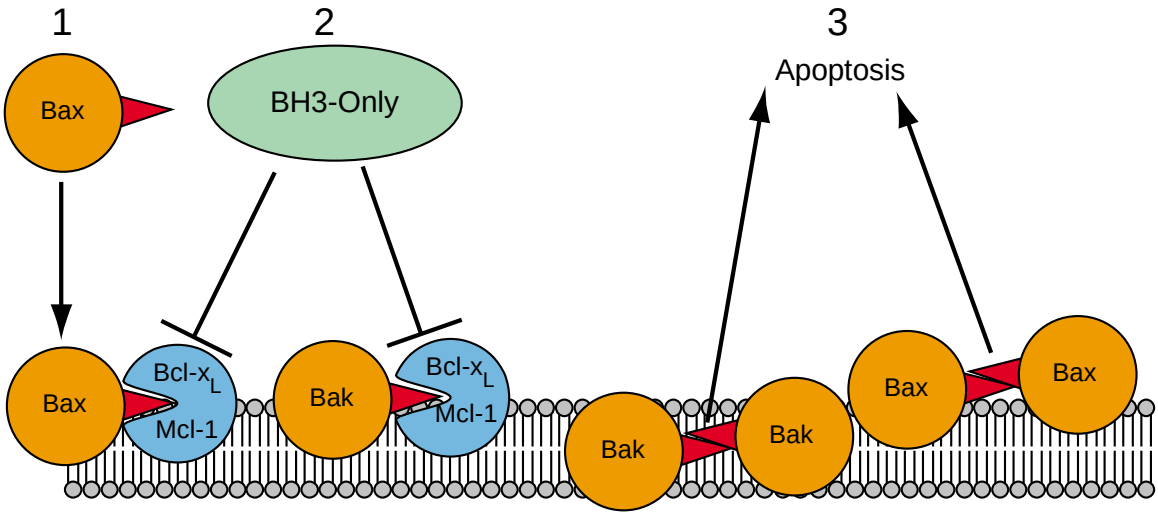

Figure 4.5. Regulation of the mitochondrial pathway of apoptosis. In step 1, cytosolic Bax translocates to the mitochondria, where it is sequestered by anti-apoptotic proteins such as Bcl-x_L, Mcl-1 or Bcl-2. In step 2, proapoptotic BH3 proteins such as Bad, Bim, tBid, Puma and Noxa activate Bax and Bak and displace them from antiapoptotic proteins. In step 3, active Bax and Bak dimerize and form pores in the mitochondrial membrane thereby inducing apoptosis (702).

In Ramos B cells, Bz-423 causes the translocation of the proapoptotic protein Bax to the mitochondria and activates both Bax and Bak, as assayed by

immunofluorescence (683). Decreasing Bax and Bak levels with siRNA inhibited Bz-423-induced apoptosis, confirming their importance in this pathway (683). Importantly, Ramos cells with decreased Bax and Bak levels produced as much O_2^- in response to Bz-423 as wild type cells, confirming that O_2^- production is proximal to Bax and Bak activation (683). In Ramos cells, O_2^- activates Bax and Bak by inducing the degradation of the anti-apoptotic protein Mcl-1 and the generalized activation of BH_3-only proteins (683).

Similar to its effects in Ramos cells, Bz-423-induced O_2^- activates Bax and Bak in MEFs (172). However, the signaling pathways between O_2^- and Bax and Bak differ between these two cell types. In MEFs, Bz-423 treatment increases the levels of the BH3-only protein Bad within 1 h of treatment (172). Preventing this increase in Bad, either by inhibiting protein synthesis with cyclohexamide or by using Bad-deficient MEFs, decreases Bz-423-induced apoptosis (172). This contrasts with Ramos cells, in which cyclohexamide does not inhibit Bz-423-induced apoptosis (395). While Bz-423-induced apoptosis was inhibited in both cyclohexamide-treated and Bad-deficient MEFs, it was not eliminated completely, which suggests that Bz-423 might activate Bad-independent pro-apoptotic pathways (172). In support of this hypothesis, Bz-423 activates apoptosis signaling regulating kinase-1 (ASK1) and the MAP kinase JNK (172), both of which are involved in apoptosis induced by other pro-oxidants such as H_2O_2 and TNF-α (705, 706). This ASK1-JNK signaling appears to be important in Bz-423-mediated apoptosis in MEFs, as inhibiting JNK with a selective kinase inhibitor almost completely abrogates Bz-423-induced apoptosis (172).

Another important difference between Bz-423-induced apoptosis in MEFs and Ramos cells is the [Bz-423] at which apoptosis occurs. Ramos cells require 3-4 h of exposure to [Bz-423] of 6 μM and higher for apoptosis to occur (683). In contrast, inducing apoptosis in MEFs requires longer exposure (> 10 h) to higher [Bz-423] (10 μM and higher) (172). This decreased sensitivity to Bz-423-induced apoptosis in MEFs could be due to increased levels of endogenous antioxidants, as MEFs have 2-fold more cytosolic and mitochondrial glutathione than Ramos cells. In support of this hypothesis, experimentally lowering MEF glutathione levels with the γ-glutamylcysteine synthetase inhibitor buthionine sulfoxide (BSO) increases Bz-423-induced apoptosis 3-fold (172).

In Jurkat T cells, Bz-423 activates Bak within 4 h of treatment, while Bax activation occurs later (i.e., at 8 h). This is different than the results in Ramos or MEF cells, where Bax and Bak activation was not temporally separated (172, 683). siRNA experiments showed that lowering Bak levels inhibits Bz-423-induced apoptosis in Jurkat cells, but lowering Bax alone has no effect. Bz-423 also activates JNK and inactivates the prosurvival kinase AKT in Jurkat T cells. However, blocking these two processes does not inhibit Bz-423-induced apoptosis, which suggests that other pathways may couple Bz-423-induced O_2^- to apoptosis. As in Ramos cells, Bz-423 induces the degradation of the anti-apoptotic protein Mcl-1 (173), possibly by inducing the expression of the BH3-only protein noxa. Indeed, reducing noxa levels with siRNA decreases Bz-423-induced apoptosis by 2-3-fold (173). Together, these observations show that the mechanisms coupling Bz-423-induced O_2^- to apoptosis vary between cell types

and suggest that such variations could cause differential sensitivity to Bz-423 across cell types *in vivo*.

Statement of problem. GVHD is the major morbidity associated with allogeneic bone marrow transplantion and current treatments lack efficacy and have numerous side effects, including high rates of opportunistic infection. Bz-423 is a novel pro-apoptotic small molecule that selectively induces apoptosis in activated lymphocytes in models of lupus by modulating the F_1F_o-ATPase and forming a O_2^- signal. High rates of OXPHOS and depleted antioxidants in alloreactive donor T cells suggest that Bz-423 may induce apoptosis in these cells and therefore have utility in models of GVHD. The low rates of OXPHOS and intact antioxidants in unstimulated T cells and proliferating bone marrow cells suggest that, unlike current treatments for GVHD, Bz-423 may *specifically* affect alloreactive donor T cells.

Results

Effects of Bz-423 on T cell $\Delta\psi_m$ and ROS production in vitro. Bz-423 modulates the F_1F_O-ATPase, which hyperpolarizes $\Delta\psi_m$ leading to O_2^- production and apoptosis (169, 170, 172, 173, 395). Increased OXPHOS in alloreactive donor T cells compared to unactivated cells suggests an increased flow of protons through the F_1F_O-ATPase (153). Hence, modulating the F_1F_O-ATPase with Bz-423 may induce increased hyperpolarization in cells with greater oxidative metabolism, resulting in a larger ROS signal (167, 707).

We first tested this hypothesis *in vitro* by measuring the effects of Bz-423 on $\Delta\psi_m$ hyperpolarization in unstimulated and stimulated T cells using the dye tetramethylrhodamine (TMRM). T cells stimulated for 48 h with anti-CD3 and anti-CD28 antibodies consumed 0.4 nMoles O_2/(min x 10^6 cells) (Figure 4.6 A), which is 2-fold faster than rates observed in unstimulated T cells (0.2 nMoles O_2/(min x 10^6 cells). Similarly, CD3/28-stimulated T cells had 3-4-fold more TMRM staining than unstimulated cells following Bz-423 treatment (Fig 4.6 B, $p<0.0001$ for all [Bz]). These results suggest that the ability of Bz-423 to hyperpolarize $\Delta\psi_m$ increases as O_2 consumption increases. However, unstimulated and stimulated T cells differ in many ways aside from their oxidative metabolism, including increased intracellular [Ca^{2+}] and activated NFAT and NF-κB in stimulated T cells (430). An alternative interpretation of our data is that a change independent of O_2 consumption sensitized activated T cells to Bz-423-mediated $\Delta\psi_m$ hyperpolarization.

The experiments described above were performed in standard DMEM media, which contains 25 mM glucose. To further test if cells with increased OXPHOS were more sensitive to Bz-423-induced $\Delta\psi_m$ hyperpolarization, we increased O_2 consumption in activated T cells by culturing these cells in media containing low glucose (0.5 mM). Although restricting glucose could potentially decrease OXPHOS by limiting flux through pyruvate dehydrogenase (Chapter 3), others have shown that stimulating T cells in low (0.4 mM) glucose media increases O_2 consumption 3-fold compared to T cells stimulated with high glucose (11 mM), likely due to increased fatty acid and glutamine oxidation (59, 376).

T cells stimulated in low glucose media consumed O_2 2-fold faster than T cells stimulated in high glucose media (Figure 4.6 A, $p=0.002$) and had 20-30% more TMRM staining following Bz-423 treatment (Figure 4.6 B, $p<0.02$ for [Bz-423] > 2 μM). Together, these results show that as T cells increase their rates of O_2 consumption, they become more sensitive to Bz-423-induced $\Delta\psi_m$ hyperpolarization. These results are consistent with studies in isolated mitochondria showing that inhibition of the F_1F_O-ATPase with oligomycin caused a greater rise in $\Delta\psi_m$ in quickly respiring mitochondria than in slowly respiring mitochondria (707).

A potential caveat in interpreting these data is that the concentrations of TMRM used (50 nM) may measure contributions from both the plasma and mitochondrial membrane potentials (145, 338). However, Bz-423 is not known to bind to proteins on the plasma membrane (170) and the OSCP, to which Bz-423

does bind (170), is not a component of extramitochondrial ATPases such as the vacuolar H^+-ATPase (708). These observations suggest that Bz-423-induced changes in TMRM fluorescence are due to alterations in $\Delta\psi_m$ rather than changes in the plasma membrane potential.

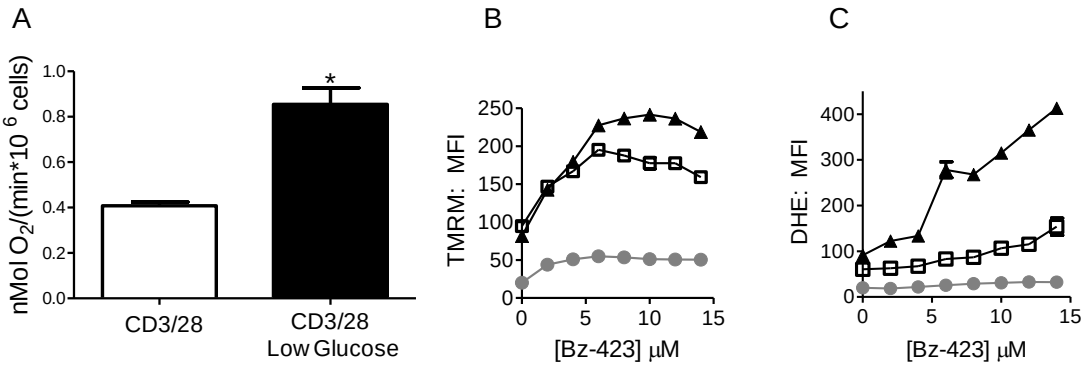

Figure 4.6. Bz-423-induced $\Delta\psi_m$ hyperpolarization and ROS production in T cells *in vitro*. A-C. T cells were stimulated for 48 h with anti-CD3/28 antibodies (0.5 μg/mL) in DMEM media with 25 mM glucose (CD3/28, white squares) or 0.5 mM glucose (CD3/28 Low Glucose, black triangles) prior to analysis. Unstimulated T cells (Unstim, gray circles)were purified from naïve mice immediately before being analyzed in DMEM media with 25 mM glucose. **A**. Oxygen consumption of CD3/28 (n=3) or CD3/28 Low Glucose (n=3) T cells performed in DMEM media with the indicated glucose concentrations. * p=0.002. **B-C**. After isolation (Unstim) or 48 h of culture (CD3/28, CD3/28 Low glucose) in media with 10% FBS, cells were washed, resuspended in media with the appropriate glucose concentration and 2% FBS and treated with the indicated concentration of Bz-423 for 1 h before analysis of TMRM (B) or DHE (C) staining. Data points are the average of median fluorescence intensity (MFI) for 3 independent treatments and error bars indicate standard error.

Because Bz-423 generates O_2^- as a consequence of its ability to hyperpolarize $\Delta\psi_m$ (170, 175), we hypothesized that T cells in which Bz-423 hyperpolarized $\Delta\psi_m$ would also increase O_2^- in response to Bz-423. Consistent with this hypothesis, Bz-423 produced 2-4-fold more DHE staining in T cells stimulated in high glucose media than in unstimulated cells (Figure 4.6 C,

p<0.002 at all [Bz-423]). This observation parallels the 3-4-fold increase in Bz-423-induced TMRM staining in stimulated cells compared to unstimulated T cells (Figure 4.6 B). T cells stimulated in low glucose had the highest levels of DHE staining following Bz-423 treatment (10-15-fold over unstimulated, 3-4-fold over high glucose, Figure 3.C, p<0.001 at all [Bz-423]). These data are consistent with the observation that T cells stimulated in media containing low glucose hyperpolarize $\Delta\psi_m$ in response to Bz-423 to a greater extent than do unstimulated T cells or T cells stimulated in media containing high glucose (Figure 4.6 B).

The difference in DHE staining between T cells stimulated in high and low glucose media (3-4-fold, Figure 4.6 C) was greater in magnitude than the difference seen in TMRM staining (20-30%, Figure 4.6 B). Although neither TMRM nor DHE reports on $\Delta\psi_m$ or ROS production quantitatively as used (145, 340), this difference in magnitude could occur because small increases in $\Delta\psi_m$ cause large increases in ROS production (168). For example, a 20% increase in $\Delta\psi_m$ increases H_2O_2 production 10-fold in isolated mitochondria (167). Alternatively, T cells stimulated in low glucose could have decreased antioxidants compared to T cells stimulated in high glucose, which could increase the ROS levels detected following Bz-423 treatment (343, 376, 491).

Effects of Bz-423 on $\Delta\psi_m$ hyperpolarization, ROS production and apoptosis in T cells during GVHD. The bioenergetic measurements detailed in Chapter 3 revealed two important and possibly related features of alloreactive donor T cells that could sensitize them to Bz-423. First, alloreactive donor T cells

increase OXPHOS 2.5-fold compared to unstimulated T cells (Figure 3.16), which could sensitize them to Bz-423-induced $\Delta\psi_m$ hyperpolarization and ROS production (Figure 4.4). Second, alloreactive donor T cells have decreased glutathione and pyruvate levels compared to unstimulated T cells (Figure 3.27), which could lead to increased ROS-mediated apoptosis (172).

To examine the effects of Bz-423 on $\Delta\psi_m$ hyperpolarization and ROS production in alloreactive donor T cells, we labeled B6-Ly5.2 splenocytes with the fluorescent cytoplasmic dye carboxyfluorescein diacetate succinimidyl ester (CFSE) (510, 511). The amount of CFSE in a cell decreases by half following each division, which causes a 2-fold decrease in fluorescence (510, 511). We infused CFSE-labeled B6-Ly5.2 splenocytes into allogeneic (B6D2F1) and syngeneic (B6) recipients, and treated mice with Bz-423 or vehicle 4 d after transplant. We distinguished donor cells based on their expression of CD45.1, as lymphocytes from B6-Ly5.2 mice express the CD45.1 phosphatase isoform, while those from B6 or F1 mice express CD45.2 (497, 498). We further identified donor T cells as either divided (i.e. 1 or more divisions) or undivided based on their CFSE fluorescence (Figure 3.18, Figure 3.26).

Bz-423 increased TMRM staining 40-50% in divided $CD4^+$ and $CD8^+$ donor T cells compared to cells from mice treated with vehicle (Figure 4.7 A, $p<0.02$). However, Bz-423 did not alter TMRM staining in undivided donor T cells or host T cells (Figure 4.7 A). These findings show that Bz-423 induces $\Delta\psi_m$ hyperpolarization preferentially in alloreactive donor T cells rather than in unstimulated donor or host T cells. Similarly, Bz-423 increased DHE staining 50-

60% in divided donor T cells as compared to cells from mice treated with vehicle (Figure 4.7 B, p=0.001). However, Bz-423 did not change DHE staining in undivided donor T cells or host T cells. These data show that, like $\Delta\psi_m$ hyperpolarization, Bz-423 produces O_2^- primarily in alloreactive donor T cells and not in unactivated T cells.

Because Bz-423 can induce redox regulated apoptosis *in vitro* (169, 172, 173, 683), we next examined the effects of Bz-423 on apoptosis in T cells post-transplant. We infused donor cells into allogeneic recipients, treated mice with Bz-423 or vehicle and analyzed the ability of donor and host T cells to bind annexin-V, a protein that selectively binds phosphatidylserine externalized by dying cells (709). Bz-423 doubled annexin-V staining in alloreactive donor T cells compared to vehicle ($p<0.001$, Figure 4.7 C), consistent with increased apoptosis in these cells (710). Bz-423 did not increase annexin-V staining in unactivated host T cells. This differential sensitivity to Bz-423-mediate apoptosis could be related to the differences in oxidative metabolism and antioxidant status in host T cells as compared to alloreactive donor T cells (Figures 3.16, 3.27).

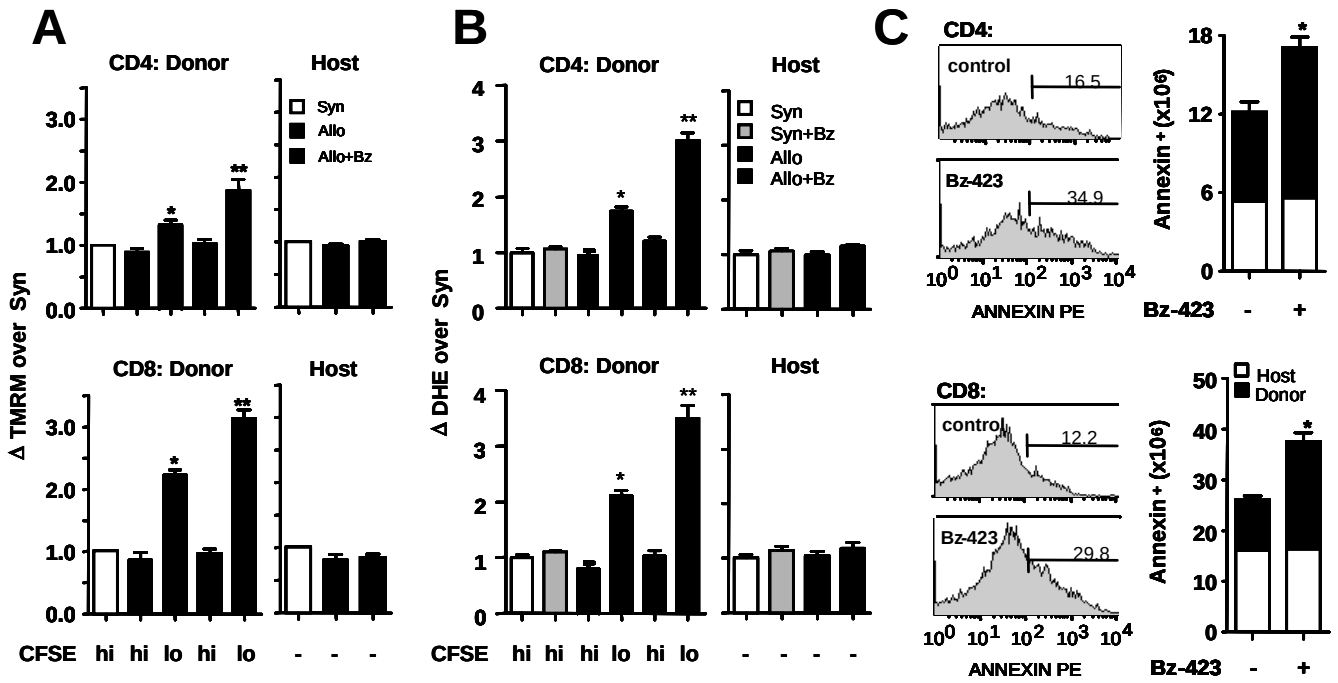

Figure 4.7. Effects of Bz-423 on $\Delta\psi_m$ hyperpolarization, ROS production and apoptosis in alloreactive donor T cells post-transplant. A and B. B6-Ly5.2 splenocytes (50 x 10^6, CFSE-labeled) were injected into F1 (Allo) or B6 (Syn) mice. On d 4 after transplant, mice were injected i.p. with Bz-423 (60 mg/kg) or vehicle. 2 h after injection, splenocytes were harvested and stained for flow cytometry. Donor ($CD45.1^+$) T cells ($CD4^+$ or $CD8^+$) that had undgergone 1+ division by CFSE were classified as $CFSE^{LO}$. Host ($CD45.2^+$) T cells were gated based on $CD4^+$ or $CD8^+$ expression. For each mouse, a sample without TMRM or DHE was included as a background control and was subtracted from the stained sample. Results were normalized to the MFI of the syngeneic sample. **A**. n=8 mice/group, *p<0.0001, **p<0.02. **B**. n=6 mice/group, * and ** p=0.001. **C**. Annexin-V staining of donor (black bars) and host (white bars) $CD4^+$ and $CD8^+$ cells from allogeneic recipient mice 7 days after donor cell infusion and 6h after a single Bz-423 or control injection (n=12/group); *p<0.001.

Effects of Bz-423 on donor T cell infiltration into recipient liver and bone marrow and host survival during non-irradiated GVHD. In the non-irradiated B6→F1 model of GVHD, alloreactive parental T cells infiltrate into target tissues such as the liver and the bone marrow where they damage host tissues and lead to high rates of mortality ~21 d after transplant (451, 453). Because a single dose of Bz-423 induces apoptosis in alloreactive donor T cells, we hypothesized that a series of Bz-423 doses could improve disease in this model. To test this hypothesis, F1 (Allo, $CD45.2^+$) or B6 (Syn, $CD45.2^+$) mice were transplanted with B6-Ly5.2 splenocytes ($CD45.1^+$, 35×10^6) and treated every other day with vehicle or Bz-423 (60 mg/kg, i.p.) from d 3 to d 13. We chose this dosing schedule because our measurements indicate that donor T cells have increased rates of OXPHOS during this period (Figure 3.16).

As expected, vehicle-treated mice with GVHD (allo) showed an increased percentage of donor T cells infiltrating into the liver (6-30%) and bone marrow (2-6%) compared to syngeneic controls (< 0.5%, $p<0.02$ for each T cell population) 14 d after transplant (Figure 4.8 A). The majority of infiltrating donor T cells were $CD8^+$ (Figure 4.8 A, $p<0.001$ for liver and bone marrow), which is consistent with the proposed role for CD8-mediated CTL activity in this model (453, 500). Treatment with Bz-423 reduced infiltrating donor $CD8^+$ T cells from 16% of bone marrow lymphocytes in vehicle treated mice to 7% ($p=0.01$), and infiltrating donor $CD4^+$ T cells also decreased from 1.8% in vehicle treated mice to 0.3% in Bz-423 treated mice ($p=0.002$, Figure 4.8 A). In addition, Bz-423 decreased donor T cell infiltration into the liver (Figure 4.8 B). $CD8^+$ donor T cells comprised 39% of liver

lymphocytes in vehicle treated mice, compared to 24% of liver lymphocytes in Bz-423 treated mice (p=0.01). Similarly, Bz-423 treatment decreased donor $CD4^+$ T cells levels from 6.4% in vehicle treated mice to 2.1% (p=0.001, Figure 4.8 B).

Donor T cells infiltrating into the BM induce apoptosis of target host hematopoietic cells which leads to lethal BM hypoplasia ~21 d after transplant (461, 500). Vehicle-treated mice with GVHD showed a 45% decrease in host bone marrow cellularity compared to untreated F1 mice 14 d after GVHD induction (Figure 4.8 C, p=0.02). However, mice receiving allogeneic splenocytes and treated with Bz-423 showed only a 9% loss in bone marrow cellularity (Figure 4.8 C, p=0.01 vs. vehicle), which was not statistically different compared to the bone marrow cellularity of untreated F1 mice (p=0.3). Hence, Bz-423 treatment prevented target cell destruction and subsequent loss of cellularity.

Because mortality in this model results from bone marrow aplasia (453, 500), we hypothesized that the ability of Bz-423 to prevent bone marrow loss would result in a survival benefit in mice with GVHD. To test this hypothesis, we performed syngeneic (F1→F1) and allogeneic (B6-Ly5.2→F1) transplants and treated mice with either Bz-423 or vehicle from d3 to d15. As expected, 100% of F1 mice injected with syngeneic F1 splenocytes (Figure 4.8 D, syn, black) survived out to d 50 post-transplant, after which the study was terminated. F1 mice injected with 35 x 10^6 parental B6-Ly5.2 splenocytes (Figure 4.8 D, red) and treated with vehicle showed significant mortality (~67%) by d 30 after transplant. Treatment with Bz-423 eliminated mortality as measured on d 50 in F1 mice injected with 35 x 10^6 B6-Ly5.2 splenocytes (Figure 4.8 D, p=0.02). Bz-423 treatment may also provided a survival benefit when GVHD is induced using an increased dose of donor splenocytes (50 x 10^6, Figure 4.8 D, blue, p=0.15).

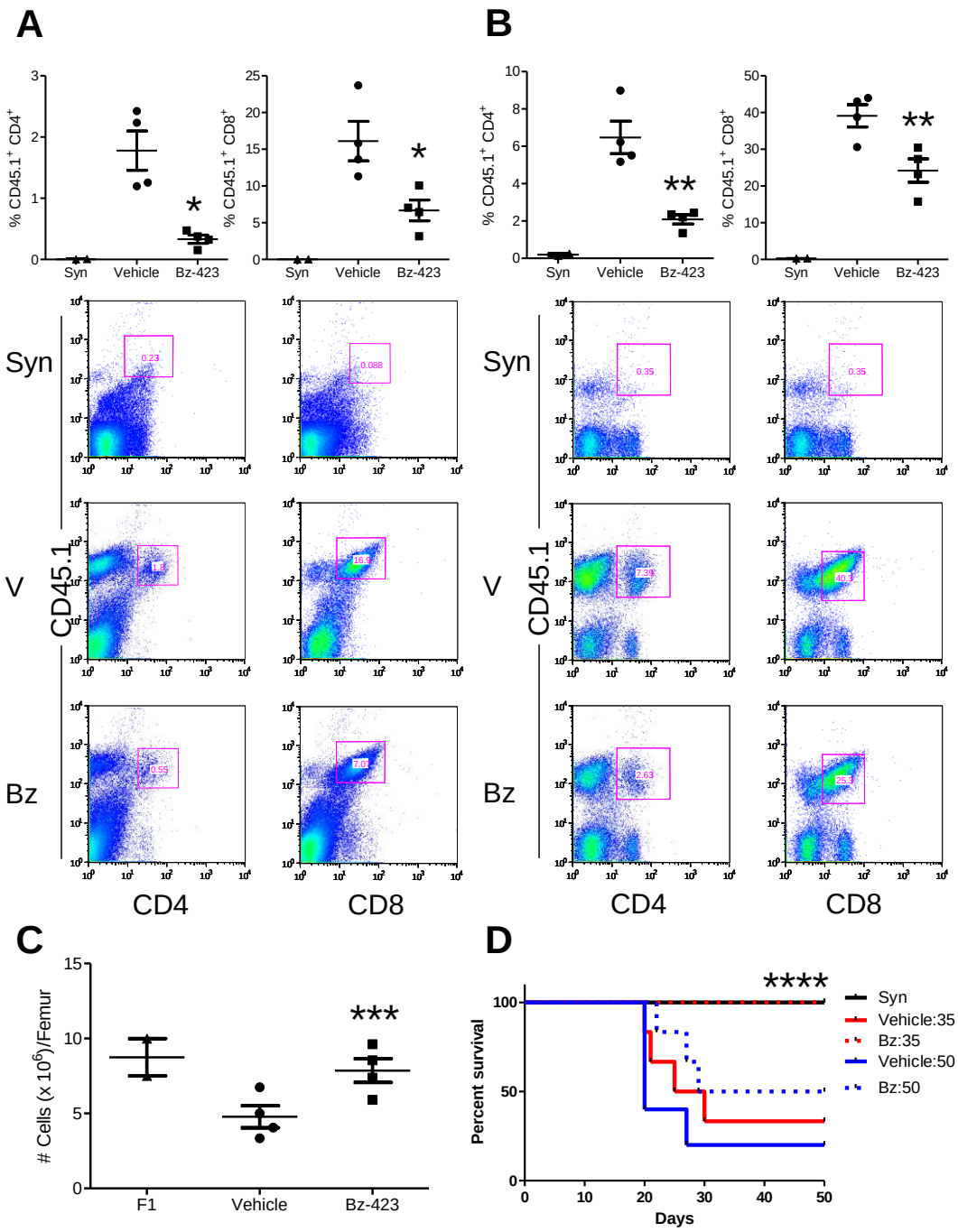
A
B
% CD45.1+ CD4+
% CD45.1+ CD8+
Syn
Vehicle
Bz-423
**
*
Syn
V
Bz
CD45.1
CD4
CD8
C
Cells (x 10^6)/Femur
F1
Vehicle
Bz-423
***
D
Percent survival
Days
****
Syn
Vehicle:35
Bz:35
Vehicle:50
Bz:50

Figure 4.8. Effect of Bz-423 treatment on donor T cell infiltration, tissue damage and mortality in non-irradiated GVHD. A-C. B6-Ly5.2 splenocytes (35 x 10^6) were injected into F1 (Vehicle or Bz-423) or B6 (Syn) mice. Mice were treated 7x from d 3 to d 13 (every other day) with i.p. injections of Bz-423 (60 mg/kg, Bz-423) or vehicle (Vehicle, Syn) and tissues were harvested on d 14 after transplant. **A**. The percentage of bone marrow cells staining positively as donor (CD45.1) T cells (CD8, left or CD4, right) was quantified by flow cytometry as shown for syn (n=2), Vehicle (n=4) and Bz-423 (n=4) mice. * $p \leq 0.01$ Bz-423 vs. Vehicle. **B**. The percentage of infiltrating liver lymphocytes staining positively as donor (CD45.1) T cells (CD8, left or CD4, right) was quantified by flow cytometry as shown for syn (n=2), Vehicle (n=4) and Bz-423 (n=4) mice. ** $p \leq 0.01$ Bz-423 vs. Vehicle. **C**. Number of non-red blood cells per femur was quantified for untreated F1 mice (F1, n=2)) and for Bz-423 (n=4) or vehicle-treated mice with GVHD (n=4). *** p=0.01 Bz-423 vs. vehicle, p=0.6 Bz-423 vs. F1. **D**. F1 mice were injected with 35 (red lines) or 50 x 10^6 (blue lines) B6-Ly5.2 splenocytes and treated with 7 i.p. injections of Bz-423 (60 mg/kg, dotted lines) or vehicle (solid lines) from d 3 to d 15. n=6 mice per group with GVHD, except for Vehicle:50 (n=5). Vehicle-treated F1 mice receiving F1 splenocytes (n=4, syn, black line) served as a control. Survival curves were compared using the Log-rank (Mantel-Cox) Test. **** p=0.02 Bz:35 vs. Vehicle:35.

Effects of Bz-423 on post-transplant bone marrow cells. Unlike alloreactive donor T cells, post-transplant bone marrow cells do not increase OXPHOS or have decreased antioxidants compared to cells from naïve mice (Chapter 3). Additionally, proliferating post-transplant bone marrow consume O_2 2-fold slower than alloreactive donor T cells (0.23 vs. 0.48 nMoles O_2/(min x 10^6 cells), p<0.0001). Because of these differences, we hypothesized that, unlike proliferating alloreactive T cells, post-transplant bone marrow cells would be resistant to Bz-423-induced $\Delta\psi_m$ hyperpolarization, O_2^- production, and apoptosis.

We transfused donor (B6) bone marrow into lethally irradiated syngeneic recipients and treated mice with Bz-423 or vehicle on d 7-8 to assess the ability of Bz-423 to induce $\Delta\psi_m$ hyperpolarization, O_2^- production and apoptosis in proliferating bone marrow cells (Figure 4.9). Bz-423 treatment did not increase TMRM staining in post-transplant bone marrow cells, indicating a lack of $\Delta\psi_m$ hyperpolarization (Figure 4.9 A, p=0.9). Similar results were obtained using a lower concentration of TMRM (10 nM), which is more specific for $\Delta\psi_m$ (Figure 4.9 B) (145, 338). Consistent with this lack of hyperpolarization, Bz-423 treatment did not increase DHE staining in post-transplant bone marrow cells. (Figure 4.9 C, p=0.3 vehicle vs. Bz-423). The lack of Bz-423-induced $\Delta\psi_m$ hyperpolarization and O_2^- production suggested that Bz-423 treatment would not induce apoptosis in post-transplant bone marrow cells. Indeed, similar percentages of donor bone marrow cells in vehicle- and Bz-423-treated mice stained positive for annexin V (Figure 4.9 D, 23% vs. 19%, p=0.2).

These results suggest that Bz-423 may preferentially induce $\Delta\psi_m$ hyperpolarization, O_2^- production and apoptosis in alloreactive donor T cells, and may spare other proliferating cells post-transplant. In addition to the rapid proliferation of granulocytes in the bone marrow (Chapter 3), the *de novo* generation of mature T cells in the thymus is critical for reconstitution of the host immune system (711). After lethal irradiation, host thymocytes undergo apoptosis and the thymus is reconstituted from bone-marrow derived donor cells to regenerate the T cell compartment of the immune system (531, 711, 712).

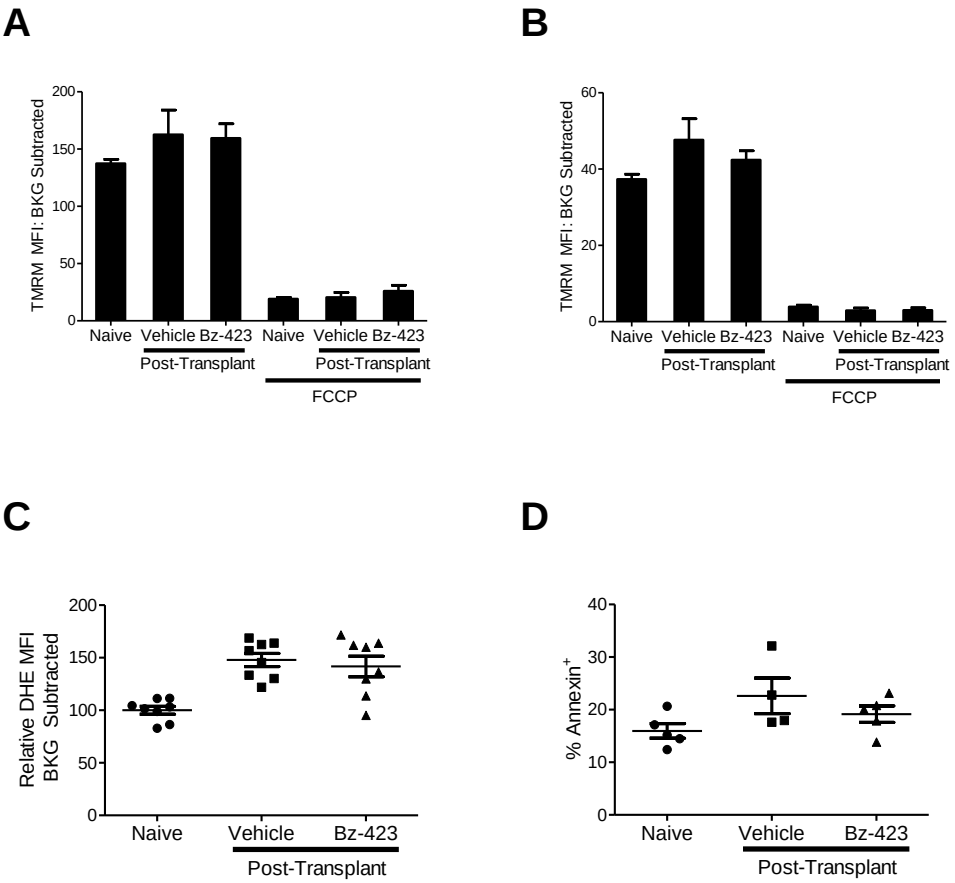

Figure 4.9 Effects of Bz-423 on post-transplant bone marrow cells. Lethally irradiated (1100 cGy) B6-Ly5.2 mice were transplanted with B6 bone marrow cells (5 x 10^6). **A and B**. Naïve B6 mice were injected i.p. with vehicle (n=8) and post-transplant mice were injected with vehicle (n=8) or Bz-423 (60 mg/kg, n=8) 2 h before analysis on d 7-8 after transplant. Bone marrow cells were stained with TMRM (50 nM in A, 10 nM in B) and immediately analyzed. The background fluorescence from unstained samples was subtracted from the TMRM fluorescence for each mouse analyzed. Samples stained with TMRM and treated with FCCP (30 μM) served as a control for disruption of $\Delta\psi_m$. **C.** Naïve B6 mice were injected i.p. with vehicle (n=8) and post-transplant mice were injected with vehicle (n=8) or Bz-423 (60 mg/kg, n=8) 2 h before analysis. Bone marrow cells were stained with DHE (4 μM) and immediately analyzed. The background fluorescence from unstained samples was subtracted from the TMRM fluorescence for each mouse analyzed. Results are combined from two separate experiments. In each experiment, the average naïve DHE MFI was normalized to 100. **D.** Naïve B6 mice were injected i.p. with vehicle (n=5) and post-transplant mice were injected with vehicle (n=4) or Bz-423 (60 mg/kg, n=5) 6 h before analysis. The % annexin V^+ was calculated using an unstained sample for each mouse.

To determine if Bz-423 affected post-transplant thymocytes, we performed syngeneic transplants, treated mice with Bz-423 or vehicle and measured TMRM, DHE and Annexin-V staining in thymocytes. Thymocytes were distinguished into $CD4^+$ or $CD8^+$ single positive, $CD4^+CD8^+$ double positive or $CD4^-CD8^-$ double negative populations (Figures 4.11-4.14). Bz-423 treatment did not cause increased TMRM staining (50 or 10 nM), DHE staining, or Annexin-V staining in $CD8^+CD4^-$ (Figure 4.11), $CD8^-CD4^+$ (Figure 4.12), $CD8^-CD4^-$ (Figure 4.13), or $CD8^+CD4^+$ (Figure 4.14) thymocytes post transplant ($p > 0.05$ for all comparisons, Bz-423 vs. vehicle). These results suggest that, like post-transplant bone marrow cells, post-transplant thymocytes are insensitive to Bz-423.

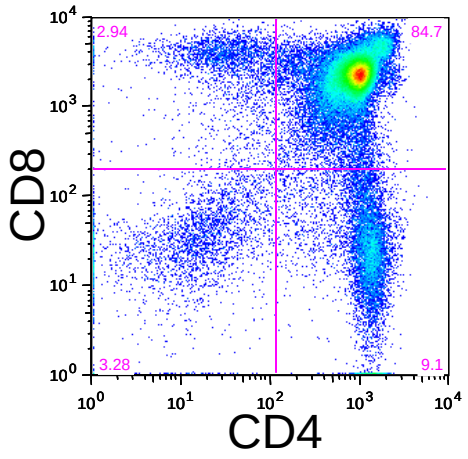

Figure 4.10. Thymocyte gating strategy. Thymocytes were stained with CD4 and CD8 and gated as shown. Cells falling into quadrants were defined as $CD8^+CD4^-$, $CD8^-CD4^+$, $CD8^+CD4^+$, or $CD8^-CD4^-$ and analyzed for TMRM, DHE and Annexin V staining.

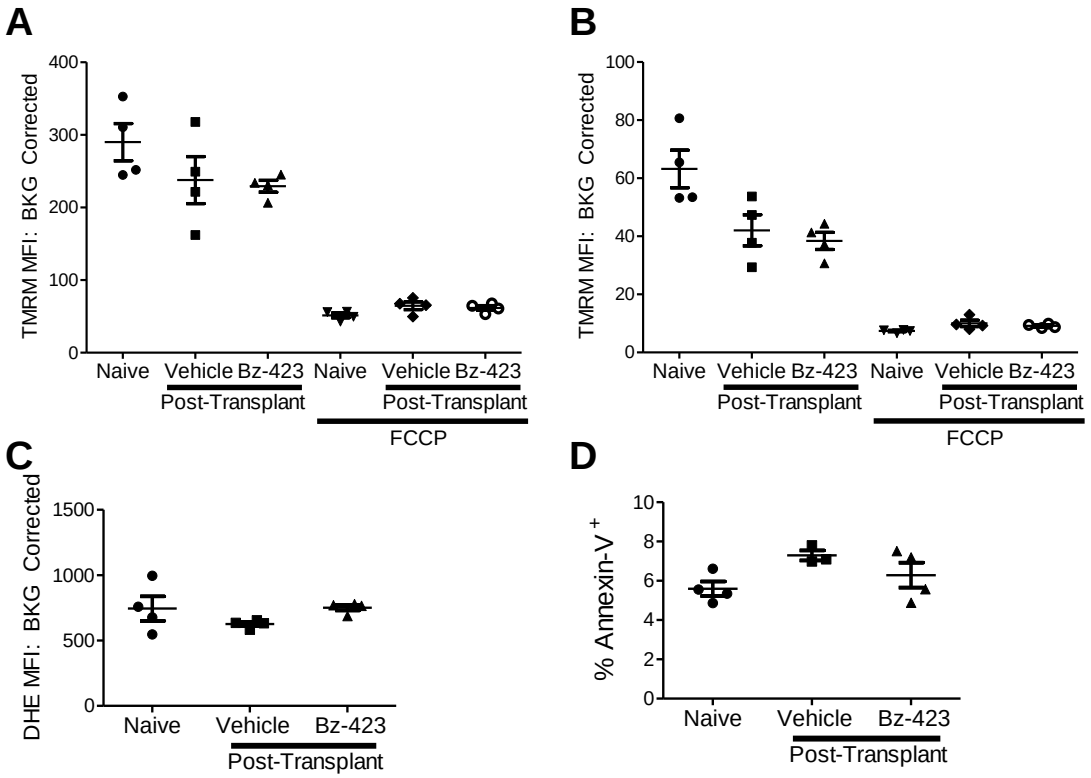

Figure 4.11. Effects of Bz-423 on $\Delta\psi_m$, ROS production, and apoptosis on CD8$^+$ post-transplant thymocytes. Lethally irradiated (1100 cGy) B6-Ly5.2 mice were transplanted with B6 bone marrow cells (5 x 10^6) and thymocytes were analyzed 20-21 d post-transplant. CD8$^+$ CD4$^-$ thymocytes were identified as shown in Figure 4.10. **A-C**. Naïve B6 mice were injected i.p. with vehicle (n=4) and post-transplant mice were injected with vehicle (n=4) or Bz-423 (60 mg/kg, n=4) 2 h before analysis. Thymocytes were stained for surface markers and TMRM (50 nM in A, 10 nM in B) or DHE (4 μM, C) and immediately analyzed. . The background fluorescence from unstained samples was subtracted from the TMRM or DHE fluorescence for each mouse analyzed. Samples stained with TMRM and treated with FCCP (30 μM) served as a control for disruption of $\Delta\psi_m$. **D**. Naïve B6 mice were injected i.p. with vehicle (n=4) and post-transplant mice were injected with vehicle (n=3) or Bz-423 (60 mg/kg, n=4) 6 h before staining for Annexin V. For each mouse, a sample not incubated with PE-Annexin V served as a gating control.

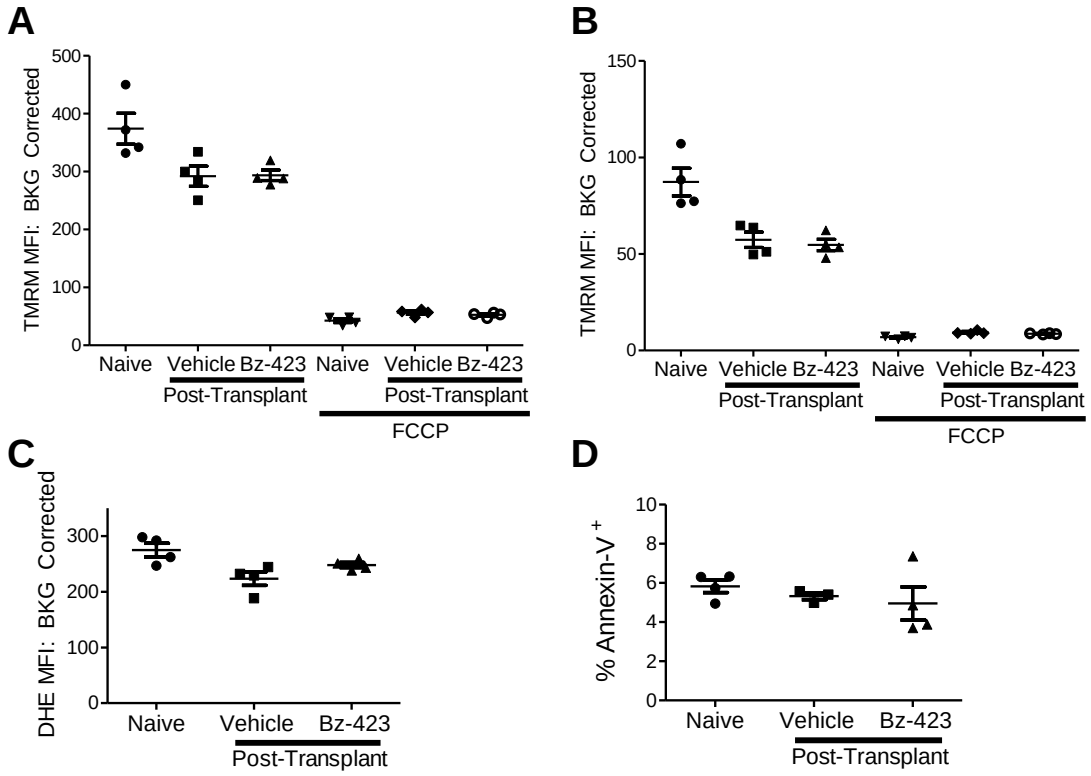

Figure 4.12. Effects of Bz-423 on $\Delta\psi_m$, ROS production, and apoptosis on CD4$^+$ post-transplant thymocytes. Lethally irradiated (1100 cGy) B6-Ly5.2 mice were transplanted with B6 bone marrow cells (5 x 10^6) and thymocytes were analyzed 20-21 d post-transplant. CD4$^+$ CD8$^-$ thymocytes were identified as shown in Figure 4.10. **A-D** are as in Figure 4.11

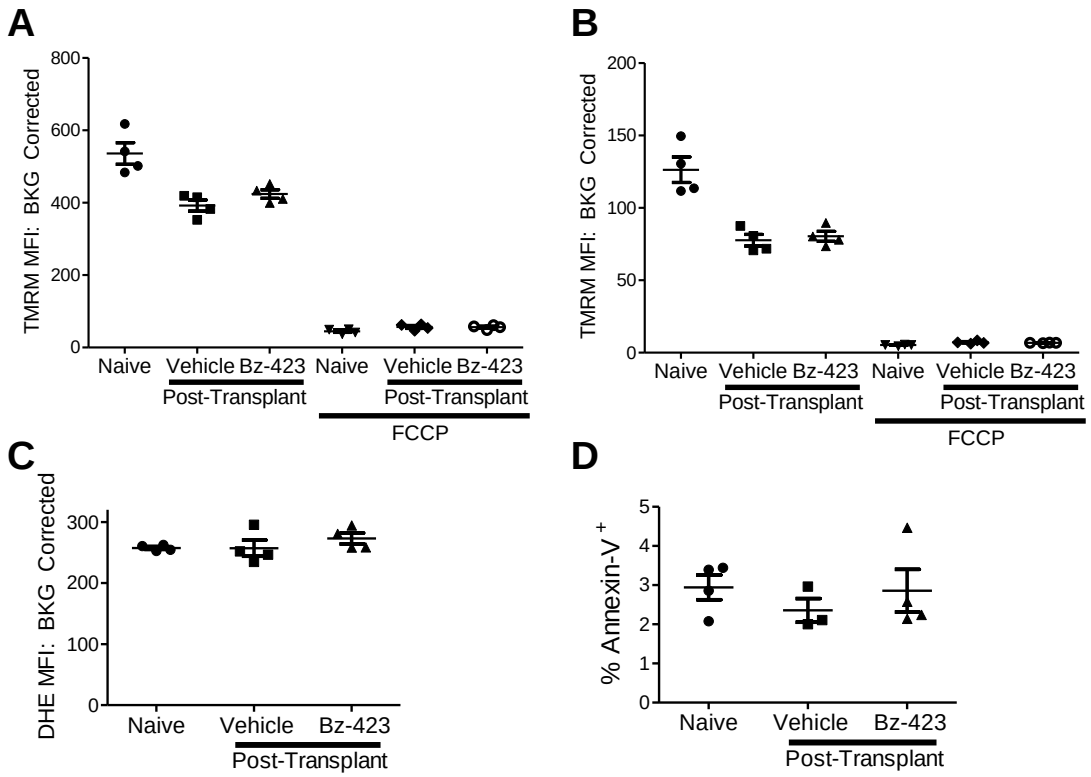

Figure 4.13. Effects of Bz-423 on $\Delta\psi_m$, ROS production, and apoptosis on double negative post-transplant thymocytes. Lethally irradiated (1100 cGy) B6-Ly5.2 mice were transplanted with B6 bone marrow cells (5 x 10^6) and thymocytes were analyzed 20-21 d post-transplant. $CD4^-$ $CD8^-$ thymocytes were identified as shown in Figure 4.10. **A-D** are as in Figure 4.11

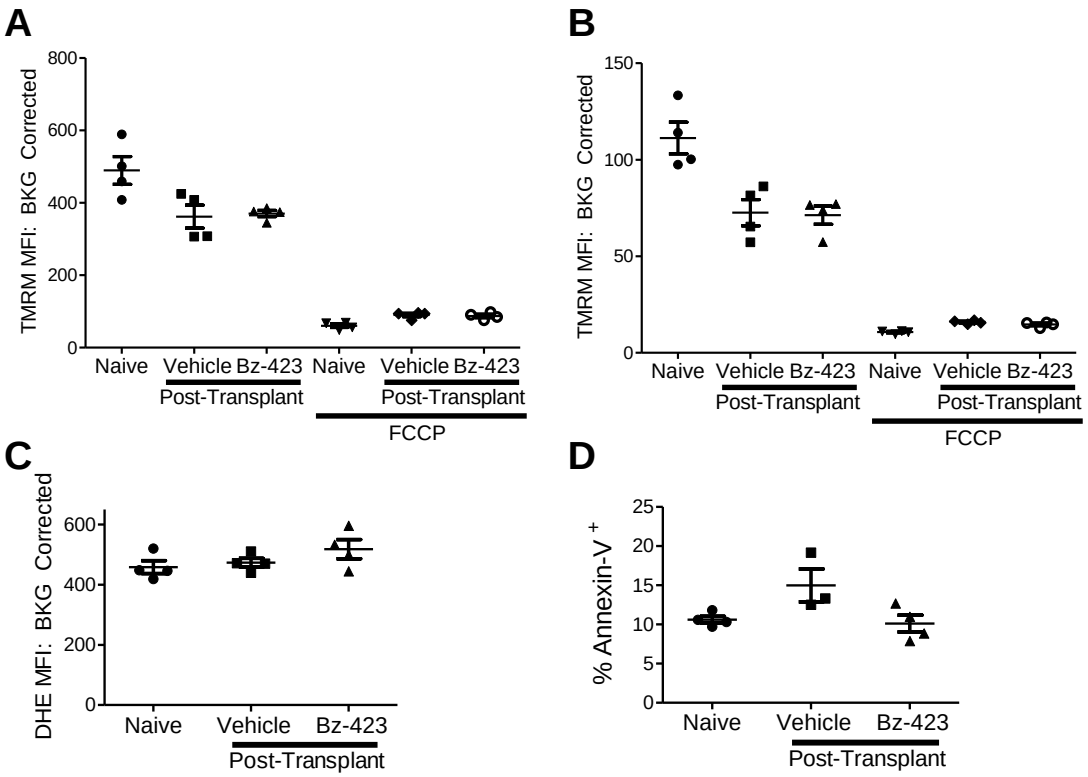

Figure 4.14. Effects of Bz-423 on $\Delta\psi_m$, ROS production, and apoptosis on double positive post-transplant thymocytes. Lethally irradiated (1100 cGy) B6-Ly5.2 mice were transplanted with B6 bone marrow cells (5 x 10^6) and thymocytes were analyzed 20-21 d post-transplant. $CD4^+$ $CD8^+$ thymocytes were identified as shown in Figure 4.10. **A-D** are as in Figure 4.11

The lack of Bz-423-induced apoptosis in post-transplant bone marrow cells or thymocytes suggested that treatment would not inhibit reconstitution of the host immune system following BMT. Such selectivity would distinguish Bz-423 from immunosuppressive agents such as glucocorticoids, which inhibit reconstitution of natural killer cells (255) and dendritic cells (596) following transplant. To examine the effects of Bz-423 on immune-system reconstitution, syngeneic transplants were performed and mice were treated with Bz-423 or vehicle from d 7 to d 21 post-transplant. Analysis of donor reconstitution in the spleen showed no significant differences between Bz-423 and vehicle-treated mice with regards to the number of donor CD4 or CD8 T cells, B cells ($CD19^+$), neutrophils ($CD11b^+Gr\text{-}1^+$), or NK cells ($CD11b^+Ly49d^+$). Bz-423 treatment also did not decrease the numbers of CD4 single positive, CD8 single positive or double positive thymocytes (Table 4.2). These results show that Bz-423 does not deplete cells in any of several lineages of the repopulating immune system (713). Together, these results suggest that Bz-423 selectively induces ROS production and apoptosis in proliferating alloreactive donor T cells but not in unstimulated T cells or proliferating post-transplant bone marrow cells or thymocytes.

Table 4.2. Effect of Bz-423 treatment on hematopoietic reconstitution after transplant. B6-Ly5.2 mice were lethally irradiated (900 cGy), injected i.v. with B6 bone marrow and T cells (5 x 10^6 BM cells, 4 x 10^6 T cells) and treated with Bz-423 (60 mg/kg, i.p.) or vehicle 3 x weekly from d 7 to d 21 post-transplant. Splenocytes and thymocytes were counted and stained for donor and lineage markers and analyzed by flow cytometry. Numbers in the table are means and nubers in parentheses indicate standard error from six individual animals per group. p> 0.05 for each comparison.

	Vehicle	**Bz-423**
Thymocytes		
Total	69.2 (4.7)	66.3 (1.2)
$CD4^+CD8^-$	3.3 (0.6)	2.7 (0.8)
$CD4^-CD8^+$	0.4 (0.1)	0.6 (0.3)
$CD4^+CD8^+$	65.7 (6.3)	62.8 (1.1)
Splenocytes		
Total	89.6 (22.0)	82.9 (19.0)
$CD4^+$	5.0 (1.0)	4.4 (0.6)
$CD8^+$	4.6 (0.8)	3.6 (0.8)
$CD19^+$	38.8 (10.0)	33.8 (10.9)
$CD11b^+Gr\text{-}1^+$	12.2 (3.8)	16.4 (4.6)
$CD11b^+Ly49d^+$	6.2 (1.7)	9.8 (2.9)

Discussion

Cellular bioenergetics and Bz-423 sensitivity. Bz-423 exerts its apoptotic effects by slowing H^+ flow through the F_1F_o-ATPase, thereby leading to $\Delta\psi_m$ hyperpolarization, O_2^- production and apoptosis (169-172). Our results suggest that the sensitivity of a T cell to Bz-423 is related to its respiratory activity. Stimulated T cells respire 2-fold faster than unstimulated T cells, and Bz-423 treatment causes 3-4-fold more TMRM staining in stimulated T cells than in unstimulated T cells. In isolation, these results suggest that T cell activation sensitizes cells to Bz-423-induced $\Delta\psi_m$ hyperpolarization, but they do not specifically implicate respiratory activity. However, culturing stimulated T cells in media with low (0.5 mM) glucose further doubles their respiration rate and increases Bz-423-induced TMRM staining by 20-30% (Figure 4.6). Together, these results show that as a T cell increases its respiratory activity, it becomes more sensitive to Bz-423-induced $\Delta\psi_m$ hyperpolarization.

These results are consistent with studies showing that, as the respiratory activity of isolated mitochondria increases, inhibition of the F_1F_o-ATPase causes increased hyperpolarization of $\Delta\psi_m$ (707). In these experiments, respiration in isolated mitochondria was stimulated by succinate and ADP, and the rate of O_2 consumption was modulated by the addition of malonate, which inhibits succinate metabolism at complex II (714). When respiration rates were highest (i.e., no malonate present), oligomycin caused the greatest increase in $\Delta\psi_m$ (707). Similarly, when respiration was inhibited by 80% through the addition of malonate, oligomycin had no effect on $\Delta\psi_m$ (Figure 4.15). This study suggests

that inhibiting the flow of a system with a large amount of flux (i.e., high levels of H^+ flow through the ATPase) will cause a greater back-up (i.e., increased $\Delta\psi_m$) than will the same amount of inhibition in a system with low flux (Figure 4.15).

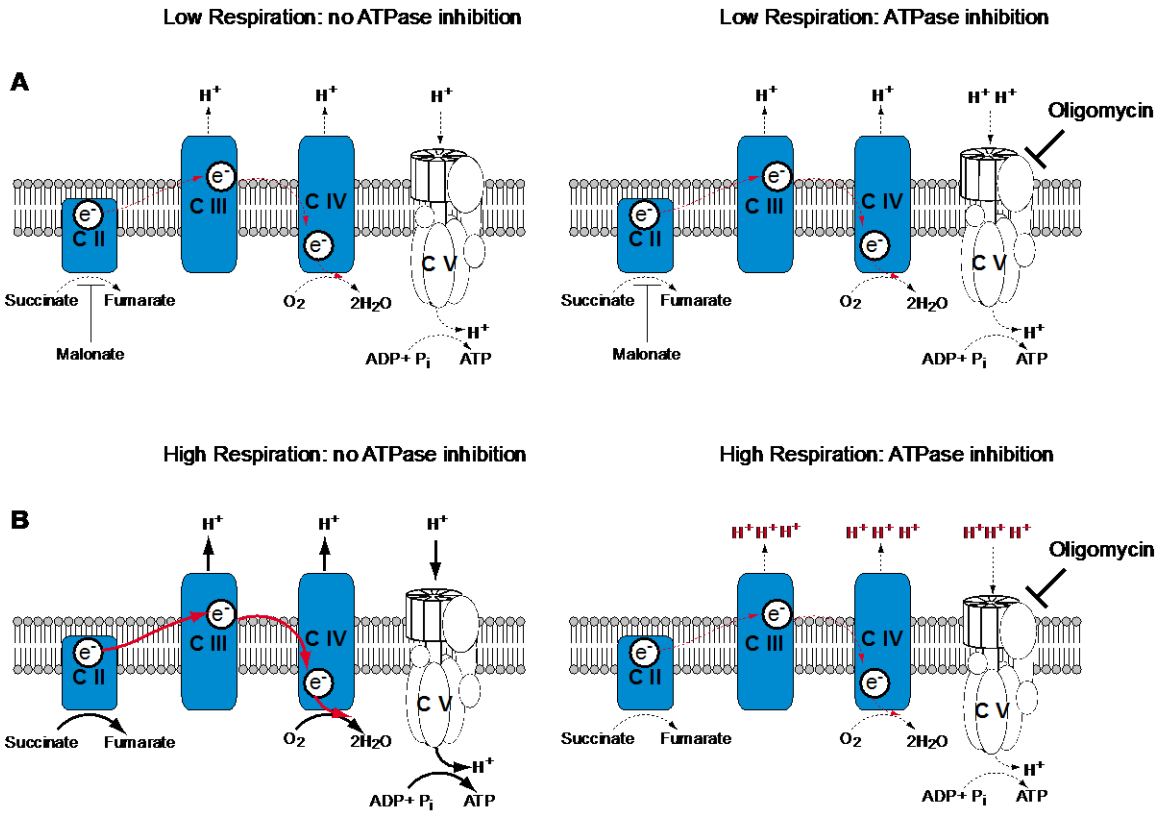

Figure 4.15. Effects of ATPase inhibition on $\Delta\psi_m$ at high and low respiratory activity. A. When malonate is present, mitochondria respire at 20% of their maximal rate and the rate of H^+ flow through the ATPase is low (left). When oligomycin is added to the system (right), H^+ does not accumulate in the intermembrane space, and $\Delta\psi_m$ does not hyperpolarize. **B.** When malonate is absent, mitochondria respire at their maximal rate, and the rate of H^+ flow through the ATPase is high (left). When oligomycin is added to the system (right), H^+ accumates in the intermembrane space (in red) and $\Delta\psi_m$ hyperpolarizes (707).

In isolated mitochondria, ROS production increases as $\Delta\psi_m$ increases (167, 168). In the experiments demonstrating this phenomenon, respiratory substrate (either succinate, malate and glutamate, or α-ketoglutarate) is added to isolated mitochondria in buffer containing only inorganic phosphate (P_i). The presence of respiratory substrate causes the electron transport chain (ETC) to pump H^+ into the intermembrane space (715). However, the lack of ADP limits H^+ flow through the F_1F_o-ATPase and causes H^+ accumulation in the intermembrane space, leading to $\Delta\psi_m$ values of 180 mV in rat brain mitochondria, which is 30 mV greater than the $\Delta\psi_m$ of normally respiring mitochondria (168, 715). H_2O_2 production was measured by monitoring the fluorescence of a horseradish peroxidase substrate (167, 168, 716), and was maximal at this high $\Delta\psi_m$. Three techniques were then used to lower $\Delta\psi_m$: ADP was added to the system to allow H^+ to flow through the F_1F_o-ATPase, chemical uncouplers such as carbonylcyanide-p-trifluoromethoxyphenylhydrazone (FCCP) were added to allow non-specific H^+ leak through the mitochondrial membrane, or malonate was added to decrease succinate-stimulated H^+ pumping into the intermembrane space. Each of these manipulations lowered $\Delta\psi_m$ and subsequently lowered H_2O_2 production by the mitochondria (167, 168). Small changes in $\Delta\psi_m$ caused large changes in ROS production. For example, decreasing $\Delta\psi_m$ from 180 to 150 mV decreased H_2O_2 production 4-fold in rat brain mitochondria (168).

Increasing $\Delta\psi_m$ by inhibiting the F_1F_o-ATPase also increases ROS production both in isolated mitochondria and in intact cells. The addition of oligomycin to isolated mitochondria respiring on succinate increases O_2^-

production 4-fold as measured by EPR spectroscopy (174). Similarly, treating actively respiring mitochondria with other inhibitors of the F_1F_o-ATPase, such as diindoylmethane (DIM) and Bz-423, leads to increased ROS production as measured by the fluorescent dyes DCF and DHE (169, 717). These effects also occur in intact cells. Bz-423 induces $\Delta\psi_m$ hyperpolarization and O_2^- production in Ramos B cells (169, 170), while DIM induces $\Delta\psi_m$ hyperpolarization and H_2O_2 production in MCF-7 mammary carcinoma cells (717).

Together, these studies demonstrate the relationship between $\Delta\psi_m$ and mitochondrial ROS production. Consistent with this relationship, the ability of Bz-423 to produce O_2^- coincided with its ability to hyperpolarize $\Delta\psi_m$. Unstimulated T cells treated with Bz-423 *in vitro* produce nearly undetectable levels of O_2^-, consistent with the lack of Bz-423-induced $\Delta\psi_m$ hyperpolarization (Figure 4.6) in these cells. Bz-423 produces 2-4-fold more DHE staining in control stimulated T cells than in unstimulated cells, which is consistent with the increased $\Delta\psi_m$ hyperpolarization seen in these cells (Figure 4.6). Bz-423 produced the most DHE fluorescence (10-15-fold over unstimulated) in stimulated T cells cultured in low glucose media (Figure 4.6). As expected, these changes mirror Bz-423's effects on $\Delta\psi_m$. The relationship between Bz-423-induced $\Delta\psi_m$ hyperpolarization and O_2^- production could be confirmed by incubating cells with an uncoupler such as FCCP, which collapses $\Delta\psi_m$ at low micromolar concentrations (519, 718). If the ability of Bz-423 to form O_2^- depends on its ability to increase $\Delta\psi_m$, uncouplers such as FCCP should significantly reduce the amount of DHE oxidized by Bz-423 treatment (176).

Adding Bz-423 to activated T cells cultured in low rather than high glucose leads to a greater increase in DHE fluorescence (3-4-fold) than in TMRM fluorescence (20-30%). This disproportionate change may occur because small changes in $\Delta\psi_m$ can cause large changes in ROS production (167, 168). For example, a 20% increase in $\Delta\psi_m$ increases H_2O_2 production by 10-fold in isolated mitochondria (167). Another factor that may contribute to increased Bz-423-induced O_2^- in activated T cells cultured in low rather than high glucose is the relative intracellular antioxidant levels under these two conditions. As discussed in Chapter 3, glucose metabolism is a crucial aspect of both pyruvate and glutathione generation (252, 343, 535). Indeed, astrocytes cultured in media lacking glucose lose 75% of their reduced glutathione within 12 h, while astrocytes cultured in media with 5.5 mM glucose lose only 10-20% (343). Similarly, decreasing the glucose concentration of cell culture media from 12 mM to 2.5 mM reduces the intracellular pyruvate levels of a pancreatic β-cell line by 12-fold (535). Together, these results suggest that glutathione and pyruvate may be depleted in activated T cells cultured in media with low glucose.

Differences in endogenous antioxidant levels can alter the amount of ROS observed following treatment with pro-oxidants (489). For example, depleting endogenous glutathione levels in U937 lymphoma cells with BSO causes a 10-fold increase in H_2O_2 production following treatment with arsenic trioxide, a pro-oxidant used clinically to treat acute promyelocytic leukemia (APL) (489, 607). This observation suggests that the increased Bz-423-induced O_2^- in activated T

cells cultured in low glucose could partially be due to depleted antioxidants in these cells, in addition to Bz-423's greater ability to hyperpolarize $\Delta\psi_m$.

The importance of endogenous antioxidants in determining sensitivity to pro-oxidant drugs is well documented. The ability of arsenic trioxide to induce apoptosis in leukemia cell lines *in vitro* is inversely related to intracellular glutathione content (488). Increasing glutathione levels ~2-fold by pretreating cells with NAC decreases arsenic trioxide-induced apoptosis by 4-fold. Similarly, depleting glutathione levels with BSO increases arsenic trioxide-induced apoptosis up to 10-fold (488, 489, 719, 720). N-(4-hydroxyphenyl) retinamide (4-HPR) is a synthetic retinoid that induces apoptosis in leukemia cells by producing ROS (721). In a manner similar to arsenic trioxide, endogenous intracellular glutathione content is inversely related to sensitivity to 4-HPR-mediated apoptosis across numerous cell lines (722). Furthermore, depleting intracellular glutathione levels with BSO increases 4-HPR apoptosis approximately 2-fold in MOLT-4 leukemia cells (721). ROS production also plays a role in cell death induced by paclitaxel, a common chemotherapeutic agent (723). In a screen of 16 different cell lines, the total antioxidant capacity of a cell line correlated with its sensitivity to growth inhibition by paclitaxel (606). The importance of endogenous antioxidants for paclitaxel sensitivity was confirmed by experiments showing that increasing antioxidant levels with NAC or glutathione treatment reduced the sensitivity of lung cancer cells to paclitaxel 4-fold, while depleting endogenous glutathione levels with BSO sensitized these cells to paclitaxel-induced apoptosis (723).

Several studies provide direct and indirect evidence regarding the importance of endogenous antioxidants in determining sensitivity to Bz-423. MEFs have 2-fold more cytosolic and mitochondrial glutathione than Ramos B cells and require nearly 2-fold greater [Bz-423] for the induction of apoptosis (172, 683). Decreasing MEF glutathione levels by 99% using BSO increases the sensitivity of these cells to Bz-423-induced apoptosis by approximately 3-fold (172). Indirect evidence for the effect of endogenous antioxidants on sensitivity to Bz-423 comes from the analysis of non-lymphoid tissue. The molecular target of Bz-423, the OSCP, is a mitochondrial protein expressed in all nucleated cells (170). If cellular sensitivity to Bz-423 were solely determined by respiratory activity, tissues engaging in high rates of oxidative phosphorylation, such as the heart and liver (724), might be susceptible to the pro-apoptotic effects of Bz-423. However, neither hepatic nor cardiac toxicity has ever been observed following *in vivo* administration of Bz-423 (169, 395). This lack of toxicity could be due to increased endogenous antioxidants in hepatic and cardiac tissue as compared to lymphatic tissue. One important set of antioxidant enzymes are the SODs, which catalyze the conversion of O_2^- into H_2O_2 (177). The activities of Cu/Zn-SOD and Mn-SOD are 10-15-fold greater in mouse liver and heart as compared to mouse spleen (725). Because the SOD-mimetic MnTBAP decreases Bz-423-induced apoptosis in B cells, T cells and fibroblasts, it is likely that cardiac and hepatic tissue will be relatively resistant to Bz-423-induced apoptosis as compared to lymphocytes (169, 172, 173, 683). Similarly, the activity of glutathione peroxidase, which catalyzes the GSH-dependent conversion of H_2O_2 to H_2O

(196), is 10-15-times higher in heart and liver tissue than in spleen (725). Because glutathione levels are important in determining cellular sensitivity to Bz-423 (172), increased glutathione peroxidase could provide protection against Bz-423-mediated apoptosis in heart and liver tissue.

Together, these observations suggest a 2-part bioenergetic model that defines cellular sensitivity to Bz-423 (Figure 4.16). The first element of this model is cellular respiratory activity. If cells respire at a low rate (i.e., unstimulated T cells), Bz-423 will not hyperpolarize $\Delta\psi_m$, will not form O_2^- and will not induce apoptosis. However, if cells respire at a high rate (i.e., stimulated T cells), Bz-423 will hyperpolarize $\Delta\psi_m$ and will, to some extent, generate O_2^-. The second factor of the model is cellular antioxidant status. If cells with high rates of respiration have high levels of antioxidants (i.e., heart and liver tissue, MEFs, activated T cells in high glucose, cells treated with MnTBAP), Bz-423-mediated O_2^- will be detoxified and cells will be relatively resistant to apoptosis. However, if cells with high rates of respiration also have low levels of antioxidants (i.e. BSO-treated MEFs, Ramos B cells, T cells stimulated in low-glucose media), Bz-423-mediated O_2^- production will be increased and cells will undergo apoptosis.

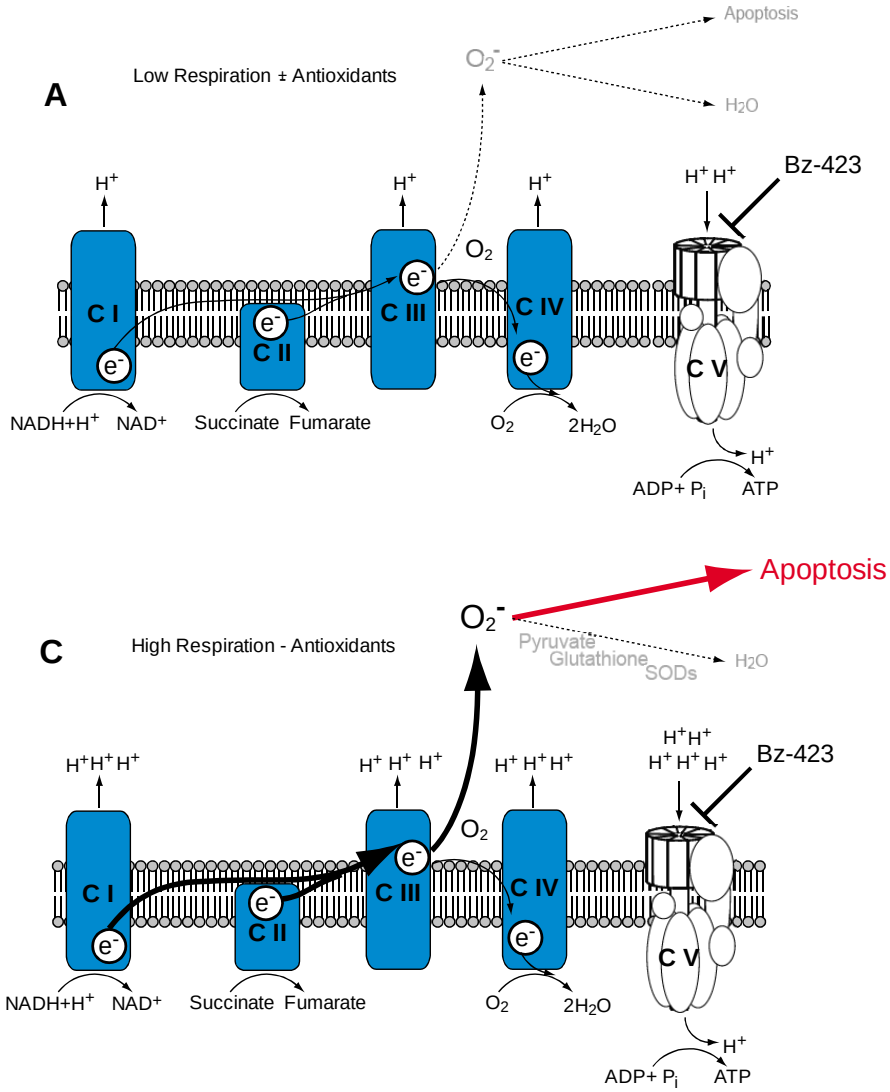

Figure 4.16. Bioenergetic model for Bz-423 sensitivity. **A.** In cells with low respiratory activity, Bz-423 does not hyperpolarize $\Delta\psi_m$ and does not produce significant O_2^-. Because O_2^- production is low, antioxidants are not needed to prevent apoptosis. **B and C.** In cells with high respiratory activity, Bz-423 hyperpolarizes $\Delta\psi_m$ and produces O_2^-. If antioxidants are present in high amounts (**B**), O_2^- is detoxified to water and apoptosis is prevented. If antioxidants are depleted (**C**), cells undergo apoptosis.

Selective killing of pathogenic T cells by Bz-423. The model described above has important implications that help explain Bz-423's effects in the B6→F1 model of GVHD. Alloreactive donor T cells consume oxygen 2.5-fold faster than unstimulated T cells (Figure 3.16). This observation suggests that alloreactive donor T cells will be more sensitive to $\Delta\psi_m$ hyperpolarization mediated by inhibition of the F_1F_o-ATPase than will unstimulated cells. Indeed, a single i.p. injection of Bz-423 causes a 50% increase in TMRM staining in divided alloreactive donor T cells (Figure 4.7), but does not alter TMRM staining in unactivated cells. These results support our *in vitro* studies that demonstrate the relationship between T cell respiration rate and Bz-423-induced $\Delta\psi_m$ hyperpolarization.

Bz-423 also selectively produces O_2^- in alloreactive donor T cells, but not in unactivated cells. While this increased O_2^- production in pathogenic T cells is likely due to the ability of Bz-423 to induce $\Delta\psi_m$ hyperpolarization in these cells (167, 168), it may be accentuated by pyruvate and glutathione depletion (Chapter 3, (488)). Finally, Bz-423 selectively induced apoptosis in alloreactive donor T cells, which is consistent with the previously established link between Bz-423-induced O_2^- production and apoptosis (169, 170, 172, 173, 683). This increased apoptosis was associated with decreased donor T cell infiltration into the liver and bone marrow, decreased bone marrow loss, and improved survival in the nonirradiated model of GVHD (Figure 4.8). These beneficial effects are consistent with a mechanism in which Bz-423 hyperpolarizes $\Delta\psi_m$, produces O_2^-

and induces apoptosis in alloreactive donor T cells, thereby preventing them from migrating into target tissues and mediating lethal GVHD.

Several alternative explanations exist that could also explain the efficacy of Bz-423 in the treatment of GVHD. Bz-423 could induce apoptosis and disease improvement through an ROS-independent mechanism. While the inhibition of Bz-423-mediated apoptosis by antioxidants such as MnTBAP and vitamin E makes the link between O_2^- and apoptosis clear *in vitro* (169, 172, 173, 683), this hypothesis has not yet been tested *in vivo*. Concurrently treating mice with antioxidants such as NAC (478) or ethyl pyruvate (493, 495, 496) and Bz-423 could reverse Bz-423's ability to induce apoptosis in alloreactive donor T cells and its subsequent ability to improve GVHD.

The beneficial effects of Bz-423 on GVHD could also be explained by inhibition of T cell trafficking to target tissues, independent of its ability to induce apoptosis. Such a situation is seen in the nonirradiated B6→F1 model when donor T cells lack the chemokine receptor CXCR6 (464). In this model, WT alloreactive donor T cells increase their expression of CXCR6 3-4 fold 7 d after infusion into allogeneic recipients(464). However, donor T cells lacking CXCR6 show a 2-fold reduction in liver infiltration compared to WT T cells, despite an identical rates of proliferation and apoptosis (464). Similarly, FTY720, a sphingosine-1-phosphate agonist, improves GVHD by directly inhibiting T cell migration into target tissues (726, 727). While Bz-423 has not been shown to affect T cell migration, it does have anti-proliferative effects which are independent of apoptosis (695, 699, 700). To exclude Bz-423 effects that are

independent of apoptosis, donor T cells should be used that are resistant to Bz-423-mediated apoptosis. T cells lacking Bax and Bak would be an obvious choice, however these cells do not proliferate in response to antigen (254) and would be unlikely to mediate GVHD. Because Jurkat T cells lacking Bak alone are resistant to Bz-423-mediated apoptosis (173), Bak-deficient T cells would be of potential use (254). Alternatively, Bz-423-mediated apoptosis could be blocked with a caspase inhibitor such as quinolyl-valyl-O-methylaspartyl-[-2, 6-difluorophenoxy]-methyl ketone (QVD-OPh) (728). Regardless of the strategy used, if Bz-423-mediated apoptosis is important for its ability to treat GVHD, these beneficial effects should be abrogated if donor T cells are insensitive to Bz-423-mediated apoptosis.

This bioenergetic model suggests that Bz-423 may have efficacy in other diseases where pathogenic cells have increased oxidative metabolism and depleted antioxidants. Several lines of evidence suggest that autoreactive lymphocytes from patients with SLE or mouse models of lupus exhibit increased oxidative metabolism and depleted antioxidants. T cells from patients with SLE have 2-3-fold more mitochondria and show a 50% increase in mitotracker green staining compared to cells from healthy volunteers (302). This finding shows that autoreactive lymphocytes have increased mitochondrial mass and suggests that they may have increased mitochondrial metabolism (302). Similarly, PBMCs from patients with active rheumatic diseases (including lupus, rheumatoid arthritis, arteritis and others) consume 25% more O_2 than cells from healthy controls (335). Furthermore, splenocytes from NZB/W mice with active lupus

convert 40% more glucose into CO_2 than do healthy Balb/c controls, which is suggestive of increased oxidative ATP production (Chapter 2). While these studies do not distinguish between autoreactive and non-autoreactive lymphocytes, these results are consistent with the interpretation that lymphocytes from patients or animals with autoimmune diseases have increased oxidative metabolism compared to healthy controls, possibly due to increased respiration in autoreactive lymphocytes.

Antioxidant levels are also abnormal in lymphocytes from autoimmune patients and animals. PBMCs from patients with lupus have 30% less glutathione than cells from healthy controls based on direct HPLC measurements from cellular lysates (339). Similarly, splenocytes from MRL-*lpr* mice with active lupus-like disease have 4-5-fold decreased glutathione levels compared to control mice as measured by fluorescence of the thiol-reactive probe CMFDA (380).

Together, increased oxidative metabolism and depleted antioxidants in autoreactive lymphocytes suggests that they will be sensitive to Bz-423-mediated apoptosis (Figure 4.17). Consistent with this hypothesis, a single dose of Bz-423 increased apoptosis in germinal centers in NZB/W mice with active lupus as measured by terminal deoxynucleotidyl transferase nick end labeling (TUNEL) staining (169). Additionally, a 12 week treatment with Bz-423 reduces germinal center hyperplasia and glomerulonephritis in NZB/W mice and decreases the percentage of disease-causing splenic B cells by 18% (169). Similarly, Bz-423 treatment reduces by 13% the percentage of pathologic splenic $CD4^+$ cells in

MRL-*lpr* mice and significantly reduces proteinuria, nephritis and arthritis (395). These results suggest that, as in the B6→F1 model of GVHD, treatment with Bz-423 can reduce disease in models of lupus, likely by inducing apoptosis in pathogenic lymphocytes with high rates of OXPHOS and low levels of antioxidants.

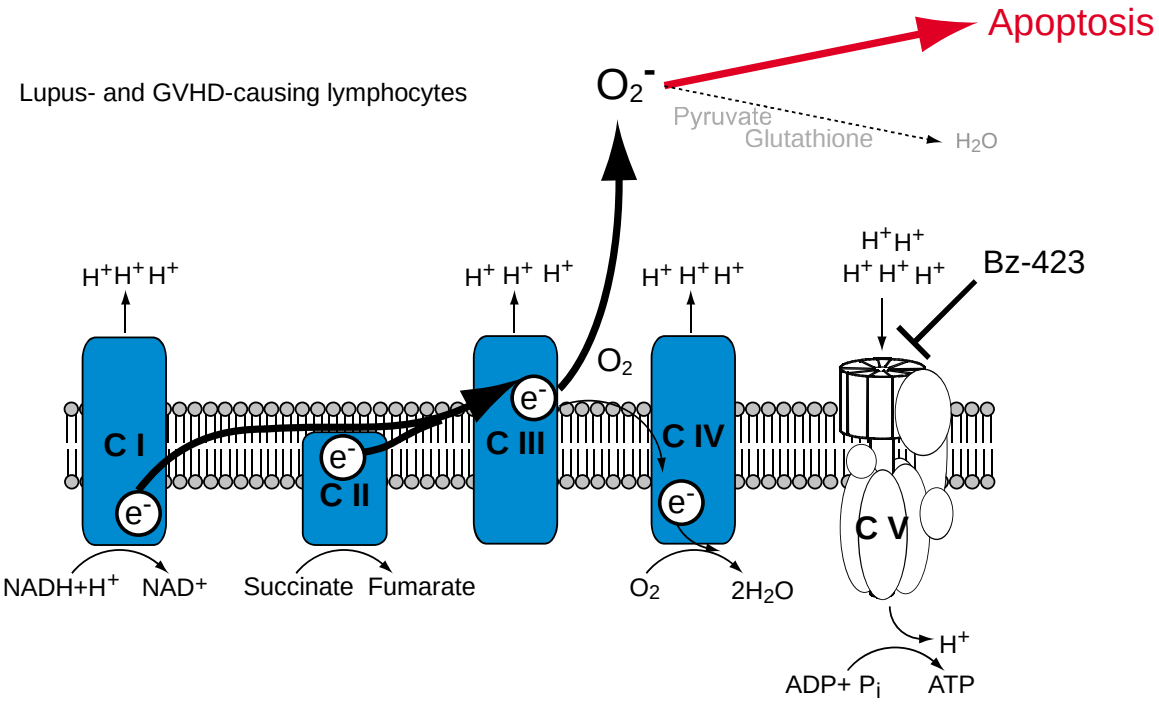

Figure 4.17. Bz-423-induced apoptosis in disease causing lymphocytes. Disease-causing lymphocytes have increased OXPHOS, thus inhibition of the F_1F_o ATPase will likely induce $\Delta\psi_m$ hyperpolarization and O_2^- production in these cells. Because these cells also have depleted levels of pyruvate and glutathione, any O_2^- formed is likely to induce apoptosis.

In both the NZB/W and MRL-*lpr* models of lupus, Bz-423 selectively depletes disease-causing lymphocytes (B cells in NZB/W, $CD4^+$ T cells in MRL-*lpr)* without broad depletion of other lymphoid subsets (169, 395). Similarly, Bz-423 induces apoptosis in dividing donor T cells during GVHD, but spares unactivated T cells and proliferating bone marrow cells. These results suggest

that the metabolic characteristics of unstimulated lymphocytes and proliferating cells in the bone marrow (i.e., low OXPHOS, intact antioxidants), may protect these cells from Bz-423-mediated apoptosis (Figure 4.18). This selectivity distinguishes Bz-423 from most current GVHD treatments, which broadly deplete T cells regardless of their activation status (441, 598, 625). ATG (670), OKT3 (669), and visilizumab (668) deplete T cells nonspecifically, while glucocorticoids (594, 654-656) and alemtuzumab (666, 667) are broadly leukotoxic. For example, a single dose of methylprednisone (25 mg/kg) reduces peripheral blood lymphocyte counts in healthy guinea pigs by 50% after 4 h (656). This lack of specificity is associated with high rates of infectious complications during treatment with such agents (417, 598, 662, 664, 666, 667). Unlike these agents, Bz-423 induces apoptosis only in alloreactive donor T cells. Similarly, healthy Balb/c mice treated for 7 d with Bz-423 maintain B and T cell numbers, which further supports the specificity of Bz-423 for activated, disease causing lymphocytes. This selectivity may account for the absence of any association between opportunistic infection and Bz-423 treatment (169, 395).

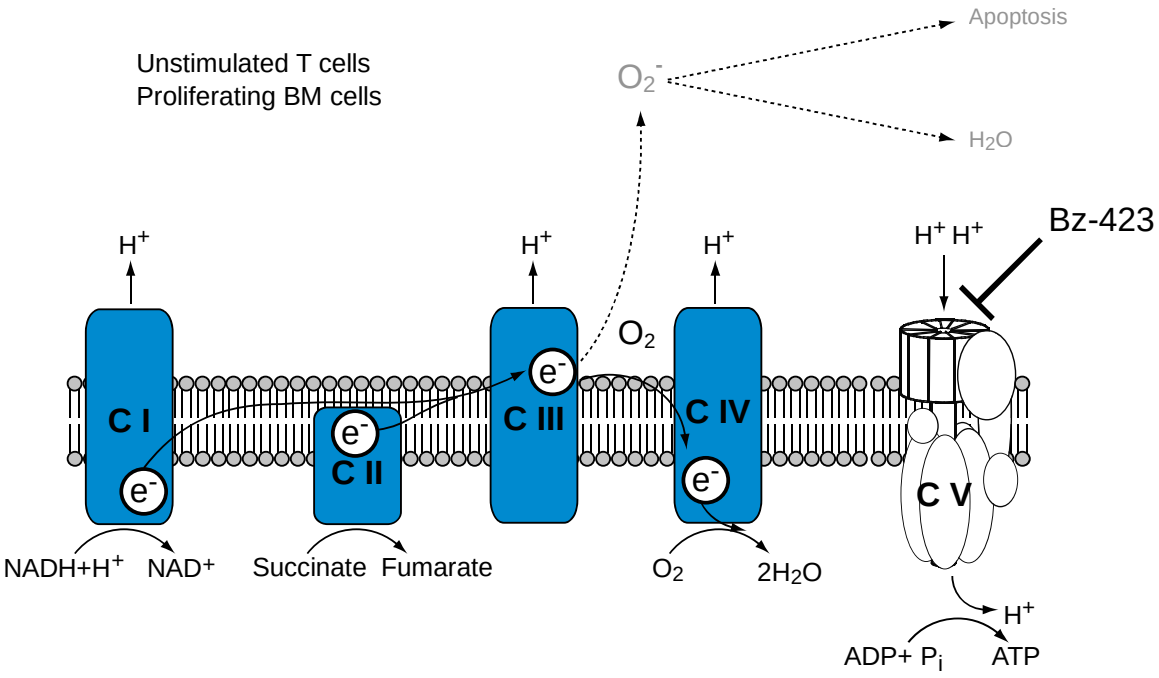

Figure 4.18. Lack of Bz-423-mediated apoptosis in unstimulated lymphocytes and proliferating bone marrow cells. Unstimulated lymphocytes respire at a low rate (dotted lines), thus inhibition of the F_1F_o ATPase does not induce large $\Delta\psi_m$ hyperpolarization or O_2^- in these cells. Because these cells have intact levels of antioxidants, any O_2^- formed is likely detoxified before inducing apoptosis.

Interestingly, continuous treatment with Bz-423 does not inhibit cell mediated inflammation in response to a delayed type hypersensitivity (DTH) test or antibody production following immunization with keyhole limpet hemocyanin (KLH) (395). The metabolic parameters of the lymphocytes mediating these KLH and DTH responses are unknown. However, our studies suggest that both acutely activated T cells (i.e., T cells stimulated for 48 h with anti-CD3/28 antibodies) and disease causing T cells (i.e., donor T cells from mice with GVHD) increase OXPHOS compared to unstimulated cells (Chapter 3). Furthermore,

CD8 T cells responding to LCMV infection *in vivo* increase TMRM staining 5-fold compared to unstimulated cells, which suggests increased OXPHOS in these cells (471). If the lymphocytes mediating KLH and DTH responses have similarly increased rates of OXPHOS, they would be expected to undergo $\Delta\psi_m$ hyperpolarization in response to Bz-423, and to some extent, produce O_2^- (Figure 4.16). However, if these lymphocytes maintain their antioxidant capacity, they may be relatively resistant to O_2^- generated by Bz-423 (Figure 4.19) (172, 173, 683). Acutely activated T cells *in vitro* have rates of glycolysis 7-fold greater than those seen in alloreactive donor T cells. As discussed in Chapter 3, high rates of glycolysis can help maintain both cellular glutathione and pyruvate levels (50, 343, 376, 491, 535). Hence, it is possible that acutely activated lymphocytes mediating KLH and DTH responses maintain their levels of antioxidants, and are therefore resistant to the proapoptotic effects of Bz-423. In support of this hypothesis, human PBMCs activated with conA *in vitro* increase glutathione levels by as much as 2-fold over 2-4 d (344). Further investigations that directly measure the cellular metabolism and antioxidant status of activated T cells in DTH and KLH responses are needed to fully understand their insensitivity to inhibition by Bz-423.

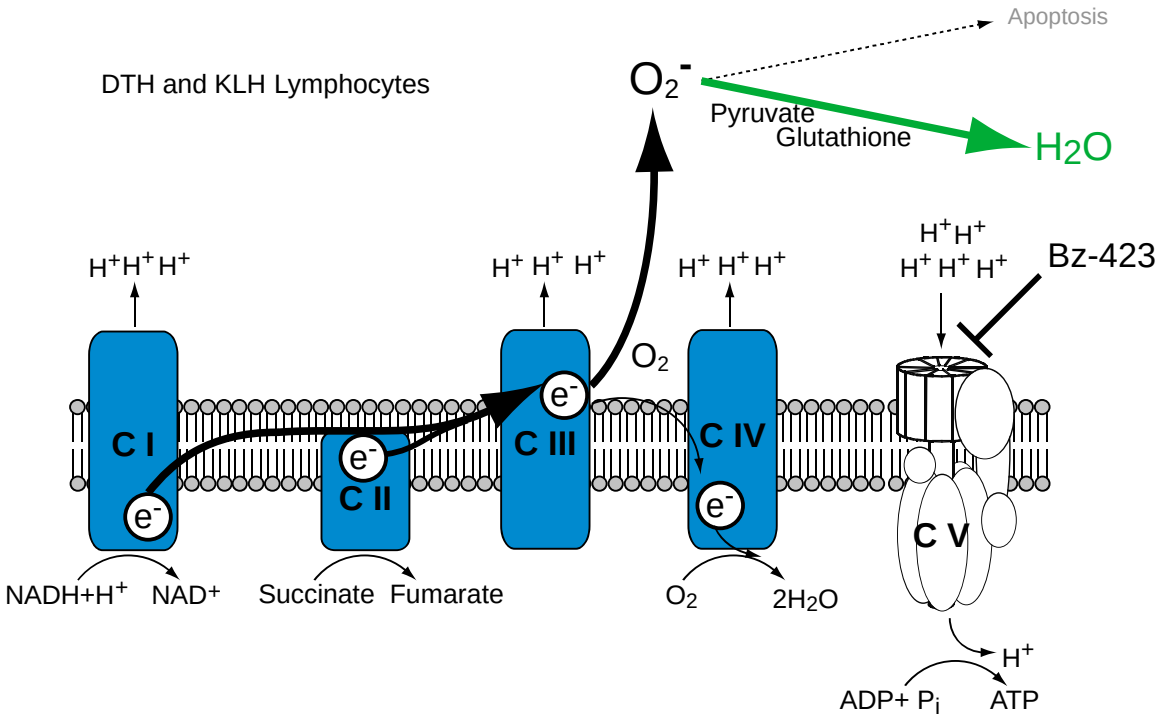

Figure 4.19. Potential model explaining lack of Bz-423 effect on DTH and KLH responses. Activated lymphocytes may have increased OXPHOS, thus inhibition of the F_1F_o ATPase will likely induce $\Delta\psi_m$ hyperpolarization and O_2^- production in these cells. However, because these cells may have intact levels of pyruvate and glutathione, any O_2^- formed is likely detoxified before inducing apoptosis.

Comparison of Bz-423 to standard GVHD therapies. Following myeloablative conditioning, the host immune system disappears and donor stem cells and progenitor cells proliferate in the bone marrow to repopulate the immune system (408, 411, 591, 592). Dendritic cells, B cells, granulocytes and NK cells are produced from progenitors in the bone marrow and released into the periphery, while immature T cells must migrate to the thymus for full maturation (408, 531).

As mentioned previously, glucocorticoid (GC) treatment is the current standard therapy for GVHD (441, 473). However, GCs inhibit reconstitution of NK cells and interferon α/β-producing plasmacytoid dendritic cells following transplant (596, 597). This inhibition of reconstitution is an undesired side effect of GG, as delayed reconstitution is associated with an increased frequency of cytomegalovirus (CMV), adenovirus and herpes zoster virus in the post-transplant period (596). GC treatment can also affect the the generation of T cells in the thymus. A single injection of cortisone into healthy mice reduces by 10-fold the percentage of $CD4^+$ $CD8^+$ cells present in the thymus (729). Similarly, an injection of cortisone into mice suffering from GVHD reduced CD4 single positive cells in the thymus by 4-fold (729). Like GCs, cyclosporine A, an agent used for GVHD prophylaxis, has negative effects on thymus reconstitution in mice. Mice undergoing lethal irradiation, syngeneic transplantation, and a 3-week treatment with CsA had 50% fewer thymocytes than transplanted animals treated with control injections (730).

Unlike GCs and CsA, Bz-423 selectively affects cells with increased oxidative metabolism and depleted antioxidants. As shown in Chapter 3, bone marrow cells increase glycolysis 3-fold as they proliferate post-transplant, but their rate of OXPHOS remain low. Based on our observations in T cells, low rates of OXPHOS in post-transplant bone marrow cells suggests that these cells will be insensitive to Bz-423-mediated $\Delta\psi_m$ hyperpolarization and O_2^- production. Furthermore, bone marrow cells maintain their intracellular pyruvate as they proliferate (Figure 3.32), suggesting that any O_2^- generated by Bz-423 will be

detoxified before activating pro-apoptotic proteins. Indeed, a single dose of Bz-423 failed to hyperpolarize $\Delta\psi_m$, generate O_2^- or induce apoptosis in proliferating bone marrow cells following syngeneic transplant. Consistent with these results, 6 doses of Bz-423 did not decrease the number of splenic B cells, neutrophils or NK cells following syngeneic transplant.

Similarly, a single dose of Bz-423 did not induce $\Delta\psi_m$ hyperpolarization, O_2^- production, or apoptosis in thymocytes following syngeneic transplantation. While we did not measure metabolic parameters or antioxidant status of these cells, literature reports indicate that actively cycling thymocytes increase GLUT1 expression and therefore may preferentially utilize glycolysis. Indeed, $CD4^+CD8^+$ thymocytes that express the transferrin receptor, a marker of active metabolism and cell division (731), also express increased levels of surface GLUT1 (732). Consistent with its inability to induce apoptosis in thymocytes, treatment with 6 doses of Bz-423 did not decrease the number of any thymocyte populations or mature splenic T cells 21 d after syngeneic transplant.

Together, these results suggest that Bz-423 selectively induces apoptosis in alloreactive donor T cells during GVHD, but spares nonreactive T cells and proliferating cells in the bone marrow and thymus. This selectivity may be due to a combination of high rates of oxidative phosphorylation and depleted antioxidants, which is present in alloreactive donor T cells and autoreactive lymphocytes, but not in unstimulated cells or proliferating cells in the bone marrow or thymus. These studies suggest that, unlike many of the current

treatments for GVHD, Bz-423 may be able to reverse GVHD without predisposing patients to opportunistic infections.

Materials and Methods

Reagents. Bz-423 was stored as a solid at -20 °C and dissolved in DMSO prior to injections. Dihydroethidium (DHE), 5-(and-6)-chloromethyl-2',7'dichlorodihydrofluorescein diacetate, acetyl ester (DCFDA) and tetramethylrhodamine methyl ester (TMRM) were purchased from Invitrogen. DMEM media was purchased from Gibco and contained 10% heat-inactivated fetal bovine serum (FBS: Gibco), glucose (25 mM), glutamine (4 mM), HEPES (1 mM), penicillin (100 units/ml), streptomycin (100 μg/ml), minimal non-essential amino acids (1x), sodium pyruvate (1 mM) and 2-mercaptoethanol (0.05 mM). Unless indicated, all other reagents were purchased from Sigma.

Mice. Female C57Bl/6 (B6; H-2^b, CD45.2^+Thy1.2^+) and B6.Ly-5a (B6-Ly5.2; H-2^b, CD45.1^+Thy1.2^+) were purchased from Charles River Laboratories or Jackson Laboraties. Female B6.PL-Thy1a (B6-Thy1.1; H-2^b, CD45.2^+Thy1.1^+) and C3H.SW (H-2^b, CD45.2^+) were purchased from the Jackson Laboratory (Bar Harbor, ME). B6D2F1 (F1) mice were purchased from Charles River Laboratories or Taconic Laboratories. Mice were housed in specific pathogen free conditions and cared for according to the Guidelines for Laboratory Animal Medicine at the University of Michigan. All mice were at least seven weeks old prior to use.

T cell purification. T cells were purified from the spleens of B6 or B6-Ly5.2 mice by CD90$^+$ positive selection according to the manufacturer's protocol. Mice were anesthetized with isoflurane and euthanized by CO_2 asphyxiation. Spleens

were harvested and placed into sterile MACS running buffer (PBS, 0.5% BSA (w/v, Fischer), 2 mM EDTA). Spleens were dissociated using sterile frosted microscope slides and strained over a 40 μM filter (BD Falcon) into 50 ml conical vials. Dishes and filters were then rinsed once with MACS running buffer. Cells were pelleted at 1400 RPM and resuspended in 50 μl anti-CD90 microbeads and 950 μl MACS running buffer per spleen and placed on ice for 15 min. Greater than 10x excess MACS running buffer was added and cells were pelleted at 1400 RPM and resuspended in MACS running buffer (500 μl) and up to 3 spleens were applied to a single LS magnetic column in a MidiMACS magnetic. After three rinses with MACS running buffer, the column was removed from the magnetic field and the positively labeled cells were flushed out using 5 ml of buffer. Cells were washed once with DMEM media, counted, stained for purity and placed on ice until use. T cells were typically >85% TCR-β positive.

In vitro T cell stimulation, Bz-423 treatment and DHE and TMRM staining. For antibody stimulation, T cells from B6-Ly5.2 mice were resuspended at 1 x 10^6 TCR-β^+ cells/ml in DMEM media containing 25 or 0.5 mM glucose. Functional grade anti-CD3 (clone 145-2C11; eBioscience) and anti-CD28 (clone 37.51; eBioscience) were added to cells at a final concentration of 0.5 μg/ml. 200 μL of cells (0.2 x 10^6 cells) were cultured in flat-bottomed 96 well plates at 37 °C.

After 48 h, these cells were washed and resuspended in fresh DMEM media containing either 0.5 or 25 mM glucose and 2% FBS at a concentration of 1 x 10^6 cells/ml . Freshly purified unstimulated T cells were also suspended in media with 25 mM glucose and 2% FBS. T cells were treated with the indicated

concentrations of Bz-423 for 1 h at 37 °C. Intracellular superoxide was measured by adding freshly prepared DHE (4 μM final concentration) directly to cell cultures and incubating for 30 min at 37 °C. Cells were then immediately analyzed using the FL-2 channel of a FACSCalibur flow cytometer (BD Biosciences) or an Accuri C6 flow cytometer to assess ethidium fluorescence. The mitochondrial membrane potential ($\Delta\psi_m$) was measured by incubating cells with TMRM (50 nM) for 30 min at 37 °C. Cells were immediately analyzed using the FL-2 channel of a FACSCalibur flow cytometer (BD Biosciences)

CFSE labeling. Vybrant CFDA SE Cell Tracer Kit was purchased from Invitrogen. Cells were suspended in L-15 media or MACS running buffer consisting of PBS, 0.5% BSA (w/v, Fischer) and 2 mM EDTA at a concentration < 20 x 10^6 cells/ml. 5(6)-carboxyfluorescein diacetate, succinimidyl ester (CFSE) was dissolved in DMSO and added to cells at a final concentration of 5 μM and cells were incubated at 37 °C for 15-30 minutes. After two washes with DMEM media, cells were placed on ice until use.

Bone marrow transplantation. To induce GVHD in non-irradiated recipients, syngeneic (B6) and allogeneic (F1) recipient mice were infused through the tail vein with 50.0x10^6 bulk splenocytes from B6-Ly5.2 or B6-Thy1.1 donor mice in L-15 media (250 μl, Cellgro). In irradiated models, B6-Ly5.2 mice were conditioned with a single dose of 900 or 1100 cGy TBI (^{137}Cs source), followed by tail vein infusion of 5.0 x 10^6 bone marrow (BM) cells in L-15 media (250 μL). In some cases, mice also received 4.0 x 10^6 positively-selected CD90$^+$ syngeneic (B6) T cells. After transplant, animals were kept in specific pathogen

free housing and given hyperchlorinated (pH=3.0) drinking water for 3 weeks. Survival after BMT was monitored daily.

In vivo treatment with Bz-423. Solid Bz-423 was dissolved in DMSO and then a mixture of 0.51% carboxymethylcellulose (w/v, Hercules) in L-15 media was added to the Bz-423 such that the final composition of the vehicle was 2% DMSO (v/v) and 0.5% CMC (w/v) in L-15. Before injection, tubes containing Bz-423 in vehicle or vehicle alone were sonicated in a water bath sonicator (Fisher) for 20 min. For survival experiments, mice were injected i.p. with Bz-423 (60 mg/kg) or vehicle (250 μl) every other day from d 7 to d 21 after transplant using a 23 gauge needle. A single dose of Bz-423 was administered 4 or 7 d following BMT to measure apoptosis, ROS levels and $\Delta\psi_m$ of donor T cells.

Flow cytometry. Cells (1×10^6) in single cell suspension were resuspended in Fc Block buffer composed of PBS, FBS (2% v/v) and anti-mouse CD16/CD32 Fc III/II receptor (1:250 dilution; BD Biosciences) for 10 min at 4 °C to minimize non-specific binding. Cells were spun (1400 RPM, 5 min) and resuspended in PBS containing 2 % fetal bovine serum (FACS wash, 100 μl) with antibodies against cell surface antigens (1:200 dilution) for 20 min at 4 °C. Cells were then washed twice with FACS wash and either analyzed immediately or fixed and analyzed 1-2 days later. The mitochondrial membrane potential ($\Delta\Psi_m$) was measured by labeling cells with TMRM (50nM; Invitrogen) and antibodies to cell surface antigens for 30 minutes at 37°C in pre-warmed FACS wash. Stained cells were washed once prior to analysis. Carbonyl cyanide 4-(trifluoromethoxy) phenylhydrazone (FCCP; 30μM; Sigma-Aldrich) was used as a positive control

for disruption of $\Delta\Psi_m$. To detect O_2^-, cells were stained for cell surface markers for 15 min at 37°C in pre-warmed FACS wash followed by incubation with DHE (4μM; Invitrogen) for 30 min at 37°C. Annexin-V staining was performed in 1x Annexin Binding Buffer (BD Biosciences) containing cell surface antibodies and 1μl/sample Annexin-V for 30 minutes on ice. The cells were washed and were either resuspended in Annexin Binding Buffer for immediate analysis or fixed in PBS containing 4% Paraformaldehyde for 20 min on ice for later analysis. The following antibodies and their isotype controls were used: anti-mouse CD4 (FITC, PerCP-Cy5.5, APC, PE, Pacific Blue, Pacific Orange clone RM4-5, Rat IgG2a), CD8a (FITC, APC, PerCP-Cy5.5, APC-Cy7 and Pacific Blue, clone 53-6.7, Rat IgG2a)**,** CD45.1 (FITC, PE, APC, PerCP-Cy5.5, APC-Alexa750 clone A20, Ms IgG2a)**,** CD45.2 (FITC, PE, PerCP-Cy5.5 and APC-eFluor780 clone 104, Ms IgG2a), CD90.1 (FITC and PE, clone HIS51, Rat IgG2a), Gr-1 (eFluor450, clone RB6-8C5, Rat IgG2b), CD19 (FITC, PE, APC, clone 1D3, Rat IgG2a), and B220 (APC, clone RA3-6B2, Rat IgG2a) (BD Biosciences and eBioscience).

Bone marrow and liver analysis. Femurs were harvested from animals 14-18 d after nonirradiated GVHD induction. Tissue was cleaned off of the bones with a scalpel and the epiphysis were cut to expose the marrow cavity. Marrow was flushed with DMEM media using a 10 ml syringe and a 27 gauge needle. Cells were passed through a 40 μM filter and then stained for flow cytometry analysis as indicated. Livers were harvested from animals 14-18 d after nonirradiated GVHD induction. Livers were homogenized in DMEM media with razorblades and, disrupted using frosted glass slides and strained over 40 μM

filters. Cells were layered over 50% Percoll and spun for 20 min at 2200 RPM and lymphocytes were collected from the bottom of the tube. Liver infiltrating lymphocytes were then stained for flow cytometry as indicated.

BIBLIOGRAPHY

1. Janeway, C., Travers, P., Walport, M., and Shlomchik, M.J. 2005. An introduction to immunobiology and innate immunity. In *Immunobiology : the immune system in health and disease*. New York: Garland Science. 1-100.
2. Matsunaga, T., and Rahman, A. 1998. What brought the adaptive immune system to vertebrates?--The jaw hypothesis and the seahorse. *Immunol Rev* 166:177-186.
3. Burnet, F.M. 1961. The cellular basis of immunology. *Jpn J Microbiol* 5:1-10.
4. Davis, M.M., and Bjorkman, P.J. 1988. T-cell antigen receptor genes and T-cell recognition. *Nature* 334:395-402.
5. Nikolich-Zugich, J., Slifka, M.K., and Messaoudi, I. 2004. The many important facets of T-cell repertoire diversity. *Nat Rev Immunol* 4:123-132.
6. Arstila, T.P., Casrouge, A., Baron, V., Even, J., Kanellopoulos, J., and Kourilsky, P. 1999. A direct estimate of the human alphabeta T cell receptor diversity. *Science* 286:958-961.
7. Casrouge, A., Beaudoing, E., Dalle, S., Pannetier, C., Kanellopoulos, J., and Kourilsky, P. 2000. Size estimate of the alpha beta TCR repertoire of naive mouse splenocytes. *J Immunol* 164:5782-5787.
8. Weant, A.E., Michalek, R.D., Khan, I.U., Holbrook, B.C., Willingham, M.C., and Grayson, J.M. 2008. Apoptosis regulators Bim and Fas function concurrently to control autoimmunity and CD8+ T cell contraction. *Immunity* 28:218-230.
9. Hughes, P.D., Belz, G.T., Fortner, K.A., Budd, R.C., Strasser, A., and Bouillet, P. 2008. Apoptosis regulators Fas and Bim cooperate in shutdown of chronic immune responses and prevention of autoimmunity. *Immunity* 28:197-205.
10. Bouillet, P., and O'Reilly, L.A. 2009. CD95, BIM and T cell homeostasis. *Nat Rev Immunol* 9:514-519.
11. Hutcheson, J., Scatizzi, J.C., Siddiqui, A.M., Haines, G.K., 3rd, Wu, T., Li, Q.Z., Davis, L.S., Mohan, C., and Perlman, H. 2008. Combined deficiency of proapoptotic regulators Bim and Fas results in the early onset of systemic autoimmunity. *Immunity* 28:206-217.

12. Green, D.R. 2008. Fas Bim boom! *Immunity* 28:141-143.
13. Dutton, R.W., Bradley, L.M., and Swain, S.L. 1998. T cell memory. *Annu Rev Immunol* 16:201-223.
14. Kurosaki, T., Shinohara, H., and Baba, Y. B cell signaling and fate decision. *Annu Rev Immunol* 28:21-55.
15. Chavez-Galan, L., Arenas-Del Angel, M.C., Zenteno, E., Chavez, R., and Lascurain, R. 2009. Cell death mechanisms induced by cytotoxic lymphocytes. *Cell Mol Immunol* 6:15-25.
16. Hoves, S., Trapani, J.A., and Voskoboinik, I. The battlefield of perforin/granzyme cell death pathways. *J Leukoc Biol* 87:237-243.
17. Constant, S.L., and Bottomly, K. 1997. Induction of Th1 and Th2 CD4+ T cell responses: the alternative approaches. *Annu Rev Immunol* 15:297-322.
18. Boehm, U., Klamp, T., Groot, M., and Howard, J.C. 1997. Cellular responses to interferon-gamma. *Annu Rev Immunol* 15:749-795.
19. Banchereau, J., Bazan, F., Blanchard, D., Briere, F., Galizzi, J.P., van Kooten, C., Liu, Y.J., Rousset, F., and Saeland, S. 1994. The CD40 antigen and its ligand. *Annu Rev Immunol* 12:881-922.
20. Khader, S.A., Bell, G.K., Pearl, J.E., Fountain, J.J., Rangel-Moreno, J., Cilley, G.E., Shen, F., Eaton, S.M., Gaffen, S.L., Swain, S.L., et al. 2007. IL-23 and IL-17 in the establishment of protective pulmonary CD4+ T cell responses after vaccination and during Mycobacterium tuberculosis challenge. *Nat Immunol* 8:369-377.
21. Sato, K., Suematsu, A., Okamoto, K., Yamaguchi, A., Morishita, Y., Kadono, Y., Tanaka, S., Kodama, T., Akira, S., Iwakura, Y., et al. 2006. Th17 functions as an osteoclastogenic helper T cell subset that links T cell activation and bone destruction. *J Exp Med* 203:2673-2682.
22. Kebir, H., Kreymborg, K., Ifergan, I., Dodelet-Devillers, A., Cayrol, R., Bernard, M., Giuliani, F., Arbour, N., Becher, B., and Prat, A. 2007. Human TH17 lymphocytes promote blood-brain barrier disruption and central nervous system inflammation. *Nat Med* 13:1173-1175.
23. Janeway, C. 2005. *Immunobiology : the immune system in health and disease*. New York: Garland Science. xxiii, 823 p. pp.
24. Cresswell, P., Ackerman, A.L., Giodini, A., Peaper, D.R., and Wearsch, P.A. 2005. Mechanisms of MHC class I-restricted antigen processing and cross-presentation. *Immunol Rev* 207:145-157.
25. Delves, P.J., and Roitt, I.M. 2000. The immune system. First of two parts. *N Engl J Med* 343:37-49.
26. Aderem, A., and Underhill, D.M. 1999. Mechanisms of phagocytosis in macrophages. *Annu Rev Immunol* 17:593-623.
27. Gordon, S. 2002. Pattern recognition receptors: doubling up for the innate immune response. *Cell* 111:927-930.
28. Zamze, S., Martinez-Pomares, L., Jones, H., Taylor, P.R., Stillion, R.J., Gordon, S., and Wong, S.Y. 2002. Recognition of bacterial capsular polysaccharides and lipopolysaccharides by the macrophage mannose receptor. *J Biol Chem* 277:41613-41623.

29. Segal, A.W. 2005. How neutrophils kill microbes. *Annu Rev Immunol* 23:197-223.
30. Wagner, J.G., and Roth, R.A. 2000. Neutrophil migration mechanisms, with an emphasis on the pulmonary vasculature. *Pharmacol Rev* 52:349-374.
31. Carroll, M.C. 1998. The role of complement and complement receptors in induction and regulation of immunity. *Annu Rev Immunol* 16:545-568.
32. Reis e Sousa, C., Sher, A., and Kaye, P. 1999. The role of dendritic cells in the induction and regulation of immunity to microbial infection. *Curr Opin Immunol* 11:392-399.
33. Sallusto, F., Schaerli, P., Loetscher, P., Schaniel, C., Lenig, D., Mackay, C.R., Qin, S., and Lanzavecchia, A. 1998. Rapid and coordinated switch in chemokine receptor expression during dendritic cell maturation. *Eur J Immunol* 28:2760-2769.
34. Acuto, O., and Michel, F. 2003. CD28-mediated co-stimulation: a quantitative support for TCR signalling. *Nat Rev Immunol* 3:939-951.
35. Parish, I.A., and Heath, W.R. 2008. Too dangerous to ignore: self-tolerance and the control of ignorant autoreactive T cells. *Immunol Cell Biol* 86:146-152.
36. Joffre, O., Nolte, M.A., Sporri, R., and Reis e Sousa, C. 2009. Inflammatory signals in dendritic cell activation and the induction of adaptive immunity. *Immunol Rev* 227:234-247.
37. Cumano, A., and Godin, I. 2007. Ontogeny of the hematopoietic system. *Annu Rev Immunol* 25:745-785.
38. Blom, B., and Spits, H. 2006. Development of human lymphoid cells. *Annu Rev Immunol* 24:287-320.
39. Petrie, H.T., and Kincade, P.W. 2005. Many roads, one destination for T cell progenitors. *J Exp Med* 202:11-13.
40. Fink, P.J., and Bevan, M.J. 1995. Positive selection of thymocytes. *Adv Immunol* 59:99-133.
41. Hare, K.J., Jenkinson, E.J., and Anderson, G. 2001. Specialisation of thymic epithelial cells for positive selection of CD4+8+ thymocytes. *Cell Mol Biol (Noisy-le-grand)* 47:119-127.
42. Starr, T.K., Jameson, S.C., and Hogquist, K.A. 2003. Positive and negative selection of T cells. *Annu Rev Immunol* 21:139-176.
43. Rahman, A., and Isenberg, D.A. 2008. Systemic lupus erythematosus. *N Engl J Med* 358:929-939.
44. Cutolo, M., Sulli, A., Pizzorni, C., Seriolo, B., and Straub, R.H. 2001. Anti-inflammatory mechanisms of methotrexate in rheumatoid arthritis. *Ann Rheum Dis* 60:729-735.
45. Beeton, C., and Chandy, K.G. 2005. Potassium channels, memory T cells, and multiple sclerosis. *Neuroscientist* 11:550-562.
46. Bell, P.R., Briggs, J.D., Calman, K.C., Paton, A.M., Wood, R.F., Macpherson, S.G., and Kyle, K. 1971. Reversal of acute clinical and experimental organ rejection using large doses of intravenous prednisolone. *Lancet* 1:876-880.

47. Ferrara, J.L.M., Cooke, K.R., and Deeg, H.J. 2005. *Graft-vs.-host disease*. New York: Marcel Dekker. xvii, 645 p. pp.
48. Ferrara, J.L., Levine, J.E., Reddy, P., and Holler, E. 2009. Graft-versus-host disease. *Lancet* 373:1550-1561.
49. Voet, D., and Voet, J.G. 2004. *Biochemistry*. New York: J. Wiley & Sons. xv, 1591 pp.
50. Vaughn, A.E., and Deshmukh, M. 2008. Glucose metabolism inhibits apoptosis in neurons and cancer cells by redox inactivation of cytochrome c. *Nat Cell Biol* 10:1477-1483.
51. Ben-Yoseph, O., Boxer, P.A., and Ross, B.D. 1996. Assessment of the role of the glutathione and pentose phosphate pathways in the protection of primary cerebrocortical cultures from oxidative stress. *J Neurochem* 66:2329-2337.
52. Bauer, D.E., Hatzivassiliou, G., Zhao, F., Andreadis, C., and Thompson, C.B. 2005. ATP citrate lyase is an important component of cell growth and transformation. *Oncogene* 24:6314-6322.
53. Hatzivassiliou, G., Zhao, F., Bauer, D.E., Andreadis, C., Shaw, A.N., Dhanak, D., Hingorani, S.R., Tuveson, D.A., and Thompson, C.B. 2005. ATP citrate lyase inhibition can suppress tumor cell growth. *Cancer Cell* 8:311-321.
54. Manolescu, A.R., Witkowska, K., Kinnaird, A., Cessford, T., and Cheeseman, C. 2007. Facilitated hexose transporters: new perspectives on form and function. *Physiology (Bethesda)* 22:234-240.
55. Mueckler, M., Caruso, C., Baldwin, S.A., Panico, M., Blench, I., Morris, H.R., Allard, W.J., Lienhard, G.E., and Lodish, H.F. 1985. Sequence and structure of a human glucose transporter. *Science* 229:941-945.
56. Barrett, M.P., Walmsley, A.R., and Gould, G.W. 1999. Structure and function of facilitative sugar transporters. *Curr Opin Cell Biol* 11:496-502.
57. Bell, G.I., Burant, C.F., Takeda, J., and Gould, G.W. 1993. Structure and function of mammalian facilitative sugar transporters. *J Biol Chem* 268:19161-19164.
58. Jacobs, S.R., Herman, C.E., Maciver, N.J., Wofford, J.A., Wieman, H.L., Hammen, J.J., and Rathmell, J.C. 2008. Glucose uptake is limiting in T cell activation and requires CD28-mediated Akt-dependent and independent pathways. *J Immunol* 180:4476-4486.
59. Frauwirth, K.A., Riley, J.L., Harris, M.H., Parry, R.V., Rathmell, J.C., Plas, D.R., Elstrom, R.L., June, C.H., and Thompson, C.B. 2002. The CD28 signaling pathway regulates glucose metabolism. *Immunity* 16:769-777.
60. Chakrabarti, R., Jung, C.Y., Lee, T.P., Liu, H., and Mookerjee, B.K. 1994. Changes in glucose transport and transporter isoforms during the activation of human peripheral blood lymphocytes by phytohemagglutinin. *J Immunol* 152:2660-2668.
61. Netzker, R., Hermfisse, U., Wein, K.H., and Brand, K. 1994. Expression of glycolytic isozymes in rat thymocytes during cell cycle progression. *Biochim Biophys Acta* 1224:371-376.

62. Brand, K. 1985. Glutamine and glucose metabolism during thymocyte proliferation. Pathways of glutamine and glutamate metabolism. *Biochem J* 228:353-361.
63. Greiner, E.F., Guppy, M., and Brand, K. 1994. Glucose is essential for proliferation and the glycolytic enzyme induction that provokes a transition to glycolytic energy production. *J Biol Chem* 269:31484-31490.
64. Marjanovic, S., Eriksson, I., and Nelson, B.D. 1990. Expression of a new set of glycolytic isozymes in activated human peripheral lymphocytes. *Biochim Biophys Acta* 1087:1-6.
65. Kester, M.V., Phillips, T.L., and Gracy, R.W. 1977. Changes in glycolytic enzyme levels and isozyme expression in human lymphocytes during blast transformation. *Arch Biochem Biophys* 183:700-709.
66. Netzker, R., Greiner, E., Eigenbrodt, E., Noguchi, T., Tanaka, T., and Brand, K. 1992. Cell cycle-associated expression of M2-type isozyme of pyruvate kinase in proliferating rat thymocytes. *J Biol Chem* 267:6421-6424.
67. Marjanovic, S., Skog, S., Heiden, T., Tribukait, B., and Nelson, B.D. 1991. Expression of glycolytic isoenzymes in activated human peripheral lymphocytes: cell cycle analysis using flow cytometry. *Exp Cell Res* 193:425-431.
68. Zhao, Y., Wieman, H.L., Jacobs, S.R., and Rathmell, J.C. 2008. Mechanisms and methods in glucose metabolism and cell death. *Methods Enzymol* 442:439-457.
69. Maciver, N.J., Jacobs, S.R., Wieman, H.L., Wofford, J.A., Coloff, J.L., and Rathmell, J.C. 2008. Glucose metabolism in lymphocytes is a regulated process with significant effects on immune cell function and survival. *J Leukoc Biol* 84:949-957.
70. Fu, Y., Maianu, L., Melbert, B.R., and Garvey, W.T. 2004. Facilitative glucose transporter gene expression in human lymphocytes, monocytes, and macrophages: a role for GLUT isoforms 1, 3, and 5 in the immune response and foam cell formation. *Blood Cells Mol Dis* 32:182-190.
71. Stentz, F.B., and Kitabchi, A.E. 2007. Transcriptome and proteome expressions involved in insulin resistance in muscle and activated T-lymphocytes of patients with type 2 diabetes. *Genomics Proteomics Bioinformatics* 5:216-235.
72. Printz, R.L., Magnuson, M.A., and Granner, D.K. 1993. Mammalian glucokinase. *Annu Rev Nutr* 13:463-496.
73. Ureta, T. 1982. The comparative isozymology of vertebrate hexokinases. *Comp Biochem Physiol B* 71:549-555.
74. Iyer, N.V., Kotch, L.E., Agani, F., Leung, S.W., Laughner, E., Wenger, R.H., Gassmann, M., Gearhart, J.D., Lawler, A.M., Yu, A.Y., et al. 1998. Cellular and developmental control of O2 homeostasis by hypoxia-inducible factor 1 alpha. *Genes Dev* 12:149-162.
75. Rathmell, J.C., Fox, C.J., Plas, D.R., Hammerman, P.S., Cinalli, R.M., and Thompson, C.B. 2003. Akt-directed glucose metabolism can prevent Bax

conformation change and promote growth factor-independent survival. *Mol Cell Biol* 23:7315-7328.
76. Chehtane, M., and Khaled, A.R. Interleukin-7 mediates glucose utilization in lymphocytes through transcriptional regulation of the hexokinase II gene. *Am J Physiol Cell Physiol* 298:C1560-1571.
77. Kletzien, R.F., Harris, P.K., and Foellmi, L.A. 1994. Glucose-6-phosphate dehydrogenase: a "housekeeping" enzyme subject to tissue-specific regulation by hormones, nutrients, and oxidant stress. *FASEB J* 8:174-181.
78. Vander Heiden, M.G., Cantley, L.C., and Thompson, C.B. 2009. Understanding the Warburg effect: the metabolic requirements of cell proliferation. *Science* 324:1029-1033.
79. Wagle, A., Jivraj, S., Garlock, G.L., and Stapleton, S.R. 1998. Insulin regulation of glucose-6-phosphate dehydrogenase gene expression is rapamycin-sensitive and requires phosphatidylinositol 3-kinase. *J Biol Chem* 273:14968-14974.
80. Dunaway, G.A., Kasten, T.P., Sebo, T., and Trapp, R. 1988. Analysis of the phosphofructokinase subunits and isoenzymes in human tissues. *Biochem J* 251:677-683.
81. Meienhofer, M.C., Lagrange, J.L., Cottreau, D., Lenoir, G., Dreyfus, J.C., and Kahn, A. 1979. Phosphofructokinase in human blood cells. *Blood* 54:389-400.
82. Deprez, J., Vertommen, D., Alessi, D.R., Hue, L., and Rider, M.H. 1997. Phosphorylation and activation of heart 6-phosphofructo-2-kinase by protein kinase B and other protein kinases of the insulin signaling cascades. *J Biol Chem* 272:17269-17275.
83. Mukai, T., Joh, K., Arai, Y., Yatsuki, H., and Hori, K. 1986. Tissue-specific expression of rat aldolase A mRNAs. Three molecular species differing only in the 5'-terminal sequences. *J Biol Chem* 261:3347-3354.
84. Paolella, G., Santamaria, R., Izzo, P., Costanzo, P., and Salvatore, F. 1984. Isolation and nucleotide sequence of a full-length cDNA coding for aldolase B from human liver. *Nucleic Acids Res* 12:7401-7410.
85. Buono, P., D'Armiento, F.P., Terzi, G., Alfieri, A., and Salvatore, F. 2001. Differential distribution of aldolase A and C in the human central nervous system. *J Neurocytol* 30:957-965.
86. Gomez, P.F., Ito, K., Huang, Y., Otsu, K., Kuzumaki, T., and Ishikawa, K. 1994. Dietary and hormonal regulation of aldolase B gene transcription in rat liver. *Arch Biochem Biophys* 314:307-314.
87. Munnich, A., Besmond, C., Darquy, S., Reach, G., Vaulont, S., Dreyfus, J.C., and Kahn, A. 1985. Dietary and hormonal regulation of aldolase B gene expression. *J Clin Invest* 75:1045-1052.
88. Zelzer, E., Levy, Y., Kahana, C., Shilo, B.Z., Rubinstein, M., and Cohen, B. 1998. Insulin induces transcription of target genes through the hypoxia-inducible factor HIF-1alpha/ARNT. *EMBO J* 17:5085-5094.

89. Kester, M.V., and Gracy, R.W. 1975. Alteration of human lymphocyte triosephosphate isomerase isozymes during blastogenesis. *Biochem Biophys Res Commun* 65:1270-1277.
90. Asakawa, J., and Iida, S. 1985. Origin of human triosephosphate isomerase isozymes: further evidence for the single structural locus hypothesis with Japanese variants. *Hum Genet* 71:22-26.
91. Rubinson, H., Meienhofer, M.C., and Dreyfus, J.C. 1973. A new isozyme of triose phosphate isomerase specific to hominoids. *J Mol Evol* 2:243-250.
92. Knowles, J.R. 1991. Enzyme catalysis: not different, just better. *Nature* 350:121-124.
93. Barber, R.D., Harmer, D.W., Coleman, R.A., and Clark, B.J. 2005. GAPDH as a housekeeping gene: analysis of GAPDH mRNA expression in a panel of 72 human tissues. *Physiol Genomics* 21:389-395.
94. Goto, M., Koji, T., Mizuno, K., Tamaru, M., Koikeda, S., Nakane, P.K., Mori, N., Masamune, Y., and Nakanishi, Y. 1990. Transcription switch of two phosphoglycerate kinase genes during spermatogenesis as determined with mouse testis sections in situ. *Exp Cell Res* 186:273-278.
95. Zhang, J., Yu, L., Fu, Q., Gao, J., Xie, Y., Chen, J., Zhang, P., Liu, Q., and Zhao, S. 2001. Mouse phosphoglycerate mutase M and B isozymes: cDNA cloning, enzyme activity assay and mapping. *Gene* 264:273-279.
96. Omenn, G.S., and Cheung, S.C. 1974. Phosphoglycerate mutase isozyme marker for tissue differentiation in man. *Am J Hum Genet* 26:393-399.
97. Pancholi, V. 2001. Multifunctional alpha-enolase: its role in diseases. *Cell Mol Life Sci* 58:902-920.
98. Ibsen, K.H. 1977. Interrelationships and functions of the pyruvate kinase isozymes and their variant forms: a review. *Cancer Res* 37:341-353.
99. Mazurek, S., Boschek, C.B., Hugo, F., and Eigenbrodt, E. 2005. Pyruvate kinase type M2 and its role in tumor growth and spreading. *Semin Cancer Biol* 15:300-308.
100. Christofk, H.R., Vander Heiden, M.G., Harris, M.H., Ramanathan, A., Gerszten, R.E., Wei, R., Fleming, M.D., Schreiber, S.L., and Cantley, L.C. 2008. The M2 splice isoform of pyruvate kinase is important for cancer metabolism and tumour growth. *Nature* 452:230-233.
101. Noguchi, T., Inoue, H., and Tanaka, T. 1986. The M1- and M2-type isozymes of rat pyruvate kinase are produced from the same gene by alternative RNA splicing. *J Biol Chem* 261:13807-13812.
102. Mellati, A.A., Yucel, M., Altinors, N., and Gunduz, U. 1992. Regulation of M2-type pyruvate kinase from human meningioma by allosteric effectors fructose 1,6 diphosphate and L-alanine. *Cancer Biochem Biophys* 13:33-41.
103. Jurica, M.S., Mesecar, A., Heath, P.J., Shi, W., Nowak, T., and Stoddard, B.L. 1998. The allosteric regulation of pyruvate kinase by fructose-1,6-bisphosphate. *Structure* 6:195-210.
104. Murray, C.M., Hutchinson, R., Bantick, J.R., Belfield, G.P., Benjamin, A.D., Brazma, D., Bundick, R.V., Cook, I.D., Craggs, R.I., Edwards, S., et al.

2005. Monocarboxylate transporter MCT1 is a target for immunosuppression. *Nat Chem Biol* 1:371-376.
105. Behal, R.H., Buxton, D.B., Robertson, J.G., and Olson, M.S. 1993. Regulation of the pyruvate dehydrogenase multienzyme complex. *Annu Rev Nutr* 13:497-520.
106. Kolobova, E., Tuganova, A., Boulatnikov, I., and Popov, K.M. 2001. Regulation of pyruvate dehydrogenase activity through phosphorylation at multiple sites. *Biochem J* 358:69-77.
107. Jitrapakdee, S., St Maurice, M., Rayment, I., Cleland, W.W., Wallace, J.C., and Attwood, P.V. 2008. Structure, mechanism and regulation of pyruvate carboxylase. *Biochem J* 413:369-387.
108. Reis, G.J., Kaufman, H.W., Horowitz, G.L., and Pasternak, R.C. 1988. Usefulness of lactate dehydrogenase and lactate dehydrogenase isoenzymes for diagnosis of acute myocardial infarction. *Am J Cardiol* 61:754-758.
109. Markert, C.L. 1963. Lactate Dehydrogenase Isozymes: Dissociation and Recombination of Subunits. *Science* 140:1329-1330.
110. Drent, M., Cobben, N.A., Henderson, R.F., Wouters, E.F., and van Dieijen-Visser, M. 1996. Usefulness of lactate dehydrogenase and its isoenzymes as indicators of lung damage or inflammation. *Eur Respir J* 9:1736-1742.
111. Wollberg, P., and Nelson, B.D. 1992. Regulation of the expression of lactate dehydrogenase isozymes in human lymphocytes. *Mol Cell Biochem* 110:161-164.
112. Voet, D., and Voet, J.G. 2004. Citric Acid Cycle. In *Biochemistry*. D. Harris, and P. Fitzgerald, editors: John Wiley and Sons. 765-796.
113. DeBerardinis, R.J., and Cheng, T. Q's next: the diverse functions of glutamine in metabolism, cell biology and cancer. *Oncogene* 29:313-324.
114. Marti, H.H., Jung, H.H., Pfeilschifter, J., and Bauer, C. 1994. Hypoxia and cobalt stimulate lactate dehydrogenase (LDH) activity in vascular smooth muscle cells. *Pflugers Arch* 429:216-222.
115. Thomas, A.P., and Halestrap, A.P. 1981. Identification of the protein responsible for pyruvate transport into rat liver and heart mitochondria by specific labelling with [3H]N-phenylmaleimide. *Biochem J* 196:471-479.
116. Hildyard, J.C., and Halestrap, A.P. 2003. Identification of the mitochondrial pyruvate carrier in Saccharomyces cerevisiae. *Biochem J* 374:607-611.
117. Sugden, M.C., and Holness, M.J. 2003. Trials, tribulations and finally, a transporter: the identification of the mitochondrial pyruvate transporter. *Biochem J* 374:e1-2.
118. Wiegand, G., and Remington, S.J. 1986. Citrate synthase: structure, control, and mechanism. *Annu Rev Biophys Biophys Chem* 15:97-117.
119. Barrera, C.R., Namihira, G., Hamilton, L., Munk, P., Eley, M.H., Linn, T.C., and Reed, L.J. 1972. -Keto acid dehydrogenase complexes. XVI. Studies on the subunit structure of the pyruvate dehydrogenase complexes from bovine kidney and heart. *Arch Biochem Biophys* 148:343-358.

120. Pinheiro, A., Faustino, I., Silva, M.J., Silva, J., Sa, R., Sousa, M., Barros, A., de Almeida, I.T., and Rivera, I. Human testis-specific PDHA2 gene: methylation status of a CpG island in the open reading frame correlates with transcriptional activity. *Mol Genet Metab* 99:425-430.
121. Kim, J.W., Tchernyshyov, I., Semenza, G.L., and Dang, C.V. 2006. HIF-1-mediated expression of pyruvate dehydrogenase kinase: a metabolic switch required for cellular adaptation to hypoxia. *Cell Metab* 3:177-185.
122. Kirito, K., Hu, Y., and Komatsu, N. 2009. HIF-1 prevents the overproduction of mitochondrial ROS after cytokine stimulation through induction of PDK-1. *Cell Cycle* 8:2844-2849.
123. Baumgarten, E., Brand, M.D., and Pozzan, T. 1983. Mechanism of activation of pyruvate dehydrogenase by mitogens in pig lymphocytes. *Biochem J* 216:359-367.
124. Walker, M.E., Baker, E., Wallace, J.C., and Sutherland, G.R. 1995. Assignment of the human pyruvate carboxylase gene (PC) to 11q13.4 by fluorescence in situ hybridisation. *Cytogenet Cell Genet* 69:187-189.
125. Legge, G.B., Branson, J.P., and Attwood, P.V. 1996. Effects of acetyl CoA on the pre-steady-state kinetics of the biotin carboxylation reaction of pyruvate carboxylase. *Biochemistry* 35:3849-3856.
126. Curi, R., Newsholme, P., and Newsholme, E.A. 1988. Metabolism of pyruvate by isolated rat mesenteric lymphocytes, lymphocyte mitochondria and isolated mouse macrophages. *Biochem J* 250:383-388.
127. O'Rourke, A.M., and Rider, C.C. 1989. Glucose, glutamine and ketone body utilisation by resting and concanavalin A activated rat splenic lymphocytes. *Biochim Biophys Acta* 1010:342-345.
128. Brand, K., Fekl, W., von Hintzenstern, J., Langer, K., Luppa, P., and Schoerner, C. 1989. Metabolism of glutamine in lymphocytes. *Metabolism* 38:29-33.
129. Brandt, U. 2006. Energy converting NADH:quinone oxidoreductase (complex I). *Annu Rev Biochem* 75:69-92.
130. Hinchliffe, P., and Sazanov, L.A. 2005. Organization of iron-sulfur clusters in respiratory complex I. *Science* 309:771-774.
131. Lambert, A.J., and Brand, M.D. 2009. Reactive oxygen species production by mitochondria. *Methods Mol Biol* 554:165-181.
132. Wikstrom, M. 1984. Two protons are pumped from the mitochondrial matrix per electron transferred between NADH and ubiquinone. *FEBS Lett* 169:300-304.
133. Godemann, R., Biernat, J., Mandelkow, E., and Mandelkow, E.M. 1999. Phosphorylation of tau protein by recombinant GSK-3beta: pronounced phosphorylation at select Ser/Thr-Pro motifs but no phosphorylation at Ser262 in the repeat domain. *FEBS Lett* 454:157-164.
134. Cecchini, G. 2003. Function and structure of complex II of the respiratory chain. *Annu Rev Biochem* 72:77-109.
135. Schultz, B.E., and Chan, S.I. 2001. Structures and proton-pumping strategies of mitochondrial respiratory enzymes. *Annu Rev Biophys Biomol Struct* 30:23-65.

136. Lehninger, A., Nelson, D., and Cox, M. 1993. Oxidative phosphorylation and photophosphorylation. In *Principles of Biochemistry*. New York: Worth Publishers. 542-561.
137. Wikstrom, M. 2004. Cytochrome c oxidase: 25 years of the elusive proton pump. *Biochim Biophys Acta* 1655:241-247.
138. Crofts, A.R. 2004. The cytochrome bc1 complex: function in the context of structure. *Annu Rev Physiol* 66:689-733.
139. Hunte, C., Palsdottir, H., and Trumpower, B.L. 2003. Protonmotive pathways and mechanisms in the cytochrome bc1 complex. *FEBS Lett* 545:39-46.
140. Michel, H., Behr, J., Harrenga, A., and Kannt, A. 1998. Cytochrome c oxidase: structure and spectroscopy. *Annu Rev Biophys Biomol Struct* 27:329-356.
141. Faxen, K., Gilderson, G., Adelroth, P., and Brzezinski, P. 2005. A mechanistic principle for proton pumping by cytochrome c oxidase. *Nature* 437:286-289.
142. Sariban-Sohraby, S., Magrath, I.T., and Balaban, R.S. 1983. Comparison of energy metabolism in human normal and neoplastic (Burkitt's lymphoma) lymphoid cells. *Cancer Res* 43:4662-4664.
143. Harris, S.I., Balaban, R.S., and Mandel, L.J. 1980. Oxygen consumption and cellular ion transport: evidence for adenosine triphosphate to O2 ratio near 6 in intact cell. *Science* 208:1148-1150.
144. Scheffler, I.E. 1999. Mitochondrial Electron Transport and Oxidative Phosphorylation. In *Mitochondria*. New York: Wile-Liss, Inc. 141-252.
145. Nicholls, D.G., and Ward, M.W. 2000. Mitochondrial membrane potential and neuronal glutamate excitotoxicity: mortality and millivolts. *Trends Neurosci* 23:166-174.
146. Nicholls, D.G. 2004. Mitochondrial membrane potential and aging. *Aging Cell* 3:35-40.
147. Boyer, P.D. 1997. The ATP synthase--a splendid molecular machine. *Annu Rev Biochem* 66:717-749.
148. Devenish, R.J., Prescott, M., Boyle, G.M., and Nagley, P. 2000. The oligomycin axis of mitochondrial ATP synthase: OSCP and the proton channel. *J Bioenerg Biomembr* 32:507-515.
149. Rastogi, V.K., and Girvin, M.E. 1999. Structural changes linked to proton translocation by subunit c of the ATP synthase. *Nature* 402:263-268.
150. Noji, H., Yasuda, R., Yoshida, M., and Kinosita, K., Jr. 1997. Direct observation of the rotation of F1-ATPase. *Nature* 386:299-302.
151. Yasuda, R., Noji, H., Kinosita, K., Jr., and Yoshida, M. 1998. F1-ATPase is a highly efficient molecular motor that rotates with discrete 120 degree steps. *Cell* 93:1117-1124.
152. Saraste, M. 1999. Oxidative phosphorylation at the fin de siecle. *Science* 283:1488-1493.
153. Leyva, J.A., Bianchet, M.A., and Amzel, L.M. 2003. Understanding ATP synthesis: structure and mechanism of the F1-ATPase (Review). *Mol Membr Biol* 20:27-33.

154. Murphy, M.P. 2009. How mitochondria produce reactive oxygen species. *Biochem J* 417:1-13.
155. Degli Esposti, M. 1998. Inhibitors of NADH-ubiquinone reductase: an overview. *Biochim Biophys Acta* 1364:222-235.
156. Okun, J.G., Lummen, P., and Brandt, U. 1999. Three classes of inhibitors share a common binding domain in mitochondrial complex I (NADH:ubiquinone oxidoreductase). *J Biol Chem* 274:2625-2630.
157. Kudin, A.P., Bimpong-Buta, N.Y., Vielhaber, S., Elger, C.E., and Kunz, W.S. 2004. Characterization of superoxide-producing sites in isolated brain mitochondria. *J Biol Chem* 279:4127-4135.
158. Genova, M.L., Ventura, B., Giuliano, G., Bovina, C., Formiggini, G., Parenti Castelli, G., and Lenaz, G. 2001. The site of production of superoxide radical in mitochondrial Complex I is not a bound ubisemiquinone but presumably iron-sulfur cluster N2. *FEBS Lett* 505:364-368.
159. Muller, F.L., Liu, Y., and Van Remmen, H. 2004. Complex III releases superoxide to both sides of the inner mitochondrial membrane. *J Biol Chem* 279:49064-49073.
160. Turrens, J.F., Alexandre, A., and Lehninger, A.L. 1985. Ubisemiquinone is the electron donor for superoxide formation by complex III of heart mitochondria. *Arch Biochem Biophys* 237:408-414.
161. Brand, M.D. The sites and topology of mitochondrial superoxide production. *Exp Gerontol* 45:466-472.
162. St-Pierre, J., Buckingham, J.A., Roebuck, S.J., and Brand, M.D. 2002. Topology of superoxide production from different sites in the mitochondrial electron transport chain. *J Biol Chem* 277:44784-44790.
163. Adam-Vizi, V., and Chinopoulos, C. 2006. Bioenergetics and the formation of mitochondrial reactive oxygen species. *Trends Pharmacol Sci* 27:639-645.
164. Demin, O.V., Kholodenko, B.N., and Skulachev, V.P. 1998. A model of O2.-generation in the complex III of the electron transport chain. *Mol Cell Biochem* 184:21-33.
165. Lambert, A.J., and Brand, M.D. 2004. Superoxide production by NADH:ubiquinone oxidoreductase (complex I) depends on the pH gradient across the mitochondrial inner membrane. *Biochem J* 382:511-517.
166. Votyakova, T.V., and Reynolds, I.J. 2001. DeltaPsi(m)-Dependent and -independent production of reactive oxygen species by rat brain mitochondria. *J Neurochem* 79:266-277.
167. Korshunov, S.S., Skulachev, V.P., and Starkov, A.A. 1997. High protonic potential actuates a mechanism of production of reactive oxygen species in mitochondria. *FEBS Lett* 416:15-18.
168. Starkov, A.A., and Fiskum, G. 2003. Regulation of brain mitochondrial H2O2 production by membrane potential and NAD(P)H redox state. *J Neurochem* 86:1101-1107.
169. Blatt, N.B., Bednarski, J.J., Warner, R.E., Leonetti, F., Johnson, K.M., Boitano, A., Yung, R., Richardson, B.C., Johnson, K.J., Ellman, J.A., et al.

2002. Benzodiazepine-induced superoxide signals B cell apoptosis: mechanistic insight and potential therapeutic utility. *J Clin Invest* 110:1123-1132.

170. Johnson, K.M., Chen, X., Boitano, A., Swenson, L., Opipari, A.W., Jr., and Glick, G.D. 2005. Identification and validation of the mitochondrial F1F0-ATPase as the molecular target of the immunomodulatory benzodiazepine Bz-423. *Chem Biol* 12:485-496.
171. Johnson, K.M., Cleary, J., Fierke, C.A., Opipari, A.W., Jr., and Glick, G.D. 2006. Mechanistic basis for therapeutic targeting of the mitochondrial F1F0-ATPase. *ACS Chem Biol* 1:304-308.
172. Blatt, N.B., Boitano, A.E., Lyssiotis, C.A., Opipari, A.W., Jr., and Glick, G.D. 2008. Bz-423 superoxide signals apoptosis via selective activation of JNK, Bak, and Bax. *Free Radic Biol Med* 45:1232-1242.
173. Sundberg, T.B., Swenson, L., Wahl, D.R., Opipari, A.W., Jr., and Glick, G.D. 2009. Apoptotic signaling activated by modulation of the F0F1-ATPase: implications for selective killing of autoimmune lymphocytes. *J Pharmacol Exp Ther* 331:437-444.
174. Fink, B.D., Reszka, K.J., Herlein, J.A., Mathahs, M.M., and Sivitz, W.I. 2005. Respiratory uncoupling by UCP1 and UCP2 and superoxide generation in endothelial cell mitochondria. *Am J Physiol Endocrinol Metab* 288:E71-79.
175. Cleary, J., Johnson, K.M., Opipari, A.W., Jr., and Glick, G.D. 2007. Inhibition of the mitochondrial F1F0-ATPase by ligands of the peripheral benzodiazepine receptor. *Bioorg Med Chem Lett* 17:1667-1670.
176. Machida, K., and Tanaka, T. 1999. Farnesol-induced generation of reactive oxygen species dependent on mitochondrial transmembrane potential hyperpolarization mediated by F(0)F(1)-ATPase in yeast. *FEBS Lett* 462:108-112.
177. Fridovich, I. 1995. Superoxide radical and superoxide dismutases. *Annu Rev Biochem* 64:97-112.
178. Bulteau, A.L., Lundberg, K.C., Ikeda-Saito, M., Isaya, G., and Szweda, L.I. 2005. Reversible redox-dependent modulation of mitochondrial aconitase and proteolytic activity during in vivo cardiac ischemia/reperfusion. *Proc Natl Acad Sci U S A* 102:5987-5991.
179. Bulteau, A.L., Ikeda-Saito, M., and Szweda, L.I. 2003. Redox-dependent modulation of aconitase activity in intact mitochondria. *Biochemistry* 42:14846-14855.
180. Abreu, I.A., and Cabelli, D.E. Superoxide dismutases-a review of the metal-associated mechanistic variations. *Biochim Biophys Acta* 1804:263-274.
181. Przedborski, S., Kostic, V., Jackson-Lewis, V., Naini, A.B., Simonetti, S., Fahn, S., Carlson, E., Epstein, C.J., and Cadet, J.L. 1992. Transgenic mice with increased Cu/Zn-superoxide dismutase activity are resistant to N-methyl-4-phenyl-1,2,3,6-tetrahydropyridine-induced neurotoxicity. *J Neurosci* 12:1658-1667.

182. Li, Y., Huang, T.T., Carlson, E.J., Melov, S., Ursell, P.C., Olson, J.L., Noble, L.J., Yoshimura, M.P., Berger, C., Chan, P.H., et al. 1995. Dilated cardiomyopathy and neonatal lethality in mutant mice lacking manganese superoxide dismutase. *Nat Genet* 11:376-381.
183. Camello-Almaraz, C., Gomez-Pinilla, P.J., Pozo, M.J., and Camello, P.J. 2006. Mitochondrial reactive oxygen species and Ca2+ signaling. *Am J Physiol Cell Physiol* 291:C1082-1088.
184. Poole, L.B., Karplus, P.A., and Claiborne, A. 2004. Protein sulfenic acids in redox signaling. *Annu Rev Pharmacol Toxicol* 44:325-347.
185. Juarez, J.C., Manuia, M., Burnett, M.E., Betancourt, O., Boivin, B., Shaw, D.E., Tonks, N.K., Mazar, A.P., and Donate, F. 2008. Superoxide dismutase 1 (SOD1) is essential for H2O2-mediated oxidation and inactivation of phosphatases in growth factor signaling. *Proc Natl Acad Sci U S A* 105:7147-7152.
186. Genestra, M. 2007. Oxyl radicals, redox-sensitive signalling cascades and antioxidants. *Cell Signal* 19:1807-1819.
187. Arany, I., Megyesi, J.K., Kaneto, H., Tanaka, S., and Safirstein, R.L. 2004. Activation of ERK or inhibition of JNK ameliorates H(2)O(2) cytotoxicity in mouse renal proximal tubule cells. *Kidney Int* 65:1231-1239.
188. Ichijo, H., Nishida, E., Irie, K., ten Dijke, P., Saitoh, M., Moriguchi, T., Takagi, M., Matsumoto, K., Miyazono, K., and Gotoh, Y. 1997. Induction of apoptosis by ASK1, a mammalian MAPKKK that activates SAPK/JNK and p38 signaling pathways. *Science* 275:90-94.
189. Matsuzawa, A., Nishitoh, H., Tobiume, K., Takeda, K., and Ichijo, H. 2002. Physiological roles of ASK1-mediated signal transduction in oxidative stress- and endoplasmic reticulum stress-induced apoptosis: advanced findings from ASK1 knockout mice. *Antioxid Redox Signal* 4:415-425.
190. Dasgupta, J., Subbaram, S., Connor, K.M., Rodriguez, A.M., Tirosh, O., Beckman, J.S., Jourd'Heuil, D., and Melendez, J.A. 2006. Manganese superoxide dismutase protects from TNF-alpha-induced apoptosis by increasing the steady-state production of H2O2. *Antioxid Redox Signal* 8:1295-1305.
191. Imlay, J.A. 2003. Pathways of oxidative damage. *Annu Rev Microbiol* 57:395-418.
192. Halliwell, B., and Aruoma, O.I. 1991. DNA damage by oxygen-derived species. Its mechanism and measurement in mammalian systems. *FEBS Lett* 281:9-19.
193. Fridovich, I. 1999. Fundamental aspects of reactive oxygen species, or what's the matter with oxygen? *Ann N Y Acad Sci* 893:13-18.
194. Michalik, V., Spotheim Maurizot, M., and Charlier, M. 1995. Calculation of hydroxyl radical attack on different forms of DNA. *J Biomol Struct Dyn* 13:565-575.
195. Zamocky, M., Furtmuller, P.G., and Obinger, C. 2008. Evolution of catalases from bacteria to humans. *Antioxid Redox Signal* 10:1527-1548.
196. Meister, A., and Anderson, M.E. 1983. Glutathione. *Annu Rev Biochem* 52:711-760.

197. Yuan, L., and Kaplowitz, N. 2009. Glutathione in liver diseases and hepatotoxicity. *Mol Aspects Med* 30:29-41.
198. Sies, H. 1999. Glutathione and its role in cellular functions. *Free Radic Biol Med* 27:916-921.
199. Constantopoulos, G., and Barranger, J.A. 1984. Nonenzymatic decarboxylation of pyruvate. *Anal Biochem* 139:353-358.
200. Mallet, R.T., and Sun, J. 2003. Antioxidant properties of myocardial fuels. *Mol Cell Biochem* 253:103-111.
201. Sileri, P., Schena, S., Morini, S., Rastellini, C., Pham, S., Benedetti, E., and Cicalese, L. 2001. Pyruvate inhibits hepatic ischemia-reperfusion injury in rats. *Transplantation* 72:27-30.
202. Cicalese, L., Lee, K., Schraut, W., Watkins, S., Borle, A., and Stanko, R. 1996. Pyruvate prevents ischemia-reperfusion mucosal injury of rat small intestine. *Am J Surg* 171:97-100; discussion 100-101.
203. Wang, X., Perez, E., Liu, R., Yan, L.J., Mallet, R.T., and Yang, S.H. 2007. Pyruvate protects mitochondria from oxidative stress in human neuroblastoma SK-N-SH cells. *Brain Res* 1132:1-9.
204. Desagher, S., Glowinski, J., and Premont, J. 1997. Pyruvate protects neurons against hydrogen peroxide-induced toxicity. *J Neurosci* 17:9060-9067.
205. Warburg, O. 1956. On the origin of cancer cells. *Science* 123:309-314.
206. Guppy, M., Greiner, E., and Brand, K. 1993. The role of the Crabtree effect and an endogenous fuel in the energy metabolism of resting and proliferating thymocytes. *Eur J Biochem* 212:95-99.
207. Fox, C.J., Hammerman, P.S., and Thompson, C.B. 2005. Fuel feeds function: energy metabolism and the T-cell response. *Nat Rev Immunol* 5:844-852.
208. Moreno-Sanchez, R., Rodriguez-Enriquez, S., Marin-Hernandez, A., and Saavedra, E. 2007. Energy metabolism in tumor cells. *FEBS J* 274:1393-1418.
209. Kelloff, G.J., Hoffman, J.M., Johnson, B., Scher, H.I., Siegel, B.A., Cheng, E.Y., Cheson, B.D., O'Shaughnessy, J., Guyton, K.Z., Mankoff, D.A., et al. 2005. Progress and promise of FDG-PET imaging for cancer patient management and oncologic drug development. *Clin Cancer Res* 11:2785-2808.
210. Ramanathan, A., Wang, C., and Schreiber, S.L. 2005. Perturbational profiling of a cell-line model of tumorigenesis by using metabolic measurements. *Proc Natl Acad Sci U S A* 102:5992-5997.
211. Robey, R.B., and Hay, N. 2009. Is Akt the "Warburg kinase"?-Akt-energy metabolism interactions and oncogenesis. *Semin Cancer Biol* 19:25-31.
212. Eskey, C.J., Koretsky, A.P., Domach, M.M., and Jain, R.K. 1993. Role of oxygen vs. glucose in energy metabolism in a mammary carcinoma perfused ex vivo: direct measurement by 31P NMR. *Proc Natl Acad Sci U S A* 90:2646-2650.
213. Zu, X.L., and Guppy, M. 2004. Cancer metabolism: facts, fantasy, and fiction. *Biochem Biophys Res Commun* 313:459-465.

214. Gauthier, T., Denis-Pouxviel, C., and Murat, J.C. 1990. Respiration of mitochondria isolated from differentiated and undifferentiated HT29 colon cancer cells in the presence of various substrates and ADP generating systems. *Int J Biochem* 22:411-417.
215. Rodriguez-Enriquez, S., Vital-Gonzalez, P.A., Flores-Rodriguez, F.L., Marin-Hernandez, A., Ruiz-Azuara, L., and Moreno-Sanchez, R. 2006. Control of cellular proliferation by modulation of oxidative phosphorylation in human and rodent fast-growing tumor cells. *Toxicol Appl Pharmacol* 215:208-217.
216. Lanks, K.W., Hitti, I.F., and Chin, N.W. 1986. Substrate utilization for lactate and energy production by heat-shocked L929 cells. *J Cell Physiol* 127:451-456.
217. Semenza, G.L. 2009. Regulation of cancer cell metabolism by hypoxia-inducible factor 1. *Semin Cancer Biol* 19:12-16.
218. Jiang, B.H., Semenza, G.L., Bauer, C., and Marti, H.H. 1996. Hypoxia-inducible factor 1 levels vary exponentially over a physiologically relevant range of O2 tension. *Am J Physiol* 271:C1172-1180.
219. Ivan, M., Kondo, K., Yang, H., Kim, W., Valiando, J., Ohh, M., Salic, A., Asara, J.M., Lane, W.S., and Kaelin, W.G., Jr. 2001. HIFalpha targeted for VHL-mediated destruction by proline hydroxylation: implications for O2 sensing. *Science* 292:464-468.
220. Jaakkola, P., Mole, D.R., Tian, Y.M., Wilson, M.I., Gielbert, J., Gaskell, S.J., Kriegsheim, A., Hebestreit, H.F., Mukherji, M., Schofield, C.J., et al. 2001. Targeting of HIF-alpha to the von Hippel-Lindau ubiquitylation complex by O2-regulated prolyl hydroxylation. *Science* 292:468-472.
221. Maxwell, P.H., Wiesener, M.S., Chang, G.W., Clifford, S.C., Vaux, E.C., Cockman, M.E., Wykoff, C.C., Pugh, C.W., Maher, E.R., and Ratcliffe, P.J. 1999. The tumour suppressor protein VHL targets hypoxia-inducible factors for oxygen-dependent proteolysis. *Nature* 399:271-275.
222. Haase, V.H. 2009. The VHL tumor suppressor: master regulator of HIF. *Curr Pharm Des* 15:3895-3903.
223. Zhang, H., Gao, P., Fukuda, R., Kumar, G., Krishnamachary, B., Zeller, K.I., Dang, C.V., and Semenza, G.L. 2007. HIF-1 inhibits mitochondrial biogenesis and cellular respiration in VHL-deficient renal cell carcinoma by repression of C-MYC activity. *Cancer Cell* 11:407-420.
224. Wofford, J.A., Wieman, H.L., Jacobs, S.R., Zhao, Y., and Rathmell, J.C. 2008. IL-7 promotes Glut1 trafficking and glucose uptake via STAT5-mediated activation of Akt to support T-cell survival. *Blood* 111:2101-2111.
225. Parsons, R. 2004. Human cancer, PTEN and the PI-3 kinase pathway. *Semin Cell Dev Biol* 15:171-176.
226. Cantley, L.C., and Neel, B.G. 1999. New insights into tumor suppression: PTEN suppresses tumor formation by restraining the phosphoinositide 3-kinase/AKT pathway. *Proc Natl Acad Sci U S A* 96:4240-4245.
227. Kang, S., Bader, A.G., and Vogt, P.K. 2005. Phosphatidylinositol 3-kinase mutations identified in human cancer are oncogenic. *Proc Natl Acad Sci U S A* 102:802-807.

228. Bhaskar, P.T., and Hay, N. 2007. The two TORCs and Akt. *Dev Cell* 12:487-502.
229. Bae, S.S., Cho, H., Mu, J., and Birnbaum, M.J. 2003. Isoform-specific regulation of insulin-dependent glucose uptake by Akt/protein kinase B. *J Biol Chem* 278:49530-49536.
230. Gottlob, K., Majewski, N., Kennedy, S., Kandel, E., Robey, R.B., and Hay, N. 2001. Inhibition of early apoptotic events by Akt/PKB is dependent on the first committed step of glycolysis and mitochondrial hexokinase. *Genes Dev* 15:1406-1418.
231. Frauwirth, K.A., and Thompson, C.B. 2004. Regulation of T lymphocyte metabolism. *J Immunol* 172:4661-4665.
232. Nogueira, V., Park, Y., Chen, C.C., Xu, P.Z., Chen, M.L., Tonic, I., Unterman, T., and Hay, N. 2008. Akt determines replicative senescence and oxidative or oncogenic premature senescence and sensitizes cells to oxidative apoptosis. *Cancer Cell* 14:458-470.
233. Berwick, D.C., Hers, I., Heesom, K.J., Moule, S.K., and Tavare, J.M. 2002. The identification of ATP-citrate lyase as a protein kinase B (Akt) substrate in primary adipocytes. *J Biol Chem* 277:33895-33900.
234. Vaupel, P., and Mayer, A. 2007. Hypoxia in cancer: significance and impact on clinical outcome. *Cancer Metastasis Rev* 26:225-239.
235. Boag, J.M., Beesley, A.H., Firth, M.J., Freitas, J.R., Ford, J., Hoffmann, K., Cummings, A.J., de Klerk, N.H., and Kees, U.R. 2006. Altered glucose metabolism in childhood pre-B acute lymphoblastic leukaemia. *Leukemia* 20:1731-1737.
236. Kostakoglu, L., Leonard, J.P., Coleman, M., and Goldsmith, S.J. 2004. The role of FDG-PET imaging in the management of lymphoma. *Clin Adv Hematol Oncol* 2:115-121.
237. Bellance, N., Benard, G., Furt, F., Begueret, H., Smolkova, K., Passerieux, E., Delage, J.P., Baste, J.M., Moreau, P., and Rossignol, R. 2009. Bioenergetics of lung tumors: alteration of mitochondrial biogenesis and respiratory capacity. *Int J Biochem Cell Biol* 41:2566-2577.
238. Mashima, T., Seimiya, H., and Tsuruo, T. 2009. De novo fatty-acid synthesis and related pathways as molecular targets for cancer therapy. *Br J Cancer* 100:1369-1372.
239. Li, D., Zhu, Y., Tang, Q., Lu, H., Li, H., Yang, Y., Li, Z., and Tong, S. 2009. A new G6PD knockdown tumor-cell line with reduced proliferation and increased susceptibility to oxidative stress. *Cancer Biother Radiopharm* 24:81-90.
240. Rais, B., Comin, B., Puigjaner, J., Brandes, J.L., Creppy, E., Saboureau, D., Ennamany, R., Lee, W.N., Boros, L.G., and Cascante, M. 1999. Oxythiamine and dehydroepiandrosterone induce a G1 phase cycle arrest in Ehrlich's tumor cells through inhibition of the pentose cycle. *FEBS Lett* 456:113-118.
241. Boros, L.G., Puigjaner, J., Cascante, M., Lee, W.N., Brandes, J.L., Bassilian, S., Yusuf, F.I., Williams, R.D., Muscarella, P., Melvin, W.S., et al. 1997. Oxythiamine and dehydroepiandrosterone inhibit the

nonoxidative synthesis of ribose and tumor cell proliferation. *Cancer Res* 57:4242-4248.
242. Le, A., Cooper, C.R., Gouw, A.M., Dinavahi, R., Maitra, A., Deck, L.M., Royer, R.E., Vander Jagt, D.L., Semenza, G.L., and Dang, C.V. Inhibition of lactate dehydrogenase A induces oxidative stress and inhibits tumor progression. *Proc Natl Acad Sci U S A* 107:2037-2042.
243. Fantin, V.R., St-Pierre, J., and Leder, P. 2006. Attenuation of LDH-A expression uncovers a link between glycolysis, mitochondrial physiology, and tumor maintenance. *Cancer Cell* 9:425-434.
244. Lin, X., Zhang, F., Bradbury, C.M., Kaushal, A., Li, L., Spitz, D.R., Aft, R.L., and Gius, D. 2003. 2-Deoxy-D-glucose-induced cytotoxicity and radiosensitization in tumor cells is mediated via disruptions in thiol metabolism. *Cancer Res* 63:3413-3417.
245. Buttgereit, F., Brand, M.D., and Muller, M. 1992. ConA induced changes in energy metabolism of rat thymocytes. *Biosci Rep* 12:381-386.
246. Ardawi, M.S., and Newsholme, E.A. 1984. Metabolism of ketone bodies, oleate and glucose in lymphocytes of the rat. *Biochem J* 221:255-260.
247. Schieke, S.M., Phillips, D., McCoy, J.P., Jr., Aponte, A.M., Shen, R.F., Balaban, R.S., and Finkel, T. 2006. The mammalian target of rapamycin (mTOR) pathway regulates mitochondrial oxygen consumption and oxidative capacity. *J Biol Chem* 281:27643-27652.
248. Cooper, E.H., Barkhan, P., and Hale, A.J. 1963. Observations on the proliferation of human leucocytes cultured with phytohaemagglutinin. *Br J Haematol* 9:101-111.
249. Hedeskov, C.J. 1968. Early effects of phytohaemagglutinin on glucose metabolism of normal human lymphocytes. *Biochem J* 110:373-380.
250. Roos, D., and Loos, J.A. 1970. Changes in the carbohydrate metabolism of mitogenically stimulated human peripheral lymphocytes. I. Stimulation by phytohaemagglutinin. *Biochim Biophys Acta* 222:565-582.
251. Roos, D., and Loos, J.A. 1973. Changes in the carbohydrate metabolism of mitogenically stimulated human peripheral lymphocytes. II. Relative importance of glycolysis and oxidative phosphorylation on phytohaemagglutinin stimulation. *Exp Cell Res* 77:127-135.
252. Brand, K.A., and Hermfisse, U. 1997. Aerobic glycolysis by proliferating cells: a protective strategy against reactive oxygen species. *FASEB J* 11:388-395.
253. Krauss, S., Buttgereit, F., and Brand, M.D. 1999. Effects of the mitogen concanavalin A on pathways of thymocyte energy metabolism. *Biochim Biophys Acta* 1412:129-138.
254. Jones, R.G., Bui, T., White, C., Madesh, M., Krawczyk, C.M., Lindsten, T., Hawkins, B.J., Kubek, S., Frauwirth, K.A., Wang, Y.L., et al. 2007. The proapoptotic factors Bax and Bak regulate T Cell proliferation through control of endoplasmic reticulum Ca(2+) homeostasis. *Immunity* 27:268-280.
255. Parry, R.V., Chemnitz, J.M., Frauwirth, K.A., Lanfranco, A.R., Braunstein, I., Kobayashi, S.V., Linsley, P.S., Thompson, C.B., and Riley, J.L. 2005.

CTLA-4 and PD-1 receptors inhibit T-cell activation by distinct mechanisms. *Mol Cell Biol* 25:9543-9553.
256. Buttgereit, F., and Brand, M.D. 1995. A hierarchy of ATP-consuming processes in mammalian cells. *Biochem J* 312 (Pt 1):163-167.
257. Tripmacher, R., Gaber, T., Dziurla, R., Haupl, T., Erekul, K., Grutzkau, A., Tschirschmann, M., Scheffold, A., Radbruch, A., Burmester, G.R., et al. 2008. Human CD4(+) T cells maintain specific functions even under conditions of extremely restricted ATP production. *Eur J Immunol* 38:1631-1642.
258. Moreau, B., Nelson, C., and Parekh, A.B. 2006. Biphasic regulation of mitochondrial Ca2+ uptake by cytosolic Ca2+ concentration. *Curr Biol* 16:1672-1677.
259. McCormack, J.G., Halestrap, A.P., and Denton, R.M. 1990. Role of calcium ions in regulation of mammalian intramitochondrial metabolism. *Physiol Rev* 70:391-425.
260. Robb-Gaspers, L.D., Burnett, P., Rutter, G.A., Denton, R.M., Rizzuto, R., and Thomas, A.P. 1998. Integrating cytosolic calcium signals into mitochondrial metabolic responses. *Embo J* 17:4987-5000.
261. Tamas, P., Hawley, S.A., Clarke, R.G., Mustard, K.J., Green, K., Hardie, D.G., and Cantrell, D.A. 2006. Regulation of the energy sensor AMP-activated protein kinase by antigen receptor and Ca2+ in T lymphocytes. *J Exp Med* 203:1665-1670.
262. Lee, W.J., Kim, M., Park, H.S., Kim, H.S., Jeon, M.J., Oh, K.S., Koh, E.H., Won, J.C., Kim, M.S., Oh, G.T., et al. 2006. AMPK activation increases fatty acid oxidation in skeletal muscle by activating PPARalpha and PGC-1. *Biochem Biophys Res Commun* 340:291-295.
263. Hardie, D.G. 2007. AMP-activated/SNF1 protein kinases: conserved guardians of cellular energy. *Nat Rev Mol Cell Biol* 8:774-785.
264. D'Souza, A.D., Parikh, N., Kaech, S.M., and Shadel, G.S. 2007. Convergence of multiple signaling pathways is required to coordinately up-regulate mtDNA and mitochondrial biogenesis during T cell activation. *Mitochondrion* 7:374-385.
265. Pendergrass, W., Wolf, N., and Poot, M. 2004. Efficacy of MitoTracker Green and CMXrosamine to measure changes in mitochondrial membrane potentials in living cells and tissues. *Cytometry A* 61:162-169.
266. Doughty, C.A., Bleiman, B.F., Wagner, D.J., Dufort, F.J., Mataraza, J.M., Roberts, M.F., and Chiles, T.C. 2006. Antigen receptor-mediated changes in glucose metabolism in B lymphocytes: role of phosphatidylinositol 3-kinase signaling in the glycolytic control of growth. *Blood* 107:4458-4465.
267. Jacobson, D.L., Gange, S.J., Rose, N.R., and Graham, N.M. 1997. Epidemiology and estimated population burden of selected autoimmune diseases in the United States. *Clin Immunol Immunopathol* 84:223-243.
268. Wakeland, E.K., Liu, K., Graham, R.R., and Behrens, T.W. 2001. Delineating the genetic basis of systemic lupus erythematosus. *Immunity* 15:397-408.

269. Tan, E.M., Cohen, A.S., Fries, J.F., Masi, A.T., McShane, D.J., Rothfield, N.F., Schaller, J.G., Talal, N., and Winchester, R.J. 1982. The 1982 revised criteria for the classification of systemic lupus erythematosus. *Arthritis Rheum* 25:1271-1277.
270. Sullivan, K.E. 2000. Genetics of systemic lupus erythematosus. Clinical implications. *Rheum Dis Clin North Am* 26:229-256, v-vi.
271. Deapen, D., Escalante, A., Weinrib, L., Horwitz, D., Bachman, B., Roy-Burman, P., Walker, A., and Mack, T.M. 1992. A revised estimate of twin concordance in systemic lupus erythematosus. *Arthritis Rheum* 35:311-318.
272. Mohan, C., Alas, E., Morel, L., Yang, P., and Wakeland, E.K. 1998. Genetic dissection of SLE pathogenesis. Sle1 on murine chromosome 1 leads to a selective loss of tolerance to H2A/H2B/DNA subnucleosomes. *J Clin Invest* 101:1362-1372.
273. Mohan, C., Morel, L., Yang, P., and Wakeland, E.K. 1997. Genetic dissection of systemic lupus erythematosus pathogenesis: Sle2 on murine chromosome 4 leads to B cell hyperactivity. *J Immunol* 159:454-465.
274. Mohan, C., Yu, Y., Morel, L., Yang, P., and Wakeland, E.K. 1999. Genetic dissection of Sle pathogenesis: Sle3 on murine chromosome 7 impacts T cell activation, differentiation, and cell death. *J Immunol* 162:6492-6502.
275. Morel, L., Croker, B.P., Blenman, K.R., Mohan, C., Huang, G., Gilkeson, G., and Wakeland, E.K. 2000. Genetic reconstitution of systemic lupus erythematosus immunopathology with polycongenic murine strains. *Proc Natl Acad Sci U S A* 97:6670-6675.
276. Borchers, A.T., Keen, C.L., and Gershwin, M.E. 2007. Drug-induced lupus. *Ann N Y Acad Sci* 1108:166-182.
277. Quddus, J., Johnson, K.J., Gavalchin, J., Amento, E.P., Chrisp, C.E., Yung, R.L., and Richardson, B.C. 1993. Treating activated CD4+ T cells with either of two distinct DNA methyltransferase inhibitors, 5-azacytidine or procainamide, is sufficient to cause a lupus-like disease in syngeneic mice. *J Clin Invest* 92:38-53.
278. Wardemann, H., Yurasov, S., Schaefer, A., Young, J.W., Meffre, E., and Nussenzweig, M.C. 2003. Predominant autoantibody production by early human B cell precursors. *Science* 301:1374-1377.
279. Lieby, P., Soley, A., Knapp, A.M., Cerutti, M., Freyssinet, J.M., Pasquali, J.L., and Martin, T. 2003. Memory B cells producing somatically mutated antiphospholipid antibodies are present in healthy individuals. *Blood* 102:2459-2465.
280. Anolik, J., and Sanz, I. 2004. B cells in human and murine systemic lupus erythematosus. *Curr Opin Rheumatol* 16:505-512.
281. Theofilopoulos, A.N., and Dixon, F.J. 1985. Murine models of systemic lupus erythematosus. *Adv Immunol* 37:269-390.
282. Klinman, D.M. 1997. B-cell abnormalities characteristic of systemic lupus erythematosus. In *Dubois' Lupus Erythematosus*. D.J. Wallace, and B.H. Hahn, editors. Baltimore: Williams and Wilkins. 195-206.

283. Klinman, D.M. 1990. Polyclonal B cell activation in lupus-prone mice precedes and predicts the development of autoimmune disease. *J Clin Invest* 86:1249-1254.
284. Desai-Mehta, A., Lu, L., Ramsey-Goldman, R., and Datta, S.K. 1996. Hyperexpression of CD40 ligand by B and T cells in human lupus and its role in pathogenic autoantibody production. *J Clin Invest* 97:2063-2073.
285. Liebig, T.M., Fiedler, A., Klein-Gonzalez, N., Shimabukuro-Vornhagen, A., and von Bergwelt-Baildon, M. Murine model of CD40-activation of B cells. *J Vis Exp*.
286. Datta, S.K. 1998. Production of pathogenic antibodies: cognate interactions between autoimmune T and B cells. *Lupus* 7:591-596.
287. Mohan, C., Shi, Y., Laman, J.D., and Datta, S.K. 1995. Interaction between CD40 and its ligand gp39 in the development of murine lupus nephritis. *J Immunol* 154:1470-1480.
288. Ono, M., Bolland, S., Tempst, P., and Ravetch, J.V. 1996. Role of the inositol phosphatase SHIP in negative regulation of the immune system by the receptor Fc(gamma)RIIB. *Nature* 383:263-266.
289. Mackay, M., Stanevsky, A., Wang, T., Aranow, C., Li, M., Koenig, S., Ravetch, J.V., and Diamond, B. 2006. Selective dysregulation of the FcgammaIIB receptor on memory B cells in SLE. *J Exp Med* 203:2157-2164.
290. Floto, R.A., Clatworthy, M.R., Heilbronn, K.R., Rosner, D.R., MacAry, P.A., Rankin, A., Lehner, P.J., Ouwehand, W.H., Allen, J.M., Watkins, N.A., et al. 2005. Loss of function of a lupus-associated FcgammaRIIb polymorphism through exclusion from lipid rafts. *Nat Med* 11:1056-1058.
291. Kyogoku, C., Dijstelbloem, H.M., Tsuchiya, N., Hatta, Y., Kato, H., Yamaguchi, A., Fukazawa, T., Jansen, M.D., Hashimoto, H., van de Winkel, J.G., et al. 2002. Fcgamma receptor gene polymorphisms in Japanese patients with systemic lupus erythematosus: contribution of FCGR2B to genetic susceptibility. *Arthritis Rheum* 46:1242-1254.
292. De Silva-Udawatta, M., Kumar, S.R., Greidinger, E.L., and Hoffman, R.W. 2004. Cloned human TCR from patients with autoimmune disease can respond to two structurally distinct autoantigens. *J Immunol* 172:3940-3947.
293. Hoffman, R.W., Takeda, Y., Sharp, G.C., Lee, D.R., Hill, D.L., Kaneoka, H., and Caldwell, C.W. 1993. Human T cell clones reactive against U-small nuclear ribonucleoprotein autoantigens from connective tissue disease patients and healthy individuals. *J Immunol* 151:6460-6469.
294. Datta, S.K., Patel, H., and Berry, D. 1987. Induction of a cationic shift in IgG anti-DNA autoantibodies. Role of T helper cells with classical and novel phenotypes in three murine models of lupus nephritis. *J Exp Med* 165:1252-1268.
295. Sainis, K., and Datta, S.K. 1988. CD4+ T cell lines with selective patterns of autoreactivity as well as CD4- CD8- T helper cell lines augment the production of idiotypes shared by pathogenic anti-DNA autoantibodies in the NZB x SWR model of lupus nephritis. *J Immunol* 140:2215-2224.

296. Shlomchik, M.J., Craft, J.E., and Mamula, M.J. 2001. From T to B and back again: positive feedback in systemic autoimmune disease. *Nat Rev Immunol* 1:147-153.
297. Schwartz, R.H. 2003. T cell anergy. *Annu Rev Immunol* 21:305-334.
298. Janeway, C.A., Jr., and Medzhitov, R. 2002. Innate immune recognition. *Annu Rev Immunol* 20:197-216.
299. Datta, S.K., Zhang, L., and Xu, L. 2005. T-helper cell intrinsic defects in lupus that break peripheral tolerance to nuclear autoantigens. *J Mol Med* 83:267-278.
300. Zielinski, C.E., Jacob, S.N., Bouzahzah, F., Ehrlich, B.E., and Craft, J. 2005. Naive CD4+ T cells from lupus-prone Fas-intact MRL mice display TCR-mediated hyperproliferation due to intrinsic threshold defects in activation. *J Immunol* 174:5100-5109.
301. Vratsanos, G.S., Jung, S., Park, Y.M., and Craft, J. 2001. CD4(+) T cells from lupus-prone mice are hyperresponsive to T cell receptor engagement with low and high affinity peptide antigens: a model to explain spontaneous T cell activation in lupus. *J Exp Med* 193:329-337.
302. Nagy, G., Barcza, M., Gonchoroff, N., Phillips, P.E., and Perl, A. 2004. Nitric oxide-dependent mitochondrial biogenesis generates Ca2+ signaling profile of lupus T cells. *J Immunol* 173:3676-3683.
303. Bouzahzah, F., Jung, S., and Craft, J. 2003. CD4+ T cells from lupus-prone mice avoid antigen-specific tolerance induction in vivo. *J Immunol* 170:741-748.
304. Green, D.R., Droin, N., and Pinkoski, M. 2003. Activation-induced cell death in T cells. *Immunol Rev* 193:70-81.
305. Brunner, T., Mogil, R.J., LaFace, D., Yoo, N.J., Mahboubi, A., Echeverri, F., Martin, S.J., Force, W.R., Lynch, D.H., Ware, C.F., et al. 1995. Cell-autonomous Fas (CD95)/Fas-ligand interaction mediates activation-induced apoptosis in T-cell hybridomas. *Nature* 373:441-444.
306. Dhein, J., Walczak, H., Baumler, C., Debatin, K.M., and Krammer, P.H. 1995. Autocrine T-cell suicide mediated by APO-1/(Fas/CD95). *Nature* 373:438-441.
307. Ju, S.T., Panka, D.J., Cui, H., Ettinger, R., el-Khatib, M., Sherr, D.H., Stanger, B.Z., and Marshak-Rothstein, A. 1995. Fas(CD95)/FasL interactions required for programmed cell death after T-cell activation. *Nature* 373:444-448.
308. Ow, Y.P., Green, D.R., Hao, Z., and Mak, T.W. 2008. Cytochrome c: functions beyond respiration. *Nat Rev Mol Cell Biol* 9:532-542.
309. Vaishnaw, A.K., Toubi, E., Ohsako, S., Drappa, J., Buys, S., Estrada, J., Sitarz, A., Zemel, L., Chu, J.L., and Elkon, K.B. 1999. The spectrum of apoptotic defects and clinical manifestations, including systemic lupus erythematosus, in humans with CD95 (Fas/APO-1) mutations. *Arthritis Rheum* 42:1833-1842.
310. Kovacs, B., Vassilopoulos, D., Vogelgesang, S.A., and Tsokos, G.C. 1996. Defective CD3-mediated cell death in activated T cells from patients

with systemic lupus erythematosus: role of decreased intracellular TNF-alpha. *Clin Immunol Immunopathol* 81:293-302.
311. Xu, L., Zhang, L., Yi, Y., Kang, H.K., and Datta, S.K. 2004. Human lupus T cells resist inactivation and escape death by upregulating COX-2. *Nat Med* 10:411-415.
312. Bagnoli, M., Canevari, S., and Mezzanzanica, D. Cellular FLICE-inhibitory protein (c-FLIP) signalling: a key regulator of receptor-mediated apoptosis in physiologic context and in cancer. *Int J Biochem Cell Biol* 42:210-213.
313. Koffler, D., Schur, P.H., and Kunkel, H.G. 1967. Immunological studies concerning the nephritis of systemic lupus erythematosus. *J Exp Med* 126:607-624.
314. Amoura, Z., Koutouzov, S., Chabre, H., Cacoub, P., Amoura, I., Musset, L., Bach, J.F., and Piette, J.C. 2000. Presence of antinucleosome autoantibodies in a restricted set of connective tissue diseases: antinucleosome antibodies of the IgG3 subclass are markers of renal pathogenicity in systemic lupus erythematosus. *Arthritis Rheum* 43:76-84.
315. Berden, J.H., Licht, R., van Bruggen, M.C., and Tax, W.J. 1999. Role of nucleosomes for induction and glomerular binding of autoantibodies in lupus nephritis. *Curr Opin Nephrol Hypertens* 8:299-306.
316. Kramers, C., Hylkema, M.N., van Bruggen, M.C., van de Lagemaat, R., Dijkman, H.B., Assmann, K.J., Smeenk, R.J., and Berden, J.H. 1994. Anti-nucleosome antibodies complexed to nucleosomal antigens show anti-DNA reactivity and bind to rat glomerular basement membrane in vivo. *J Clin Invest* 94:568-577.
317. Mostoslavsky, G., Fischel, R., Yachimovich, N., Yarkoni, Y., Rosenmann, E., Monestier, M., Baniyash, M., and Eilat, D. 2001. Lupus anti-DNA autoantibodies cross-react with a glomerular structural protein: a case for tissue injury by molecular mimicry. *Eur J Immunol* 31:1221-1227.
318. Helyer, B.J., and Howie, J.B. 1963. Spontaneous auto-immune disease in NZB/BL mice. *Br J Haematol* 9:119-131.
319. Helyer, B.J., and Howie, J.B. 1963. Renal disease associated with positive lupus erythematosus tests in a cross-bred strain of mice. *Nature* 197:197.
320. Andrews, B.S., Eisenberg, R.A., Theofilopoulos, A.N., Izui, S., Wilson, C.B., McConahey, P.J., Murphy, E.D., Roths, J.B., and Dixon, F.J. 1978. Spontaneous murine lupus-like syndromes. Clinical and immunopathological manifestations in several strains. *J Exp Med* 148:1198-1215.
321. Roubinian, J.R., Talal, N., Greenspan, J.S., Goodman, J.R., and Siiteri, P.K. 1978. Effect of castration and sex hormone treatment on survival, anti-nucleic acid antibodies, and glomerulonephritis in NZB/NZW F1 mice. *J Exp Med* 147:1568-1583.
322. Munns, T.W., Liszewski, M.K., and Hahn, B.H. 1984. Antibody-nucleic acid complexes. Conformational and base specificities associated with spontaneously occurring poly- and monoclonal anti-DNA antibodies from autoimmune mice. *Biochemistry* 23:2964-2970.

323. Howie, J.B., and Helyer, B.J. 1968. The immunology and pathology of NZB mice. *Adv Immunol* 9:215-266.
324. Wofsy, D., and Seaman, W.E. 1985. Successful treatment of autoimmunity in NZB/NZW F1 mice with monoclonal antibody to L3T4. *J Exp Med* 161:378-391.
325. Carteron, N.L., Schimenti, C.L., and Wofsy, D. 1989. Treatment of murine lupus with F(ab')2 fragments of monoclonal antibody to L3T4. Suppression of autoimmunity does not depend on T helper cell depletion. *J Immunol* 142:1470-1475.
326. Wofsy, D., and Seaman, W.E. 1987. Reversal of advanced murine lupus in NZB/NZW F1 mice by treatment with monoclonal antibody to L3T4. *J Immunol* 138:3247-3253.
327. Haas, K.M., Watanabe, R., Matsushita, T., Nakashima, H., Ishiura, N., Okochi, H., Fujimoto, M., and Tedder, T.F. Protective and pathogenic roles for B cells during systemic autoimmunity in NZB/W F1 mice. *J Immunol* 184:4789-4800.
328. Beeton, C., Wulff, H., Barbaria, J., Clot-Faybesse, O., Pennington, M., Bernard, D., Cahalan, M.D., Chandy, K.G., and Beraud, E. 2001. Selective blockade of T lymphocyte K(+) channels ameliorates experimental autoimmune encephalomyelitis, a model for multiple sclerosis. *Proc Natl Acad Sci U S A* 98:13942-13947.
329. Decker, P., Kotter, I., Klein, R., Berner, B., and Rammensee, H.G. 2006. Monocyte-derived dendritic cells over-express CD86 in patients with systemic lupus erythematosus. *Rheumatology (Oxford)* 45:1087-1095.
330. Folzenlogen, D., Hofer, M.F., Leung, D.Y., Freed, J.H., and Newell, M.K. 1997. Analysis of CD80 and CD86 expression on peripheral blood B lymphocytes reveals increased expression of CD86 in lupus patients. *Clin Immunol Immunopathol* 83:199-204.
331. Koshy, M., Berger, D., and Crow, M.K. 1996. Increased expression of CD40 ligand on systemic lupus erythematosus lymphocytes. *J Clin Invest* 98:826-837.
332. Vallejo, A.N. 2005. CD28 extinction in human T cells: altered functions and the program of T-cell senescence. *Immunol Rev* 205:158-169.
333. Wulff, H., Calabresi, P.A., Allie, R., Yun, S., Pennington, M., Beeton, C., and Chandy, K.G. 2003. The voltage-gated Kv1.3 K(+) channel in effector memory T cells as new target for MS. *J Clin Invest* 111:1703-1713.
334. Benke, P.J., Drisko, J., and Ahmad, P. 1991. Increased oxidative metabolism in phytohemagglutinin-stimulated lymphocytes from patients with systemic lupus erythematosus is associated with serum SSA antibody. *Biochem Med Metab Biol* 45:28-40.
335. Kuhnke, A., Burmester, G.R., Krauss, S., and Buttgereit, F. 2003. Bioenergetics of immune cells to assess rheumatic disease activity and efficacy of glucocorticoid treatment. *Ann Rheum Dis* 62:133-139.
336. Hitchon, C.A., and El-Gabalawy, H.S. 2004. Oxidation in rheumatoid arthritis. *Arthritis Res Ther* 6:265-278.

337. Zhou, Q., Mrowietz, U., and Rostami-Yazdi, M. 2009. Oxidative stress in the pathogenesis of psoriasis. *Free Radic Biol Med* 47:891-905.
338. Nicholls, D.G. 2006. Simultaneous monitoring of ionophore- and inhibitor-mediated plasma and mitochondrial membrane potential changes in cultured neurons. *J Biol Chem* 281:14864-14874.
339. Gergely, P., Jr., Grossman, C., Niland, B., Puskas, F., Neupane, H., Allam, F., Banki, K., Phillips, P.E., and Perl, A. 2002. Mitochondrial hyperpolarization and ATP depletion in patients with systemic lupus erythematosus. *Arthritis Rheum* 46:175-190.
340. Benov, L., Sztejnberg, L., and Fridovich, I. 1998. Critical evaluation of the use of hydroethidine as a measure of superoxide anion radical. *Free Radic Biol Med* 25:826-831.
341. Gergely, P., Jr., Niland, B., Gonchoroff, N., Pullmann, R., Jr., Phillips, P.E., and Perl, A. 2002. Persistent mitochondrial hyperpolarization, increased reactive oxygen intermediate production, and cytoplasmic alkalinization characterize altered IL-10 signaling in patients with systemic lupus erythematosus. *J Immunol* 169:1092-1101.
342. Jones, R.G., and Thompson, C.B. 2007. Revving the engine: signal transduction fuels T cell activation. *Immunity* 27:173-178.
343. Papadopoulos, M.C., Koumenis, I.L., Dugan, L.L., and Giffard, R.G. 1997. Vulnerability to glucose deprivation injury correlates with glutathione levels in astrocytes. *Brain Res* 748:151-156.
344. Walsh, A.C., Michaud, S.G., Malossi, J.A., and Lawrence, D.A. 1995. Glutathione depletion in human T lymphocytes: analysis of activation-associated gene expression and the stress response. *Toxicol Appl Pharmacol* 133:249-261.
345. Ohsako, S., Hara, M., Harigai, M., Fukasawa, C., and Kashiwazaki, S. 1994. Expression and function of Fas antigen and bcl-2 in human systemic lupus erythematosus lymphocytes. *Clin Immunol Immunopathol* 73:109-114.
346. Beeton, C., Wulff, H., Standifer, N.E., Azam, P., Mullen, K.M., Pennington, M.W., Kolski-Andreaco, A., Wei, E., Grino, A., Counts, D.R., et al. 2006. Kv1.3 channels are a therapeutic target for T cell-mediated autoimmune diseases. *Proc Natl Acad Sci U S A* 103:17414-17419.
347. Vallejo, A.N., Bryl, E., Klarskov, K., Naylor, S., Weyand, C.M., and Goronzy, J.J. 2002. Molecular basis for the loss of CD28 expression in senescent T cells. *J Biol Chem* 277:46940-46949.
348. Vallejo, A.N., Brandes, J.C., Weyand, C.M., and Goronzy, J.J. 1999. Modulation of CD28 expression: distinct regulatory pathways during activation and replicative senescence. *J Immunol* 162:6572-6579.
349. Markovic-Plese, S., Cortese, I., Wandinger, K.P., McFarland, H.F., and Martin, R. 2001. CD4+CD28- costimulation-independent T cells in multiple sclerosis. *J Clin Invest* 108:1185-1194.
350. Martens, P.B., Goronzy, J.J., Schaid, D., and Weyand, C.M. 1997. Expansion of unusual CD4+ T cells in severe rheumatoid arthritis. *Arthritis Rheum* 40:1106-1114.

351. Honda, M., Mengesha, E., Albano, S., Nichols, W.S., Wallace, D.J., Metzger, A., Klinenberg, J.R., and Linker-Israeli, M. 2001. Telomere shortening and decreased replicative potential, contrasted by continued proliferation of telomerase-positive CD8+CD28(lo) T cells in patients with systemic lupus erythematosus. *Clin Immunol* 99:211-221.
352. Kaneko, H., Saito, K., Hashimoto, H., Yagita, H., Okumura, K., and Azuma, M. 1996. Preferential elimination of CD28+ T cells in systemic lupus erythematosus (SLE) and the relation with activation-induced apoptosis. *Clin Exp Immunol* 106:218-229.
353. Schmidt, D., Goronzy, J.J., and Weyand, C.M. 1996. CD4+ CD7- CD28- T cells are expanded in rheumatoid arthritis and are characterized by autoreactivity. *J Clin Invest* 97:2027-2037.
354. Park, W., Weyand, C.M., Schmidt, D., and Goronzy, J.J. 1997. Co-stimulatory pathways controlling activation and peripheral tolerance of human CD4+CD28- T cells. *Eur J Immunol* 27:1082-1090.
355. Liu, Y., Chen, Y., and Richardson, B. 2009. Decreased DNA methyltransferase levels contribute to abnormal gene expression in "senescent" CD4(+)CD28(-) T cells. *Clin Immunol* 132:257-265.
356. Rajagopalan, S., Fu, J., and Long, E.O. 2001. Cutting edge: induction of IFN-gamma production but not cytotoxicity by the killer cell Ig-like receptor KIR2DL4 (CD158d) in resting NK cells. *J Immunol* 167:1877-1881.
357. Katz, J., Lee, W.N., Wals, P.A., and Bergner, E.A. 1989. Studies of glycogen synthesis and the Krebs cycle by mass isotopomer analysis with [U-13C]glucose in rats. *J Biol Chem* 264:12994-13004.
358. Jongstra-Bilen, J., Vukusic, B., Boras, K., and Wither, J.E. 1997. Resting B cells from autoimmune lupus-prone New Zealand Black and (New Zealand Black x New Zealand White)F1 mice are hyper-responsive to T cell-derived stimuli. *J Immunol* 159:5810-5820.
359. Ye, Y.L., Suen, J.L., Chen, Y.Y., and Chiang, B.L. 1998. Phenotypic and functional analysis of activated B cells of autoimmune NZB x NZW F1 mice. *Scand J Immunol* 47:122-126.
360. Pawelec, G., Rehbein, A., Haehnel, K., Merl, A., and Adibzadeh, M. 1997. Human T-cell clones in long-term culture as a model of immunosenescence. *Immunol Rev* 160:31-42.
361. Beger, R.D., Hansen, D.K., Schnackenberg, L.K., Cross, B.M., Fatollahi, J.J., Lagunero, F.T., Sarnyai, Z., and Boros, L.G. 2009. Single valproic acid treatment inhibits glycogen and RNA ribose turnover while disrupting glucose-derived cholesterol synthesis in liver as revealed by the [U-C(6)]-d-glucose tracer in mice. *Metabolomics* 5:336-345.
362. Maechler, P., Kennedy, E.D., Pozzan, T., and Wollheim, C.B. 1997. Mitochondrial activation directly triggers the exocytosis of insulin in permeabilized pancreatic beta-cells. *EMBO J* 16:3833-3841.
363. Lee, W.N., Boros, L.G., Puigjaner, J., Bassilian, S., Lim, S., and Cascante, M. 1998. Mass isotopomer study of the nonoxidative pathways of the pentose cycle with [1,2-13C2]glucose. *Am J Physiol* 274:E843-851.

364. Boros, L.G., Steinkamp, M.P., Fleming, J.C., Lee, W.N., Cascante, M., and Neufeld, E.J. 2003. Defective RNA ribose synthesis in fibroblasts from patients with thiamine-responsive megaloblastic anemia (TRMA). *Blood* 102:3556-3561.
365. Lee, W.N., Guo, P., Lim, S., Bassilian, S., Lee, S.T., Boren, J., Cascante, M., Go, V.L., and Boros, L.G. 2004. Metabolic sensitivity of pancreatic tumour cell apoptosis to glycogen phosphorylase inhibitor treatment. *Br J Cancer* 91:2094-2100.
366. Chen, Y., Gorelik, G.J., Strickland, F.M., and Richardson, B.C. 2009. Decreased ERK and JNK signaling contribute to gene overexpression in "senescent" CD4+CD28- T cells through epigenetic mechanisms. *J Leukoc Biol*.
367. Homann, D., Teyton, L., and Oldstone, M.B. 2001. Differential regulation of antiviral T-cell immunity results in stable CD8+ but declining CD4+ T-cell memory. *Nat Med* 7:913-919.
368. Foulds, K.E., Zenewicz, L.A., Shedlock, D.J., Jiang, J., Troy, A.E., and Shen, H. 2002. Cutting edge: CD4 and CD8 T cells are intrinsically different in their proliferative responses. *J Immunol* 168:1528-1532.
369. Seder, R.A., and Ahmed, R. 2003. Similarities and differences in CD4+ and CD8+ effector and memory T cell generation. *Nat Immunol* 4:835-842.
370. Buttgereit, F., Burmester, G.R., and Brand, M.D. 2000. Therapeutically targeting lymphocyte energy metabolism by high-dose glucocorticoids. *Biochem Pharmacol* 59:597-603.
371. Lukashev, D., Caldwell, C., Ohta, A., Chen, P., and Sitkovsky, M. 2001. Differential regulation of two alternatively spliced isoforms of hypoxia-inducible factor-1 alpha in activated T lymphocytes. *J Biol Chem* 276:48754-48763.
372. Lum, J.J., Bui, T., Gruber, M., Gordan, J.D., DeBerardinis, R.J., Covello, K.L., Simon, M.C., and Thompson, C.B. 2007. The transcription factor HIF-1alpha plays a critical role in the growth factor-dependent regulation of both aerobic and anaerobic glycolysis. *Genes Dev* 21:1037-1049.
373. Vander Heiden, M.G., Plas, D.R., Rathmell, J.C., Fox, C.J., Harris, M.H., and Thompson, C.B. 2001. Growth factors can influence cell growth and survival through effects on glucose metabolism. *Mol Cell Biol* 21:5899-5912.
374. Semenza, G.L., Jiang, B.H., Leung, S.W., Passantino, R., Concordet, J.P., Maire, P., and Giallongo, A. 1996. Hypoxia response elements in the aldolase A, enolase 1, and lactate dehydrogenase A gene promoters contain essential binding sites for hypoxia-inducible factor 1. *J Biol Chem* 271:32529-32537.
375. Papandreou, I., Cairns, R.A., Fontana, L., Lim, A.L., and Denko, N.C. 2006. HIF-1 mediates adaptation to hypoxia by actively downregulating mitochondrial oxygen consumption. *Cell Metab* 3:187-197.
376. Aulwurm, U.R., and Brand, K.A. 2000. Increased formation of reactive oxygen species due to glucose depletion in primary cultures of rat thymocytes inhibits proliferation. *Eur J Biochem* 267:5693-5698.

377. Moroni, G., Novembrino, C., Quaglini, S., De Giuseppe, R., Gallelli, B., Uva, V., Montanari, V., Messa, P., and Bamonti, F. 2009. Oxidative stress and homocysteine metabolism in patients with lupus nephritis. *Lupus*.
378. Boveris, A., and Chance, B. 1973. The mitochondrial generation of hydrogen peroxide. General properties and effect of hyperbaric oxygen. *Biochem J* 134:707-716.
379. Perl, A., Gergely, P., Jr., and Banki, K. 2004. Mitochondrial dysfunction in T cells of patients with systemic lupus erythematosus. *Int Rev Immunol* 23:293-313.
380. Bobe, P., Bonardelle, D., Benihoud, K., Opolon, P., and Chelbi-Alix, M.K. 2006. Arsenic trioxide: A promising novel therapeutic agent for lymphoproliferative and autoimmune syndromes in MRL/lpr mice. *Blood* 108:3967-3975.
381. Perl, A., Gergely, P., Jr., Nagy, G., Koncz, A., and Banki, K. 2004. Mitochondrial hyperpolarization: a checkpoint of T-cell life, death and autoimmunity. *Trends Immunol* 25:360-367.
382. Barber, D.F., Bartolome, A., Hernandez, C., Flores, J.M., Redondo, C., Fernandez-Arias, C., Camps, M., Ruckle, T., Schwarz, M.K., Rodriguez, S., et al. 2005. PI3Kgamma inhibition blocks glomerulonephritis and extends lifespan in a mouse model of systemic lupus. *Nat Med* 11:933-935.
383. Xie, C., Patel, R., Wu, T., Zhu, J., Henry, T., Bhaskarabhatla, M., Samudrala, R., Tus, K., Gong, Y., Zhou, H., et al. 2007. PI3K/AKT/mTOR hypersignaling in autoimmune lymphoproliferative disease engendered by the epistatic interplay of Sle1b and FASlpr. *Int Immunol* 19:509-522.
384. Ramanathan, A., and Schreiber, S.L. 2009. Direct control of mitochondrial function by mTOR. *Proc Natl Acad Sci U S A* 106:22229-22232.
385. Cunningham, J.T., Rodgers, J.T., Arlow, D.H., Vazquez, F., Mootha, V.K., and Puigserver, P. 2007. mTOR controls mitochondrial oxidative function through a YY1-PGC-1alpha transcriptional complex. *Nature* 450:736-740.
386. Wardman, P. 2007. Fluorescent and luminescent probes for measurement of oxidative and nitrosative species in cells and tissues: progress, pitfalls, and prospects. *Free Radic Biol Med* 43:995-1022.
387. Weng, N.P., Akbar, A.N., and Goronzy, J. 2009. CD28(-) T cells: their role in the age-associated decline of immune function. *Trends Immunol* 30:306-312.
388. Hirashima, M., Fukazawa, T., Abe, K., Morita, Y., Kusaoi, M., and Hashimoto, H. 2004. Expression and activity analyses of CTLA4 in peripheral blood lymphocytes in systemic lupus erythematosus patients. *Lupus* 13:24-31.
389. Sharpe, A.H., Wherry, E.J., Ahmed, R., and Freeman, G.J. 2007. The function of programmed cell death 1 and its ligands in regulating autoimmunity and infection. *Nat Immunol* 8:239-245.
390. Wu, T., Qin, X., Kurepa, Z., Kumar, K.R., Liu, K., Kanta, H., Zhou, X.J., Satterthwaite, A.B., Davis, L.S., and Mohan, C. 2007. Shared signaling

networks active in B cells isolated from genetically distinct mouse models of lupus. *J Clin Invest* 117:2186-2196.
391. Tuscano, J.M., Hsu, T.C., McKnight, H., Ansari, A.A., and Gershwin, M.E. 2002. Phosphorylation abnormalities: NZB mice exhibit a B-cell signalling defect. *J Autoimmun* 19:103-109.
392. Kojima, H., Gu, H., Nomura, S., Caldwell, C.C., Kobata, T., Carmeliet, P., Semenza, G.L., and Sitkovsky, M.V. 2002. Abnormal B lymphocyte development and autoimmunity in hypoxia-inducible factor 1alpha -deficient chimeric mice. *Proc Natl Acad Sci U S A* 99:2170-2174.
393. Ahmed, N.N., Grimes, H.L., Bellacosa, A., Chan, T.O., and Tsichlis, P.N. 1997. Transduction of interleukin-2 antiapoptotic and proliferative signals via Akt protein kinase. *Proc Natl Acad Sci U S A* 94:3627-3632.
394. Kelly, E., Won, A., Refaeli, Y., and Van Parijs, L. 2002. IL-2 and related cytokines can promote T cell survival by activating AKT. *J Immunol* 168:597-603.
395. Bednarski, J.J., Warner, R.E., Rao, T., Leonetti, F., Yung, R., Richardson, B.C., Johnson, K.J., Ellman, J.A., Opipari, A.W., Jr., and Glick, G.D. 2003. Attenuation of autoimmune disease in Fas-deficient mice by treatment with a cytotoxic benzodiazepine. *Arthritis Rheum* 48:757-766.
396. Boumezbeur, F., Besret, L., Valette, J., Gregoire, M.C., Delzescaux, T., Maroy, R., Vaufrey, F., Gervais, P., Hantraye, P., Bloch, G., et al. 2005. Glycolysis versus TCA cycle in the primate brain as measured by combining 18F-FDG PET and 13C-NMR. *J Cereb Blood Flow Metab* 25:1418-1423.
397. Gautier, J.F., Pirnay, F., Lacroix, M., Mosora, F., Scheen, A.J., Cathelineau, G., and Lefebvre, P.J. 1996. Changes in breath 13CO2/12CO2 during exercise of different intensities. *J Appl Physiol* 81:1096-1102.
398. Kaibara, T., Sutherland, G.R., Colbourne, F., and Tyson, R.L. 1999. Hypothermia: depression of tricarboxylic acid cycle flux and evidence for pentose phosphate shunt upregulation. *J Neurosurg* 90:339-347.
399. Boren, J., Cascante, M., Marin, S., Comin-Anduix, B., Centelles, J.J., Lim, S., Bassilian, S., Ahmed, S., Lee, W.N., and Boros, L.G. 2001. Gleevec (STI571) influences metabolic enzyme activities and glucose carbon flow toward nucleic acid and fatty acid synthesis in myeloid tumor cells. *J Biol Chem* 276:37747-37753.
400. Lee, W.N., Bergner, E.A., and Guo, Z.K. 1992. Mass isotopomer pattern and precursor-product relationship. *Biol Mass Spectrom* 21:114-122.
401. Ruzzin, J., Peronnet, F., Tremblay, J., Massicotte, D., and Lavoie, C. 2003. Breath [13CO2] recovery from an oral glucose load during exercise: comparison between [U-13C] and [1,2-13C]glucose. *J Appl Physiol* 95:477-482.
402. Schmit-Pokorny, K. 2009. Expanding indications for stem cell transplantation. *Semin Oncol Nurs* 25:105-114.
403. Sanders, J.E. 1999. Stem-cell transplant preparative regimens. *Pediatr Transplant* 3 Suppl 1:23-34.

404. Negrin, R. 2010. Preparative regimens for hematopoietic cell transplantation. In *UpToDate*. D. Basow, editor. Waltham, MA: UpToDate.
405. Negrin, R. 2010. Sources of hematopoietic stem cells. In *UpToDate*. D. Basow, editor. Waltham, MA: UpToDate.
406. Klumpp, T.R., Mangan, K.F., Goldberg, S.L., Pearlman, E.S., and Macdonald, J.S. 1995. Granulocyte colony-stimulating factor accelerates neutrophil engraftment following peripheral-blood stem-cell transplantation: a prospective, randomized trial. *J Clin Oncol* 13:1323-1327.
407. Chunduri, S., Dobogai, L.C., Peace, D., Sauntharajah, Y., Chen, H.Y., Mahmud, N., Quigley, J., Hoffman, R., Jessop, E., Beri, R., et al. 2006. Comparable kinetics of myeloablation between fludarabine/full-dose busulfan and fludarabine/melphalan conditioning regimens in allogeneic peripheral blood stem cell transplantation. *Bone Marrow Transplant* 38:477-482.
408. Storek, J., Geddes, M., Khan, F., Huard, B., Helg, C., Chalandon, Y., Passweg, J., and Roosnek, E. 2008. Reconstitution of the immune system after hematopoietic stem cell transplantation in humans. *Semin Immunopathol* 30:425-437.
409. Storek, J., Zhao, Z., Lin, E., Berger, T., McSweeney, P.A., Nash, R.A., Akatsuka, Y., Metcalf, M.D., Lu, H., Kalina, T., et al. 2004. Recovery from and consequences of severe iatrogenic lymphopenia (induced to treat autoimmune diseases). *Clin Immunol* 113:285-298.
410. von Vietinghoff, S., and Ley, K. 2008. Homeostatic regulation of blood neutrophil counts. *J Immunol* 181:5183-5188.
411. Panopoulos, A.D., and Watowich, S.S. 2008. Granulocyte colony-stimulating factor: molecular mechanisms of action during steady state and 'emergency' hematopoiesis. *Cytokine* 42:277-288.
412. Weaver, C.H., Hazelton, B., Birch, R., Palmer, P., Allen, C., Schwartzberg, L., and West, W. 1995. An analysis of engraftment kinetics as a function of the CD34 content of peripheral blood progenitor cell collections in 692 patients after the administration of myeloablative chemotherapy. *Blood* 86:3961-3969.
413. Welniak, L.A., Blazar, B.R., and Murphy, W.J. 2007. Immunobiology of allogeneic hematopoietic stem cell transplantation. *Annu Rev Immunol* 25:139-170.
414. Fry, T.J., and Mackall, C.L. 2005. The many faces of IL-7: from lymphopoiesis to peripheral T cell maintenance. *J Immunol* 174:6571-6576.
415. Sable, C.A., and Donowitz, G.R. 1994. Infections in bone marrow transplant recipients. *Clin Infect Dis* 18:273-281; quiz 282-274.
416. Leather, H.L., and Wingard, J.R. 2001. Infections following hematopoietic stem cell transplantation. *Infect Dis Clin North Am* 15:483-520.
417. Hovi, L., Saarinen-Pihkala, U.M., Vettenranta, K., and Saxen, H. 2000. Invasive fungal infections in pediatric bone marrow transplant recipients:

single center experience of 10 years. *Bone Marrow Transplant* 26:999-1004.
418. Meyers, J.D., Flournoy, N., and Thomas, E.D. 1980. Infection with herpes simplex virus and cell-mediated immunity after marrow transplant. *J Infect Dis* 142:338-346.
419. Wagner, J.E., Thompson, J.S., Carter, S.L., and Kernan, N.A. 2005. Effect of graft-versus-host disease prophylaxis on 3-year disease-free survival in recipients of unrelated donor bone marrow (T-cell Depletion Trial): a multi-centre, randomised phase II-III trial. *Lancet* 366:733-741.
420. Billingham, R.E. 1966. The biology of graft-versus-host reactions. *Harvey Lect* 62:21-78.
421. Hill, G.R., Crawford, J.M., Cooke, K.R., Brinson, Y.S., Pan, L., and Ferrara, J.L. 1997. Total body irradiation and acute graft-versus-host disease: the role of gastrointestinal damage and inflammatory cytokines. *Blood* 90:3204-3213.
422. Champlin, R.E., Passweg, J.R., Zhang, M.J., Rowlings, P.A., Pelz, C.J., Atkinson, K.A., Barrett, A.J., Cahn, J.Y., Drobyski, W.R., Gale, R.P., et al. 2000. T-cell depletion of bone marrow transplants for leukemia from donors other than HLA-identical siblings: advantage of T-cell antibodies with narrow specificities. *Blood* 95:3996-4003.
423. Marmont, A.M., Horowitz, M.M., Gale, R.P., Sobocinski, K., Ash, R.C., van Bekkum, D.W., Champlin, R.E., Dicke, K.A., Goldman, J.M., Good, R.A., et al. 1991. T-cell depletion of HLA-identical transplants in leukemia. *Blood* 78:2120-2130.
424. Shlomchik, W.D. 2007. Graft-versus-host disease. *Nat Rev Immunol* 7:340-352.
425. Loiseau, P., Busson, M., Balere, M.L., Dormoy, A., Bignon, J.D., Gagne, K., Gebuhrer, L., Dubois, V., Jollet, I., Bois, M., et al. 2007. HLA Association with hematopoietic stem cell transplantation outcome: the number of mismatches at HLA-A, -B, -C, -DRB1, or -DQB1 is strongly associated with overall survival. *Biol Blood Marrow Transplant* 13:965-974.
426. Ruggeri, L., Capanni, M., Urbani, E., Perruccio, K., Shlomchik, W.D., Tosti, A., Posati, S., Rogaia, D., Frassoni, F., Aversa, F., et al. 2002. Effectiveness of donor natural killer cell alloreactivity in mismatched hematopoietic transplants. *Science* 295:2097-2100.
427. Shlomchik, W.D., Couzens, M.S., Tang, C.B., McNiff, J., Robert, M.E., Liu, J., Shlomchik, M.J., and Emerson, S.G. 1999. Prevention of graft versus host disease by inactivation of host antigen-presenting cells. *Science* 285:412-415.
428. Teshima, T., Ordemann, R., Reddy, P., Gagin, S., Liu, C., Cooke, K.R., and Ferrara, J.L. 2002. Acute graft-versus-host disease does not require alloantigen expression on host epithelium. *Nat Med* 8:575-581.
429. Duffner, U.A., Maeda, Y., Cooke, K.R., Reddy, P., Ordemann, R., Liu, C., Ferrara, J.L., and Teshima, T. 2004. Host dendritic cells alone are

sufficient to initiate acute graft-versus-host disease. *J Immunol* 172:7393-7398.
430. Smith-Garvin, J.E., Koretzky, G.A., and Jordan, M.S. 2009. T cell activation. *Annu Rev Immunol* 27:591-619.
431. Valenzuela, J.O., Iclozan, C., Hossain, M.S., Prlic, M., Hopewell, E., Bronk, C.C., Wang, J., Celis, E., Engelman, R.W., Blazar, B.R., et al. 2009. PKCtheta is required for alloreactivity and GVHD but not for immune responses toward leukemia and infection in mice. *J Clin Invest* 119:3774-3786.
432. Lu, S.X., Alpdogan, O., Lin, J., Balderas, R., Campos-Gonzalez, R., Wang, X., Gao, G.J., Suh, D., King, C., Chow, M., et al. 2008. STAT-3 and ERK 1/2 phosphorylation are critical for T-cell alloactivation and graft-versus-host disease. *Blood* 112:5254-5258.
433. Ratanatharathorn, V., Nash, R.A., Przepiorka, D., Devine, S.M., Klein, J.L., Weisdorf, D., Fay, J.W., Nademanee, A., Antin, J.H., Christiansen, N.P., et al. 1998. Phase III study comparing methotrexate and tacrolimus (prograf, FK506) with methotrexate and cyclosporine for graft-versus-host disease prophylaxis after HLA-identical sibling bone marrow transplantation. *Blood* 92:2303-2314.
434. Ferrara, J.L., Marion, A., McIntyre, J.F., Murphy, G.F., and Burakoff, S.J. 1986. Amelioration of acute graft vs host disease due to minor histocompatibility antigens by in vivo administration of anti-interleukin 2 receptor antibody. *J Immunol* 137:1874-1877.
435. Jacobsohn, D.A., and Vogelsang, G.B. 2004. Anti-cytokine therapy for the treatment of graft-versus-host disease. *Curr Pharm Des* 10:1195-1205.
436. Chen, X., Das, R., Komorowski, R., Beres, A., Hessner, M.J., Mihara, M., and Drobyski, W.R. 2009. Blockade of interleukin-6 signaling augments regulatory T-cell reconstitution and attenuates the severity of graft-versus-host disease. *Blood* 114:891-900.
437. Radojcic, V., Pletneva, M.A., Yen, H.R., Ivcevic, S., Panoskaltsis-Mortari, A., Gilliam, A.C., Drake, C.G., Blazar, B.R., and Luznik, L. STAT3 signaling in CD4+ T cells is critical for the pathogenesis of chronic sclerodermatous graft-versus-host disease in a murine model. *J Immunol* 184:764-774.
438. Anderson, B.E., McNiff, J.M., Jain, D., Blazar, B.R., Shlomchik, W.D., and Shlomchik, M.J. 2005. Distinct roles for donor- and host-derived antigen-presenting cells and costimulatory molecules in murine chronic graft-versus-host disease: requirements depend on target organ. *Blood* 105:2227-2234.
439. Saito, K., Yagita, H., Hashimoto, H., Okumura, K., and Azuma, M. 1996. Effect of CD80 and CD86 blockade and anti-interleukin-12 treatment on mouse acute graft-versus-host disease. *Eur J Immunol* 26:3098-3106.
440. Blazar, B.R., Taylor, P.A., Linsley, P.S., and Vallera, D.A. 1994. In vivo blockade of CD28/CTLA4: B7/BB1 interaction with CTLA4-Ig reduces lethal murine graft-versus-host disease across the major histocompatibility complex barrier in mice. *Blood* 83:3815-3825.

441. Chao, N. 2010. Prevention and treatment of acute graft-versus-host disease: Recommendations. In *UpToDate*. D. Basow, editor. Waltham, MA: UpToDate.
442. Linsley, P.S., Greene, J.L., Brady, W., Bajorath, J., Ledbetter, J.A., and Peach, R. 1994. Human B7-1 (CD80) and B7-2 (CD86) bind with similar avidities but distinct kinetics to CD28 and CTLA-4 receptors. *Immunity* 1:793-801.
443. Michel, F., Attal-Bonnefoy, G., Mangino, G., Mise-Omata, S., and Acuto, O. 2001. CD28 as a molecular amplifier extending TCR ligation and signaling capabilities. *Immunity* 15:935-945.
444. Marinari, B., Costanzo, A., Viola, A., Michel, F., Mangino, G., Acuto, O., Levrero, M., Piccolella, E., and Tuosto, L. 2002. Vav cooperates with CD28 to induce NF-kappaB activation via a pathway involving Rac-1 and mitogen-activated kinase kinase 1. *Eur J Immunol* 32:447-456.
445. Boise, L.H., Minn, A.J., Noel, P.J., June, C.H., Accavitti, M.A., Lindsten, T., and Thompson, C.B. 1995. CD28 costimulation can promote T cell survival by enhancing the expression of Bcl-XL. *Immunity* 3:87-98.
446. Malek, T.R. 2008. The biology of interleukin-2. *Annu Rev Immunol* 26:453-479.
447. Baecher-Allan, C., Viglietta, V., and Hafler, D.A. 2004. Human CD4+CD25+ regulatory T cells. *Semin Immunol* 16:89-98.
448. Xun, C.Q., Thompson, J.S., Jennings, C.D., Brown, S.A., and Widmer, M.B. 1994. Effect of total body irradiation, busulfan-cyclophosphamide, or cyclophosphamide conditioning on inflammatory cytokine release and development of acute and chronic graft-versus-host disease in H-2-incompatible transplanted SCID mice. *Blood* 83:2360-2367.
449. Dienz, O., and Rincon, M. 2009. The effects of IL-6 on CD4 T cell responses. *Clin Immunol* 130:27-33.
450. Fischer Lindahl, K. 1997. On naming H2 haplotypes: functional significance of MHC class Ib alleles. *Immunogenetics* 46:53-62.
451. Pulaiev, R.A., Puliaeva, I.A., Ryan, A.E., and Via, C.S. 2005. The Parent-into-F1 Model of Graft-vs-Host Disease as a Model of In Vivo T Cell Function and Immunomodulation. *Curr Med Chem Immunol Endocr Metab Agents* 5:575-583.
452. Kumar, V., George, T., Yu, Y.Y., Liu, J., and Bennett, M. 1997. Role of murine NK cells and their receptors in hybrid resistance. *Curr Opin Immunol* 9:52-56.
453. Bloom, M.L., Wolk, A.G., Simon-Stoos, K.L., Bard, J.S., Chen, J., and Young, N.S. 2004. A mouse model of lymphocyte infusion-induced bone marrow failure. *Exp Hematol* 32:1163-1172.
454. Hakim, F.T., Sharrow, S.O., Payne, S., and Shearer, G.M. 1991. Repopulation of host lymphohematopoietic systems by donor cells during graft-versus-host reaction in unirradiated adult F1 mice injected with parental lymphocytes. *J Immunol* 146:2108-2115.
455. Via, C.S. 1991. Kinetics of T cell activation in acute and chronic forms of murine graft-versus-host disease. *J Immunol* 146:2603-2609.

456. Hurchla, M.A., Sedy, J.R., and Murphy, K.M. 2007. Unexpected role of B and T lymphocyte attenuator in sustaining cell survival during chronic allostimulation. *J Immunol* 178:6073-6082.
457. Rus, V., Svetic, A., Nguyen, P., Gause, W.C., and Via, C.S. 1995. Kinetics of Th1 and Th2 cytokine production during the early course of acute and chronic murine graft-versus-host disease. Regulatory role of donor CD8+ T cells. *J Immunol* 155:2396-2406.
458. Via, C.S., Rus, V., Nguyen, P., Linsley, P., and Gause, W.C. 1996. Differential effect of CTLA4Ig on murine graft-versus-host disease (GVHD) development: CTLA4Ig prevents both acute and chronic GVHD development but reverses only chronic GVHD. *J Immunol* 157:4258-4267.
459. Puliaev, R., Nguyen, P., Finkelman, F.D., and Via, C.S. 2004. Differential requirement for IFN-gamma in CTL maturation in acute murine graft-versus-host disease. *J Immunol* 173:910-919.
460. Strasser, A., Jost, P.J., and Nagata, S. 2009. The many roles of FAS receptor signaling in the immune system. *Immunity* 30:180-192.
461. Iwasaki, T., Hamano, T., Saheki, K., Kuroiwa, T., Kataoka, Y., Takemoto, Y., Ogata, A., Fujimoto, J., and Kakishita, E. 2000. Graft-versus-host-disease-associated donor cell engraftment in an F1 hybrid model is dependent upon the Fas pathway. *Immunology* 99:94-100.
462. Shustov, A., Luzina, I., Nguyen, P., Papadimitriou, J.C., Handwerger, B., Elkon, K.B., and Via, C.S. 2000. Role of perforin in controlling B-cell hyperactivity and humoral autoimmunity. *J Clin Invest* 106:R39-47.
463. Baker, M.B., Riley, R.L., Podack, E.R., and Levy, R.B. 1997. Graft-versus-host-disease-associated lymphoid hypoplasia and B cell dysfunction is dependent upon donor T cell-mediated Fas-ligand function, but not perforin function. *Proc Natl Acad Sci U S A* 94:1366-1371.
464. Sato, T., Thorlacius, H., Johnston, B., Staton, T.L., Xiang, W., Littman, D.R., and Butcher, E.C. 2005. Role for CXCR6 in recruitment of activated CD8+ lymphocytes to inflamed liver. *J Immunol* 174:277-283.
465. Blazar, B.R., Carreno, B.M., Panoskaltsis-Mortari, A., Carter, L., Iwai, Y., Yagita, H., Nishimura, H., and Taylor, P.A. 2003. Blockade of programmed death-1 engagement accelerates graft-versus-host disease lethality by an IFN-gamma-dependent mechanism. *J Immunol* 171:1272-1277.
466. Habicht, A., Kewalaramani, R., Vu, M.D., Demirci, G., Blazar, B.R., Sayegh, M.H., and Li, X.C. 2007. Striking dichotomy of PD-L1 and PD-L2 pathways in regulating alloreactive CD4(+) and CD8(+) T cells in vivo. *Am J Transplant* 7:2683-2692.
467. Blazar, B.R., Taylor, P.A., Panoskaltsis-Mortari, A., Sharpe, A.H., and Vallera, D.A. 1999. Opposing roles of CD28:B7 and CTLA-4:B7 pathways in regulating in vivo alloresponses in murine recipients of MHC disparate T cells. *J Immunol* 162:6368-6377.
468. Nowak, M., Carrasquillo, J.A., Yarboro, C.H., Bacharach, S.L., Whatley, M., Valencia, X., Takada, K., Brust, D.G., and Illei, G.G. 2004. A pilot study of the use of 2-[18F]-fluoro-2-deoxy-D-glucose-positron emission

tomography to assess the distribution of activated lymphocytes in patients with systemic lupus erythematosus. *Arthritis Rheum* 50:1233-1238.
469. Radu, C.G., Shu, C.J., Shelly, S.M., Phelps, M.E., and Witte, O.N. 2007. Positron emission tomography with computed tomography imaging of neuroinflammation in experimental autoimmune encephalomyelitis. *Proc Natl Acad Sci U S A* 104:1937-1942.
470. Stelljes, M., Hermann, S., Albring, J., Kohler, G., Loffler, M., Franzius, C., Poremba, C., Schlosser, V., Volkmann, S., Opitz, C., et al. 2008. Clinical molecular imaging in intestinal graft-versus-host disease: mapping of disease activity, prediction, and monitoring of treatment efficiency by positron emission tomography. *Blood* 111:2909-2918.
471. Grayson, J.M., Laniewski, N.G., Lanier, J.G., and Ahmed, R. 2003. Mitochondrial potential and reactive oxygen intermediates in antigen-specific CD8+ T cells during viral infection. *J Immunol* 170:4745-4751.
472. Nagy, G., Koncz, A., and Perl, A. 2005. T- and B-cell abnormalities in systemic lupus erythematosus. *Crit Rev Immunol* 25:123-140.
473. Chao, N. 2010. Treatment of acute graft-versus-host disease: Clinical trials. In *UpToDate*. D. Basow, editor. Waltham, MA: UpToDate.
474. Wegrzyn, J., Potla, R., Chwae, Y.J., Sepuri, N.B., Zhang, Q., Koeck, T., Derecka, M., Szczepanek, K., Szelag, M., Gornicka, A., et al. 2009. Function of mitochondrial Stat3 in cellular respiration. *Science* 323:793-797.
475. Unwin, R.D., Smith, D.L., Blinco, D., Wilson, C.L., Miller, C.J., Evans, C.A., Jaworska, E., Baldwin, S.A., Barnes, K., Pierce, A., et al. 2006. Quantitative proteomics reveals posttranslational control as a regulatory factor in primary hematopoietic stem cells. *Blood* 107:4687-4694.
476. Maianski, N.A., Geissler, J., Srinivasula, S.M., Alnemri, E.S., Roos, D., and Kuijpers, T.W. 2004. Functional characterization of mitochondria in neutrophils: a role restricted to apoptosis. *Cell Death Differ* 11:143-153.
477. Rathmell, J.C., Farkash, E.A., Gao, W., and Thompson, C.B. 2001. IL-7 enhances the survival and maintains the size of naive T cells. *J Immunol* 167:6869-6876.
478. Chen, C., Liu, Y., Liu, R., Ikenoue, T., Guan, K.L., and Zheng, P. 2008. TSC-mTOR maintains quiescence and function of hematopoietic stem cells by repressing mitochondrial biogenesis and reactive oxygen species. *J Exp Med* 205:2397-2408.
479. Borregaard, N., and Herlin, T. 1982. Energy metabolism of human neutrophils during phagocytosis. *J Clin Invest* 70:550-557.
480. Schafer, E., Seelert, H., Reifschneider, N.H., Krause, F., Dencher, N.A., and Vonck, J. 2006. Architecture of active mammalian respiratory chain supercomplexes. *J Biol Chem* 281:15370-15375.
481. van Raam, B.J., Sluiter, W., de Wit, E., Roos, D., Verhoeven, A.J., and Kuijpers, T.W. 2008. Mitochondrial membrane potential in human neutrophils is maintained by complex III activity in the absence of supercomplex organisation. *PLoS One* 3:e2013.

482. Schrader, M., and Fahimi, H.D. 2006. Peroxisomes and oxidative stress. *Biochim Biophys Acta* 1763:1755-1766.
483. Cross, A.R., and Segal, A.W. 2004. The NADPH oxidase of professional phagocytes--prototype of the NOX electron transport chain systems. *Biochim Biophys Acta* 1657:1-22.
484. Marnett, L.J. 1999. Lipid peroxidation-DNA damage by malondialdehyde. *Mutat Res* 424:83-95.
485. Sari, I., Cetin, A., Kaynar, L., Saraymen, R., Hacioglu, S.K., Ozturk, A., Kocyigit, I., Altuntas, F., and Eser, B. 2008. Disturbance of pro-oxidative/antioxidative balance in allogeneic peripheral blood stem cell transplantation. *Ann Clin Lab Sci* 38:120-125.
486. Ziegler, T.R., Panoskaltsus-Mortari, A., Gu, L.H., Jonas, C.R., Farrell, C.L., Lacey, D.L., Jones, D.P., and Blazar, B.R. 2001. Regulation of glutathione redox status in lung and liver by conditioning regimens and keratinocyte growth factor in murine allogeneic bone marrow transplantation. *Transplantation* 72:1354-1362.
487. Amer, J., Weiss, L., Reich, S., Shapira, M.Y., Slavin, S., and Fibach, E. 2007. The oxidative status of blood cells in a murine model of graft-versus-host disease. *Ann Hematol* 86:753-758.
488. Dai, J., Weinberg, R.S., Waxman, S., and Jing, Y. 1999. Malignant cells can be sensitized to undergo growth inhibition and apoptosis by arsenic trioxide through modulation of the glutathione redox system. *Blood* 93:268-277.
489. Chen, D., Chan, R., Waxman, S., and Jing, Y. 2006. Buthionine sulfoximine enhancement of arsenic trioxide-induced apoptosis in leukemia and lymphoma cells is mediated via activation of c-Jun NH2-terminal kinase and up-regulation of death receptors. *Cancer Res* 66:11416-11423.
490. Hollins, D.L., Suliman, H.B., Piantadosi, C.A., and Carraway, M.S. 2006. Glutathione regulates susceptibility to oxidant-induced mitochondrial DNA damage in human lymphocytes. *Free Radic Biol Med* 40:1220-1226.
491. Ruckenstuhl, C., Buttner, S., Carmona-Gutierrez, D., Eisenberg, T., Kroemer, G., Sigrist, S.J., Frohlich, K.U., and Madeo, F. 2009. The Warburg effect suppresses oxidative stress induced apoptosis in a yeast model for cancer. *PLoS One* 4:e4592.
492. Bassenge, E., Sommer, O., Schwemmer, M., and Bunger, R. 2000. Antioxidant pyruvate inhibits cardiac formation of reactive oxygen species through changes in redox state. *Am J Physiol Heart Circ Physiol* 279:H2431-2438.
493. Fink, M.P. 2007. Ethyl pyruvate: a novel anti-inflammatory agent. *J Intern Med* 261:349-362.
494. Tawadrous, Z.S., Delude, R.L., and Fink, M.P. 2002. Resuscitation from hemorrhagic shock with Ringer's ethyl pyruvate solution improves survival and ameliorates intestinal mucosal hyperpermeability in rats. *Shock* 17:473-477.

495. Yu, Y.M., Kim, J.B., Lee, K.W., Kim, S.Y., Han, P.L., and Lee, J.K. 2005. Inhibition of the cerebral ischemic injury by ethyl pyruvate with a wide therapeutic window. *Stroke* 36:2238-2243.
496. Ulloa, L., Ochani, M., Yang, H., Tanovic, M., Halperin, D., Yang, R., Czura, C.J., Fink, M.P., and Tracey, K.J. 2002. Ethyl pyruvate prevents lethality in mice with established lethal sepsis and systemic inflammation. *Proc Natl Acad Sci U S A* 99:12351-12356.
497. Morse, H.C., 3rd, Shen, F.W., and Hammerling, U. 1987. Genetic nomenclature for loci controlling mouse lymphocyte antigens. *Immunogenetics* 25:71-78.
498. Newton, M.R., Wood, K.J., and Fabre, J.W. 1986. A monoclonal alloantibody detecting a polymorphism of the rat leucocyte common (LC) antigen. *J Immunogenet* 13:41-50.
499. Karp, G. 2002. *Cell and molecular biology : concepts and experiments*. New York: J. Wiley. xxi, 785, [748] pp.
500. Chen, J., Lipovsky, K., Ellison, F.M., Calado, R.T., and Young, N.S. 2004. Bystander destruction of hematopoietic progenitor and stem cells in a mouse model of infusion-induced bone marrow failure. *Blood* 104:1671-1678.
501. Reyes, J., Borriero, L., Tanphaichitr, N., Bellve, A.R., and Benos, D.J. 1986. Energy metabolism of cultured TM4 cells and the action of gossypol. *Biol Reprod* 34:809-819.
502. Brand, M.D. 2005. The efficiency and plasticity of mitochondrial energy transduction. *Biochem Soc Trans* 33:897-904.
503. Dranka, B.P., Hill, B.G., and Darley-Usmar, V.M. Mitochondrial reserve capacity in endothelial cells: The impact of nitric oxide and reactive oxygen species. *Free Radic Biol Med* 48:905-914.
504. Hill, B.G., Dranka, B.P., Zou, L., Chatham, J.C., and Darley-Usmar, V.M. 2009. Importance of the bioenergetic reserve capacity in response to cardiomyocyte stress induced by 4-hydroxynonenal. *Biochem J* 424:99-107.
505. Owerbach, D., Rich, C., and Taneja, K. 1986. Characterization of three HLA-DR beta genes isolated from an HLA-DR 3/4 insulin-dependent diabetic patient. *Immunogenetics* 24:41-46.
506. Chen, B.J., Cui, X., Sempowski, G.D., Domen, J., and Chao, N.J. 2004. Hematopoietic stem cell dose correlates with the speed of immune reconstitution after stem cell transplantation. *Blood* 103:4344-4352.
507. Kruisbeek, A.M., Shevach, E., and Thornton, A.M. 2004. Proliferative assays for T cell function. *Curr Protoc Immunol* Chapter 3:Unit 3 12.
508. Suchin, E.J., Langmuir, P.B., Palmer, E., Sayegh, M.H., Wells, A.D., and Turka, L.A. 2001. Quantifying the frequency of alloreactive T cells in vivo: new answers to an old question. *J Immunol* 166:973-981.
509. Swain, S.L., Croft, M., Dubey, C., Haynes, L., Rogers, P., Zhang, X., and Bradley, L.M. 1996. From naive to memory T cells. *Immunol Rev* 150:143-167.

510. Quah, B.J., Warren, H.S., and Parish, C.R. 2007. Monitoring lymphocyte proliferation in vitro and in vivo with the intracellular fluorescent dye carboxyfluorescein diacetate succinimidyl ester. *Nat Protoc* 2:2049-2056.
511. Fazekas de St Groth, B., Smith, A.L., Koh, W.P., Girgis, L., Cook, M.C., and Bertolino, P. 1999. Carboxyfluorescein diacetate succinimidyl ester and the virgin lymphocyte: a marriage made in heaven. *Immunol Cell Biol* 77:530-538.
512. Anderson, B.E., Taylor, P.A., McNiff, J.M., Jain, D., Demetris, A.J., Panoskaltsis-Mortari, A., Ager, A., Blazar, B.R., Shlomchik, W.D., and Shlomchik, M.J. 2008. Effects of donor T-cell trafficking and priming site on graft-versus-host disease induction by naive and memory phenotype CD4 T cells. *Blood* 111:5242-5251.
513. Mitchell, D.M., and Williams, M.A. An activation marker finds a function. *Immunity* 32:9-11.
514. Wieman, H.L., Wofford, J.A., and Rathmell, J.C. 2007. Cytokine stimulation promotes glucose uptake via phosphatidylinositol-3 kinase/Akt regulation of Glut1 activity and trafficking. *Mol Biol Cell* 18:1437-1446.
515. Ormerod, M.G. 1994. *Flow Cytometry, A Practical Approach*: IRL Press.
516. Crellin, N.K., Garcia, R.V., and Levings, M.K. 2007. Altered activation of AKT is required for the suppressive function of human CD4+CD25+ T regulatory cells. *Blood* 109:2014-2022.
517. Crellin, N.K., Garcia, R.V., and Levings, M.K. 2007. Flow cytometry-based methods for studying signaling in human CD4+CD25+FOXP3+ T regulatory cells. *J Immunol Methods* 324:92-104.
518. Bonnevier, J.L., Yarke, C.A., and Mueller, D.L. 2006. Sustained B7/CD28 interactions and resultant phosphatidylinositol 3-kinase activity maintain G1-->S phase transitions at an optimal rate. *Eur J Immunol* 36:1583-1597.
519. Floryk, D., and Houstek, J. 1999. Tetramethyl rhodamine methyl ester (TMRM) is suitable for cytofluorometric measurements of mitochondrial membrane potential in cells treated with digitonin. *Biosci Rep* 19:27-34.
520. Laurindo, F.R., Fernandes, D.C., and Santos, C.X. 2008. Assessment of superoxide production and NADPH oxidase activity by HPLC analysis of dihydroethidium oxidation products. *Methods Enzymol* 441:237-260.
521. Invitrogen. 2010. TMRM Product Structure. Molecular Probes.
522. Grinstein, S., and Dixon, S.J. 1989. Ion transport, membrane potential, and cytoplasmic pH in lymphocytes: changes during activation. *Physiol Rev* 69:417-481.
523. Gelfand, E.W., and Or, R. 1991. Charybdotoxin-sensitive, Ca(2+)-dependent membrane potential changes are not involved in human T or B cell activation and proliferation. *J Immunol* 147:3452-3458.
524. Rader, R.K., Kahn, L.E., Anderson, G.D., Martin, C.L., Chinn, K.S., and Gregory, S.A. 1996. T cell activation is regulated by voltage-dependent and calcium-activated potassium channels. *J Immunol* 156:1425-1430.
525. Tsien, R.Y., Pozzan, T., and Rink, T.J. 1982. T-cell mitogens cause early changes in cytoplasmic free Ca2+ and membrane potential in lymphocytes. *Nature* 295:68-71.

526. Bindokas, V.P., Jordan, J., Lee, C.C., and Miller, R.J. 1996. Superoxide production in rat hippocampal neurons: selective imaging with hydroethidine. *J Neurosci* 16:1324-1336.
527. Young, I.S., and Woodside, J.V. 2001. Antioxidants in health and disease. *J Clin Pathol* 54:176-186.
528. Ballatori, N., Krance, S.M., Marchan, R., and Hammond, C.L. 2009. Plasma membrane glutathione transporters and their roles in cell physiology and pathophysiology. *Mol Aspects Med* 30:13-28.
529. Zhu, A., Romero, R., and Petty, H.R. A sensitive fluorimetric assay for pyruvate. *Anal Biochem* 396:146-151.
530. Rahman, I., Kode, A., and Biswas, S.K. 2006. Assay for quantitative determination of glutathione and glutathione disulfide levels using enzymatic recycling method. *Nat Protoc* 1:3159-3165.
531. Cavazzana-Calvo, M., Andre-Schmutz, I., Dal Cortivo, L., Neven, B., Hacein-Bey-Abina, S., and Fischer, A. 2009. Immune reconstitution after haematopoietic stem cell transplantation: obstacles and anticipated progress. *Curr Opin Immunol* 21:544-548.
532. Leif, R.C., Stein, J.H., and Zucker, R.M. 2004. A short history of the initial application of anti-5-BrdU to the detection and measurement of S phase. *Cytometry A* 58:45-52.
533. Beaty, S.R., Rose, C.E., Jr., and Sung, S.S. 2007. Diverse and potent chemokine production by lung CD11bhigh dendritic cells in homeostasis and in allergic lung inflammation. *J Immunol* 178:1882-1895.
534. Hickman, S.P., and Turka, L.A. 2005. Homeostatic T cell proliferation as a barrier to T cell tolerance. *Philos Trans R Soc Lond B Biol Sci* 360:1713-1721.
535. Jensen, M.V., Joseph, J.W., Ilkayeva, O., Burgess, S., Lu, D., Ronnebaum, S.M., Odegaard, M., Becker, T.C., Sherry, A.D., and Newgard, C.B. 2006. Compensatory responses to pyruvate carboxylase suppression in islet beta-cells. Preservation of glucose-stimulated insulin secretion. *J Biol Chem* 281:22342-22351.
536. Hume, D.A., Radik, J.L., Ferber, E., and Weidemann, M.J. 1978. Aerobic glycolysis and lymphocyte transformation. *Biochem J* 174:703-709.
537. Bennett, M.J. 2007. Assays of fatty acid beta-oxidation activity. *Methods Cell Biol* 80:179-197.
538. Parry-Billings, M., Evans, J., Calder, P.C., and Newsholme, E.A. 1990. Does glutamine contribute to immunosuppression after major burns? *Lancet* 336:523-525.
539. Ardawi, M.S., and Newsholme, E.A. 1983. Glutamine metabolism in lymphocytes of the rat. *Biochem J* 212:835-842.
540. Yaqoob, P., and Calder, P.C. 1997. Glutamine requirement of proliferating T lymphocytes. *Nutrition* 13:646-651.
541. Wise, D.R., DeBerardinis, R.J., Mancuso, A., Sayed, N., Zhang, X.Y., Pfeiffer, H.K., Nissim, I., Daikhin, E., Yudkoff, M., McMahon, S.B., et al. 2008. Myc regulates a transcriptional program that stimulates

mitochondrial glutaminolysis and leads to glutamine addiction. *Proc Natl Acad Sci U S A* 105:18782-18787.
542. Gao, P., Tchernyshyov, I., Chang, T.C., Lee, Y.S., Kita, K., Ochi, T., Zeller, K.I., De Marzo, A.M., Van Eyk, J.E., Mendell, J.T., et al. 2009. c-Myc suppression of miR-23a/b enhances mitochondrial glutaminase expression and glutamine metabolism. *Nature* 458:762-765.
543. Yang, C., Sudderth, J., Dang, T., Bachoo, R.M., McDonald, J.G., and DeBerardinis, R.J. 2009. Glioblastoma cells require glutamate dehydrogenase to survive impairments of glucose metabolism or Akt signaling. *Cancer Res* 69:7986-7993.
544. Curthoys, N.P., and Watford, M. 1995. Regulation of glutaminase activity and glutamine metabolism. *Annu Rev Nutr* 15:133-159.
545. Deberardinis, R.J., Sayed, N., Ditsworth, D., and Thompson, C.B. 2008. Brick by brick: metabolism and tumor cell growth. *Curr Opin Genet Dev* 18:54-61.
546. Lindsten, T., June, C.H., and Thompson, C.B. 1988. Multiple mechanisms regulate c-myc gene expression during normal T cell activation. *EMBO J* 7:2787-2794.
547. Huang, C.Y., Bredemeyer, A.L., Walker, L.M., Bassing, C.H., and Sleckman, B.P. 2008. Dynamic regulation of c-Myc proto-oncogene expression during lymphocyte development revealed by a GFP-c-Myc knock-in mouse. *Eur J Immunol* 38:342-349.
548. Yaqoob, P., and Calder, P.C. 1998. Cytokine production by human peripheral blood mononuclear cells: differential senstivity to glutamine availability. *Cytokine* 10:790-794.
549. Shewchuk, L.D., Baracos, V.E., and Field, C.J. 1997. Dietary L-glutamine supplementation reduces the growth of the Morris Hepatoma 7777 in exercise-trained and sedentary rats. *J Nutr* 127:158-166.
550. Kew, S., Wells, S.M., Yaqoob, P., Wallace, F.A., Miles, E.A., and Calder, P.C. 1999. Dietary glutamine enhances murine T-lymphocyte responsiveness. *J Nutr* 129:1524-1531.
551. Neu, J., Roig, J.C., Meetze, W.H., Veerman, M., Carter, C., Millsaps, M., Bowling, D., Dallas, M.J., Sleasman, J., Knight, T., et al. 1997. Enteral glutamine supplementation for very low birth weight infants decreases morbidity. *J Pediatr* 131:691-699.
552. Houdijk, A.P., Rijnsburger, E.R., Jansen, J., Wesdorp, R.I., Weiss, J.K., McCamish, M.A., Teerlink, T., Meuwissen, S.G., Haarman, H.J., Thijs, L.G., et al. 1998. Randomised trial of glutamine-enriched enteral nutrition on infectious morbidity in patients with multiple trauma. *Lancet* 352:772-776.
553. Kato, K., Cui, S., Kuick, R., Mineishi, S., Hexner, E., Ferrara, J.L., Emerson, S.G., and Zhang, Y. Identification of stem cell transcriptional programs normally expressed in embryonic and neural stem cells in alloreactive CD8+ T cells mediating graft-versus-host disease. *Biol Blood Marrow Transplant* 16:751-771.

554. Ziegler, T.R., Young, L.S., Benfell, K., Scheltinga, M., Hortos, K., Bye, R., Morrow, F.D., Jacobs, D.O., Smith, R.J., Antin, J.H., et al. 1992. Clinical and metabolic efficacy of glutamine-supplemented parenteral nutrition after bone marrow transplantation. A randomized, double-blind, controlled study. *Ann Intern Med* 116:821-828.
555. Ziegler, T.R., Bye, R.L., Persinger, R.L., Young, L.S., Antin, J.H., and Wilmore, D.W. 1998. Effects of glutamine supplementation on circulating lymphocytes after bone marrow transplantation: a pilot study. *Am J Med Sci* 315:4-10.
556. Richieri, G.V., Anel, A., and Kleinfeld, A.M. 1993. Interactions of long-chain fatty acids and albumin: determination of free fatty acid levels using the fluorescent probe ADIFAB. *Biochemistry* 32:7574-7580.
557. Glatz, J.F., Luiken, J.J., and Bonen, A. Membrane fatty acid transporters as regulators of lipid metabolism: implications for metabolic disease. *Physiol Rev* 90:367-417.
558. Soupene, E., and Kuypers, F.A. 2008. Mammalian long-chain acyl-CoA synthetases. *Exp Biol Med (Maywood)* 233:507-521.
559. Zarain-Herzberg, A., and Rupp, H. 2002. Therapeutic potential of CPT I inhibitors: cardiac gene transcription as a target. *Expert Opin Investig Drugs* 11:345-356.
560. Lopaschuk, G.D., Ussher, J.R., Folmes, C.D., Jaswal, J.S., and Stanley, W.C. Myocardial fatty acid metabolism in health and disease. *Physiol Rev* 90:207-258.
561. Ruderman, N.B., Saha, A.K., and Kraegen, E.W. 2003. Minireview: malonyl CoA, AMP-activated protein kinase, and adiposity. *Endocrinology* 144:5166-5171.
562. Zhang, B.B., Zhou, G., and Li, C. 2009. AMPK: an emerging drug target for diabetes and the metabolic syndrome. *Cell Metab* 9:407-416.
563. Kudo, N., Barr, A.J., Barr, R.L., Desai, S., and Lopaschuk, G.D. 1995. High rates of fatty acid oxidation during reperfusion of ischemic hearts are associated with a decrease in malonyl-CoA levels due to an increase in 5'-AMP-activated protein kinase inhibition of acetyl-CoA carboxylase. *J Biol Chem* 270:17513-17520.
564. Samudio, I., Harmancey, R., Fiegl, M., Kantarjian, H., Konopleva, M., Korchin, B., Kaluarachchi, K., Bornmann, W., Duvvuri, S., Taegtmeyer, H., et al. Pharmacologic inhibition of fatty acid oxidation sensitizes human leukemia cells to apoptosis induction. *J Clin Invest* 120:142-156.
565. Schmidt-Schweda, S., and Holubarsch, C. 2000. First clinical trial with etomoxir in patients with chronic congestive heart failure. *Clin Sci (Lond)* 99:27-35.
566. Mayer, A., Denanglaire, S., Viollet, B., Leo, O., and Andris, F. 2008. AMP-activated protein kinase regulates lymphocyte responses to metabolic stress but is largely dispensable for immune cell development and function. *Eur J Immunol* 38:948-956.
567. Dzamko, N., Schertzer, J.D., Ryall, J.G., Steel, R., Macaulay, S.L., Wee, S., Chen, Z.P., Michell, B.J., Oakhill, J.S., Watt, M.J., et al. 2008. AMPK-

independent pathways regulate skeletal muscle fatty acid oxidation. *J Physiol* 586:5819-5831.
568. Pearce, E.L., Walsh, M.C., Cejas, P.J., Harms, G.M., Shen, H., Wang, L.S., Jones, R.G., and Choi, Y. 2009. Enhancing CD8 T-cell memory by modulating fatty acid metabolism. *Nature* 460:103-107.
569. Prlic, M., and Bevan, M.J. 2009. Immunology: A metabolic switch to memory. *Nature* 460:41-42.
570. Deberardinis, R.J., Lum, J.J., and Thompson, C.B. 2006. Phosphatidylinositol 3-kinase-dependent modulation of carnitine palmitoyltransferase 1A expression regulates lipid metabolism during hematopoietic cell growth. *J Biol Chem* 281:37372-37380.
571. Anderson, B.E., McNiff, J., Yan, J., Doyle, H., Mamula, M., Shlomchik, M.J., and Shlomchik, W.D. 2003. Memory CD4+ T cells do not induce graft-versus-host disease. *J Clin Invest* 112:101-108.
572. Chen, B.J., Cui, X., Sempowski, G.D., Liu, C., and Chao, N.J. 2004. Transfer of allogeneic CD62L- memory T cells without graft-versus-host disease. *Blood* 103:1534-1541.
573. Zhang, Y., Joe, G., Hexner, E., Zhu, J., and Emerson, S.G. 2005. Alloreactive memory T cells are responsible for the persistence of graft-versus-host disease. *J Immunol* 174:3051-3058.
574. Zauner, C., Rabitsch, W., Schneeweiss, B., Schiefermeier, M., Greinix, H.T., Keil, F., Ratheiser, K., and Kalhs, P. 2001. Energy and substrate metabolism in patients with chronic extensive graft-versus-host disease. *Transplantation* 71:524-528.
575. Koves, T.R., Ussher, J.R., Noland, R.C., Slentz, D., Mosedale, M., Ilkayeva, O., Bain, J., Stevens, R., Dyck, J.R., Newgard, C.B., et al. 2008. Mitochondrial overload and incomplete fatty acid oxidation contribute to skeletal muscle insulin resistance. *Cell Metab* 7:45-56.
576. Turcani, M., and Rupp, H. 1997. Etomoxir improves left ventricular performance of pressure-overloaded rat heart. *Circulation* 96:3681-3686.
577. Turcani, M., and Rupp, H. 1999. Modification of left ventricular hypertrophy by chronic etomixir treatment. *Br J Pharmacol* 126:501-507.
578. Holubarsch, C.J., Rohrbach, M., Karrasch, M., Boehm, E., Polonski, L., Ponikowski, P., and Rhein, S. 2007. A double-blind randomized multicentre clinical trial to evaluate the efficacy and safety of two doses of etomoxir in comparison with placebo in patients with moderate congestive heart failure: the ERGO (etomoxir for the recovery of glucose oxidation) study. *Clin Sci (Lond)* 113:205-212.
579. Robey, R.B., and Hay, N. 2006. Mitochondrial hexokinases, novel mediators of the antiapoptotic effects of growth factors and Akt. *Oncogene* 25:4683-4696.
580. Rosenthal, M.D. 1980. Selectivity in incorporation, utilization and retention of oleic and linoleic acids by human skin fibroblasts. *Lipids* 15:838-848.
581. Igal, R.A., Wang, S., Gonzalez-Baro, M., and Coleman, R.A. 2001. Mitochondrial glycerol phosphate acyltransferase directs the incorporation

of exogenous fatty acids into triacylglycerol. *J Biol Chem* 276:42205-42212.
582. Rathmell, J.C., Vander Heiden, M.G., Harris, M.H., Frauwirth, K.A., and Thompson, C.B. 2000. In the absence of extrinsic signals, nutrient utilization by lymphocytes is insufficient to maintain either cell size or viability. *Mol Cell* 6:683-692.
583. Rathmell, J.C., Elstrom, R.L., Cinalli, R.M., and Thompson, C.B. 2003. Activated Akt promotes increased resting T cell size, CD28-independent T cell growth, and development of autoimmunity and lymphoma. *Eur J Immunol* 33:2223-2232.
584. Hirrlinger, J., Konig, J., Keppler, D., Lindenau, J., Schulz, J.B., and Dringen, R. 2001. The multidrug resistance protein MRP1 mediates the release of glutathione disulfide from rat astrocytes during oxidative stress. *J Neurochem* 76:627-636.
585. Kim, S.K., Woodcroft, K.J., Khodadadeh, S.S., and Novak, R.F. 2004. Insulin signaling regulates gamma-glutamylcysteine ligase catalytic subunit expression in primary cultured rat hepatocytes. *J Pharmacol Exp Ther* 311:99-108.
586. Pardo, M., Melendez, J.A., and Tirosh, O. 2006. Manganese superoxide dismutase inactivation during Fas (CD95)-mediated apoptosis in Jurkat T cells. *Free Radic Biol Med* 41:1795-1806.
587. Grigolo, B., Borzi, R.M., Mariani, E., Monaco, M.C., Cattini, L., Porstmann, T., and Facchini, A. 1994. Intracellular Cu/Zn superoxide dismutase levels in T and non-T cells from normal aged subjects. *Mech Ageing Dev* 73:27-37.
588. Salahudeen, A.K., Clark, E.C., and Nath, K.A. 1991. Hydrogen peroxide-induced renal injury. A protective role for pyruvate in vitro and in vivo. *J Clin Invest* 88:1886-1893.
589. Jitrapakdee, S., Vidal-Puig, A., and Wallace, J.C. 2006. Anaplerotic roles of pyruvate carboxylase in mammalian tissues. *Cell Mol Life Sci* 63:843-854.
590. Mir, M.A., and Battiwalla, M. 2009. Immune deficits in allogeneic hematopoietic stem cell transplant (HSCT) recipients. *Mycopathologia* 168:271-282.
591. Podesta, M. 2001. Transplantation hematopoiesis. *Curr Opin Hematol* 8:331-336.
592. Germeshausen, M., Skokowa, J., Ballmaier, M., Zeidler, C., and Welte, K. 2008. G-CSF receptor mutations in patients with congenital neutropenia. *Curr Opin Hematol* 15:332-337.
593. Van Lint, M.T., Uderzo, C., Locasciulli, A., Majolino, I., Scime, R., Locatelli, F., Giorgiani, G., Arcese, W., Iori, A.P., Falda, M., et al. 1998. Early treatment of acute graft-versus-host disease with high- or low-dose 6-methylprednisolone: a multicenter randomized trial from the Italian Group for Bone Marrow Transplantation. *Blood* 92:2288-2293.

594. Montague, J.W., and Cidlowski, J.A. 1995. Glucocorticoid-induced death of immune cells: mechanisms of action. *Curr Top Microbiol Immunol* 200:51-65.
595. De Bosscher, K., Vanden Berghe, W., and Haegeman, G. 2000. Mechanisms of anti-inflammatory action and of immunosuppression by glucocorticoids: negative interference of activated glucocorticoid receptor with transcription factors. *J Neuroimmunol* 109:16-22.
596. Kitawaki, T., Kadowaki, N., Ishikawa, T., Ichinohe, T., and Uchiyama, T. 2003. Compromised recovery of natural interferon-alpha/beta-producing cells after allogeneic hematopoietic stem cell transplantation complicated by acute graft-versus-host disease and glucocorticoid administration. *Bone Marrow Transplant* 32:187-194.
597. Giebel, S., Dziaczkowska, J., Wojnar, J., Krawczyk-Kulis, M., Markiewicz, M., Kruzel, T., Wylezol, I., Nowak, K., Jagoda, K., and Holowiecki, J. 2005. The impact of immunosuppressive therapy on an early quantitative NK cell reconstitution after allogeneic haematopoietic cell transplantation. *Ann Transplant* 10:29-33.
598. Paczesny, S., Choi, S.W., and Ferrara, J.L. 2009. Acute graft-versus-host disease: new treatment strategies. *Curr Opin Hematol* 16:427-436.
599. Merezhinskaya, N., and Fishbein, W.N. 2009. Monocarboxylate transporters: past, present, and future. *Histol Histopathol* 24:243-264.
600. Salomon, A.R., Voehringer, D.W., Herzenberg, L.A., and Khosla, C. 2000. Understanding and exploiting the mechanistic basis for selectivity of polyketide inhibitors of F(0)F(1)-ATPase. *Proc Natl Acad Sci U S A* 97:14766-14771.
601. McKenna, M.C., Waagepetersen, H.S., Schousboe, A., and Sonnewald, U. 2006. Neuronal and astrocytic shuttle mechanisms for cytosolic-mitochondrial transfer of reducing equivalents: current evidence and pharmacological tools. *Biochem Pharmacol* 71:399-407.
602. Borle, A.B., and Stanko, R.T. 1996. Pyruvate reduces anoxic injury and free radical formation in perfused rat hepatocytes. *Am J Physiol* 270:G535-540.
603. Kutala, V.K., Khan, M., Angelos, M.G., and Kuppusamy, P. 2007. Role of oxygen in postischemic myocardial injury. *Antioxid Redox Signal* 9:1193-1206.
604. Zweier, J.L., Kuppusamy, P., Williams, R., Rayburn, B.K., Smith, D., Weisfeldt, M.L., and Flaherty, J.T. 1989. Measurement and characterization of postischemic free radical generation in the isolated perfused heart. *J Biol Chem* 264:18890-18895.
605. Pelicano, H., Feng, L., Zhou, Y., Carew, J.S., Hileman, E.O., Plunkett, W., Keating, M.J., and Huang, P. 2003. Inhibition of mitochondrial respiration: a novel strategy to enhance drug-induced apoptosis in human leukemia cells by a reactive oxygen species-mediated mechanism. *J Biol Chem* 278:37832-37839.

606. Ramanathan, B., Jan, K.Y., Chen, C.H., Hour, T.C., Yu, H.J., and Pu, Y.S. 2005. Resistance to paclitaxel is proportional to cellular total antioxidant capacity. *Cancer Res* 65:8455-8460.
607. Shen, Z.X., Chen, G.Q., Ni, J.H., Li, X.S., Xiong, S.M., Qiu, Q.Y., Zhu, J., Tang, W., Sun, G.L., Yang, K.Q., et al. 1997. Use of arsenic trioxide (As2O3) in the treatment of acute promyelocytic leukemia (APL): II. Clinical efficacy and pharmacokinetics in relapsed patients. *Blood* 89:3354-3360.
608. Passegue, E., Wagers, A.J., Giuriato, S., Anderson, W.C., and Weissman, I.L. 2005. Global analysis of proliferation and cell cycle gene expression in the regulation of hematopoietic stem and progenitor cell fates. *J Exp Med* 202:1599-1611.
609. Cho, B.K., Rao, V.P., Ge, Q., Eisen, H.N., and Chen, J. 2000. Homeostasis-stimulated proliferation drives naive T cells to differentiate directly into memory T cells. *J Exp Med* 192:549-556.
610. De Boer, R.J., Homann, D., and Perelson, A.S. 2003. Different dynamics of CD4+ and CD8+ T cell responses during and after acute lymphocytic choriomeningitis virus infection. *J Immunol* 171:3928-3935.
611. Via, C.S., Shustov, A., Rus, V., Lang, T., Nguyen, P., and Finkelman, F.D. 2001. In vivo neutralization of TNF-alpha promotes humoral autoimmunity by preventing the induction of CTL. *J Immunol* 167:6821-6826.
612. Via, C.S., and Finkelman, F.D. 1993. Critical role of interleukin-2 in the development of acute graft-versus-host disease. *Int Immunol* 5:565-572.
613. Hellwig-Burgel, T., Rutkowski, K., Metzen, E., Fandrey, J., and Jelkmann, W. 1999. Interleukin-1beta and tumor necrosis factor-alpha stimulate DNA binding of hypoxia-inducible factor-1. *Blood* 94:1561-1567.
614. Haddad, J.J., and Land, S.C. 2001. A non-hypoxic, ROS-sensitive pathway mediates TNF-alpha-dependent regulation of HIF-1alpha. *FEBS Lett* 505:269-274.
615. Bauer, D.E., Harris, M.H., Plas, D.R., Lum, J.J., Hammerman, P.S., Rathmell, J.C., Riley, J.L., and Thompson, C.B. 2004. Cytokine stimulation of aerobic glycolysis in hematopoietic cells exceeds proliferative demand. *FASEB J* 18:1303-1305.
616. Myers, M.G., Jr. 2009. Cell biology. Moonlighting in mitochondria. *Science* 323:723-724.
617. Sallusto, F., and Lanzavecchia, A. 1994. Efficient presentation of soluble antigen by cultured human dendritic cells is maintained by granulocyte/macrophage colony-stimulating factor plus interleukin 4 and downregulated by tumor necrosis factor alpha. *J Exp Med* 179:1109-1118.
618. Mohty, M., and Gaugler, B. 2008. Inflammatory cytokines and dendritic cells in acute graft-versus-host disease after allogeneic stem cell transplantation. *Cytokine Growth Factor Rev* 19:53-63.
619. De Smedt, T., Pajak, B., Muraille, E., Lespagnard, L., Heinen, E., De Baetselier, P., Urbain, J., Leo, O., and Moser, M. 1996. Regulation of dendritic cell numbers and maturation by lipopolysaccharide in vivo. *J Exp Med* 184:1413-1424.

620. Chang, C.H., Furue, M., and Tamaki, K. 1995. B7-1 expression of Langerhans cells is up-regulated by proinflammatory cytokines, and is down-regulated by interferon-gamma or by interleukin-10. *Eur J Immunol* 25:394-398.
621. Ando, M., Uehara, I., Kogure, K., Asano, Y., Nakajima, W., Abe, Y., Kawauchi, K., and Tanaka, N. Interleukin 6 enhances glycolysis through expression of the glycolytic enzymes hexokinase 2 and 6-phosphofructo-2-kinase/fructose-2,6-bisphosphatase-3. *J Nippon Med Sch* 77:97-105.
622. Kishimoto, T., Akira, S., Narazaki, M., and Taga, T. 1995. Interleukin-6 family of cytokines and gp130. *Blood* 86:1243-1254.
623. Hibi, M., Nakajima, K., and Hirano, T. 1996. IL-6 cytokine family and signal transduction: a model of the cytokine system. *J Mol Med* 74:1-12.
624. Zhong, Z., Wen, Z., and Darnell, J.E., Jr. 1994. Stat3: a STAT family member activated by tyrosine phosphorylation in response to epidermal growth factor and interleukin-6. *Science* 264:95-98.
625. Wolff, D., Steiner, B., Hildebrandt, G., Edinger, M., and Holler, E. 2009. Pharmaceutical and cellular strategies in prophylaxis and treatment of graft-versus-host disease. *Curr Pharm Des* 15:1974-1997.
626. Borel, J.F. 2002. History of the discovery of cyclosporin and of its early pharmacological development. *Wien Klin Wochenschr* 114:433-437.
627. Gallay, P.A. 2009. Cyclophilin inhibitors. *Clin Liver Dis* 13:403-417.
628. Pritchard, D.I. 2005. Sourcing a chemical succession for cyclosporin from parasites and human pathogens. *Drug Discov Today* 10:688-691.
629. Harding, M.W., Galat, A., Uehling, D.E., and Schreiber, S.L. 1989. A receptor for the immunosuppressant FK506 is a cis-trans peptidyl-prolyl isomerase. *Nature* 341:758-760.
630. Fulton, B., and Markham, A. 1996. Mycophenolate mofetil. A review of its pharmacodynamic and pharmacokinetic properties and clinical efficacy in renal transplantation. *Drugs* 51:278-298.
631. Matthews, D.A., Alden, R.A., Bolin, J.T., Freer, S.T., Hamlin, R., Xuong, N., Kraut, J., Poe, M., Williams, M., and Hoogsteen, K. 1977. Dihydrofolate reductase: x-ray structure of the binary complex with methotrexate. *Science* 197:452-455.
632. Bertino, J.R. 2009. Cancer research: from folate antagonism to molecular targets. *Best Pract Res Clin Haematol* 22:577-582.
633. Nakajima, A., Hakoda, M., Yamanaka, H., Kamatani, N., and Kashiwazaki, S. 1996. Divergent effects of methotrexate on the clonal growth of T and B lymphocytes and synovial adherent cells from patients with rheumatoid arthritis. *Ann Rheum Dis* 55:237-242.
634. Ram, R., Gafter-Gvili, A., Yeshurun, M., Paul, M., Raanani, P., and Shpilberg, O. 2009. Prophylaxis regimens for GVHD: systematic review and meta-analysis. *Bone Marrow Transplant* 43:643-653.
635. Yang, Q., and Guan, K.L. 2007. Expanding mTOR signaling. *Cell Res* 17:666-681.
636. Cutler, C., Li, S., Ho, V.T., Koreth, J., Alyea, E., Soiffer, R.J., and Antin, J.H. 2007. Extended follow-up of methotrexate-free immunosuppression

using sirolimus and tacrolimus in related and unrelated donor peripheral blood stem cell transplantation. *Blood* 109:3108-3114.
637. Nagy, S.E., Andersson, J.P., and Andersson, U.G. 1993. Effect of mycophenolate mofetil (RS-61443) on cytokine production: inhibition of superantigen-induced cytokines. *Immunopharmacology* 26:11-20.
638. Kasper, C., Sayer, H.G., Mugge, L.O., Schilling, K., Scholl, S., Issa, M.C., and Hoffken, K. 2004. Combined standard graft-versus-host disease (GvHD) prophylaxis with mycophenolate mofetil (MMF) in allogeneic peripheral blood stem cell transplantation from unrelated donors. *Bone Marrow Transplant* 33:65-69.
639. van Leeuwen, L., Guiffre, A.K., Sewell, W.A., Vos, B.J., Rainer, S., and Atkinson, K. 1997. Administration of mycophenolate mofetil in a murine model of acute graft-versus-host disease after bone marrow transplantation. *Transplantation* 64:1097-1101.
640. Mohty, M., de Lavallade, H., Faucher, C., Bilger, K., Vey, N., Stoppa, A.M., Gravis, G., Coso, D., Viens, P., Gastaut, J.A., et al. 2004. Mycophenolate mofetil and cyclosporine for graft-versus-host disease prophylaxis following reduced intensity conditioning allogeneic stem cell transplantation. *Bone Marrow Transplant* 34:527-530.
641. Hahn, T., McCarthy, P.L., Jr., Zhang, M.J., Wang, D., Arora, M., Frangoul, H., Gale, R.P., Hale, G.A., Horan, J., Isola, L., et al. 2008. Risk factors for acute graft-versus-host disease after human leukocyte antigen-identical sibling transplants for adults with leukemia. *J Clin Oncol* 26:5728-5734.
642. MacMillan, M.L., Weisdorf, D.J., Wagner, J.E., DeFor, T.E., Burns, L.J., Ramsay, N.K., Davies, S.M., and Blazar, B.R. 2002. Response of 443 patients to steroids as primary therapy for acute graft-versus-host disease: comparison of grading systems. *Biol Blood Marrow Transplant* 8:387-394.
643. Griffin, R.L., Krzesicki, R.F., Fidler, S.F., Rosenbloom, C.L., Auchampach, J.A., Manning, A.M., Haas, J.V., Cammarata, S.K., Chin, J.E., and Richards, I.M. 1994. Attenuation of oxidant-induced lung injury by 21-aminosteroids (lazaroids): correlation with the mRNA expression for E-selectin, P-selectin, ICAM-1, and VCAM-1. *Environ Health Perspect* 102 Suppl 10:193-200.
644. Ashwell, J.D., Lu, F.W., and Vacchio, M.S. 2000. Glucocorticoids in T cell development and function*. *Annu Rev Immunol* 18:309-345.
645. Charmandari, E., Tsigos, C., and Chrousos, G. 2005. Endocrinology of the stress response. *Annu Rev Physiol* 67:259-284.
646. Jaffe, H.L. 1924. The Influence of the Suprarenal Gland on the Thymus : Iii. Stimulation of the Growth of the Thymus Gland Following Double Suprarenalectomy in Young Rats. *J Exp Med* 40:753-759.
647. Kirk, L.F., Jr., Hash, R.B., Katner, H.P., and Jones, T. 2000. Cushing's disease: clinical manifestations and diagnostic evaluation. *Am Fam Physician* 62:1119-1127, 1133-1114.
648. Dougherty TF, W.A. 1943. Effect of pituitary adrenotropic hormone on lymphoid tissue. *Proc. Soc. Exp. Biol. Med.* 53:132–133.

649. Auphan, N., DiDonato, J.A., Rosette, C., Helmberg, A., and Karin, M. 1995. Immunosuppression by glucocorticoids: inhibition of NF-kappa B activity through induction of I kappa B synthesis. *Science* 270:286-290.
650. Scheinman, R.I., Cogswell, P.C., Lofquist, A.K., and Baldwin, A.S., Jr. 1995. Role of transcriptional activation of I kappa B alpha in mediation of immunosuppression by glucocorticoids. *Science* 270:283-286.
651. Brostjan, C., Anrather, J., Csizmadia, V., Stroka, D., Soares, M., Bach, F.H., and Winkler, H. 1996. Glucocorticoid-mediated repression of NFkappaB activity in endothelial cells does not involve induction of IkappaBalpha synthesis. *J Biol Chem* 271:19612-19616.
652. Heck, S., Kullmann, M., Gast, A., Ponta, H., Rahmsdorf, H.J., Herrlich, P., and Cato, A.C. 1994. A distinct modulating domain in glucocorticoid receptor monomers in the repression of activity of the transcription factor AP-1. *Embo J* 13:4087-4095.
653. Rogatsky, I., Hittelman, A.B., Pearce, D., and Garabedian, M.J. 1999. Distinct glucocorticoid receptor transcriptional regulatory surfaces mediate the cytotoxic and cytostatic effects of glucocorticoids. *Mol Cell Biol* 19:5036-5049.
654. Perandones, C.E., Illera, V.A., Peckham, D., Stunz, L.L., and Ashman, R.F. 1993. Regulation of apoptosis in vitro in mature murine spleen T cells. *J Immunol* 151:3521-3529.
655. Brokaw, J.J., White, G.W., Baluk, P., Anderson, G.P., Umemoto, E.Y., and McDonald, D.M. 1998. Glucocorticoid-induced apoptosis of dendritic cells in the rat tracheal mucosa. *Am J Respir Cell Mol Biol* 19:598-605.
656. Balow, J.E., Hurley, D.L., and Fauci, A.S. 1975. Immunosuppressive effects of glucocorticosteroids: differential effects of acute vs chronic administration on cell-mediated immunity. *J Immunol* 114:1072-1076.
657. Sentman, C.L., Shutter, J.R., Hockenbery, D., Kanagawa, O., and Korsmeyer, S.J. 1991. bcl-2 inhibits multiple forms of apoptosis but not negative selection in thymocytes. *Cell* 67:879-888.
658. Siegel, R.M., Katsumata, M., Miyashita, T., Louie, D.C., Greene, M.I., and Reed, J.C. 1992. Inhibition of thymocyte apoptosis and negative antigenic selection in bcl-2 transgenic mice. *Proc Natl Acad Sci U S A* 89:7003-7007.
659. Grillot, D.A., Merino, R., and Nunez, G. 1995. Bcl-XL displays restricted distribution during T cell development and inhibits multiple forms of apoptosis but not clonal deletion in transgenic mice. *J Exp Med* 182:1973-1983.
660. Hench, P.S., Kendall, E.C., Slocumb, C.H., and Polley, H.F. 1950. Effects of cortisone acetate and pituitary ACTH on rheumatoid arthritis, rheumatic fever and certain other conditions. *Arch Intern Med (Chic)* 85:545-666.
661. Parker, B.J., and Bruce, I.N. 2007. High dose methylprednisolone therapy for the treatment of severe systemic lupus erythematosus. *Lupus* 16:387-393.
662. Lionakis, M.S., and Kontoyiannis, D.P. 2003. Glucocorticoids and invasive fungal infections. *Lancet* 362:1828-1838.

663. Jick, S.S., Lieberman, E.S., Rahman, M.U., and Choi, H.K. 2006. Glucocorticoid use, other associated factors, and the risk of tuberculosis. *Arthritis Rheum* 55:19-26.
664. Gustafson, T.L., Schaffner, W., Lavely, G.B., Stratton, C.W., Johnson, H.K., and Hutcheson, R.H., Jr. 1983. Invasive aspergillosis in renal transplant recipients: correlation with corticosteroid therapy. *J Infect Dis* 148:230-238.
665. Orth, D.N. 1995. Cushing's syndrome. *N Engl J Med* 332:791-803.
666. Carella, A.M., Beltrami, G., Scalzulli, P.R., Carella, A.M., Jr., and Corsetti, M.T. 2004. Alemtuzumab can successfully treat steroid-refractory acute graft-versus-host disease (aGVHD). *Bone Marrow Transplant* 33:131-132.
667. Gomez-Almaguer, D., Ruiz-Arguelles, G.J., del Carmen Tarin-Arzaga, L., Gonzalez-Llano, O., Gutierrez-Aguirre, H., Cantu-Rodriguez, O., Jaime-Perez, J., Carrasco-Yalan, A., and Giralt, S. 2008. Alemtuzumab for the treatment of steroid-refractory acute graft-versus-host disease. *Biol Blood Marrow Transplant* 14:10-15.
668. Carpenter, P.A., Lowder, J., Johnston, L., Frangoul, H., Khoury, H., Parker, P., Jerome, K.R., McCune, J.S., Storer, B., Martin, P., et al. 2005. A phase II multicenter study of visilizumab, humanized anti-CD3 antibody, to treat steroid-refractory acute graft-versus-host disease. *Biol Blood Marrow Transplant* 11:465-471.
669. Knop, S., Hebart, H., Gscheidle, H., Holler, E., Kolb, H.J., Niederwieser, D., and Einsele, H. 2005. OKT3 muromonab as second-line and subsequent treatment in recipients of stem cell allografts with steroid-resistant acute graft-versus-host disease. *Bone Marrow Transplant* 36:831-837.
670. Arai, S., Margolis, J., Zahurak, M., Anders, V., and Vogelsang, G.B. 2002. Poor outcome in steroid-refractory graft-versus-host disease with antithymocyte globulin treatment. *Biol Blood Marrow Transplant* 8:155-160.
671. Wong, M., Ziring, D., Korin, Y., Desai, S., Kim, S., Lin, J., Gjertson, D., Braun, J., Reed, E., and Singh, R.R. 2008. TNFalpha blockade in human diseases: mechanisms and future directions. *Clin Immunol* 126:121-136.
672. Locksley, R.M., Killeen, N., and Lenardo, M.J. 2001. The TNF and TNF receptor superfamilies: integrating mammalian biology. *Cell* 104:487-501.
673. Mitoma, H., Horiuchi, T., Tsukamoto, H., Tamimoto, Y., Kimoto, Y., Uchino, A., To, K., Harashima, S., Hatta, N., and Harada, M. 2008. Mechanisms for cytotoxic effects of anti-tumor necrosis factor agents on transmembrane tumor necrosis factor alpha-expressing cells: comparison among infliximab, etanercept, and adalimumab. *Arthritis Rheum* 58:1248-1257.
674. Patriarca, F., Sperotto, A., Damiani, D., Morreale, G., Bonifazi, F., Olivieri, A., Ciceri, F., Milone, G., Cesaro, S., Bandini, G., et al. 2004. Infliximab treatment for steroid-refractory acute graft-versus-host disease. *Haematologica* 89:1352-1359.

675. Levine, J.E., Paczesny, S., Mineishi, S., Braun, T., Choi, S.W., Hutchinson, R.J., Jones, D., Khaled, Y., Kitko, C.L., Bickley, D., et al. 2008. Etanercept plus methylprednisolone as initial therapy for acute graft-versus-host disease. *Blood* 111:2470-2475.
676. Knobler, R., Barr, M.L., Couriel, D.R., Ferrara, J.L., French, L.E., Jaksch, P., Reinisch, W., Rook, A.H., Schwarz, T., and Greinix, H. 2009. Extracorporeal photopheresis: past, present, and future. *J Am Acad Dermatol* 61:652-665.
677. Greinix, H.T., Knobler, R.M., Worel, N., Schneider, B., Schneeberger, A., Hoecker, P., Mitterbauer, M., Rabitsch, W., Schulenburg, A., and Kalhs, P. 2006. The effect of intensified extracorporeal photochemotherapy on long-term survival in patients with severe acute graft-versus-host disease. *Haematologica* 91:405-408.
678. Lamioni, A., Parisi, F., Isacchi, G., Giorda, E., Di Cesare, S., Landolfo, A., Cenci, F., Bottazzo, G.F., and Carsetti, R. 2005. The immunological effects of extracorporeal photopheresis unraveled: induction of tolerogenic dendritic cells in vitro and regulatory T cells in vivo. *Transplantation* 79:846-850.
679. Gatza, E., Rogers, C.E., Clouthier, S.G., Lowler, K.P., Tawara, I., Liu, C., Reddy, P., and Ferrara, J.L. 2008. Extracorporeal photopheresis reverses experimental graft-versus-host disease through regulatory T cells. *Blood* 112:1515-1521.
680. Colombo, A.A., Alessandrino, E.P., Bernasconi, P., Arcese, G.W., Rabusin, M., Bacigalupo, A., and Bernasconi, C. 1999. N-acetylcysteine in the treatment of steroid-resistant acute graft-versus-host-disease: preliminary results. Gruppo Italiano Trapianto di Midollo Osseo (GITMO). *Transplantation* 68:1414-1416.
681. Atkuri, K.R., Mantovani, J.J., and Herzenberg, L.A. 2007. N-Acetylcysteine--a safe antidote for cysteine/glutathione deficiency. *Curr Opin Pharmacol* 7:355-359.
682. Gregory, C.D., Tursz, T., Edwards, C.F., Tetaud, C., Talbot, M., Caillou, B., Rickinson, A.B., and Lipinski, M. 1987. Identification of a subset of normal B cells with a Burkitt's lymphoma (BL)-like phenotype. *J Immunol* 139:313-318.
683. Blatt, N.B., Boitano, A.E., Lyssiotis, C.A., Opipari, A.W., Jr., and Glick, G.D. 2009. Bz-423 superoxide signals B cell apoptosis via Mcl-1, Bak, and Bax. *Biochem Pharmacol* 78:966-973.
684. Haefely, W. 1990. The GABA-benzodiazepine interaction fifteen years later. *Neurochem Res* 15:169-174.
685. Boitano, A., Emal, C.D., Leonetti, F., Blatt, N.B., Dineen, T.A., Ellman, J.A., Roush, W.R., Opipari, A.W., and Glick, G.D. 2003. Structure activity studies of a novel cytotoxic benzodiazepine. *Bioorg Med Chem Lett* 13:3327-3330.
686. Veenman, L., and Gavish, M. 2006. The peripheral-type benzodiazepine receptor and the cardiovascular system. Implications for drug development. *Pharmacol Ther* 110:503-524.

687. Canat, X., Carayon, P., Bouaboula, M., Cahard, D., Shire, D., Roque, C., Le Fur, G., and Casellas, P. 1993. Distribution profile and properties of peripheral-type benzodiazepine receptors on human hemopoietic cells. *Life Sci* 52:107-118.
688. Casellas, P., Galiegue, S., and Basile, A.S. 2002. Peripheral benzodiazepine receptors and mitochondrial function. *Neurochem Int* 40:475-486.
689. Hirsch, T., Decaudin, D., Susin, S.A., Marchetti, P., Larochette, N., Resche-Rigon, M., and Kroemer, G. 1998. PK11195, a ligand of the mitochondrial benzodiazepine receptor, facilitates the induction of apoptosis and reverses Bcl-2-mediated cytoprotection. *Exp Cell Res* 241:426-434.
690. Torres, S.R., Frode, T.S., Nardi, G.M., Vita, N., Reeb, R., Ferrara, P., Ribeiro-do-Valle, R.M., and Farges, R.C. 2000. Anti-inflammatory effects of peripheral benzodiazepine receptor ligands in two mouse models of inflammation. *Eur J Pharmacol* 408:199-211.
691. Waterfield, J.D., McGeer, E.G., and McGeer, P.L. 1999. The peripheral benzodiazepine receptor ligand PK 11195 inhibits arthritis in the MRL-lpr mouse model. *Rheumatology (Oxford)* 38:1068-1073.
692. Boitano, A., Ellman, J.A., Glick, G.D., and Opipari, A.W., Jr. 2003. The proapoptotic benzodiazepine Bz-423 affects the growth and survival of malignant B cells. *Cancer Res* 63:6870-6876.
693. Doble, A., Ferris, O., Burgevin, M.C., Menager, J., Uzan, A., Dubroeucq, M.C., Renault, C., Gueremy, C., and Le Fur, G. 1987. Photoaffinity labeling of peripheral-type benzodiazepine-binding sites. *Mol Pharmacol* 31:42-49.
694. Portanova, J.P., Creadon, G., Zhang, X., Smith, D.S., Kotzin, B.L., and Wysocki, L.J. 1995. An early post-mutational selection event directs expansion of autoreactive B cells in murine lupus. *Mol Immunol* 32:117-135.
695. Sundberg, T.B., Ney, G.M., Subramanian, C., Opipari, A.W., Jr., and Glick, G.D. 2006. The immunomodulatory benzodiazepine Bz-423 inhibits B-cell proliferation by targeting c-myc protein for rapid and specific degradation. *Cancer Res* 66:1775-1782.
696. Fernandez, P.C., Frank, S.R., Wang, L., Schroeder, M., Liu, S., Greene, J., Cocito, A., and Amati, B. 2003. Genomic targets of the human c-Myc protein. *Genes Dev* 17:1115-1129.
697. Cobrinik, D. 2005. Pocket proteins and cell cycle control. *Oncogene* 24:2796-2809.
698. Krueger, G.G., Bergstresser, P.R., Lowe, N.J., Voorhees, J.J., and Weinstein, G.D. 1984. Psoriasis. *J Am Acad Dermatol* 11:937-947.
699. Varani, J., Bhagavathula, N., Nerusu, K.C., Sherzer, H., Fay, K., Boitano, A.E., Glick, G.D., Johnson, K., Kang, S., and Opipari, A.W., Jr. 2005. A novel benzodiazepine selectively inhibits keratinocyte proliferation and reduces retinoid-induced epidermal hyperplasia in organ-cultured human skin. *J Pharmacol Exp Ther* 313:56-63.

700. Bhagavathula, N., Nerusu, K.C., Hanosh, A., Aslam, M.N., Sundberg, T.B., Opipari, A.W., Jr., Johnson, K., Kang, S., Glick, G.D., and Varani, J. 2008. 7-Chloro-5-(4-hydroxyphenyl)-1-methyl-3-(naphthalen-2-ylmethyl)-4,5-dihydr o-1H-benzo[b][1,4]diazepin-2(3H)-one (Bz-423), a benzodiazepine, suppresses keratinocyte proliferation and has antipsoriatic activity in the human skin-severe, combined immunodeficient mouse transplant model. *J Pharmacol Exp Ther* 324:938-947.
701. Chelikani, P., Fita, I., and Loewen, P.C. 2004. Diversity of structures and properties among catalases. *Cell Mol Life Sci* 61:192-208.
702. Adams, J.M., and Cory, S. 2007. Bcl-2-regulated apoptosis: mechanism and therapeutic potential. *Curr Opin Immunol* 19:488-496.
703. Willis, S.N., Chen, L., Dewson, G., Wei, A., Naik, E., Fletcher, J.I., Adams, J.M., and Huang, D.C. 2005. Proapoptotic Bak is sequestered by Mcl-1 and Bcl-xL, but not Bcl-2, until displaced by BH3-only proteins. *Genes Dev* 19:1294-1305.
704. Kim, B.J., Ryu, S.W., and Song, B.J. 2006. JNK- and p38 kinase-mediated phosphorylation of Bax leads to its activation and mitochondrial translocation and to apoptosis of human hepatoma HepG2 cells. *J Biol Chem* 281:21256-21265.
705. Shen, H.M., and Liu, Z.G. 2006. JNK signaling pathway is a key modulator in cell death mediated by reactive oxygen and nitrogen species. *Free Radic Biol Med* 40:928-939.
706. Tobiume, K., Matsuzawa, A., Takahashi, T., Nishitoh, H., Morita, K., Takeda, K., Minowa, O., Miyazono, K., Noda, T., and Ichijo, H. 2001. ASK1 is required for sustained activations of JNK/p38 MAP kinases and apoptosis. *EMBO Rep* 2:222-228.
707. Hafner, R.P., Brown, G.C., and Brand, M.D. 1990. Analysis of the control of respiration rate, phosphorylation rate, proton leak rate and protonmotive force in isolated mitochondria using the 'top-down' approach of metabolic control theory. *Eur J Biochem* 188:313-319.
708. Nishi, T., and Forgac, M. 2002. The vacuolar (H+)-ATPases--nature's most versatile proton pumps. *Nat Rev Mol Cell Biol* 3:94-103.
709. Bossy-Wetzel, E., and Green, D.R. 2000. Detection of apoptosis by annexin V labeling. *Methods Enzymol* 322:15-18.
710. Steensma, D.P., Timm, M., and Witzig, T.E. 2003. Flow cytometric methods for detection and quantification of apoptosis. *Methods Mol Med* 85:323-332.
711. Krenger, W., and Hollander, G.A. 2008. The immunopathology of thymic GVHD. *Semin Immunopathol* 30:439-456.
712. Parkman, R. 2008. Antigen-specific immunity following hematopoietic stem cell transplantation. *Blood Cells Mol Dis* 40:91-93.
713. Tomblyn, M., Chiller, T., Einsele, H., Gress, R., Sepkowitz, K., Storek, J., Wingard, J.R., Young, J.A., and Boeckh, M.J. 2009. Guidelines for preventing infectious complications among hematopoietic cell transplant recipients: a global perspective. Preface. *Bone Marrow Transplant* 44:453-455.

714. Wojtovich, A.P., and Brookes, P.S. 2008. The endogenous mitochondrial complex II inhibitor malonate regulates mitochondrial ATP-sensitive potassium channels: implications for ischemic preconditioning. *Biochim Biophys Acta* 1777:882-889.
715. Chance, B., and Williams, G.R. 1955. Respiratory enzymes in oxidative phosphorylation. III. The steady state. *J Biol Chem* 217:409-427.
716. Adam-Vizi, V. 2005. Production of reactive oxygen species in brain mitochondria: contribution by electron transport chain and non-electron transport chain sources. *Antioxid Redox Signal* 7:1140-1149.
717. Gong, Y., Sohn, H., Xue, L., Firestone, G.L., and Bjeldanes, L.F. 2006. 3,3'-Diindolylmethane is a novel mitochondrial H(+)-ATP synthase inhibitor that can induce p21(Cip1/Waf1) expression by induction of oxidative stress in human breast cancer cells. *Cancer Res* 66:4880-4887.
718. Terada, H. 1990. Uncouplers of oxidative phosphorylation. *Environ Health Perspect* 87:213-218.
719. Gartenhaus, R.B., Prachand, S.N., Paniaqua, M., Li, Y., and Gordon, L.I. 2002. Arsenic trioxide cytotoxicity in steroid and chemotherapy-resistant myeloma cell lines: enhancement of apoptosis by manipulation of cellular redox state. *Clin Cancer Res* 8:566-572.
720. Davison, K., Mann, K.K., Waxman, S., and Miller, W.H., Jr. 2004. JNK activation is a mediator of arsenic trioxide-induced apoptosis in acute promyelocytic leukemia cells. *Blood* 103:3496-3502.
721. Goto, H., Takahashi, H., Fujii, H., Ikuta, K., and Yokota, S. 2003. N-(4-Hydroxyphenyl)retinamide (4-HPR) induces leukemia cell death via generation of reactive oxygen species. *Int J Hematol* 78:219-225.
722. Morales, M.C., Perez-Yarza, G., Nieto-Rementeria, N., Boyano, M.D., Jangi, M., Atencia, R., and Asumendi, A. 2005. Intracellular glutathione levels determine cell sensitivity to apoptosis induced by the antineoplasic agent N-(4-hydroxyphenyl) retinamide. *Anticancer Res* 25:1945-1951.
723. Alexandre, J., Batteux, F., Nicco, C., Chereau, C., Laurent, A., Guillevin, L., Weill, B., and Goldwasser, F. 2006. Accumulation of hydrogen peroxide is an early and crucial step for paclitaxel-induced cancer cell death both in vitro and in vivo. *Int J Cancer* 119:41-48.
724. Akhmedov, R. 1972. CHANGES IN TISSUE RESPIRATION OF VARIOUS ORGANS INDUCED BY A HIGH AMBIENT TEMPERATURE
Bulletin of Experimental Biology and Medicine 73:149-150.
725. Van Remmen, H., Salvador, C., Yang, H., Huang, T.T., Epstein, C.J., and Richardson, A. 1999. Characterization of the antioxidant status of the heterozygous manganese superoxide dismutase knockout mouse. *Arch Biochem Biophys* 363:91-97.
726. Chiba, K. 2005. FTY720, a new class of immunomodulator, inhibits lymphocyte egress from secondary lymphoid tissues and thymus by agonistic activity at sphingosine 1-phosphate receptors. *Pharmacol Ther* 108:308-319.
727. Taylor, P.A., Ehrhardt, M.J., Lees, C.J., Tolar, J., Weigel, B.J., Panoskaltsis-Mortari, A., Serody, J.S., Brinkmann, V., and Blazar, B.R.

2007. Insights into the mechanism of FTY720 and compatibility with regulatory T cells for the inhibition of graft-versus-host disease (GVHD). *Blood* 110:3480-3488.
728. Brown, T.L. 2004. Q-VD-OPh, next generation caspase inhibitor. *Adv Exp Med Biol* 559:293-300.
729. Kornbluth, M., You-Ten, E., Desbarats, J., Gamache, S., Xenocostas, A., and Lapp, W.S. 1991. T cell subsets in the thymus of graft-versus-host immunosuppressed mice. Sensitivity of the L3T4+Lyt-2- subset to cortisone. *Transplantation* 51:262-267.
730. Jenkins, M.K., Schwartz, R.H., and Pardoll, D.M. 1988. Effects of cyclosporine A on T cell development and clonal deletion. *Science* 241:1655-1658.
731. Brekelmans, P., van Soest, P., Voerman, J., Platenburg, P.P., Leenen, P.J., and van Ewijk, W. 1994. Transferrin receptor expression as a marker of immature cycling thymocytes in the mouse. *Cell Immunol* 159:331-339.
732. Swainson, L., Kinet, S., Manel, N., Battini, J.L., Sitbon, M., and Taylor, N. 2005. Glucose transporter 1 expression identifies a population of cycling CD4+ CD8+ human thymocytes with high CXCR4-induced chemotaxis. *Proc Natl Acad Sci U S A* 102:12867-12872.